Thin Film Composite Membranes Derived from Interfacial Polymerization for Nanofiltration and Pervaporation Applications

by

Dihua Wu

A thesis

presented to the University of Waterloo

in fulfillment of the

thesis requirement for the degree of

Doctor of Philosophy

in

Chemical Engineering

Waterloo, Ontario, Canada, 2015

AUTHOR's DECLARATION

I hereby declare that I am the sole author of this thesis. This is a true copy of the thesis, including any required final revisions, as accepted by my examiners.

I understand that my thesis may be made electronically available to the public.

Abstract

In this study, thin film composite (TFC) membranes were prepared by interfacial polymerization on a microporous polyethersulfone (PES) substrate. These membranes were studied for salt separation by nanofiltration and ethylene glycol dehydration by pervaporation.

The membranes with a layer-by-layer structure based on polyethylenimine (PEI) and trimesoylchloride (TMC) were prepared by sequential reactant depositions and reactions. The membrane properties can be tailored by controlling the number and sequence of the reactant depositions. In general, the PEI-TMC membranes were more permeable than the TMC-PEI membranes. The membrane formed by a single cycle of interfacial polymerization with 3.5 wt% PEI and 0.7 wt% TMC had a positively charged surface and showed a good nanofiltration performance; salt rejections of 95.1% for $MgCl_2$, 94.4% for $MgSO_4$, 80.5% for Na_2SO_4 and 85.1% for NaCl with a pure water permeation flux of 24.5 $L/(m^2.h)$ were obtained at a feed solute concentration of 500 ppm and transmembrane pressure of 0.8 MPa gauge.

In another approach, monomeric amine piperazine (PIP) was embedded into the polymeric amine PEI as the amine reactant. Membranes with a single-ply polyamide layer were produced by reacting TMC with mixed amines of PEI and PIP. Incorporation of 10 wt% PIP in PEI resulted in a 6-fold increase in permeation flux while still maintaining a 91.6% $MgCl_2$ rejection. In addition, 2-ply polyamide membranes were prepared by two cycles of PEI-TMC and PIP-TMC interfacial reactions, separately. It was demonstrated that by properly controlling the PIP/PEI concentration ratio, the 2-ply polyamide membranes with both a higher permeation flux and salt rejection than conventional single-ply polyamide membranes could be produced.

The effects of chlorine exposure on the nanofiltration performance of the positively-charged polyamide membranes were studied. It was found that the PIP/TMC crosslinks on the outer sublayer improved the chlorine resistance of the membrane. Controlled exposure of the membrane to a low chlorine concentration could improve the nanofiltration performance. The effect of membrane chlorination was intensified at either an alkaline or acidic pH. The customarily used chlorination intensity (ppm.h), which is a composite parameter based on the product of chlorine concentration and chlorination time, was not adequate for use as a standalone parameter to characterize the chlorination conditions.

The PEI/TMC nanofiltration membrane was further modified with self-polymerized polydopamine for use in dehydration of ethylene glycol by pervaporation. Deposition of polydopamine either as an outer layer (i.e., on top of the polyamide) or as a transition layer (i.e., between the polyamide and the substrate) would increase the total permeation flux and effectively improve the membrane selectivity. The modified membrane showed a total permeation flux of 81.03 g/(m^2.h) and a separation factor of 388 for a feed containing 2.4 wt% water at 38 °C. The presence of inorganic salt NaCl in the feed mixture decreased the permeation fluxes of both water and ethylene glycol, but increased the water content in the permeate.

Acknowledgements

PhD study is a long journey and this thesis is the result of intense work over several years. I have been supported, assisted and accompanied by many people during this period of study. I would like to take this opportunity to express my gratitude to all of them.

First, I want to thank the Department of Chemical Engineering, University of Waterloo for giving me the permission to study here as well as providing the departmental resources.

The first person I would like to thank is my supervisor, Dr. Xianshe Feng, who provided me opportunity, support, advice and guidance during my PhD study. His excellent knowledge and scientific vision in the field of membrane helped me to discover my passions and potentials. His valuable advice and encouragement led me to overcome difficulties in research. I am much moved by his conscientious revisions of my PhD comprehensive proposal, manuscripts and PhD thesis. His responsible and patient attitudes greatly affect me, which is not limited to the past four years guiding me to become a better scientist but will continue to influence me in my future.

I am glad to express my gratitude to my PhD examination committee members: Prof. Raja Ghosh of McMaster University, Prof. Sigrid Peldszus of Civil and Environmental Engineering, and Profs. Christine Moresoli and Boxin Zhao of Chemical Engineering, for providing valuable suggestions regarding my research.

I am thankful to all the people who helped me during my PhD studies. I would like to thank Prof. Sanchuan Yu at Zhejiang Sci-Tech University, who shared his experience and gave me valuable suggestions relating to my research. I appreciate the assistance with membrane characterization provided by Ms. Jingqun Liu and Mr. Qibo Cheng in Prof. Sanchuan Yu's

group. I also want express my thanks to the current and previous group members. Dr. Gil J. Francisco, Dr. Ying Zhang and Xincheng Xu helped me to design and set up my test unit at the beginning of my research. Dr. Prodip Kundu and Melanie Snow provided very useful suggestions for my comprehensive examination. Dr. Yong Zhou and Dr. Yongqiang Yang generously shared their research experience and provided their professional knowledge and advice on my research. Dr. Yijie Hu, Yifeng Huang, Shuixiu Lai, Boya Zhang, Min Guan and Kai Wu always kindly offered their patience and passion for assistance, listening and discussion.

I also extend my thanks to people those who influenced me in the past four years. Dr. Zhongde Wang and Dr. Xiaodong Wang gave me valuable suggestion for the development in my future career and life. Baoling Chen, my dearest friend in Waterloo, whose enthusiasm, optimism and capability always profoundly encourage me to hold a positive attitude to everything happens in life. Thank her for accompanying me at the moments of my happiness and difficulties.

Last, but not the least, I would like to appreciate my families, especially my parents and my grandmother for holding my hands with understanding, support, comfort and encouragement to pursue the choice I made. This thesis is dedicated to them.

I might not be able to name everyone who touched my life in various meaningful ways on these limited pages, but your kindness will be remembered in my mind and my heart. I express my respect and thanks to you all with the utmost sincerity and appreciation.

Table of Contents

Chapter 3

Thin film composite NF membranes formed by interfacial polymerization from PEI and TMC.. **43**

Chapter 4

Thin film composite NF membranes formed from polymeric amine PEI imbedded with monomeric amine PIP and TMC **91**

List of Figures

List of Tables

List of Symbols

A	Water permeabilit constant, $mol/(m^2.s.MPa)$
B	Salt transport paremeter, m/s
c	Concentration, mol/m^3, mol/L, mg/L
D	Diffusion coefficient, m^2/s
E_D	Activation energy for diffusion, kJ/mol
E_J	Activation energy based on permeation flux, kJ/mol
E_P	Activation energy based on membrane permeability, kJ/mol
H	Henry's law coefficient, $Pa.m^3/mol$
ΔH_S	Heat of sorption, kJ/mol
i	Total number of moles of ions given by one mole of the salt
J	Permeation flux, $mol/(m^2.s)$, $m^3/(m^2.s)$, $L/(m^2.h)$, $g/(m^2.h)$,
K	Sorption coeffiient, cm^3/g
K_{C-K}	Carman-Kozeny constant
k	Mass transfer coefficient for the solute on the high pressure side, m/s
L	Proportional coefficient related to chemcal potentail driving force
l	Membrane thickness, m
M	Molecular weights
m	Molality, mol/L
N	Mole permeation flux, $mol/(m^2.s)$
P	Permeability coefficient, m^2/s
ΔP	Pressure difference across the membrane, MPa
p	Partial vapor pressure, Pa
p^p	Permeate pressure, Pa

p^s Saturated vapor pressure, Pa

Q   Quantity of permeate, L, g

R   Gas constant, 8.314 J/(K.mol)

R_m Total resistance towards solvent flow, m^{-1}

r   Salt rejection, %

r_p Pore radius, m

S   Effective membrane area, m^2

S_m Pore internal surface area per unit volume, m^2/m^3

T   Temperature, K

Δt Time interval, h

v   Mole volume, m^3/mol

X   Mass fraction

x   Mole fraction

W_D Weights of the dried membrane, g

W_S Weights of the swollen membrane, g

Greek letters

α Separation factor

γ Activity coefficient

ε Surface porosity

η Viscosity of the liquid solvent, MPa.s

μ Chemical potential

π Osmotic pressure, MPa

ρ Molar density, mol/m^3

τ Tortuosity of the pores

Subscripts

i   Component i

j   Component j

s   Salt

w   Water

0   Position of the feed interface

b   Position of the concentrated boundary

l Position of the permeate interface

Supscript

L   Liquid phase

List of Abbreviations

Chemicals

AA   acrylic acid

AC   ammonium chloride

BPA   bisphenol A

BSA   bovine serum albumin

BTEC   biphenyl tetraacyl chloride

BTRC   3,4',5-Biphenyl triacyl chloride

CFIC   5-chloroformyloxy-isophthaloyl chloride

CHDA   1,3-cyclohexanediamine

CHMA   1,3-Cyclohexanebis (methylamine)

CPL   caprolactam

CS   chitosan

DABA   3,5-diamino-N-(4-aminophenyl) benzamide

DAPE   1,3-diaminopropane

DETA   diethylenetriamine

DHB   4,4'-dihydroxybiphenyl

DTPA   diethylene triamine pentaacetic acid

EDA   ethylenediamine

GOTMS   3-glycidyloxypropyltrimethoxy-silane

HDA   hexanediamine

HFA-   hexafluoroalcohol-

HQ   hydroquinone

HTC   1,3,5-cyclohexane-tricarbonyl chloride

ICIC	5-isocyanato-isophthaloyl chloride
IPC	isophthaloyl chloride
MAP	m-aminophenol
MDEOA	methyl-diethanolamine
MMPD	m-phenylenediamine-4-methyl
MPD	m-phenylene-diamine
MWNTs	multiwall carbon nanotubes
NaSS	sodium p-styrene sulfonate
PA	polyamide
PAA	poly(acrylic acid)
PAMAM	poly(amidoamine)
PAN	polyacrylonitrile
PBI	polybenzimidazole
PD	polydopamine
PDMS	polydimethylsiloxane
PEG	poly(ethylene glycol)
PEK	polyetherketone
PEI	polyethylenimine
PES	polyethersulfone
PIP	piperazine
PP	polypropylene
PPD	p-phenylenediamine
PTFE	poly(tetrafluoroethylene)
PVA	poly(vinylalcohol)
PVAm	polyvinylamine

PVDF   poly(vinylidene fluoride)

PVP   polyvinylpyrrolidone

SDS   sodium dodecyl sulfate

SPEEK   sulfonated poly(ether ether ketone)

SPES-NH$_2$ amine sulfonated cardo poly(arylene ether sulfone)

TDI   toluene diisocyanate

TEA   triethylamine

TEOA   triethanolamine

TMC   trimesoyl chloride

TPC   terephthaloyl chloride

Tris   tris(hydroxymethyl)aminomethane

Characterization technologies

AFM   atomic force microscope

ATR-FTIR   attenuated total reflectance Fourier transform infrared spectroscopy

IEP   isoelectric point

FE-SEM   field emission scanning electron microscopy

Membranes

MF   microfiltration

NF   nanofiltration

RO   reverse osmosis

TFC   thin film composite

UF   ultrafiltration

Special compounds

EDCs   endocrine disrupter compounds

PhACs   pharmaceutically active compounds

VOCs   volatile organic compounds

Chapter 1.

Introduction

1.1 Background

Membrane separation processes are used in a wide range of applications since they are energy efficient than conventional thermal separation processes. Based on different separation mechanisms and the size of separated particles, the widely used membrane processes include microfiltration, ultrafiltration, nanofiltration, reverse osmosis, pervaporation and gas separation. Table 1.1 illustrates the general principles (e.g., driving force, pore size and substances to be separated) of these membrane processes. For microfiltration, ultrafiltration, nanofiltration and reverse osmosis, the operation units have been well established. Several experience companies can offer the industrial membrane-based filtration system. Pervaporation and gas separation are two developing industrial membrane separation technologies. A small number of plants have been installed and the market size is being expanded. Among these processes, nanofiltration (NF) and pervaporation are two important processes for liquid separation.

Nanofiltration is a pressure-driven membrane process between reverse osmosis (RO) and ultrafiltration (UF) and rejects molecules with sizes on the order of 1 nm. It is used most often for treating water with a low content of ion (e.g., surface water and fresh ground water) with a main purpose of water softening (removal of multi valent cations) and removal of disinfection by-products such as natural and synthetic organic matters [Letterman, 1999]. Nanofiltration is

also becoming more widely used in food processing applications such as simultaneous concentration and partial (monovalent ion) demineralization of dairy products.

The process of pervaporation involves a phase transition from the feed to the permeate for the separation of liquid mixtures. That is, the liquid feed contacts one side of the membrane and the vapor-phase permeate is removed from the other side. The driving force for the mass transport is the vapor pressure difference between the feed solution and the permeate vapor. The separation is based on the difference in the transport rate of individual component through the membrane. Pervaporation is mainly used for the dehydration of organic solvents (e.g., alcohols, ethers, esters, acids and glycols), recovery of trace amounts of organics from aqueous solutions (e.g., removal of volatile organic compounds, recovery of aroma) and separation of organic-organic mixtures (e.g., methyl tert-butyl ether/methanol, dimethyl carbonate/methanol) [Baker, 2012].

Table 1.1 General principles of different membrane processes

Membrane process	Driving force	Pore size (m)	Separated substances
Microfiltration		10^{-5}-10^{-7}	Suspended and emulsified solids, yeast
Ultrafiltration		10^{-7}-10^{-9}	Colloids, proteins, bacteria
Nanofiltration		10^{-8}-10^{-9}	Divalent salts, sugars
Reverse osmosis	ΔP	10^{-9}-10^{-10}	Monovalent salts
Pervaporation		Non-porous	Solvents dehydration, organic recovery, organic-organic separation
Gas separation		Non-porous	N_2/O_2, H_2/N_2, H_2/CH_4, $N_2/$ air, CO_2/CH_4, propylene/N_2 separation

Most NF and pervaporation membranes are structurally asymmetric, which can be divided into two categories: integrally skinned membranes and composite membranes. Integrally

skinned membranes are made from the same polymer materials for both the skin layer and support layer, and these membranes are normally produced by the phase-inversion process. A breakthrough in improving the membrane performance was the development of composite membranes where the surface skin layer and the porous substrate are formed separately. This way, a broad range of polymer materials can be used and different formation procedures can be optimized for each layer, thereby maximizing the membrane performance. The resulting membranes have ultra-thin selective top layers for separation and microporous substrates for durability and compaction resistance [Petersen, 1993].

The composite membrane approach was initially developed to deposit a polymeric barrier layer onto a microporous substrate. For example, a thick cellulose acetate reverse osmosis membrane was placed on the Millipore filter paper [Riley *et al.*, 1967], leading to a decreased vulnerability to compaction. Poly (vinyl alcohol) was cross-linked on top of a porous polyacrylonitrile (PAN) substrate for the dehydration of caprolactam [Zhang *et al.*, 2007].

Interfacial polymerization appears to be a promising method for preparing thin film composite (TFC) membranes for nanofiltration. The interfacially polymerized TFC membranes also have been developed for pervaporation, especially for the dehydration of organic solvents. The barrier layers formed from interfacial polymerization have a balanced hydrophilicity and hydrophobicity as well as good membrane stability. Such membranes can be based on polyamide, polyurea and polyester, and polyamide membranes are particularly promising for water production, salt rejection and organic solvent dehydration. In the reverse osmosis/nanofiltration field, aliphatic polyamide membranes tend to have low rejections and modest fluxes, and aromatic polyamide membranes, especially those made from 1,3-benzenediamine (m-phenylene-diamine (MPD)) and trimesoyl chloride (TMC), are widely used

[Cadotte, 1981a]. Aromatic polyamide membranes not only have a high rejection and high flux, but can also withstand chlorine exposure up to 1000 ppm-h. In the pervaporation field, both aliphatic and aromatic TFC polyamide membranes have been studied, and many attempts are made to produce membranes with good separation performance for the dehydration of organic solvents [Huang *et al.*, 2008].

The amine structures play an important role in the properties of the resulting polyamide membranes. Polyethylenimine (PEI) was used previously as an aqueous reactant for interfacial polymerization. In 1969-1970, Cadotte used branched PEI with a 3:4:3 ratio of primary: secondary: tertiary amine groups and a molecular weight of 10,000 to 60,000 for the interfacial reaction, and this led to the commercial NS-100 [Cadotte and Roxelle, 1972; Cadotte, 1977; Rozelle *et al.*, 1977], RC-100 and PA-300 [RiIey *et al.*, 1977] composite membranes. Presently, PEI still attracts significant interest for fabricating NF membranes based on interfacial polymerization. Ruaan's group [Yang, 2008; Chiang, 2009] studied four NF membranes formed from PEI/TMC, PEI/terephthaloyl chloride (TPC), ethylenediamine (EDA)/TMC and diethylenetriamine (DETA)/TMC, and it was found that the PEI/TPC membrane had a pore size similar to that of the EDA/TMC membrane but with both a higher salt rejection and permeation flux, while the PEI/TMC membrane had a pore size as large as 1.5 nm but still had a higher NaCl rejection than the EDA/TMC membrane whose pore size was only 0.43 nm. This special rejection character is derived from the flexible pendant amine groups of PEI. The amine groups may drift inside the pores and interact with the ions, which will hinder the transport of ions but have little effect on water permeation. A TFC hollow fiber NF membrane from PEI and isophthaloyl chloride (IPC) was fabricated by Sun *et al.* [2012] and the membrane showed very high rejections (over 99%) for both positively and negatively charged dye molecules as

well as a high rejection for cephalexin over a wide pH range. PEI was chosen as the aqueous phase reactant for interfacial polymerization on microporous polypropylene (PP) supports to fabricate solvent-resistant TFC ultrafiltration [Korikov *et al.*, 2006] and nanofiltration membranes [Kosaraju and Sirkar, 2008]. PEI/TMC TFC hollow fiber membranes have also been employed to pervaporation for isopropanol dehydration [Zuo *et al.*, 2012] and their pervaporation flux was reported to be higher than that of a MPD/TMC membrane. Therefore, PEI is a promising amine reactant, and we chose it for the fabrication of TFC membranes in this study.

After the discovery of PEI, several monomeric amines had been tried and none of them provided attractive salt rejection until Cadotte found that high rejection composite membranes could be made by interfacial reaction of piperazine (PIP) and IPC through an optimization of membrane preparation conditions [Cadotte *et al.*, 1976]. The first commercial membrane based on PIP and TMC, named NS-300, exhibited a high water flux and $MgSO_4$ rejection [Cadotte *et al.*, 1978; Cadotte, 1981b]. Several PIP/TMC commercial membranes were developed following the NS-300 membrane, including NF series membranes (e.g., NF-40, NF-40HF and NF-70) [Freeman and Stocker, 1987; Cadotte *et al.*, 1988; Eriksson, 1988] and XP series membranes (e.g., XP-20 and XP-45) [Cadotte *et al.*, 1988] made by FilmTec Corporation, NTR series membranes (e.g., NTR-7100, NTR-7250, NTR-729HF and NTR-739HF) [Kamiyama *et al.*, 1984; Kawada *et al.*, 1987] made by Nitto Electric Industrial Company and UTC series membranes (e.g., UTC-20, UTC-50 and UTC-60) [Kurihara *et al.*, 1985; Kurihara and Himeshima, 1991] made by Toray Industries. Thus, PIP is also a reactive amine reactant and was used for interfacial polymerization in this study.

The interfacially polymerized nanofiltration membranes with very small pores have the potential to be modified to the non-porous pervaporation membranes. Inspired by the adhesive proteins excreted by marine mussels, the self-polymerized polydopamine has also attracted much attention for modifications of various types of surfaces, including membrane surface [Xi *et al.*, 2009; Karkhanechi *et al.*, 2014]. This self-polymerized polydopamine was also used in this study to modify the self-made polyamide nanofiltration membrane by a simple coating method for pervaporation uses.

1.2 Research objectives

The objectives of this research were to study the TFC polyamide membranes based on interfacial polymerization for salt separation by nanofiltration and ethylene glycol dehydration by pervaporation. The research consisted of the followings:

(1) To develop TFC nanofiltration membranes based on the reactant system of hyperbranched PEI and TMC by interfacial polymerization for salt separations.

(2) To develop TFC nanofiltration membranes from polymeric amine PEI imbedded with monomeric amine PIP for enhanced salt separations.

(3) To investigate the effects of chlorine exposure on the nanofiltration performance of the multiple-layered polyamide composite membranes based on [(PEI/TMC)-(PIP/TMC)].

(4) To modify the PEI-based polyamide composite nanofiltration membrane to make it suitable for pervaporative dehydration of ethylene glycol by depositing additional layers of self-polymerized polydopamine.

1.3 Outline of the thesis

This thesis consists of seven chapters as follows:

Chapter 1 presents the background of this study, including an introduction of the membrane processes and materials of nanofiltration and pervaporation. The objectives of this study are also described.

Chapter 2 presents a literature review of nanofiltration and pervaporation. This chapter briefly introduces the basic characteristics and mass transport of these two membrane processes. This chapter also provides the development and features of TFC membranes in nanofiltration and pervaporation. In addition, the approach of interfacial polymerization for membrane preparation is described and the effects of the parameters involved in the procedure of interfacial polymerization on the membrane properties are discussed.

Chapter 3 studies the TFC polyamide membranes prepared from hyperbranched PEI and TMC. Membranes with a layer-by-layer structure were prepared by a repeated sequence of reactant depositions/reactions to improve the salt rejection. The effects of the number of cycles of reactant deposition/reaction, the sequence of reactant deposition, the concentrations of the reactant solutions, and temperature of thermal treatment on the membrane performance were investigated. The influence of operating conditions on the membrane performance, including the feed concentration and operating pressure, was also studied.

Chapter 4 presents the development of TFC membranes fabricated from polymeric amine PEI imbedded with monomeric amine PIP. Membranes with a single polyamide layer were prepared using a blend of PEI and PIP as the aqueous phase reactant to react with TMC for interfacial polymerization. The effects of the compositions of the amine mixtures on the membrane performance were studied. Two series of 2-plies polyamide membranes were prepared (one with a PEI/TMC inner-layer and a PIP/TMC outer-layer and the other with a PIP/TMC inner-layer and a PEI/TMC outer-layer) by two cycles of interfacial polymerization.

The effects of the concentrations of PIP/PEI for the formation of different polyamide layers on the membrane performance were investigated.

The PEI-based polyamide has a high chlorine sensitivity ascribed from the large amounts of end amine groups and the N-H linkages from amide bonds. Chapter 5 focuses on the effects of chlorine exposure on nanofiltration performance of the multiple-layered polyamide composite membranes. The chlorine resistance of the PEI-based polyamide membranes was improved by an additional interfacial polymerization from PIP and TMC on the top. The effects of the concentrations of PIP/PEI for the formation of different polyamide layers and the number of PIP/TMC polyamide top-layers on the chlorine resistance of the membrane were studied. The effects of the chlorination conditions (including pH of the chlorination solutions, chlorine concentration (ppm) and exposure time (h)) on the separation performance were also studied.

Chapter 6 investigates the modification of the PEI-based polyamide nanofiltration membrane for pervaporation use by simply depositing additional layers of self-polymerized polydopamine. The separation performance of the modified membranes was evaluated for dehydration of ethylene glycol. The effects of the number and sequence of the polydopamine depositions on the pervaporation performance were studied. The effects of feed water concentration, operating temperature and feed NaCl contents on the pervaporation performance were also studied.

The general conclusions and original contributions of this research are described in Chapter 7. Some recommendations for future work are also proposed. In order to have a clear understanding of this thesis, Figure 1.1 briefly describes the structure of this thesis

```
                    ┌─────────────────────────────┐
                    │  Introduction (Chapter 1)   │
                    └─────────────────────────────┘
                                  │
                                  ▼
                ┌───────────────────────────────────┐
                │  Literature Review (Chapter 2)    │
                └───────────────────────────────────┘
                                  │
                                  ▼
                      ╭───────────────────────╮
                      │  Membrane Fabrication  │
                      ╰───────────────────────╯
                      ↙                       ↘
```

Interfacially polymerized TFC NF membranes from polymeric amine PEI and TMC (Chapter 3)

Interfacially polymerized TFC NF membranes from polymeric amine PEI embedded with monomeric amine PIP and TMC (Chapter 4)

TFC membranes based on PEI/TMC and polydopamine for pervaporative dehydration of ethylene glycol (Chapter 6)

Effect of chlorine exposure on nanofiltration performance (Chapter 5)

General conclusions, contributions and recommendations (Chapter 7)

Figure 1.1 Thesis structure illustrated in terms of chapters and content relevance.

Chapter 2.

Literature Review

Membrane technologies are used in a wide range of applications and cover the separations of gaseous and liquid stream mixtures. Comparing to the conventional thermal separation processes (e.g., distillation, sublimation or crystallization), membrane processes are energy efficient since they do not need continuous heating or cooling. In addition, membrane processes are environmentally friendly since no chemical reaction is involved. Furthermore, membrane processes are gentle and mild processes and hence very effective for separation of those mixtures which cannot operate under the harsh conditions.

Nanofiltration and pervaporation are two promising processes for liquid separation. Nanofiltration is a filtration process for the removal of multivalent ions and organic matters. Pervaporation is a method for the separation of liquid mixtures by partial vaporization through the membrane. This chapter intends to provide an overview of the principles of nanofiltration and pervaporation, including the basic characteristics and mass transport. The development of thin film composite membrane based on interfacial polymerization used in nanofiltration and pervaporation are also reviewed. In addition, a brief review of the procedure of interfacial polymerization is presented as it is the method used for preparing thin film composite membranes in this study. The effects of the parameters involved in the procedure of interfacial polymerization on the membrane properties are also discussed.

2.1 Nanofiltration process

2.1.1 Characteristics of nanofiltration

Nanofiltration (NF) is a pressure-driven membrane process developed since the late 1970s as a loose reverse osmosis (RO) process. In general, NF has two distinct properties [Rautenbach and Gröschl, 1990]:

1. The pore size of the membrane corresponds to a molecular weight cut off of approximately 300-500 g/mol. Therefore, components with higher molecular weights can be separated from solvents with smaller molecular weights.

2. Because the dimensions of the pores are close to the size of ions, charge interactions are normally important to the separation of ions with different valences when the NF membrane has a charged surface.

Based on these properties, nanofiltration is typically used for the separation of non-ionic components having different molecular weights (e.g., viruses and bacteria) and ions of different valences. Generally, nanofiltration membranes have a greater rejection to multivalent ions, but less resistant to permeation of monovalent ions. A major advantage of nanofiltration over reverse osmosis is its greater fluxes due to its bigger pore sizes. Also, it operates at a lower pressure than reverse osmosis and hence costs less in module construction and fluid pumping.

2.1.2 Mass transport in nanofiltration

The separation ability of membranes is based on the control of permeation rate of different species. Generally, there are two models used to describe the mass transport through the membranes. One is pore-flow model, in which permeation occurs by the pressure-driven convective flow through the pores and separation is based on the exclusion of permeants from the pores. The other is the solution-diffusion model, in which permeants first dissolve in the

11

membrane and then diffuse through the membrane by a concentration gradient. The separation

is based on the difference in solubility and diffusivity of different permeants in the membrane.

The pore-flow model applies to the porous membrane such as microfiltration and ultrafiltration,

and the solution-diffusion model applies to the non-porous membrane such as reverse osmosis,

pervaporation and gas separation. Nanofiltration is an intermediate between ultrafiltration and

reverse osmosis, and hence the mass transport in nanofiltration is the transition between pore-

flow and solution-diffusion.

Pore-flow model

The separation mechanism of porous membranes can be the sieving filtration taking place at the

membranes surface or the depth filtration taking place in the interior of the membranes. The

pore geometries greatly affect the mass transport through the membrane. Depending on the

shapes and sizes of the pores in the membrane, the flux of water through a membrane can be

modeled using empirical equations based on the Hagen-Poiseuille or Carman-Kozeny equations

[Mulder, 1997] as follows:

(a) Hagen-Poiseuille equation

   Consider a membrane having a number of parallel cylindrical pores. The flux through such a

membrane is given by:

$$J = \left(\frac{\varepsilon r_p^2}{8\tau l}\right)\left(\frac{\Delta P}{\eta}\right) = \frac{\Delta P}{\eta R_m} \tag{2.1}$$

where J is the volumetric permeation flux of solvent through the membrane ($m^3/(m^2.s)$), ΔP is

the pressure difference across the membrane (MPa), η is the viscosity of the liquid solvent

(MPa.s), ε is the surface porosity, r_p is the pore radius (m), τ is the tortuosity of the pores, and l

is the membrane thickness (m), R_m is the total resistance towards solvent flow (m^{-1}) and equal to the term $8\tau l / \varepsilon r_p{}^2$.

(b) Carman-Kozeny equation

For membranes which consist of closely packed spheres, the solvent flux is given by:

$$J = \left(\frac{\varepsilon^3}{K_{C-K} l S_m{}^2 (1-\varepsilon)^2} \right) \left(\frac{\Delta P}{\eta} \right) \qquad (2.2)$$

where K_{C-K} is the Carman-Kozeny constant, which depends on the pore geometry, and S_m is the pore internal surface area per unit volume (m^2/m^3). Based on the Carman-Kozeny equation, Rm is equal to the term $K_{C-K} l S_m{}^2 (1-\varepsilon)^2 / \varepsilon^3$.

Solution-diffusion model

The transport of molecules based on solution-diffusion mechanism involves three consecutive steps, that is: (1) sorption of permeant into the upstream side of the membrane; (2) diffusion of the sorbed component through the membrane under a concentration gradient; and (3) desorption from the downstream side of the membrane (see Figure 2.1).
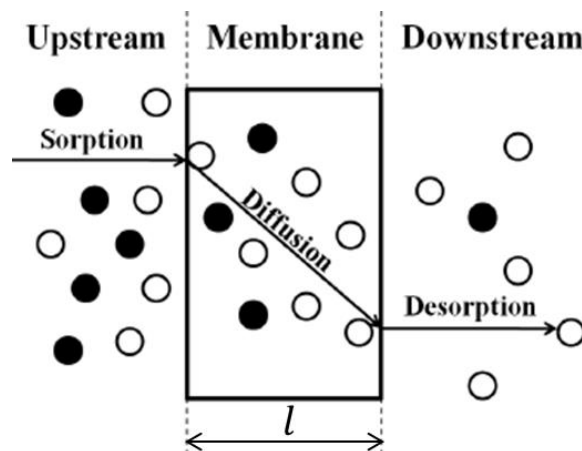
Figure 2.1 Schematic description of solution-diffusion mechanism.

The net transport of molecules occurs by the driving forces, such as gradient in pressure, temperature and concentration. The overall driving force can be expressed as chemical potential gradient, and the flux can be described by a simple equation:

$$J_i = -L_i \frac{d\mu_i}{dx} \qquad (2.3)$$

where $d\mu_i/dx$ is the chemical potential gradient of component i and L_i is a proportional coefficient related to this chemical potential driving force.

Consider a nanofiltration process involving two components, water (w) and salt (s), the flux of water (J_w) and salt (J_s) through the membrane can be written as [Baker, 2012]:

$$J_w = \frac{D_w K_w^L c_{w0} v_w (\Delta p - \pi)}{lRT} = A\, (\Delta p - \pi) \qquad (2.4)$$

$$J_s = \frac{D_s K_s^L (c_{s0} - c_{sl})}{l} = B\, (c_{s0} - c_{sl}) \qquad (2.5)$$

where D is the diffusion coefficient, K is the sorption coefficient, c is the concentration, v is the molar volume, π is the osmotic pressure, A is called the water permeabiliy constamt and equal to the term $D_w K_w^L c_{w0} v_w / lRT$, B is called the salt transport paremeter and equal to the term $D_s K_s^L / l$. The subscripts w and s represent water and salt, the term 0 and l represent the positions of the feed and permeate interfaces, respectively. The superscript L means liquid phase. The rejection (r) which evaluates the ability of the membrane to separate salt from the feed solution is given by:

$$r = \left(1 - \frac{c_{sl}}{c_{s0}}\right) \times 100\% \qquad (2.6)$$

Based on the mass transport mechanism, there are two basic types of rejection mechanisms for nanofiltration [Yaroshchuk, 1998]:

1. Steric exclusion mechanism:

This is similar to a sieving mechanism. There is a geometric exclusion of solute particles bigger than the membrane pore size. A separation between different solutes can hence be achieved based on their sizes and shapes.

2. Charge-based exclusion mechanisms (Donnan exclusion):

Due to slightly charged nature of the most NF membranes, solutes with opposite charges to the membrane surface (counter-ions) are electrostatically attracted, while solutes with the same charges (co-ions) are repelled. At the membrane surface, a distribution of co-ions and counter-ions will occur, thereby causing an additional separation.

The difference between the pore-flow and solution-diffusion mechanism lies in the relative size and permanence of the pores. In fact, the boundary between a porous and a non-porous membrane is not always clear. Even for the non-porous membranes, the pores are still present on a molecular level in order to allow transport. The existence of these "molecular pores" can be adequately described as free volume. For the porous membranes, the free volume elements are relatively large, fixed and connected to one another. Their positions or volumes do not fluctuate with the timescale of permeant motion. However, for the non-porous membranes, these free volume elements appear and disappear dynamically with the timescale of the permeant motion through the membrane. For nanofiltration membranes, whose pore sizes between porous and non-porous membranes, both large fixed and small dynamic free volumes exist. Therefore, it is necessary to interpret the mass transport mechanism from two aspects.

2.2 Pervaporation process

The term "pervaporation" is derived from the two steps: permeation through the membrane and evaporation into the vapor phase. In this process, a feed liquid mixture contacts one side of the membrane, the permeate is removed as a vapor from the other side. The driving force for

pervaporation is the difference in the partial pressures of the components between the feed and permeate side. In the laboratory, the partial pressure difference is usually maintained by a vacuum pump on the permeate side.

Pervaporation is effective for removing trace or minor amounts of the component in dilute solutions. Based on this, hydrophilic membranes are used for dehydration of organic solvents containing small amounts of water, and hydrophobic membranes are used for recovery of trace amounts of organics from aqueous solutions. Pervaporation is also used for the separation of organic-organic liquid mixtures, such as the azeotropic mixtures (e.g., ethanol-cyclohexane, methanol-methyl t-butyl ether) and isomers (e.g., xylenes).

Pervaporation membranes are dense membranes and the mass transport in the membranes can be described using the solution-diffusion model. The membrane flux can be expressed as [Baker, 2012]:

$$J_i = \frac{P_i^L}{l}\left(c_{i0} - \frac{p_{il}}{H_i}\right) \tag{2.7}$$

where P is the permeability coefficient, p is the partial vapor pressure, H is the Henry's law coefficient. The subscript i represents componet i. This equation separates the two contributions to the permeation flux, the membrane contribution P_i^L/l and the driving force contribution $(c_{i0} - p_{il}/H_i)$. The separation capability of the membrane is evaluated by the separation factor:

$$\alpha = \frac{c_{il}/c_{jl}}{c_{i0}/c_{j0}} = \frac{x_{il}/x_{jl}}{x_{i0}/x_{j0}} \tag{2.8}$$

where x represents the mole fraction and subscript j represents componet j.

The contribution of this separation factor is derived from two aspects, as shown in Figure 2.2. One is the difference in volatilities of the components in the feed liquid when they evaporate to form a saturatd vapor (α_{evap}), and the other attributes to the difference in diffusion

rate of the component vapor through the membrane (α_{mem}). The overall separation (α) achieved by the product of α_{evap} and α_{mem}, i.e.,

$$\alpha = \alpha_{evap} \cdot \alpha_{mem} \tag{2.9}$$
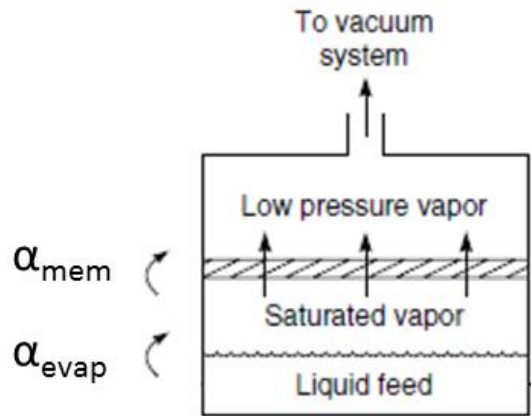
Figure 2.2 Schematic description of a conceptual pervaporation process [Wijmans and Baker, 1993].

2.3 Thin film composite membranes

Currently available nanofiltration and pervaporation membranes generally fall into two categories: integrally skinned asymmetric membranes containing one polymer, and thin film composite (TFC) membranes consisting of two or more polymer layers. Comparing to the integrally skinned asymmetric membranes, thin film composite membranes have the potential to obtain a high permeation rate and maintain a high selectivity.

   Generally a thin film composite membrane consists of three layers, as shown in Figure 2.3 [Kim *et al.*, 2003]. The ultra-thin top layer is the selective barrier responsible for the separation. This top layer is supported by a microporous sublayer; which is usually an asymmetric ultrafiltration or microfiltration membrane that provides a sufficiently smooth surface to

17

support a defect-free ultrathin top layer. This is further supported by a non-woven reinforcing fabric that provides additional mechanical strength to the composite structure while offering little resistance to mass transport through the membrane. Several techniques can be used to form the top layer of TFC, including (1) solution casting, (2) in situ graft polymerization and (3) interfacial polymerization.
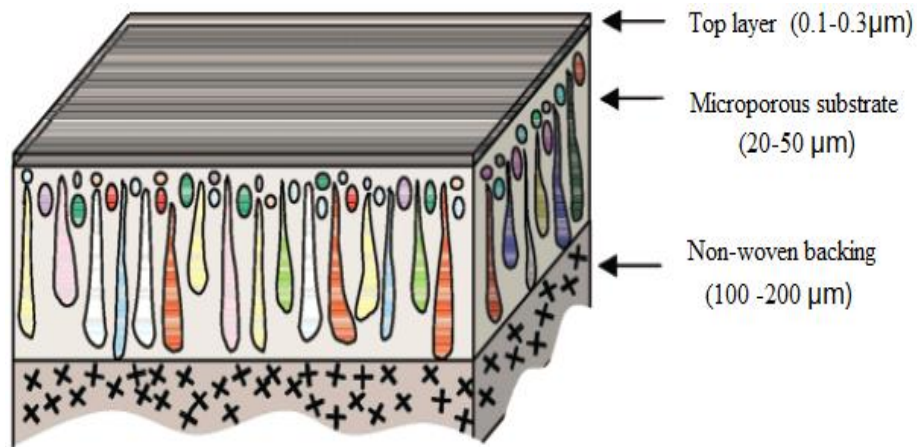
Figure 2.3 Schematic of a thin film composite membrane [Kim et al., 2003].

2.3.1 Thin film composite membranes for nanofiltration

Solution casting is a simple membrane formation method widely used in lab research and commercial production. Self-polymerized polydopamine with strong adhesion characteristics was coated on polysulfone ultrafiltration substrate to fabricate the hydrophilic nanofiltration membranes [Li *et al.*, 2012]. Poly(vinylalcohol) (PVA) [Jahanshahi *et al.*, 2010] and PVA/TiO$_2$ [Pourjafar *et al.*, 2012] were introduced on top by dip coating and then cross-linking with glutaraldehyde. Sulfonated poly(ether ether ketone) (SPEEK) based composite membranes were prepared by spin-coating [Dalwani *et al.*, 2011]. The strong chelating agent diethylene

triamine pentaacetic acid (DTPA) was spray-coated on polyethersulfone (PES) substrate by Boricha and Murthy [2009] to form a TFC NF membrane.

In situ graft polymerization is another method to obtain tailor-made membranes with specific properties by introducing specific monomers. The support membrane is exposed to an irradiation source in the presence of a monomer in the vapor or solution state. The irradiation source may be any sources commonly used in chemistry, including low temperature plasma, UV irradiation or electron-beam. Acrylic acid [Zhao *et al.*, 2004], styrene [Zhao *et al.*, 2005a; Chen *et al.*, 2007] and N-vinylpyrrolidone [Zhao *et al.*, 2005b] have been used for graft polymerization onto polyacrylonitrile (PAN) ultrafiltration membrane by low temperature plasma to form nanofiltration membranes. Single monomer acrylic acid (AA) [Qiu *et al.*, 2005] and co-monomer AA and sodium allyl sulfonate (SAS) [Qiu *et al.*, 2007] were also used for UV-induced graft polymerization on the surface of a polyetherketone (PEK) UF membrane. Sodium p-styrene sulfonate (NaSS) and (2-(acryloyloxy) ethyl)-trimethyl ammonium chloride (AC) were used to prepare nanofiltration membranes on a polysulfone substrate by UV-photografting [Akbari *et al.*, 2006]. Nylon-66, a typical semicrystalline polymer, was cross-linked through electron beam irradiation to form nanofiltration membranes by Linggawati *et al.* [2009, 2012].

Although many routes are feasible to make thin film composite nanofiltration membranes, interfacial polymerization is still of particular interest from an industrial fabrication point of view. In the early development of composite membranes, Mogan was probably the first to propose the use of interfacial polycondensation to form a thin polymeric layer onto a substrate [Morgan, 1965]. This approach, however, did not work well for industrial fabrication until Cadotte and co-workers optimized the membrane formation conditions that led to successful

development of a series of composite membranes with high fluxes by interfacial cross-linking of piperazine with trimesoyl chloride/isophthaloyl chloride mixtures [Cadotte *et al.*, 1976, 1978].

Depending on the monomers used in the interfacial polymerization, the selective layer of thin film composite membranes can be a polyamide (formed through amine and acyl chloride), a polyurea (formed by amine and cyanogen) or a polyester (prepared from alcohol/phenol and acyl chloride).

Polyamide TFC membranes

Polyamide (PA) is the most popular top layer for thin film composite membranes. The commonly used reactive monomers are aliphatic/aromatic diamines (e.g., piperazine (PIP) [Cadotte *et al.*, 1976], m-phenylenediamine (MPD) [Cadotte, 1981a] and p-phenylenediamine (PPD) [Song *et al.*, 2005]) and acid chloride monomers (e.g., trimesoyl chloride (TMC) [Cadotte *et al.*, 1976, 1978; Cadotte, 1981a] and isophthaloyl chloride (IPC) [Cadotte *et al.*, 1976]). Figure 2.4 shows the chemistry involved in preparing MPD/TMC denser layer via interfacial polymerization. Tables 2.1 and 2.2 show the chemical structures of the amine/alcohol/phenol and acyl chloride/cyanogen monomers used respectively in the formation of thin film composite membranes. Among these materials, MPD and TMC are most commonly used [Kang and Cao, 2012; Lau *et al.*, 2012].

There have been efforts to search for new monomers to improve membrane performance. In view of the importance of hydrophilicity of the TFC membrane on its performance, a novel amine monomer, 3,5-diamino-N-(4-aminophenyl) benzamide (DABA) with three amino groups, was synthesized and used together with diamine (MPD) in TFC membrane preparation [Wang *et al.*, 2010]. With an increase in the DABA content in the aqueous phase from 0 to 0.25%

(w/v), the membranes showed an increase in water flux from 37.5 to 55.4 L/(m^2 h) while maintaining a high salt rejection (about 98%) for a solution containing 2,000 ppm NaCl at 2 MPa. It was revealed that the top membrane surface became more hydrophilic, smoother and thinner as the DABA concentration was increased in the amine solution.

Chen *et al.* [2008] incorporated a water soluble amine sulfonated cardo poly(arylene ether sulfone) (SPES-NH$_2$) with MPD as the aqueous reactant. Under the optimum preparation conditions, the TFC membranes prepared from the amine solution containing SPES-NH$_2$ showed a remarkable increase in water permeability (51.2 L/(m^2 h)) and a slightly decrease in salt rejection (97.5% at 2,000 ppm NaCl, 2 MPa) as compared to membranes prepared from an amine solution without SPES-NH$_2$ (37.4 L/(m^2 h) and 99%). The improved permeation flux was attributed to the increased hydrophilicity derived from SPES-NH$_2$ and the high salt rejection was due to the chain stiffness of the copolymer and high degree of cross-linking.
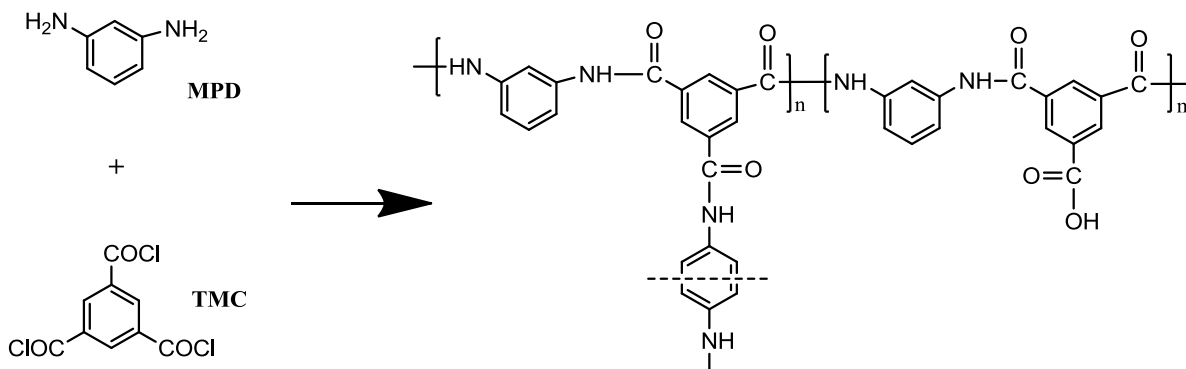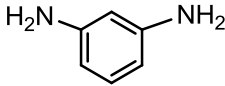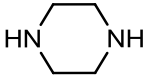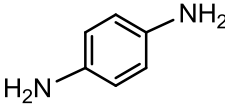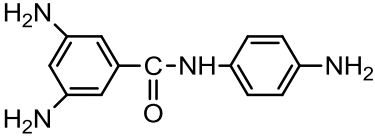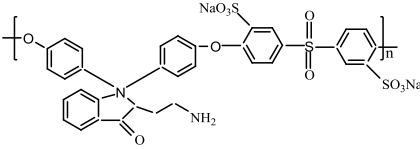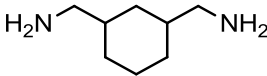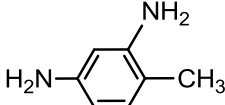
Figure 2.4 Polyamide barrier layer derived from MPD and TMC via interfacial polymerization.

21

Table 2.1 Amine/alcohol/phenol monomers for TFC membrane preparation

Amine monomer (abbreviation)	Chemical structure	Reference
m-Phenylenediamine (MPD)		[Cadotte, 1981a]
Piperazine (PIP)		[Cadotte *et al.*, 1976]
p-Phenylenediamine (PPD)		[Song *et al.*, 2005]
3,5-Diamino-N-(4-aminophenyl) benzamide (DABA)		[Wang *et al.*, 2010]
Sulfonated cardo poly(arylene ether sulfone) (SPES-NH$_2$)		[Chen *et al.*, 2008]
1,3-Cyclohexanebis (methylamine) (CHMA)		[Buch *et al.*, 2008]
m-Phenylenediamine-4-methyl (MMPD)		[Yu *et al.*, 2009b]

(Continued on next page)

22

(Table2.1 Continued)

Hexafluoroalcohol-m-phenylenediamine (HFA-MPD)		[La *et al.*, 2010]
Polyethylenimine (PEI)		[Cadotte and Roxelle, 1972; Cadotte, 1977; Rozelle *et al.*, 1977]
m-Aminophenol (MAP)		[Mudahar, 1998; Jayarani and Kulkarni, 2000; Jayarani *et al.*, 2000]
Hydroquinone (HQ)		[Mudahar, 1998; Jayarani and Kulkarni, 2000; Jayarani *et al.*, 2000]
Bisphenol A (BPA)		[Seman *et al.*, 2010, 2011]
4,4'-Dihydroxybiphenyl (DHB)		[Kim *et al.*, 1997]
Triethanolamine (TEOA)		[Tang *et al.*, 2008, 2010]
Methyl-diethanolamine (MDEOA)		[Tang *et al.*, 2010]
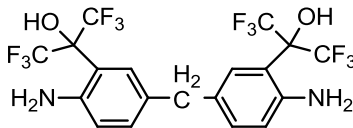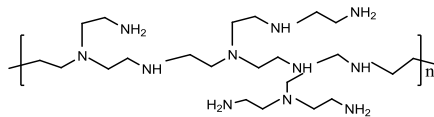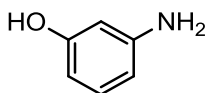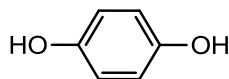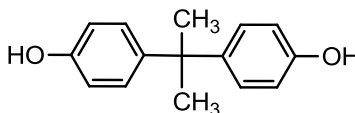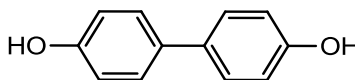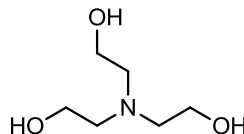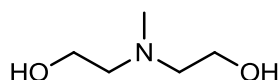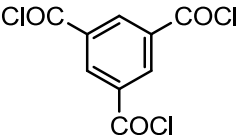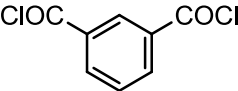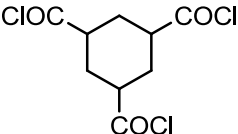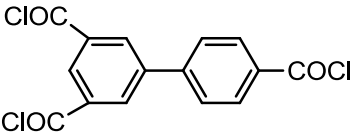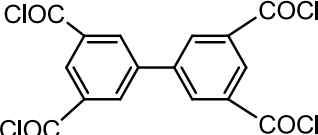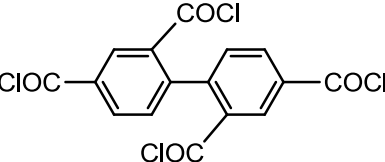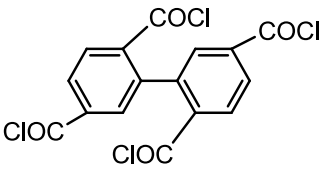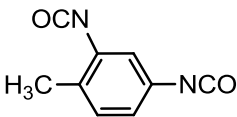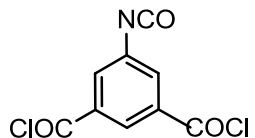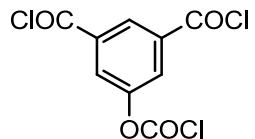
Table 2.2 Acyl chloride/cyanogen monomers for TFC membrane preparation

Acyl chloride monomer (abbreviation)	Chemical structure	Reference
Trimesoyl chloride (TMC)		[Cadotte *et al.*, 1976, 1978; Cadotte, 1981a]
Isophthaloyl chloride (IPC)		[Cadotte *et al.*, 1976]
1,3,5-Cyclohexane-tricarbonyl chloride (HTC)		[Yu *et al.*, 2009b]
3,4',5-Biphenyl triacyl chloride (BTRC)		[Li *et al.*, 2007]
mm-Biphenyl tetraacyl chloride (mm-BTEC)		[Li *et al.*, 2007, 2008]
om-Biphenyl tetraacyl chloride (om-BTEC)		[Li *et al.*, 2008]

(Continued on next page)

(Table2.2 Continued)

op-Biphenyl tetraacyl chloride (op-BTEC)	*COCl COCl ClOC ClOC* (structure)	[Li *et al.*, 2008]
Toluene diisocyanate (TDI)	*OCN H₃C—NCO* (structure)	[Cadotte and Roxelle, 1972; Cadotte, 1977; Rozelle *et al.*, 1977]
5-Isocyanato-isophthaloyl chloride (ICIC)	*NCO ClOC COCl* (structure)	[Liu *et al.*, 2006a, 2006b, 2008a, 2009]
5-Chloroformyloxy-isophthaloyl chloride (CFIC)	*ClOC COCl OCOCl* (structure)	[Arthur and Wilmington, 1992; Zhou *et al.*, 2005; Liu *et al.*, 2008b, 2009; Yu *et al.*, 2009a]

A major limitation of the commercial polyamide membranes is membrane degradation by chlorine, a common disinfectant used in water and wastewater treatment. In order to overcome this problem, Buch *et al.* [2008] attempted to develop chlorine-resistant NF membranes by interfacial polymerization of 1,3-cyclohexanebis (methylamine) (CHMA) in water with TMC in hexane. The composite membranes with aromatic-cycloaliphatic PA top layers were then exposed to NaClO-NaCl mixed solution of various NaClO concentrations to test the impact of chlorine on membrane properties. Unfortunately, the composite membrane failed to retain its performance as both water flux and salt rejection decreased considerably upon exposure to chlorine at 1 ppm for 24 h. Compared to the CHMA/TMC membrane, aromatic-cycloaliphatic PA membranes prepared from m-phenylenediamine-4-methyl (MMPD) and cyclohexane-1,3,5-tricarbonyl chloride (HTC) showed better a chlorine resistance at more than 3000 ppm.h Cl [Yu

et al., 2009b]. More recently, a new polyamide TFC membrane with a high chlorine resistance was prepared via interfacial polymerization using high molecular weight hexafluoroalcohol (HFA)-substituted aromatic diamine and TMC [La *et al.*, 2010]. As HFA is an electron withdrawing group and sterically bulky, both the electronic and steric aspects favor the protection of the amide linkages and benzene rings against chlorine attack. An examination with NMR spectroscopy showed that the HFA-PA composite membrane suffered only minor changes in its spectrum after 17 h of exposure at 500 ppm hypochlorous acid at pH 5.5. In comparison, the reference PA (MPD/TMC) membrane was severely attacked by chlorine after chlorine treatment, causing an irreversible damage to the membrane structure.

Besides the amine reactants, the structure of acyl chloride also affects the membrane properties. In the recent past, two novel biphenyl acid chlorides, 3,4',5-biphenyl triacyl chloride (BTRC) and 3,3',5,5'-biphenyl tetraacyl chloride (BTEC), with more functional groups were synthesized to prepare TFC membranes [Li *et al.*, 2007]. Due to the higher cross-linking degree and chain stiffness, the salt rejection of the membranes containing biphenyl structures was superior to the traditional commercial MPD/TMC membrane, though its flux was lower. The atomic force microscope (AFM) images showed that the MPD/BTEC membrane exhibited a smoother surface than the MPD/TMC membrane.

A series of isomeric biphenyl tetraacyl chloride (BTEC) were synthesized by Li *et al.* [2008] for formation of TFC membranes with MPD as the amine monomer. The membrane prepared from op-BTEC demonstrated the highest permeability (54.2 L/(m^2 h)), followed by membranes prepared from om-BTEC (50.0 L/(m^2 h)) and mm-BTEC (31.7 L/(m^2 h)) when tested using 2,000 ppm NaCl solution at 2 MPa. The flux enhancement was considered to be due to the rougher surface of op-BTEC membrane which had better contact with water molecules. Very

interestingly, the membrane of op-BTEC did not suffer from a commonly observed "trade-off" between permeability and selectivity as the NaCl rejection remained almost the same (> 97%).

Polyurea/Polyamide-urea/Polyamide-urethane TFC membranes

Polyurea TFC membranes were prepared from PEI and toluene diisocyanate (TDI) [Cadotte and Roxelle, 1972; Cadotte, 1977; Rozelle *et al.*, 1977] in the 1970s. Such membranes exhibited a better than 99% salt rejection and a water flux of 10.6 L/(m^2.h) when tested with 3.5% synthetic seawater at 10.4 MPa gauge.

   Membrane fouling is a common problem in practical applications. In order to improve the anti-fouling performance, polyamide-urea composite membranes were prepared from 5-isocyanato-isophthaloyl chloride (ICIC) and MPD by Liu *et al.* [2006a, 2006b, 2008a]; ICIC is a monomer with trifunctional groups containing both -COCl and -N=C=O. The MPD/ICIC membrane showed a better water flux and salt rejection than the typical commercial MPD/TMC membrane. The antifouling performance of the resultant polyamide-urea MPD/ICIC membrane was tested with lake water and four simulated aqueous solutions. Compared to the MPD/TMC membrane and ESPA membrane (a commercial polyamide RO membrane from Hydranautics Corp.), MPD/ICIC membrane showed better resistance to fouling in all the tests due to its favorable hydrophilicity and smoother surface (the static contact angle was 28.5 °, 44.3 ° and 35.0 °, and the average roughness was 43.89 nm, 54.36 nm and 160.2 nm for MPD/ICIC, MPD/TMC and ESPA membranes, respectively). In addition, a comparison of fouling resistances between polyamide and polyamide-urea membranes also showed that polyamide-urea membranes had better antifouling properties than polyamide membranes [Jenkins and Tanner, 1998]. However, due to the urea bonds (-NHCONH-) and pendant groups (-NHCOOH), it is easier for N-chlorination reaction to take place in the

MPD/ICIC TFC membrane. Thus, this membrane is less tolerant to chlorine than the MPD/TMC TFC membrane [Liu *et al.*, 2009].

Polyamide-urethane formed by reaction of haloformyloxy substituted acyl chloride with an aromatic polyamine is another approach to prepare thin film composite membranes with improved solute rejection [Arthur and Wilmington, 1992]. MPD/CFIC (5-chloroformyloxyisophthaloyl chloride) TFC membrane exhibited a higher flux and rejection than MPD/TMC TFC membrane [Zhou *et al.*, 2005]. The resulting membrane showed a salt rejection of 99.4% and a flux of 34.8 L/(m^2.h) for a feed aqueous solution containing 3.5 wt% NaCl at 5.5 MPa [Liu *et al.*, 2008b]. When subjected a heat treatment (i.e., first heat treated at a relatively low temperature for some time and then heat treated at a high temperature) during membrane formation, the water flux was enhanced to 42 L/(m^2.h) while the salt rejection was essentially the same [Yu *et al.*, 2009a].

Polyester/Polyesteramide TFC membranes

Compared to polyamide thin film composite membranes prepared by interfacial polymerization, little work is done to use a similar technique to prepare other polymeric thin films based on polyester and polyesteramide. Polyesteramide membranes are reported to have a low passage for monovalent salts, and the membranes synthesized from the mixtures of MPD incorporating with either m-aminophenol (MAP), hydroquinone (HQ) or bisphenol A (BPA) and TMC have a high NaCl rejection of 95-98% [Mudahar, 1998; Jayarani and Kulkarni, 2000; Jayarani *et al.*, 2000]. Similarly, the interfacial reaction from the mixture of 4,4'-dihydroxybiphenyl (DHB) and MPD with TMC resulted in a TFC membrane with a NaCl rejection of 96.5% [Kim *et al.*, 1997]. The polyester membranes may also be used for low pressure applications while maintaining a reasonable salt rejection. Mohammad *et al.* [2003] produced a polyester NF

membrane from BPA and TMC with a NaCl rejection of about 48% and a water flux of about 38 L/(m^2.h) at a feed NaCl concentration of 0.01M and an operating pressure of 0.45 MPa. The effect of chemical structure of bisphenol on the water flux and salt rejection was also studied, and the results showed that the methyl substitutions resulted in a higher flux and lower rejection while a reversed trend was observed with the halogen substitutions [Kwak *et al.*, 1997].

In addition, triethanolamine (TEOA), an environmentally friendly and economical monomer, was also utilized to enhance the TFC membrane performance [Tang *et al.*, 2008]. It is of great interest to use TEOA as an active monomer because its tertiary amino groups can be converted into quaternary ammonium groups at certain feed pH. This polyester composite membrane prepared from TEOA and TMC was found to be particularly suitable for treating acidic solutions. At a low feed pH, the amino groups on the membrane surface can change to -R$_3$HN$^+$ and then increase the hydrophilicity of the membrane, resulting in an increased water flux. As an extension of this study, composite membranes were also prepared from methyl-diethanolamine (MDEOA) [Tang *et al.*, 2010]. Membranes with different separation properties were obtained by adding LiBr in the aqueous phase.

It was believed that the incorporation of ester linkages would increase the oxidation resistance of the membrane and thus significantly increase the membrane tolerance to chlorine attack [Mudahar, 1998; Jayarani and Kulkarni, 2000; Jayarani *et al.*, 2000; Razdan and Kulkarni, 2004]. The highly negatively charged and uniform polyester skin layer formed from BPA and TMC is also considered to be helpful for improving fouling resistance to negatively charged humic acid molecules [Seman *et al*., 2010, 2011].

In general, TFC nanofiltration membranes have higher water fluxes and solute rejections, can withstand higher temperatures and larger pH variations, and are more immune to biological attack and compaction. However, these membranes tend to be less chlorine resistant and more susceptible to oxidation. Another important issue affecting the application of TFC membranes is membrane fouling, and efforts are needed to improve their resistance to chlorine and fouling.

2.3.2 Thin film composite membranes for pervaporation

For pervaporation applications, thin film composite membranes also have several advantages over integrally asymmetric membranes, especially the permeation flux. The membrane materials used in pervaporation can be either hydrophilic or hydrophobic depending on the applications. Hydrophobic membranes used for removing volatile organic compounds (VOCs) from water are often polydimethylsiloxane (PDMS) based [Kim *et al.*, 2002; Zhen *et al.*, 2006]. The hydrophilic membranes are used for dehydration of organic solvents, which are the main applications of pervaporation at present. Therefore, hydrophilic composite membranes are further reviewed in the following.

Hydrophilic polymeric TFC membranes

Poly(vinyl alcohol) (PVA), chitosan (CS), poly(acrylic acid) (PAA) and polyelectrolyte are the most widely used and intensively studied materials for fabrication of hydrophilic pervaporation membranes. PVA/PAN and PVA/PES crosslinked composite membranes were used for the dehydration of caprolactam (CPL) [Zhang *et al.*, 2007; Lin *et al.*, 2012] and ethylene glycol [Guo *et al.*, 2008], respectively. CS/poly(tetrafluoroethylene) (PTFE) and CS/PES composite membranes were investigated for the process of isopropanol dehydration [Liu *et al.*, 2007b] and ethanol dehydration [Chen *et al.*, 2009], respectively. The blending of PVA-CS was also applied to form the selective layer of composite membranes for dehydration of ethyl

acetate/water mixtures [Zhu *et al.*, 2010]. PAA can be used to fabricate the skin layer of composite membranes for ethanol dehydration [Choi *et al.*, 1992; Ohyaal *et al.*, 1994] due to its hydrophilictity. This polymer was also widely used as the polyanion to synthesize the polyelectrolytes composite membranes for dehydration of alcohol and diol [Xu *et al.*, 2010; Zhang *et al.*, 2013].

Interfacially polymerized TFC membranes

Interfacial polymerization, which is a commonly used technique for the fabrication of RO and NF membranes, has also been extended to form thin film composite membranes for pervaporation. The studies of interfacially polymerized TFC membranes for pervaporation mainly focused on three aspects: (1) the effects of chemical structure of reactants (especially the amine) on the membrane properties; (2) the effects of conditions of interfacial polymerization on the dehydration performance of the resulting membranes; (3) improving the membrane performance by introducing inorganic components/cross-linker/nano particles.

Four amines with different chemical structures were used to react with TMC on the PAN support membranes for the dehydration of 90 wt% isopropanol solution at 25 °C [Huang *et al.*, 2008]. It was found that the membrane formed from short aliphatic amine ethylenediamine (EDA) had the best pervaporation performance with a permeation rate of 250 g/(m^2.h) and 77 wt% water content in permeate. The membrane formed from aromatic amine MPD had a moderate pervaporation performance with a permeation rate of 180 g/(m^2.h) and 71 wt% water content in permeate. While the membranes formed from long aliphatic amine 1,6-hexanediamine (HDA) and alicyclic amine PIP showed poor pervaporation performance. Similar results were obtained while using the interfacially polymerized TFC membranes for dehydrating 90 wt% tetrahydrofuran at 25 °C [Huang *et al.*, 2014], i.e, the membrane made

from the short aliphatic amine 1,3-diaminopropane (DAPE) showed the highest selectivity (99.9 wt% water in permeate), followed by the membrane formed from the aromatic amine MPD (83.1 wt% water in permeate) while the membrane synthesized from the alicyclic amine 1,3-cyclohexanediamine (CHDA) appeared a relatively low selectivity (69.9 wt% water in permeate).

Optimizing the conditions of interfacial polymerization is another point of interest for TFC membranes. The commonly studied factors are the contact time and concentration of either amine or acyl chloride reactant [Huang *et al.*, 2009], and the annealing temperature and time [Huang *et al*., 2010a, 2010b]. In addition, the coating method was also studied for membrane formation, and the spin-coating is shown to be more favorable than a simple dip-coating for fabricating a dense and thin selective film [An *et al.*, 2012].

Introducing inorganic components, cross-linker or nano particles into the polyamide layer may modify the membrane properties hence enhance the pervaporation performance. Chung's group incorporated inorganic component 3-glycidyloxypropyltrimethoxy-silane (GOTMS) [Zuo *et al.*, 2013] or nonafluorohexylmethyldichloro silane (ClSi) [Zuo and Chung, 2013], or in situ grafted the cross-linker toluene 2,4-diisocyanate (TDI) [Zuo *et al.*, 2014] into the polyamide selective layer during interfacial polymerization to overcome the swelling problem. Moreover, the nano NaX zeolite particles were embedded into the polyamide active layer to improve the dehydration performance [Fathizadeh *et al.*, 2013].

In summary, the specific features of each individual layer in a TFC membrane can be tailored independently to obtain a composite membrane with desirable properties. The top layer of a TFC membrane can be formed independently from a vast variety of chemical materials. The hydrophilicity, permeation flux and membrane stability can be fine-tuned independent of

the substrate. The microporous substrate is generally prepared on top of a nonwoven fabric via the phase inversion technique, and can thus also be tailored separately in order to minimize its resistance to permeate flow while retaining an adequate mechanical stability.

2.4 Interfacial polymerization for preparation of thin film composite membranes

Preparation of TFC membranes is generally based on interfacial polymerization using two monomers: a polyfunctional amine dissolved in water and a polyfunctional acid chloride dissolved in a hydrocarbon solvent. By employing this approach, an ultrathin polymeric layer (300 - 400 nm) can be formed and adhered to a microporous substrate, leading to a good combination of permeability and selectivity. There are many parameters involved in the procedure of interfacial polymerization, including reactant type, reactant concentration, reactant deposition sequence and curing condition. Proper selection and control of these parameters are critical to develop membranes with good separation properties.

2.4.1 Routes of interfacial polymerization

In general, the polymerization is carried out using two reactive monomers dissolved in two immiscible solvents, respectively. The two solvents are in contact only at an interface, and this allows the reaction to take place at the interface. Figure 2.5 illustrates an interfacial polymerization process that consists of a sequence of steps. A microporous support is first impregnated with one of the solvents (usually the aqueous) containing one of the reactants. Then the impregnated support is immersed in the second phase, containing the second reactant. Since the two phases are immiscible, a distinct interface is created between them. Given that the two monomers/reactants are reactive with each other, and due to the limited partition coefficient of reactants in the two opposite phases, a very thin polymer layer is formed at the

interface between the two phases. If the two monomers are highly reactive, the interfacially formed layer is generally dense. The thin and dense film allows for a high flux and high selectivity in membrane applications. After a certain period of reaction time, the two phases are drained and the interfacially formed membrane is then subjected to heat treatment to densify the polymerized layer and/or enhance the adhesion of the ultrathin layer to the surface of the support membrane. Finally, the remaining unreacted monomers are washed away, leaving behind a thin selective film on the support.
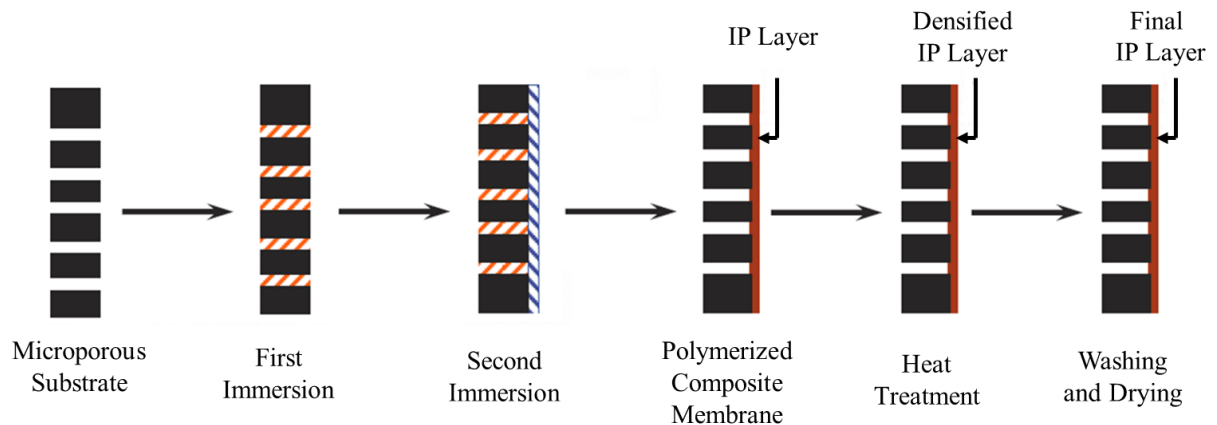
Figure 2.5 Interfacial polymerization process.

2.4.2 Parameters involved in interfacial polymerization

There are several parameters which can be varied during fabrication of TFC membranes via interfacial polymerization. The selection of the two reactants and the polymerization conditions are the key factors in interfacial polymerization. In order to engineer the ultimate membrane morphology and performance, a great deal of research focuses on these parameters related to interfacial polymerization.

Reactant (monomer) type

The selective top layer is formed by the reactants used in interfacial polymerization. Therefore, the structures of the reactants strongly influence the characteristics of the resulting membranes. Membranes made from aromatic diamines generally have denser polymer layers than those from aliphatic diamines, and these membranes thus allow for a higher selectivity at the cost of a lower flux [Petersen, 1993]. Piperazine and its derivatives are shown to be good aliphatic amines to make high performance TFC membranes [Cadotte *et al.*, 1976].

As mentioned before, efforts have been made to explore new amines and acyl chlorides as reactants. Most of these reactants are small molecules with relatively low molecular weights. However, the behavior of polymeric amines for use as aqueous reactants is expected to be very different. Based on the commonly accepted view of interfacial polymerization described by Morgan [1965], interfacial polymerization actually occurs in the organic phase rather than in aqueous phase. Because the partition of acyl chloride in the aqueous phase is highly unfavorable, the amine must diffuse into the organic phase to contact acyl chloride to induce interfacial polymerization. However, if the aqueous reactant is a polymeric amine, there is an evidence [Cadotte *et al.*, 1974] that the reaction may take place in the aqueous phase rather than in the organic phase because of the unfavorable partition of bulky polymeric amine in the organic phase. In addition, the macromolecular structures of polymeric amines offer other advantages. On the one hand, a large number of amine groups provide abundant reactive sites for interfacial polymerization. On the other hand, the macromolecules do not block the pores of the substrates. The modest reactivity of polymers makes the reactions more controllable. All these suggest that polymeric amines may be promising reactants for interfacial polymerization to form thin film composite membranes with both a high flux and rejection.

Polyethylenimine (PEI) is a favorable polymeric amine for use in interfacial polymerization. It has been used to react with toluene diisocyanate (TDI) [Cadotte and Roxelle, 1972; Cadotte, 1977; Rozelle *et al.*, 1977] to form polyurea TFC membranes with a high rejection. This is a milestone in the development of interfacially formed thin film composite membranes. Cadotte *et al.* [1981] compared the morphology of a PEI/IPC membrane with that of a PIP/IPC membrane using a scanning electron microscopy, and observed that the PEI/IPC membrane was fairly smooth with some occasional longitudinal ridges, while the PIP/IPC membrane had a very rugged surface topography. In addition, the composite membrane produced by polymeric amines may have three layers: a barrier layer of dense polyamide, an intermediate layer formed by the insolubilization of unreacted PEI, and the substrate. However, the PIP/IPC membrane does not appear to have a clear intermediate layer. The intermediate zone is likely to decrease the potential effects of discontinuities or defects of the substrate on the salt rejection of the resulting membrane. Bartels *et al.* [1987] also showed the differences between the packing of nodules formed by monomeric amine and polymeric amine: nodules in the top-most layer formed by diethylene triamine (DETA) and TDI were very closely packed, with a pore size of roughly 50 Å, whereas the nodules of PEI/TDI membrane were much looser, having a pore size on the order of 50-500 Å. Moreover, the latter membranes were thicker (3000 Å) than DETA/TDI membranes (300 Å) at similar reaction conditions.

Subsequent research work further confirmed that PEI/TMC membranes had lager pore sizes and thicker top layers than DETA/TMC membranes [Yang, 2008; Chiang, 2009]. It was found that PEI/terephthaloyl chloride (TPC) membrane had both a higher permeation flux and salt rejection than ethylenediamine (EDA)/TMC membrane, although these two membranes had similar pore sizes. The PEI/TMC membrane is reported to have a pore size of 1.5 nm but has a

higher NaCl rejection than the EDA/TMC membrane with a smaller pore size of 0.43 nm [Chiang *et al.*, 2009]. This intriguing characteristic was believed to derive from the hyperbranched structure of PEI, which allows some of the charged amine groups to drift inside the pores and interacting with the ions in the pathway. The drifting amines increased salt rejection but had little effect on water permeation.

Moreover, as mentioned in Chapter 1, PEI has been employed as a reactant to fabricate hollow fiber TFC by interfacial polymerization for removal of organic matters from water [Sun *et al.*, 2012], and dehydration of isopropanol [Zuo *et al.*, 2012]. It was also used for preparation of solvent-resistant TFC ultrafiltration [Korikov *et al.*, 2006] and nanofiltration membranes [Kosaraju and Sirkar, 2008].

Another polymeric amine, polyvinylamine (PVAm), has also attracted interest. PVAm/IPC [Yu *et al.*, 2011] and PVAm/TMC [Liu *et al.*, 2012a] membranes were prepared via interfacial polymerization, and both membranes have amphoteric surfaces with an isoelectric point (IEP) between pH 6.5-7.0. The membrane surface is relatively smooth. The root mean square roughness of PVAm/IPC membrane is 3.9 nm and that of PVAm/TMC is 4.5 nm. These values are much lower than the reported roughness (more than 30 nm) for most polyamide membranes. Besides PVAm, poly(amidoamine) (PAMAM) dendrimer [Willem *et al.*, 1997; Li *et al.*, 2006] is another potentially useful material for interfacial polymerization. The polymeric amine based thin film composite membranes are of positively charged due to the amine groups, and they are expected to perform well for treating acidic feed solutions.

Steps involved in interfacial polymerization

Conventionally, interfacial polymerization is conducted by immersing a substrate membrane in an aqueous solution followed by contact with an organic solution which is immiscible with the

first aqueous solution. Several variants are available to carry out the interfacial polymerization and to improve the membrane formation.

The first method is to change the dipping sequence. That is, the support membrane is soaked in the organic phase first, following by soaking in the aqueous phase. This method is suitable for hydrophobic substrate because of its better contact with organic solutions of acyl chloride than with aqueous solutions of amine, leading to a stable and well-distributed polyamide layer. This "reverse" steps in the interfacial polymerization procedure were used on a hydrophobic electrospun poly(vinylidene fluoride) (PVDF) nanofibrous substrate membrane [Kaur *et al.*, 2012]. The polyamide film can be formed on the PVDF substrate by interfacial polymerization with conventional dipping steps (i.e., aqueous-organic), but the TFC membrane has little salt rejection. This is probably caused by the hydrophobic nature of PVDF substrate on which the aqueous monomer cannot spread out uniformly on its surface. There were pin holes or defects on the membrane surface, and the membrane is unsuitable for filtration applications. However, when the substrate was allowed to contact the organic phase reactant first, the film showed a rejection of 80.7% for 2000 ppm $MgSO_4$ and 67.0% for 2000 ppm NaCl at a pressure of 0.48 MPa gauge, with a flux of about 0.51 and 0.52 $L/(m^2.h)$. Similar approach was also applied for making hydrophilic solvent-stable TFC ultrafiltration membranes on a hydrophobic support layers [Korikov *et al.*, 2006]. This reverse dipping sequence is also suitable to introduce a hydrophilic polyamide layer on the hydrophobic microfiltration substrates in order to increase the stabilities of supported liquid membranes [Kemperman *et al.*, 1997, 1998].

Another variant procedure is to add a dipping step before or after the conventional two-step process. The incorporation of multiwall carbon nanotubes (MWNTs) into a thin film layer has been explored to produce hydrophilic membranes for fast water transport. An improved

interfacial polymerization process was adopted by immersing the support membrane into an organic phase prior to the conventional interfacial polymerization process in the preparation of these MWNTs incorporated TFC membranes [Wu *et al.*, 2010b]. It was observed that the MWNTs were well embedded throughout the selective layer and the resulting thin film nanocomposite membrane showed an increased permeability and selectivity (4.5 L/(m^2 h) at 0.6 MPa, 78% at 5 mmol/L Na$_2$SO$_4$) when compared with membranes prepared by conventional interfacial polymerization (2.6 L/(m^2 h), 74%) without the prior immersion in organic solvent.

The method of adding one more step of amine immersion after the conventional interfacial polymerization process was used to prepare polyamide/PVDF hollow fiber composite nanofiltration membranes [Liu *et al.*, 2007a]. After the conventional interfacial polymerization process, the membrane was submerged again in an aqueous solution containing piperazine and triethylamine (TEA) for a very short period of time. Piperazine was one of the reactants, and TEA was used for neutralizing the hydrochloric acid produced by the interfacial polymerization reaction. Such a post treatment was shown to lower water flux but enhance salt rejection. It was reported that the membranes synthesized from this approach had a smoother surface since the amine introduced in the second time would react with the unreacted acyl chloride groups on the surface [Zou *et al.*, 2010]. The resultant membrane surface showed fewer 'leaf-like'' folds that are the typical structures of polyamide composite membranes prepared by the traditional interfacial polymerization process. Furthermore, the presence of amino groups (-NH$_2$) on surface would help to improve the antifouling properties of the membranes.

Reactant concentration

The reactant concentration, either in the aqueous or organic phase, is an important parameter for interfacial polymerization. In general, the effects of reactant concentration on the salt separation and water flux may be explained in terms of the effective thickness and morphology of the membrane. The polymerization will proceed slowly at a low concentration of the reactants. This results in the formation of a "thin and loose" skin layer with a low salt rejection and a high water flux. With an increase in the concentration of the reactants, the rate of the polymerization increases, leading to the formation of a skin layer with a thick and compact structure. As a consequence, the salt rejection increases, whereas the water flux decreases. When the reactant concentration is sufficiently high, a further increase in reactant concentration will decrease water flux, but the salt rejection will level off. This suggests that there is an optimum concentration of reactants. This observation can be confirmed by experimental results reported in literatures [Tang *et al.*, 2008; Liu *et al.*, 2008b; Li *et al.*, 2009b; Kaur *et al.*, 2012].

However, there are some exceptions under certain circumstances. When the aqueous reactants are polymeric amines, both water flux and salt rejection are higher at a higher concentration of polyamines [Li *et al.*, 2006; Yu *et al.*, 2011]. With an increased amine concentration, the rate of polymerization speeds up. However, the formed selective skin layer will act as a barrier to the diffusion of acyl chloride from the organic phase into the aqueous phase, resulting in a thinner barrier layer with lower resistance to water permeation. On the other hand, there will be more unreacted amino groups on the skin layer of the membrane formed at a higher concentration of polymeric amine, which can improve the hydrophilicity of the resulting membrane. This is another reason for the relatively high permeability. In the presence of water, the amine functional groups will be changed to $-RH_3N^+$ [Naylor, 1996]. As the number of $-RH_3N^+$ groups on the membrane surface increases, the electrostatic repulsion

between the membrane surface and cations in the feed will be intensified, resulting in an increase in salt rejection.

Besides the reactant concentration, the molar ratio of amine/acyl chloride also has a significant effect on the permeation flux [Xie *et al.*, 2012]. Generally, interfacial polymerization can be considered to involve two stages: an initial fast stage for contact between both monomers at the oil-water interface, followed by a slow growth stage that is controlled by the monomer diffusion [Chai and Krantz, 1994; Freger, 2003]. The initial stage forms a dense core barrier layer that is significantly thinner than the extended loose layer formed later [Freger, 2005]. At a high molar ratio of amine/acyl chloride, the larger driving force for amine diffusion into the organic phase results in a thicker barrier layer, causing a lower permeate flux. When the molar ratio of amine/acyl chloride decreases, the membrane becomes thinner and the flux tends to increase. However, compared to membranes prepared using higher amine/acid chloride molar ratios, the polyamide layer also becomes dense when the molar ratio of amine/acyl chloride tends to be close to unity [Berezkin and Khokhlov, 2006]. Thus, the molar ratios of amine/acyl chloride should be optimized in order to maximize the permeate flux.

Post treatment

Heat treatment is often used to facilitate the removal of residual organic solvent from nascent skin layer and to promote additional cross-linking by dehydration of unreacted amine and carboxyl groups. Heat treatment conditions (temperature and time) have a considerable influence on the membrane performance.

There have been some studies to indicate that the flux decreases and the rejection increases after proper heat treatment [Rao *et al.*, 1997; Zhang *et al.*, 2012], during which process residual solvent in the membrane is evaporated. In the meantime, the unreacted monomers have a

chance to come into contact with each other, and the additional reaction results in an increase in the thickness or density of the selective layer. However, the permeation flux and the salt rejection can both increase after heat treatment due to the loss of residual solvent in the film and additional cross-linking of the selective skin layer, respectively [Liu *et al.*, 2008b].

Controlling the degree of cross-linking is important when heat treatment is used to enhance the membrane properties. To achieve this, a two-stage heat treatment process may be used. For instance, when the membrane was first heat treated at a relatively low temperature for a given period of time before the temperature was increased to a higher level for further heat treatment, membrane performance was enhanced effectively [Yu *et al.*, 2009a]. The water flux of the TFC membrane increased from 34.8 to 42.5 $L/(m^2.h)$, while the salt rejection remained at a value larger than 99%. The results indicate that cross-linking is necessary but should be managed to a certain degree in order to achieve an active layer with a high permeability and selectivity.

Chapter 3.

Thin film composite NF membranes formed by interfacial polymerization from PEI and TMC[*]

3.1 Introduction

Given the importance of safe potable water, many technologies have been developed for removing salt from seawater and brackish water. Membrane technologies have been progressing rapidly because of their numerous advantages (e.g., energy saving, environmentally benign, and easy operation). In addition, the process design is flexible, and there is no complex instrumentation needed. Compared to reverse osmosis, nanofiltration generally has a higher flux and a relatively lower capital and operating costs while maintaining a high retention to multivalent ionic salts and organic molecules with molecular weights above 300. Therefore, NF is considered to be a favorable process for salt separation especially when complete removal is not needed.

   The aforementioned work in Chapter 2 reveals that TFC membranes prepared from PEI have unique characteristics that are derived from the macromolecular structure of the PEI. The lower reactivity between the macromolecules and acyl chlorides makes the interfacial reaction relatively slow and more controllable than the fast reactions between small molecular amines and acyl chlorides. It may be pointed out that almost all the TFC composite membranes based on PEI reported in the literature are composed of one selective layer (polyamide or polyurea

---

[*] Portions of this work have been published in *J. Membr. Sci.*, 472 (2014) 141-153.

layer) formed in a single step of interfacial reaction on the top of a substrate. In addition, the conventional interfacial polymerization is often accomplished by immersing a substrate membrane in one reactant solution (i.e., aqueous) followed by surface contact with the other reactant solution (i.e., organic) which is immiscible with the first reactant. In this chapter, we present a different approach based on sequential interfacial reactions for layer-by-layer assembly. This allows for better control and tailoring of the active layer of the TFC membranes to meet various application requirements. For instance, by varying the reaction conditions (e.g., reactant concentrations and reaction time in each reaction step as well as the number of sequential reactions), membranes with loose, dense or gradient layer-by-layer structures in the active layers can be produced for different applications. To demonstrate the concept, PEI and TMC were used as the aqueous phase and organic phase reactants, respectively, in this chapter to produce nanofiltration membranes. The effects of the reactant concentration, the sequence of reactant deposition on the membrane surface, the number of sequential interfacial reactions, and heat treatment on the membrane performance were investigated to provide an insight into the membrane formation by layer-by-layer interfacial polymerization. The chemical composition, surface hydrophilicity, morphology, roughness and charge property of the polyamide selective layer were characterized by ATR-FTIR, contact angle measurements, FE-SEM, AFM and streaming Zeta potential. Meanwhile, the influences of feed concentration and operating pressure were also investigated. The separation performance of the membranes was evaluated using four representative salt solutions (i.e., $MgCl_2$, $MgSO_4$, Na_2SO_4 and NaCl).

3.2 Experimental

3.2.1 Materials

Microporous flat-sheet polyethersulfone (PES) membrane (supplied by Sepro Membranes) with

a molecular weight cut-off of 10,000 was used as the substrate. The substrate membrane had a water permeability of approximately 90 L/(m^2.h.bar). Branched polyethylenimine (PEI) with a number-average molecular weight of 10,000 and a weight-average molecular weight of 25,000 was purchased from Sigma-Aldrich. Trimesoyl chloride (TMC) was purchased from Alfa Aesar, and sodium dodecyl sulfate (SDS) was purchased from Matheson Coleman & Bell Chemical. Hexane was purchased from Caledon Laboratories. MgCl$_2$ (J.T Baker Chemical Company), MgSO$_4$ (BDH Chemicals Ltd), Na$_2$SO$_4$ (McArthur Chemical Co.) and NaCl (EMD Chemical, Inc) were used to characterize the salt rejection of the TFC membranes. All these chemicals were of reagent grades.

3.2.2 Membrane preparation

The aqueous phase reactant solution was prepared by dissolving a pre-determined amount of PEI in de-ionized water to form a homogeneous solution, and then sodium dodecyl sulfate (SDS) was added as a surfactant. The organic phase reactant solution was obtained by dissolving TMC in hexane. Unless specified otherwise, the concentrations of PEI, SDS and TMC in the solutions were 2.0 wt%, 0.1 wt% and 0.4 wt%, respectively. The pH of aqueous phase solution was about 9.5. The PES substrate membrane used for interfacial polymerization was pre-soaked in de-ionized water overnight and washed thoroughly with de-ionized water to remove all preservatives in the membranes.

Preparation of TFC membranes with one polyamide layer

The water wet PES substrate was dried in air and then mounted in a cap device with the active PES surface side up and the nonwoven fabric side down. The aqueous solution of PEI was poured into the cap device to contact with the surface of the PES substrate for 3 h. The excess aqueous solution was removed by vertically positioning the membrane in the cap device for

about 2 h. Then the TMC solution was charged into the cap device to contact with the PEI-loaded PES substrate for 30 min during which period interfacial polymerization took place on the substrate surface. After the excess organic solution of TMC was removed from the membrane surface, the membrane was placed in an oven at 95 ℃ with forced air circulation for 20 min. Finally, the resulting membrane was washed and rinsed thoroughly with de-ionized water before being tested for nanofiltration of the salt solutions. The adsorption of PEI on the membrane surface was shown to have reached equilibrium well within 3 h [Xu *et al.*, 2010]. Thus a contact time of 3 h between PEI and the PES substrate was used in this study, and no additional PEI deposition would occur if the membrane was in contact with the PEI solution for a longer period of time.

As both water and hexane could wet the PES substrate, the interfacial polymerization was also carried out with a reversed sequence of reactant depositions onto the substrate to determine if this would improve the membrane performance in view that TMC molecules have a greater mobility than PEI macromolecules. This was done as follows. After air drying, the PES substrate membrane was first wetted with the organic solution of TMC dissolved in hexane for 3 h, and then the excess solution was removed from the surface of the PES substrate. After evaporation of hexane solvent in air for 30 min, the substrate was allowed to contact the PEI reactant in aqueous phase for 30 min. Finally, the membrane was subjected to the same heat treatment and rinse steps as mentioned above.

Preparation of TFC membranes with multiple polyamide layers

In order to improve the salt rejection of the membrane, the interfacial polymerization was repeated to build up a layer-by-layer structure, i.e., membranes with multiple layers formed by interfacial polymerization sequentially, one layer at a time. For convenience of discussion, the

membrane is considered to have one deposition layer after the deposition of the first reactant solution. After deposition of the second reactant phase, the membrane is considered to have two depositions of the reactants, thereby forming one interfacially polymerized layer. These steps can be repeated to form membranes with multiple interfacially polymerized layers. The process of synthesizing the thin film composite membranes with multiple polyamide layers by sequential interfacial polymerizations is shown in Figure 3.1. It may be mentioned that there was no water rinsing or other treatment between cycles of interfacial polymerization so that the unreacted acyl chloride groups would react with the PEI deposited subsequently, thereby creating a stable anchor to the PEI macromolecules on the membrane surface. In consideration of the mass transfer resistance of multiple interfacially-polymerized layers, the concentrations of PEI and TMC solutions used were 1.0 wt% and 0.2 wt%, respectively.

Throughout the multiple cycles of alternate deposition of aqueous and organic reactants during membranes preparation, the reactant deposition time for the first layer was kept at 3 h, and the drying time was 2 h for the aqueous solution and 30 min for the organic solution. The contact time between the two reactants (that is, the reaction time for the interfacial polymerization) was kept at 30 min. Finally, the membrane was thermally treated at 95 ℃ for 20 min before rinsing with de-ionized water, unless specified otherwise.

Depending on the sequence of reactant depositions and the number of interfacially polymerized layers formed in the composite membranes, membrane designations shown in Table 3.1 were used in this study. For instance, membrane (PEI/TMC)$_n$ represents a thin film composite membrane comprising of a PES substrate and n interfacially polymerized layers formed by sequential deposition of the aqueous PEI solution and the organic TMC solution,

47

and (PEI/TMC)$_n$-PEI represents a (PEI/TMC)$_n$ membrane with an additional surface deposition

of PEI.
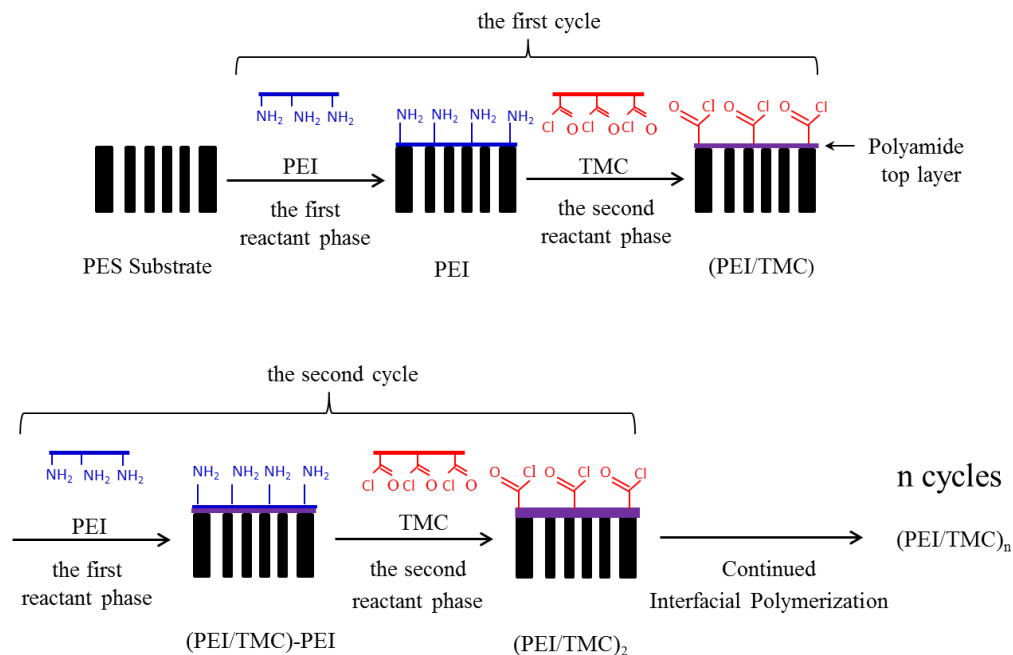
Figure 3.1 Illustration of thin film composite membrane preparation procedure with multiple cycles of reactant deposition and interfacial polymerization.

3.2.3 Membrane characterization

The membrane surface was examined using an attenuated total reflectance Fourier transform

infrared spectroscopy (ATR-FTIR) (Nicolet Aratar 370 FTIR spectrometer). For ATR-FTIR

analysis of the membrane samples, ZnSe crystal at a 45° angle of incidence was used. The

resolution of the apparatus was 4 cm^{-1}, and a total of 32 scans were recorded during the IR test

for each sample.

Table 3.1 Designation of membranes based on number and sequence of reactant depositions[*]

No. of reactant depositions	Membrane designation	Description
1	PEI	PES substrate with a surface deposition of PEI
	TMC	PES substrate with a surface deposition of TMC
2	(PEI/TMC)	Thin film composite membrane formed by interfacial polymerization of surface deposited PEI with TMC solution
	(TMC/PEI)	Thin film composite membrane formed by interfacial polymerization of surface deposited TMC with PEI solution
2n	(PEI/TMC)$_n$	Thin film composite membrane comprising of n interfacially polymerized layers from reaction of surface deposited PEI with TMC solution
	(TMC/PEI)$_n$	Thin film composite membrane comprising of n interfacially polymerized layers from reaction of surface deposited TMC with PEI solution
2n+1	(PEI/TMC)$_n$-PEI	Membrane (PEI/TMC)$_n$ deposited with PEI
	(TMC/PEI)$_n$-TMC	Membrane (TMC/PEI)$_n$ deposited with TMC

[*] n is an integer

The surface hydrophilicity of the membrane was measured using a contact angle meter (Cam-plus Micro, Tantec Inc.). The membrane samples were air dried at ambient temperature prior to the contact angle measurements. The drop size (3 μl) of de-ionized water was controlled by the microsyringe. For each contact angle measurement, at least six readings from different surface locations were taken, and the contact angles reported here are the average values. We have a 98% confidence that the variation was shown to be within 10%.

The surface charge property of the thin film composite membranes was studied with streaming potential measurements using an Anton Paar Zeta potential analysis meter (Austria). A KCl solution (0.001 M, pH = 2-11) was circulated through the measuring cell containing the

membrane sample at 25 ℃. The results presented are the average values based on at least three repeated measurements.

The cross-sectional and surface morphologies of the thin film composite membranes were investigated using a field emission scanning electron microscopy (FE-SEM) (Hitachi S-4800, Japan). For cross-sectional samples, the non-woven fabric was first detached from the composite membrane, and then the top layer (i.e., polyamide supported by PES) was fractured by a sharp scalpel. Gold sputter coating is necessary for our non-conductive membrane samples. The surface roughness of the membranes was examined under atomic force microscopy (AFM) (Park Scientific Instrument Autoprobe CT) in tapping mode. For each membrane sample, a scan area of 4 μm × 4 μm was used, and the surface roughness of the membranes was evaluated in terms of the root mean square roughness (RMS).

3.2.4 Separation performance measurements

The separation performance of the membrane was evaluated in terms of water flux and salt rejection using a laboratory-scale dead-end stirred test unit, which is shown in Figure 3.2 in a cross-sectional view. The membrane was mounted in a stainless steel test cell with an effective permeation area of 12.56 cm^2. The feed tank was 250 mL, and the feed solution was rigorously agitated using a magnetic stirrer. For every test, we adjusted the scale button at the same position to keep a similar stirring rate. The transmembrane pressure for permeation was provided by a pressurized nitrogen gas.

Prior to a permeation test, the membrane was conditioned under pressure with de-ionized water at 1.0 MPa gauge for 1 h. After that, the permeation flux of pure water was determined, followed by filtration experiments with salt solutions of $MgCl_2$, $MgSO_4$, Na_2SO_4 or NaCl at a feed concentration of 500ppm. The permeation flux (J) and salt rejection (r) were determined as:

$$J = \frac{Q}{S\Delta t} \tag{3.1}$$

$$r = \left(1 - \frac{C_{sl}}{C_{s0}}\right) \times 100\% \tag{3.2}$$

where Q is the quantity of permeate (L) collected over a time interval of Δt (h), S is the effective area of the membrane (m^2), and C_{s0} and C_{sl} are the solute concentrations in the feed and permeate, respectively. The solute concentrations in the permeate and feed solutions were determined using a conductivity meter. For a given membrane sample, the variations in the flux and salt rejection were found to be less than 2% in duplicate tests. The variation in water flux of membranes prepared from different batches was shown to be within 10%, while the variation in the salt rejection was within 5%.
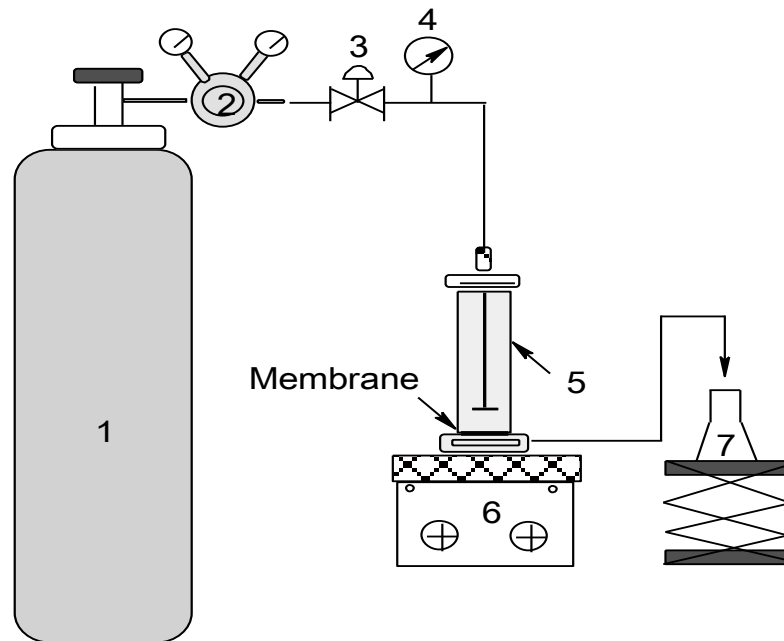
Figure 3.2 Experimental set up for membrane separation tests: (1) N$_2$ cylinder, (2) gas regulator, (3) controlling valve, (4) pressure gauge, (5) feed tank and membrane test cell, (6) magnetic stirrer, (7) permeate collector.

3.3 Results and discussion

3.3.1 Characterization of polyamide selective layer

Chemical composition of polyamide layer

The ATR-FTIR was employed to analyze the chemical composition of the top surface of the composite membrane. Figure 3.3 shows the ATR-FTIR spectra of the pristine PES substrate and two thin film composite membranes with one polyamide top layer [i.e., (PEI/TMC) and (TMC/PEI)]. For PES support membrane, the aromatic bands at 1577 and 1486 cm^{-1} are from the benzene rings and C=C bond stretching, and the peak at 1242 cm^{-1} is characteristic of the aromatic ether band. The peak appearing at 2917 cm^{-1} is characteristic of the ether (R-O-R) and hydroxyl (R-OH) groups arising from the additive poly(ethylene glycol) (PEG) used in membrane preparation, and a more significant peak at 1664 cm^{-1} is attributed to a primary amide stretch coming from additive polyvinylpyrrolidone (PVP). These additives are normally used in producing microporous membranes by the phase inversion process.

Compared to the PES substrate, two new bands at 1645 cm^{-1} and 1545 cm^{-1} appeared on the ATR-FTIR spectra for the thin film composite membranes comprising of a polyamide surface layer. This is expected because of the interfacial reaction between PEI and TMC to produce a polyamide skin layer. The chemical reaction between PEI and TMC to form a polyamide layer is proposed in Figure 3.4. The two bands at 1645 cm^{-1} and 1545 cm^{-1} are characteristic of amide-I (C=O stretching) band and amide-II (N-H) band of the amide groups (-CONH-). An absorption band observed at 1720 cm^{-1} is ascribed to the C=O stretching of carboxylic acids (-COOH) resulting from the hydrolysis of acyl chloride (-COCl). The bands at 2958 and 2846 cm^{-1} are ascribed to C-H stretching that comes from methylene (-CH$_2$) of PEI. The slight

enhancement of peak strength around 3302 cm^{-1} is attributed to N-H stretching derived from the amino groups (-NH$_2$) of PEI.

Both thin film composite membranes (PEI/TMC) and (TMC/PEI) have characteristic peaks of polyamide, PEI and TMC. This confirms the occurrence of interfacial polymerization between PEI and TMC and the formation of amide linkages (-CONH-) in the active skin layer, regardless which reactant was deposited on the PES substrate first.
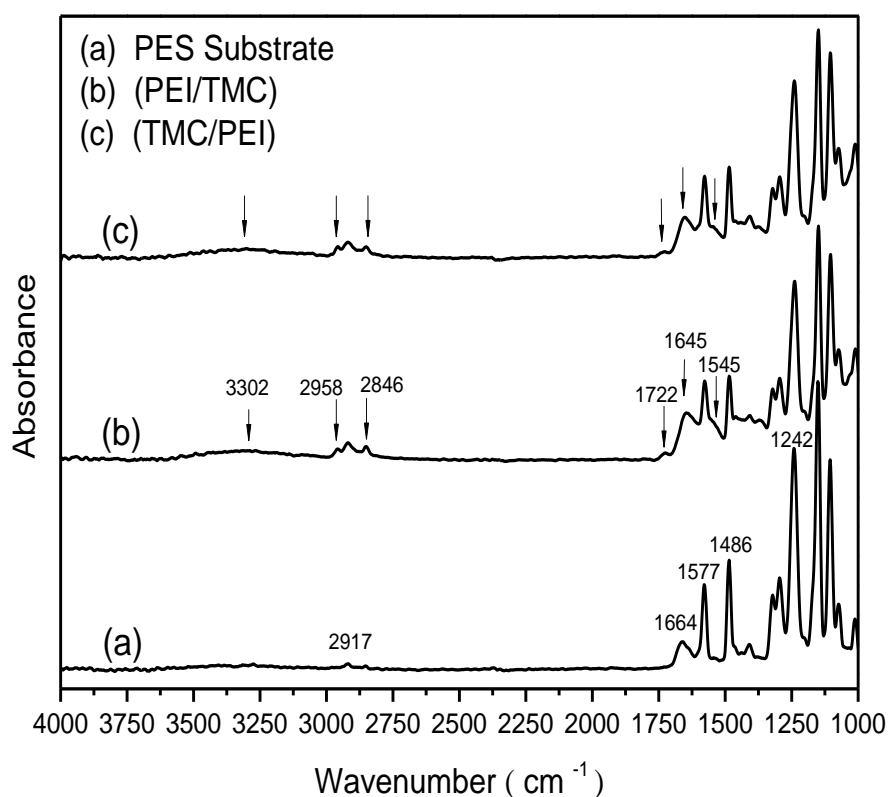
Figure 3.3 ATR-FTIR spectra of (a) PES substrate, (b) composite membrane (PEI/TMC) and (c) composite membrane (TMC/PEI).

Surface charge of the composite membrane

The charge characteristics on the surface of the membranes were studied in terms of Zeta potential. Figure 3.5 shows the Zeta potentials on the membrane surface measured at different

pH values for the two composite membranes (PEI/TMC) and (TMC/PEI). For comparison, the Zeta potential on the PES substrate surface was determined.
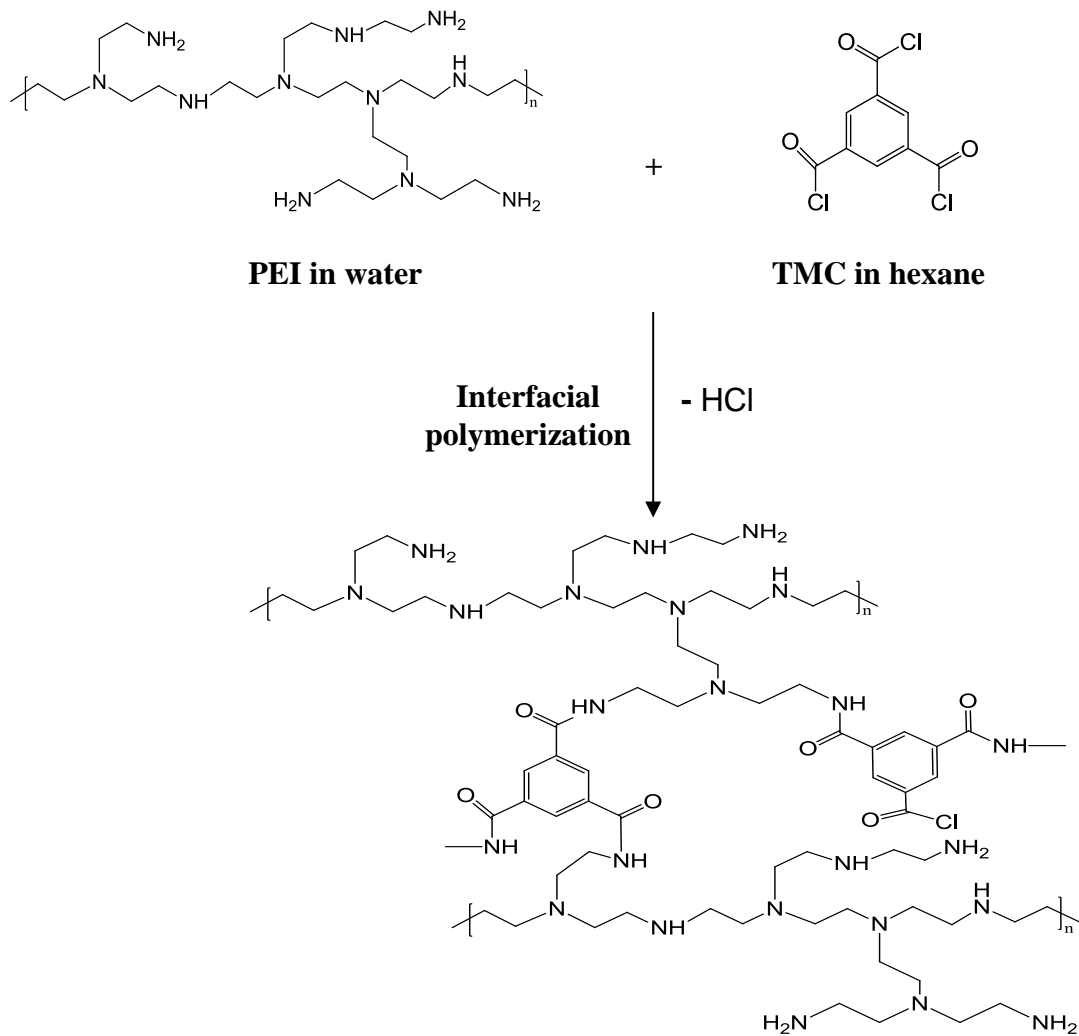
Figure 3.4 Interfacial polymerization between PEI and TMC for polyamide formation.

It is clearly shown that the PES substrate membrane is negatively charged. However, the selective polyamide layer formed by depositions of the aqueous and organic reactants in either a sequence of PEI-TMC (Figure 3.5(b)) or TMC-PEI (Figure 3.5(c)) is positively charged at a pH below 7.5. In our nanofiltration test, the pH of salt solutions is 6.8. Therefore, the

membranes are positively charged under this test condition. The positively charged surface of

the two composite membranes is caused by the unreacted primary amine of PEI.
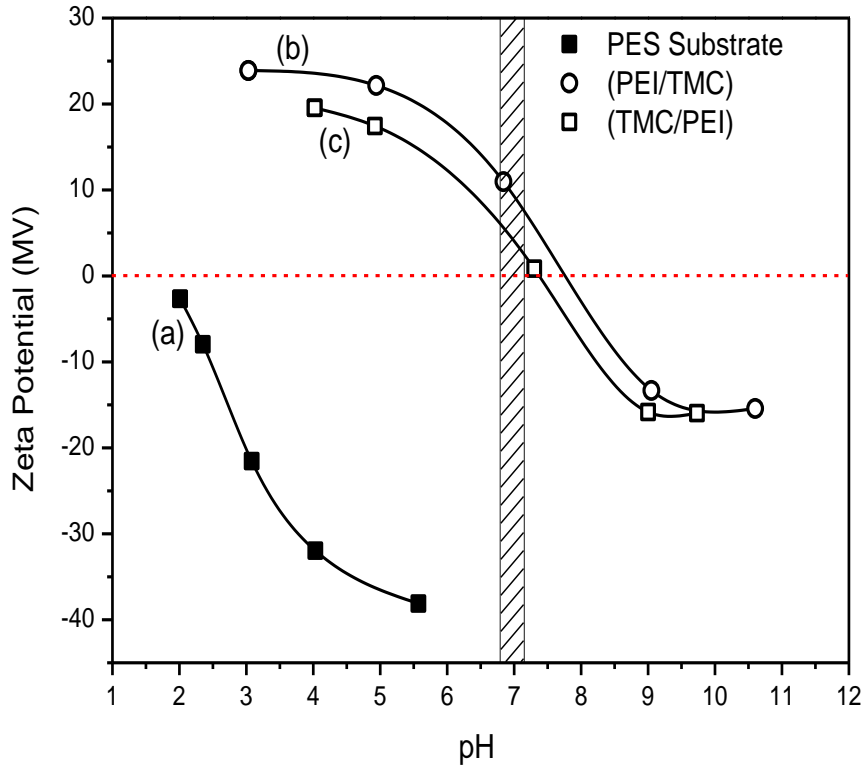
Figure 3.5 Surface Zeta potential of (a) PES substrate, (b) composite membrane (PEI/TMC) and (c) composite membrane (TMC/PEI) at various pH values (Test conditions: 0.001 M KCl, 25 °C).

Surface morphology of the composite membrane

The surface morphology of the membranes was examined using SEM. Figure 3.6 shows the

cross-section of PES substrate and that of (PEI/TMC)$_2$ polyamide composite membrane near

the top surface of the membrane. The PES substrate has a typical asymmetric structure with a

thin and dense skin and a microporous finger-like sublayer, as shown in Figure 3.6(a). The

composite membrane showed a clearly visible ultrathin active skin layer on the surface of the

PES substrate, as shown in Figure 3.6(b). The thickness of the interfacially polymerized

polyamide skin layer (i.e., the $(PEI/TMC)_2$ layer) is estimated to be 0.4 μm, suggesting that the interfacially polymerized layer (i.e., a single (PEI/TMC) layer produced in the first 2 cycles of interfacial polymerization) is approximately on the order of 0.2 μm. The individual layer thickness, however, should not be treated as constant. As shown later, the flux and rejection did not change significantly beyond 2 cycles of interfacial polymerization, which appears to indicate that the interfacially polymerized layer gradually became thinner during layer-by-layer buildup with additional cycles of interfacial polymerization, although it is difficult to accurately determine the thickness of an individual layer formed in each cycle because the interfacial layers are not stacked up distinctly.
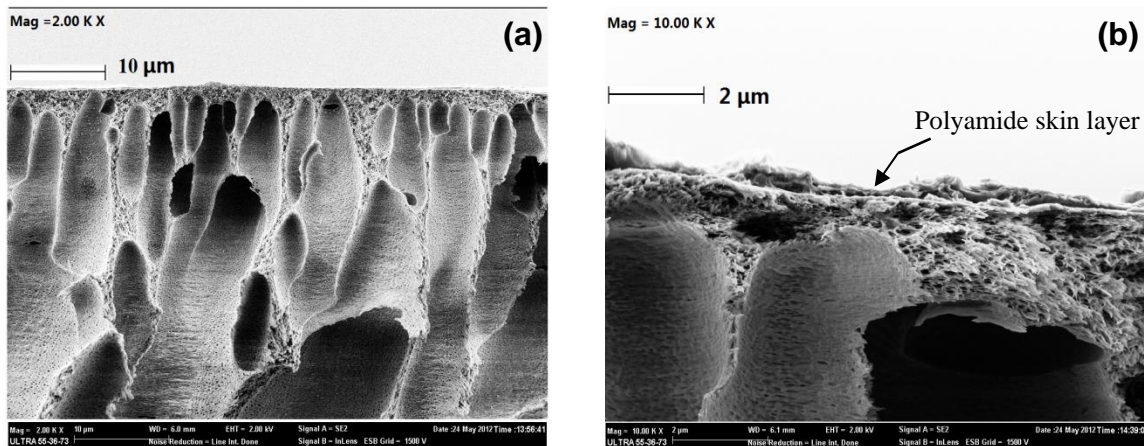
Figure 3.6 Cross-section images of (a) PES substrate and (b) composite membrane $(PEI/TMC)_2$.

Figure 3.7 displays the surface images of composite membranes formed with 1 and 2 cycles of interfacial polymerization with different reactant deposition sequences (i.e., membranes (PEI/TMC), $(PEI/TMC)_2$, (TMC/PEI) and $(TMC/PEI)_2$). Also shown in the figure for comparison is the surface image of PES substrate, which has a smooth surface with a few granular particles and pores on the surface (Figure 3.7(a)). The composite membranes based on

56

a PEI-TMC sequence of reactant deposition exhibit a valley-ridge structure evenly distributed on the surface (see Figure 3.7(b)). Doubling the interfacially polymerized polyamide layer makes the membrane surface denser but less uniform in the valley-ridge structure due to polymer aggregation, as shown in Figure 3.7(c). When the sequence of reactant deposition is reversed interfacial polymerization (i.e., deposition sequence of TMC-PEI), the membranes show nodular-like structures that are irregularly distributed on the membrane surface, and the nodules became bigger and more connected when an additional polyamide layer was assembled on the membrane surface (see Figures 3.7(d) and (e)). This indicates that the reactant deposition sequence and the number of the interfacial reaction cycles have a direct impact on the membrane structure.

AFM was also used for topological characterization of the membrane surface to complement with SEM. The three-dimensional images of a 4 μm × 4 μm scan on the membranes are shown in Figure 3.8. The surface roughness of the membranes in terms of the root mean square roughness is presented in Table 3.2. The results are in agreement with the surface morphologies observed from SEM. The surface of the PES substrate is rather plain (Figure 3.8(a)), with a roughness of only 10.9 nm. There are peaks and valleys on the surfaces of the composite membranes, whether they are formed by interfacial polymerization with sequential depositions of PEI-TMC (Figures 3.8(b) and (c)) or TMC-PEI (Figures 3.8(d) and (e)). The composite membranes showed a much rougher surface than that of the pristine PES substrate. Interestingly, when the interfacial polyamide layer is doubled, the first polyamide layer did not act as a prime coat to help produce a smoother second polyamide layer as one would expect. In fact, the distance between the peaks and valleys becomes larger (Figures 3.8(c) and (e)). The composite membranes fabricated by the TMC-PEI deposition sequence showed a larger

distance between the peaks and valleys on the membrane surface, and in general they have rougher surfaces than those of composite membranes fabricated by the PEI-TMC deposition sequence.
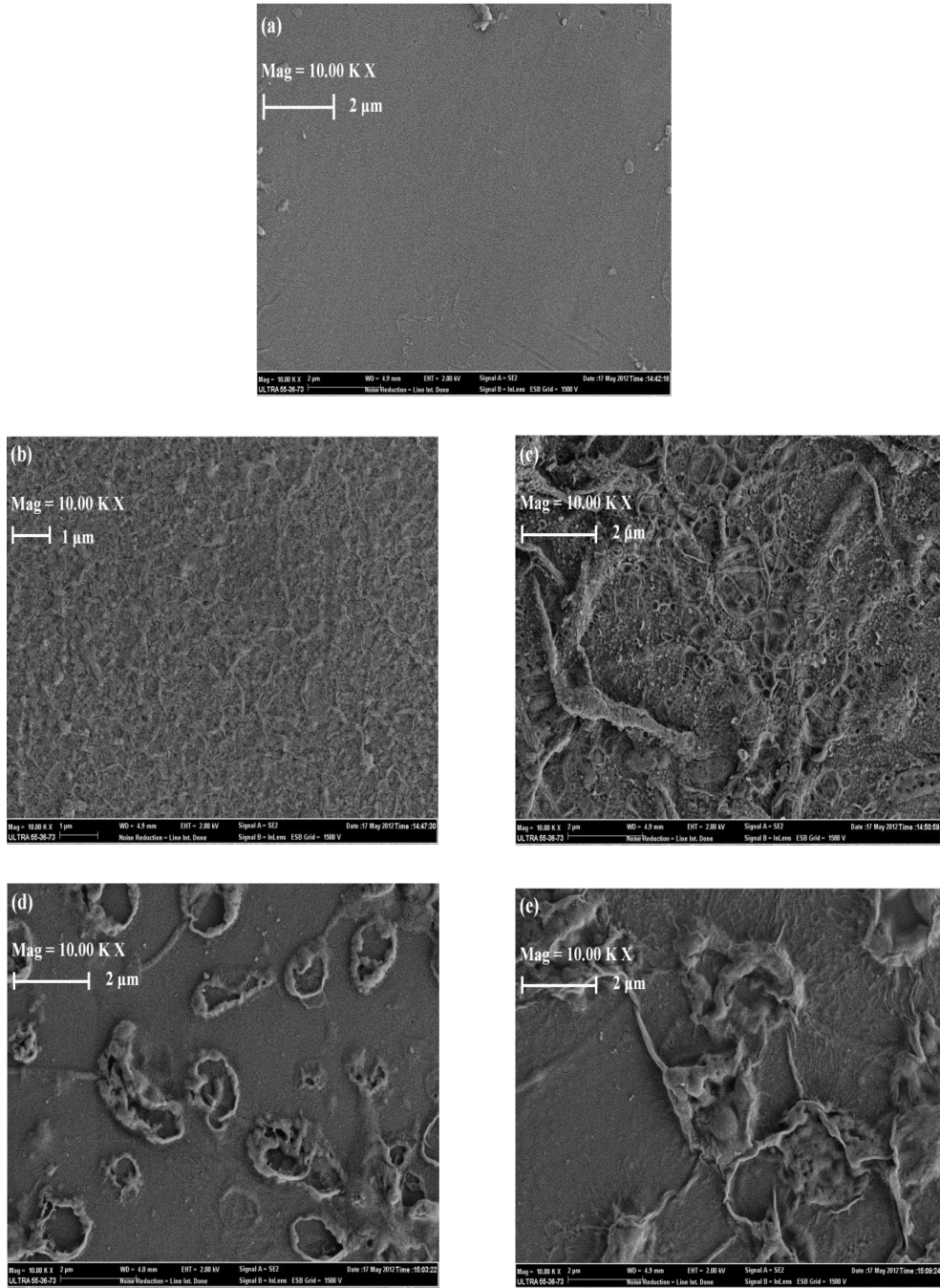
Figure 3.7 Surface images (10,000×) of (a) PES substrate, (b) composite membrane (PEI/TMC), (c) composite membrane (PEI/TMC)$_2$, (d) composite membrane (TMC/PEI) and (e) composite membrane (TMC/PEI)$_2$.
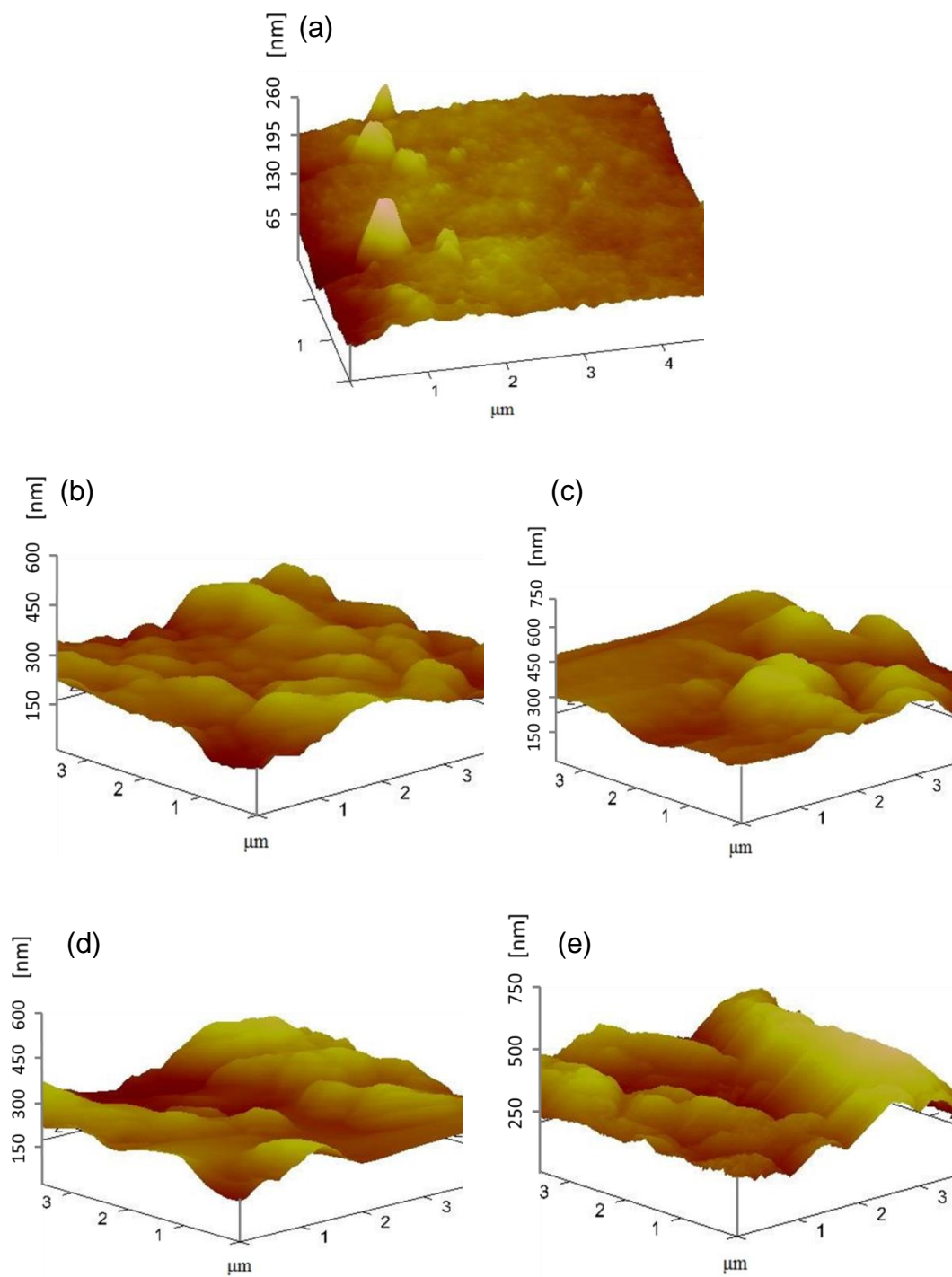
Figure 3.8 AFM images (4 μm × 4 μm) of (a) PES substrate, (b) composite membrane (PEI/TMC), (c) composite membrane $(PEI/TMC)_2$, (d) composite membrane (TMC/PEI) and (e) composite membrane $(TMC/PEI)_2$.

59

Table 3.2 Root mean square roughness of PES substrate and polyamide composite membranes analyzed by AFM

Membrane samples	Root mean square roughness (nm)
PES substrate	10.9
(PEI/TMC)	54.2
(PEI/TMC)$_2$	74.5
(TMC/PEI)	61.1
(TMC/PEI)$_2$	89.3

The latter observation can be explained based on the supramolecular assemblies during membrane formation. When the macromolecules of PEI are first deposited on the PES substrate, the amine groups are evenly distributed on substrate surface as determined by the branched polymer chains of the macromolecules. This helps develop a uniform reactive sites on the substrate surface for subsequent interfacial reaction with TMC because of the anchored amine groups. On the other hand, when the small molecules of TMC are deposited first, the local concentration of TMC on the PES substrate varies because (1) unlike PEI which cannot enter the small pores on the substrate due to its macromolecular size, the TMC solution will not only wet the substrate surface but can enter the substrate pores easily, (2) when solvent hexane is evaporated, the TMC molecules adhering to substrate surface cannot bridge the substrate pores, which will lead to an uneven distribution of the TMC molecules microscopically because of the nonuniform pore sizes of the substrate. As a result, nodular and nonuniform structures on the membrane surface will be formed.

3.3.2 Effects of membrane fabrication factors on nanofiltration performance

Effect of number of reactant depositions

The separation performance of the composite membranes with multiple polyamide active layers fabricated by interfacial polymerization with reactant depositions in the sequence of PEI and TMC is shown in Figure 3.9 for the permeation flux (a) and salt rejection (b), respectively. For comparison, the separation performance of the PES substrate alone was also tested at a lower pressure of 0.2 MPa gauge. We used dash lines from 0 to 2 since the membrane PES (number of reactant depositions "0") and PEI (number of reactant depositions "1") are not real polyamide membranes. With additional reactant depositions, the formed membranes are real polyamide membranes, and we used solid lines.

As expected, the PES substrate has a very high permeability, with a flux of 175 $L/(m^2.h)$ at a transmembrane pressure of 0.2 MPa gauge. When coated with PEI, the permeation flux drops dramatically to about 4 $L/(m^2.h)$ at a transmembrane pressure of 0.8 MPa gauge. It is interesting to note that the permeation flux increased to about 40 $L/(m^2.h)$ at 0.8 MPa gauge after the surface deposited PEI reacted with the TMC solution to form an interfacially polymerized polyamide layer (see membrane (PEI/TMC) in Figure 3.9(a)). After a second cycle of interfacial polymerization, the membrane permeability was lowered by ~50%, as shown by the permeation flux of membrane $(PEI/TMC)_2$. With a further increase in the number of sequential depositions of reactants PEI and TMC, the permeation flux began to decrease slowly and eventually leveled off.
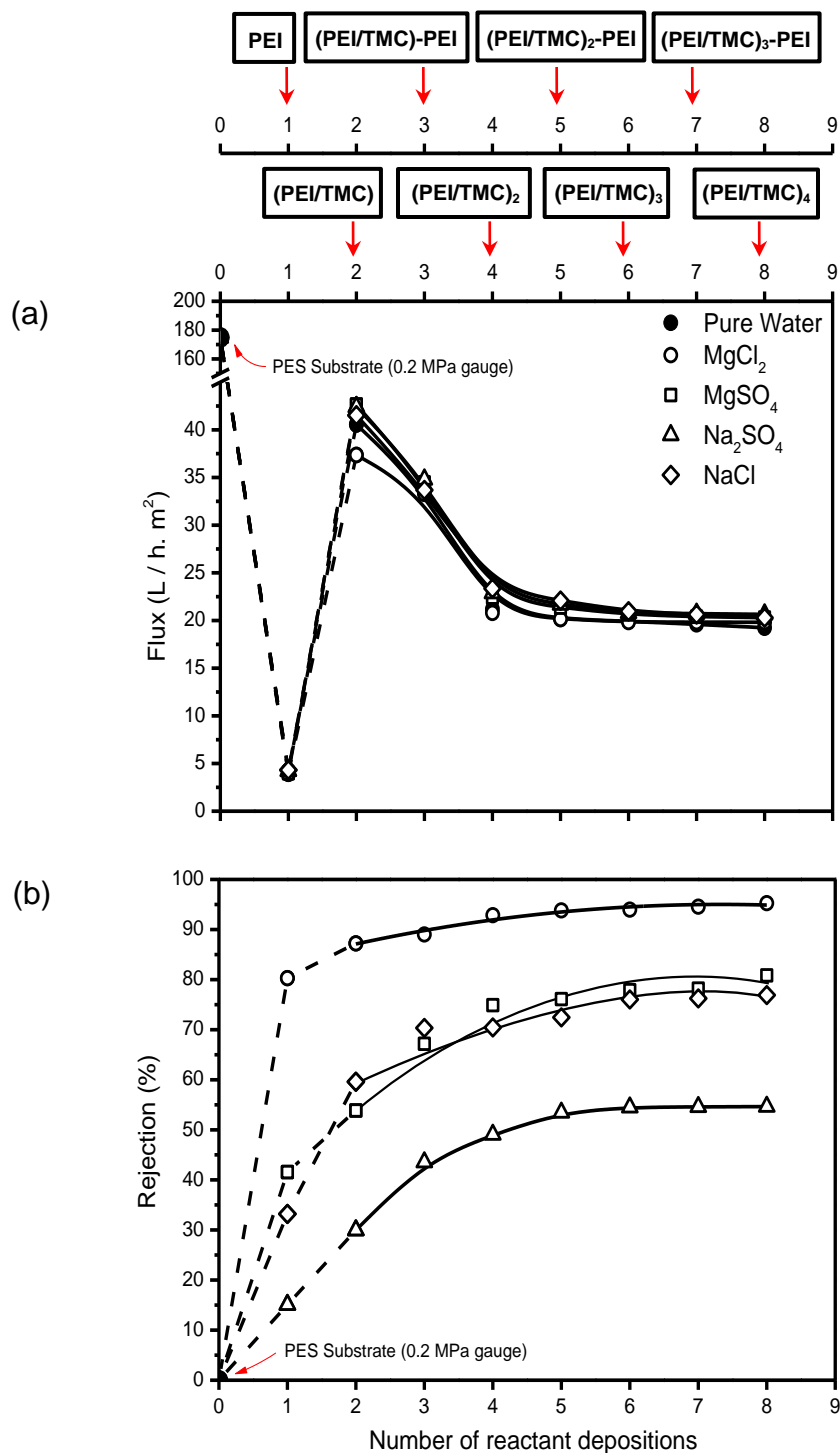
Figure 3.9 Effects of number of reactant depositions on (a) permeation flux and (b) salt rejection for membranes prepared by interfacial polymerization with a reactant deposition sequence of PEI-TMC. (Operating pressure: 0.8 MPa gauge, except for PES substrate which was tested at 0.2 MPa gauge; Salt concentration: 500 ppm; Temperature: 23°C).

The fairly low permeation flux of PEI-coated PES membrane indicates that the surface deposition layer of PEI resulted in a substantially large resistance to mass transport. This is because PEI was sufficiently adsorbed on the negatively charged surface of the PES substrate because of the primary amine groups of PEI. Upon heating at 95 °C, PEI can be insolubilized [Cadotte *et al.*, 1974]. The coated PEI would not only cover the surface of the PES substrate but also diffuse into its pores that are big enough to accommodate the macromolecules, resulting in a denser and thicker top layer and reduced pore size and porosity in the interior of the substrate. Consequently, the permeation flux decreased. However, when the surface coated PEI macromolecules were allowed to react with TMC on the membrane surface to form a polyamide layer, the PEI will be partially consumed by interfacial reaction with TMC. As a result, the PEI molecules present in the pores of the PES substrate will migrate to the interface under a concentration gradient, thereby forming a polyamide skin layer with the substrate pores that are not significantly filled with the macromolecules in comparison with PEI-coated PES. This will lead to two opposite effects. While the formation of the dense skin layer will reduce the membrane permeability, the less obstructed substrate pores relative to that in PEI-coated PES tends to make the membrane more permeable. The latter aspect appears to be more dominant as the (PEI/TMC) membrane showed a higher permeability than the PES substrate coated with PEI (i.e., PEI membrane). As expected, with additional cycles of sequential depositions with PEI and TMC for interfacial polymerization, multiple polyamide layers are built up on the membrane surface, and the interior structure of the substrate is no longer affected, resulting in a reduction in the permeation flux. However, the magnitude of the reduction in the permeation flux gradually decreases and eventually level off because the

surface characteristics of the polymerized PEI/TMC layer does not favor the adsorption of additional PEI macromolecules (see Figure 3.5).

As shown in Figure 3.9(b), there is an increase in the salt rejection with an increase in the number of reactant depositions. The salt rejection is shown to follow the order of $MgCl_2 > MgSO_4 \approx NaCl > Na_2SO_4$. It is known that the rejection rate of a charged membrane to an electrolyte is not only determined by the pore size of the membrane, but also depends on the electrostatic interactions between the membrane and the ionic feed solution [Yaroshchuk, 1998]. The Zeta potential measurements showed that the PEI-based polyamide composite membranes have a positively charged surface at the pH value (pH=6.5) of the test solutions, and they tend to have a relatively higher rejection for salts having multivalent cations and monovalent anions as a result of the Donnan exclusion between the cations and the membrane surface. Although NaCl has a smaller molecular size than Na_2SO_4, the membrane shows a higher rejection to NaCl than to Na_2SO_4, indicating that the electrostatic interaction is indeed more dominating than the steric hindrance of the permeating species in the thin film composite membranes.

Figures 3.10(a) and (b) show the permeation flux and salt rejection of multiple-layered polyamide composite membranes fabricated with a reversed sequence of reactant depositions (i.e., TMC-PEI). This series of membranes also exhibit a decreasing trend as the $(PEI/TMC)_n$ and $(PEI/TMC)_n$-PEI membranes as far as the permeation flux is concerned. However, with sequential depositions of additional reactants TMC and PEI for interfacial polymerization, the decrease in the permeation flux followed almost a linear trend up to a total of 8 depositions of the reactants (i.e., 4 cycles of interfacial polymerization) tested in this study. This is different from that for membranes formed by the TMC deposition sequence.
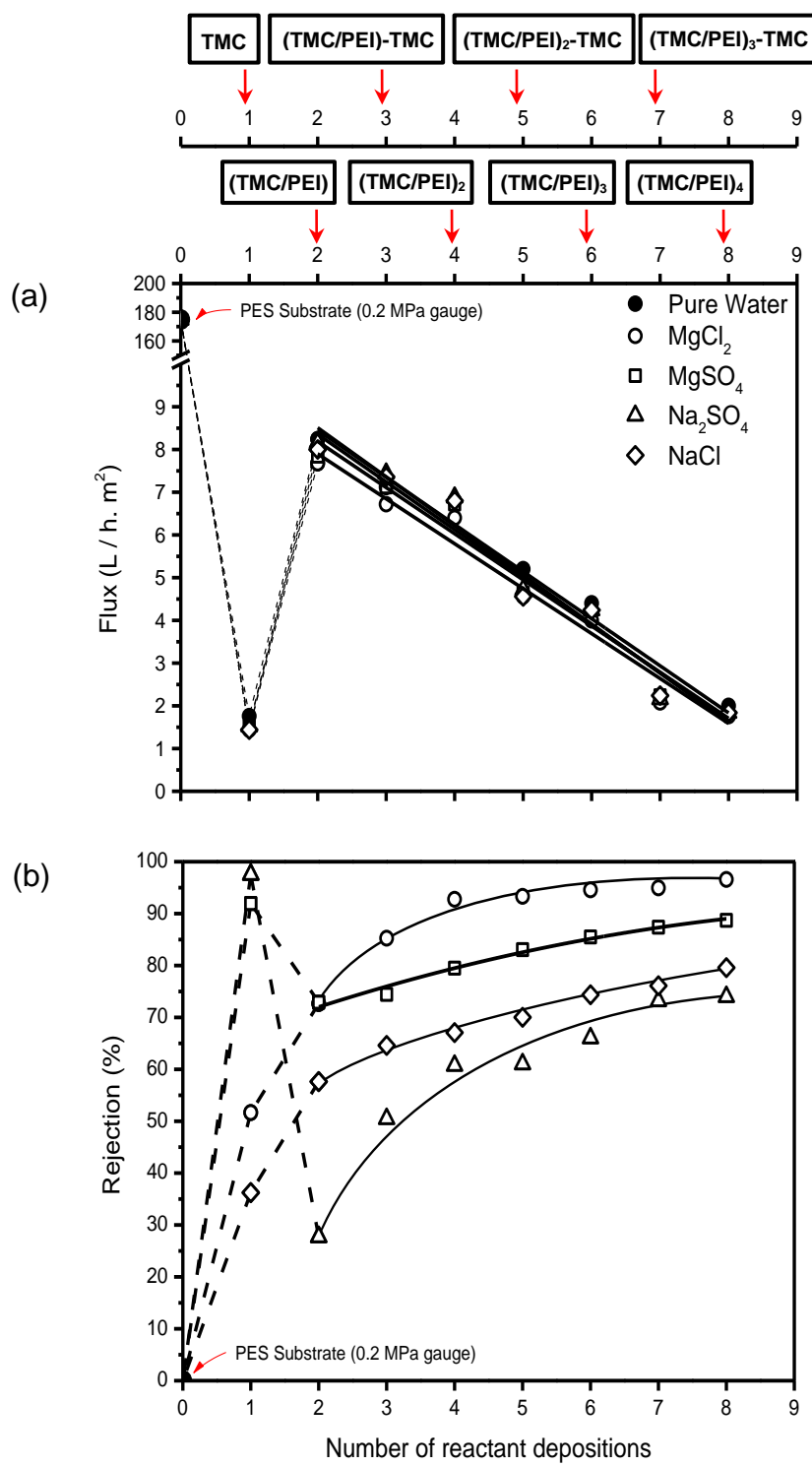
Figure 3.10 Effect of number of reactant depositions on (a) permeation flux and (b) salt rejection for membranes prepared by interfacial polymerization in sequence of TMC-PEI. (Operating pressure: 0.8 MPa gauge, except for PES substrate which was tested at 0.2 MPa gauge; Salt concentration: 500 ppm; Temperature: 23°C).

The water permeation flux of a membrane is affected by surface hydrophilicity of the membrane. Figure 3.11 shows the contact angles of the two series of composite membranes with multiple polyamide active layers. The contact angle of water on the PES substrate is 86°, and it drops to 71° and 78° after depositions with PEI (i.e., PEI membrane) and TMC (i.e., TMC membrane), respectively. As expected, PEI macromolecules are more hydrophilic than TMC molecules. With additional reactant depositions, the contact angles of water on both series of membranes further decreased slightly due to hydrophilicity of the interfacially formed polyamide layer. However, membranes fabricated with the TMC-PEI deposition sequence tend to be less hydrophilic than those membranes fabricated with the reversed sequence of reactant depositions (i.e., PEI-TMC).
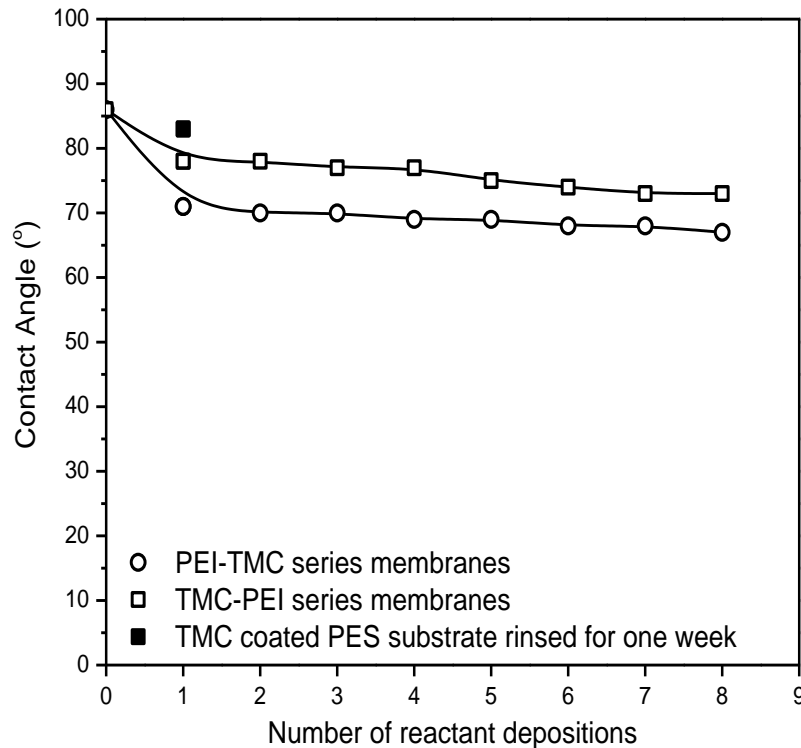
Figure 3.11 Effect of number of reactant depositions on the surface hydrophilicity characterized by contact angles.

When the PES substrate was first coated with TMC molecules, the membrane permeability decreased in spite of a slight increase in the membrane hydrophilicity. After deposition with PEI, the membrane surface becomes more hydrophilic due to formation of hydrophilic polyamide layer, and the membrane (i.e., (TMC/PEI)) became more permeable to water. When additional cycles of TMC-PEI deposition were applied, the mass transfer resistance of the skin layer continued to increase, resulting in a decrease in the permeation flux. Unlike hydrophilic PEI macromolecules, TMC molecules are smaller and more hydrophobic, and TMC adsorption onto a polyamide surface formed prior will not be affected significantly during the layer-by-layer assembly of the polyamide skin, leading to a continuous decrease in water flux.

It may be noted that the TMC-coated PES substrate showed a rather high rejection to MgSO$_4$ (91.95%) and Na$_2$SO$_4$ (97.53%). This is not unexpected in consideration of electrostatic interactions between the membrane surface and the solutes [Tang *et al.*, 2008; Li *et al.*, 2009b]. The TMC-coated PES substrate membrane has a negatively charged surface due to carboxylic groups produced from the hydrolysis of acyl chlorides. A relatively high rejection is thus anticipated to salts having multivalent anions and monovalent cations. However, such a membrane was found to be unstable for long term use as the TMC molecules on the membrane surface were gradually washed away in the feed solution over a prolonged period of time. A further buildup of a polyamide skin layer is necessary to improve the membrane stability.

Effect of sequence of reactant depositions

The above results show that polyamide composite membranes can be fabricated by reacting PEI and TMC on a substrate surface. The two reactants can be loaded onto the substrate by deposition of PEI and then TMC or vice versa. However, different deposition sequences (i.e., PEI-TMC or TMC-PEI) resulted in membranes with different surface morphologies and

separation performance. To illustrate more clearly how the reactant deposition sequence affects the membrane performance, the pure water flux and rejection data of the two series of membranes were compared, as shown in Figures 3.12 and 13. The permeabilities of the membranes fabricated with the PEI-TMC deposition sequence are generally much greater than those of membranes fabricated with the reversed sequence of reactant depositions (i.e., TMC-PEI). This can be explained using a schematic illustration of the membrane formation depicted in Figure 3.14. The PES substrate can be wetted easily with both reactant solutions. In the interfacial polymerization with the PEI-TMC deposition sequence, the aqueous solution containing the PEI macromolecules (Mw 25,000) was first deposited onto the surface of the substrate (MWCO 10,000). Because of the branched chains of PEI, it is likely and preferable for PEI to adhere onto the substrate surface, although some macromolecules may also partially enter big pores of the substrate. The pores on the substrate will be largely "bridged" over by the macromolecules and thus the polymerized polyamide layer will not deeply intrude the pores, leading to a high flux. When the reactant deposition sequence was reversed with initial deposition of the small TMC molecules onto the PES substrate surface, the TMC molecules could penetrate into the pores of the substrate. This hypothesis is supported by the fact that after TMC deposition onto the substrate the water flux was reduced substantially. As a result, the polyamide skin layer produced from TMC-PEI reaction will be anchored in the substrate pores. In addition, the substrates of composite membranes formed by the PEI-TMC deposition sequence are more hydrophilic, as discussed in the above section, and this also helps attribute to higher fluxes of the PES-(PEI/TMC)$_n$ membranes.
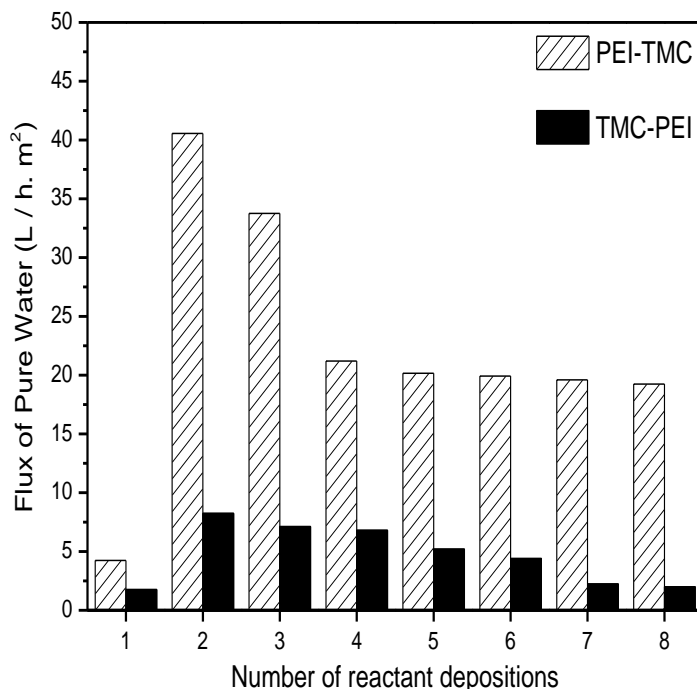
Figure 3.12 Effect of reactant deposition sequence on pure water permeation flux, Temperature: 23°C.

The difference in salt rejection between the two series of membranes appears to be more complicated. With additional buildup of polyamide layers on the PES substrate, the resulting membranes show a better rejection to all the four solutes tested for both series of composite membranes. For solutes $MgCl_2$ and NaCl, the membranes formed by the PEI-TMC deposition sequence had a better rejection than the membranes formed with the reversed reactant deposition sequence (i.e., TMC-PEI). Due to abundant amine groups on the membranes formed by the PEI-TMC deposition sequence, the membrane surface is more positively charged and thus results in a higher rejection to $MgCl_2$ and NaCl. However, when the skin layer is thick enough after a considerably large number of cycles of reactant deposition and polymerization, the membranes formed by the two different sequences of reactant depositions will exhibit a similar rejection to $MgCl_2$ and NaCl. On the other hand, for solutes $MgSO_4$ and Na_2SO_4, the

membranes formed using the TMC-PEI deposition sequence tend to have a higher rejection than the membranes formed using a reversed reactant deposition sequence.
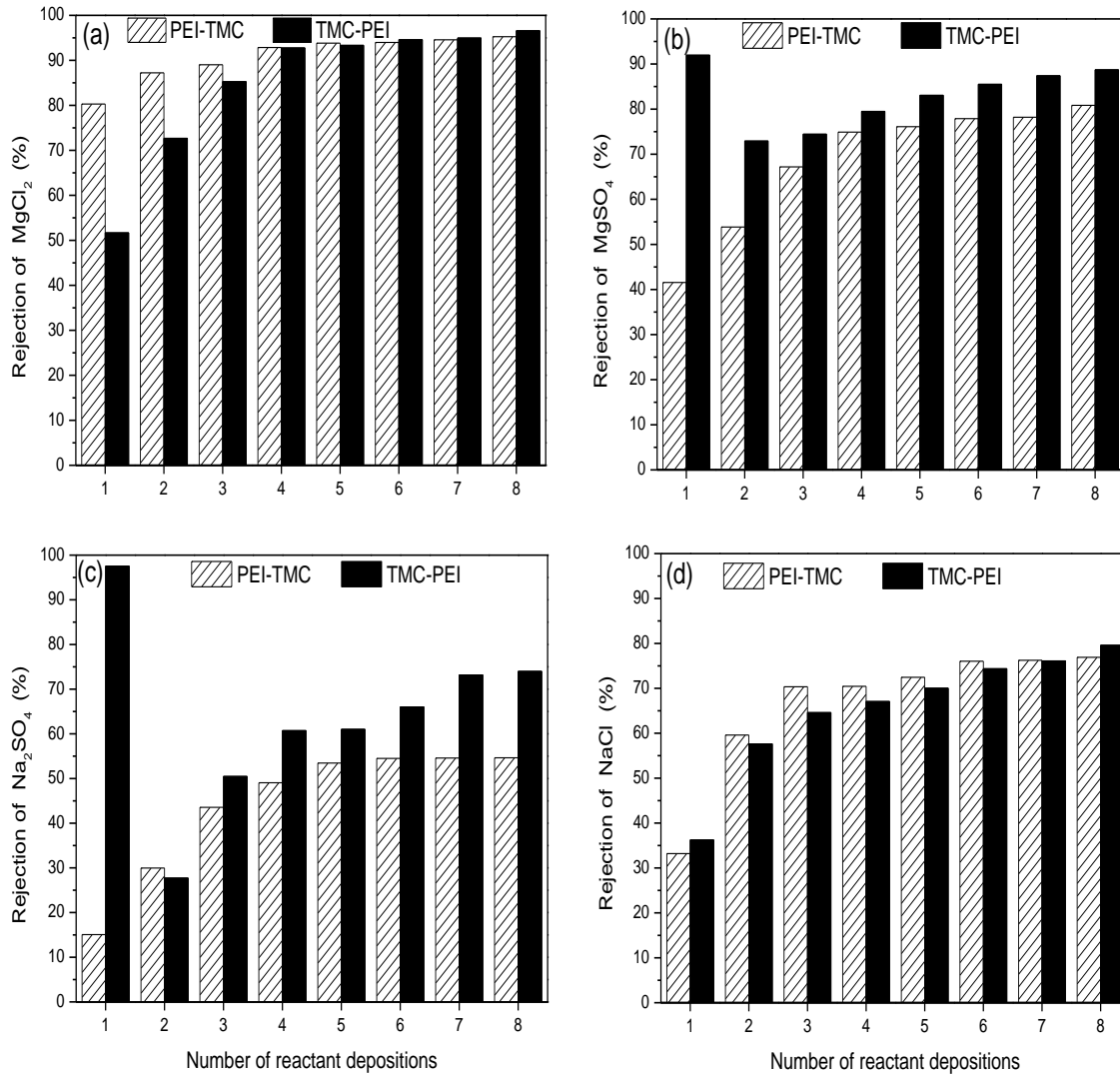
Figure 3.13 Effect of reactant deposition sequence on salt rejection: (a) $MgCl_2$, (b) $MgSO_4$, (c) Na_2SO_4, (d) NaCl (Operating pressure: 0.8 MPa gauge; Salt concentration: 500 ppm; Temperature: 23°C).

(a) Reactant deposition
sequence of PEI-TMC

(b) Reactant deposition
sequence of TMC-PEI
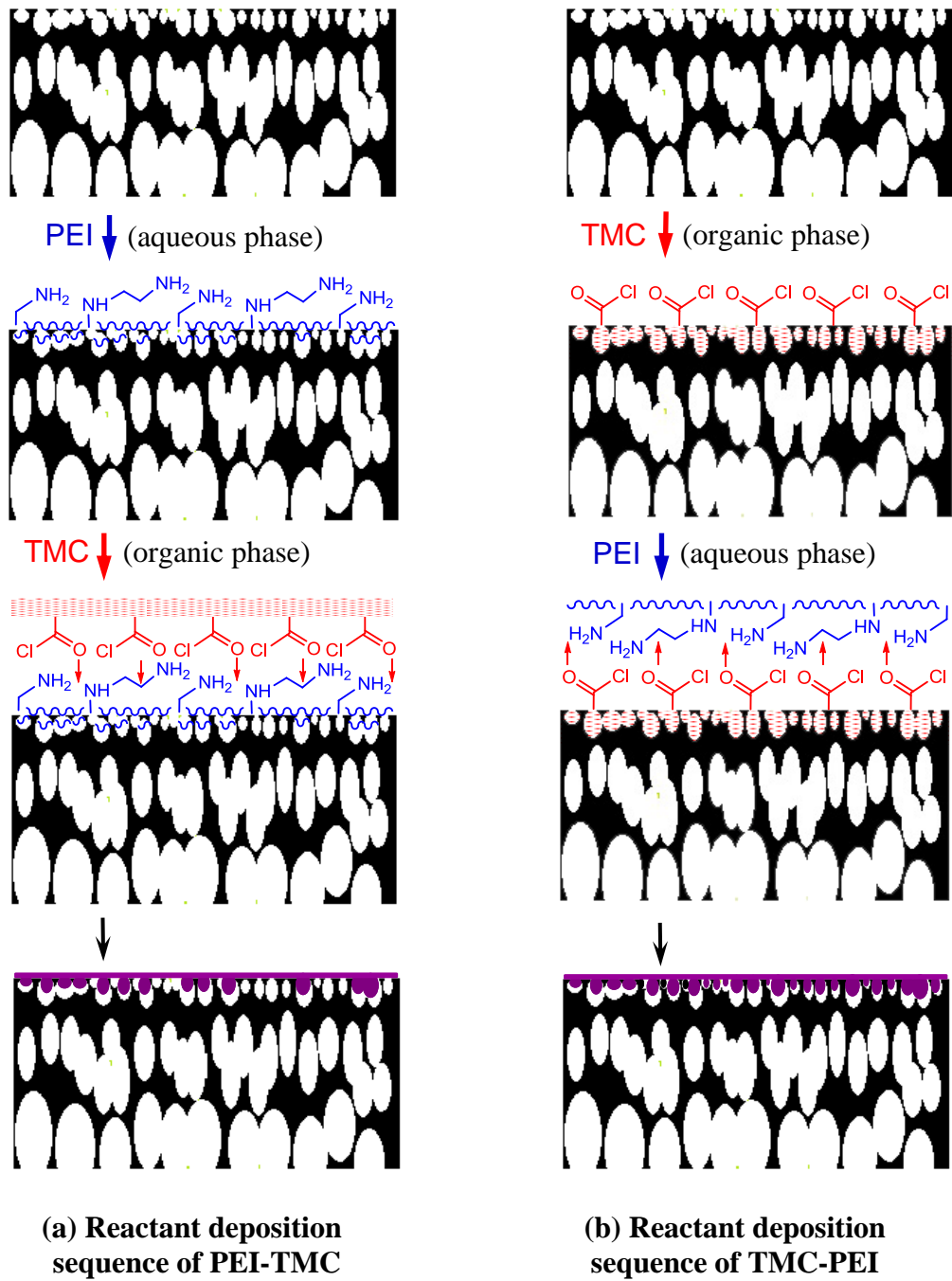
: Polyethersulfone substrate

: Polyamide thin film

: Polyethylenimine (PEI)
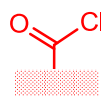
: Trimesoyl chloride (TMC)

Figure 3.14 Schematic illustration of interfacial polymerization with different reactant deposition.

Effect of concentration of reactant solution

The concentration of the reactants is an important variable for interfacial polymerization that influences the performance of resulting TFC membranes. Here, the effects of the concentrations of the aqueous reactant and the organic reactant on the membrane performance were investigated, while maintaining a fixed concentration ratio of PEI to TMC 5:1, which appeared to be a moderate value based on a range of amine to acyl chloride ratios reported in the literature for developing nanofiltration membranes [Chiang, 2009; Chiang *et al.*, 2009; Sun *et al.*, 2012].

Figure 3.15 shows the permeation flux and salt rejection of the composite membranes with one interfacially formed polyamide layer by reaction of surface deposited PEI with TMC solution (i.e., (PEI/TMC)). At a reactant concentration of 0.5 wt% for PEI and 0.1 wt% for TMC, the permeation flux reached ~45 L/(m^2.h) at a feed pressure of 0.8 MPa gauge. This membrane exhibited a rejection of 82.8% to MgCl$_2$, which is much higher than the membrane rejection to the other three salts. The permeation flux declined and the salt rejection increased with an increase in the reactant concentrations, and the decrease in the water flux and the increase in the salt rejection became less significant when the reactant concentrations were sufficiently high. At a reactant concentration of 3.5 wt% for PEI and 0.7 wt% for TMC, the formed membrane showed a rather high salt rejection (95.1% for MgCl$_2$, 94.4% for MgSO$_4$, 80.5% for Na$_2$SO$_4$ and 85.1% for NaCl) with a water permeation flux of 24.5 L/(m^2.h).
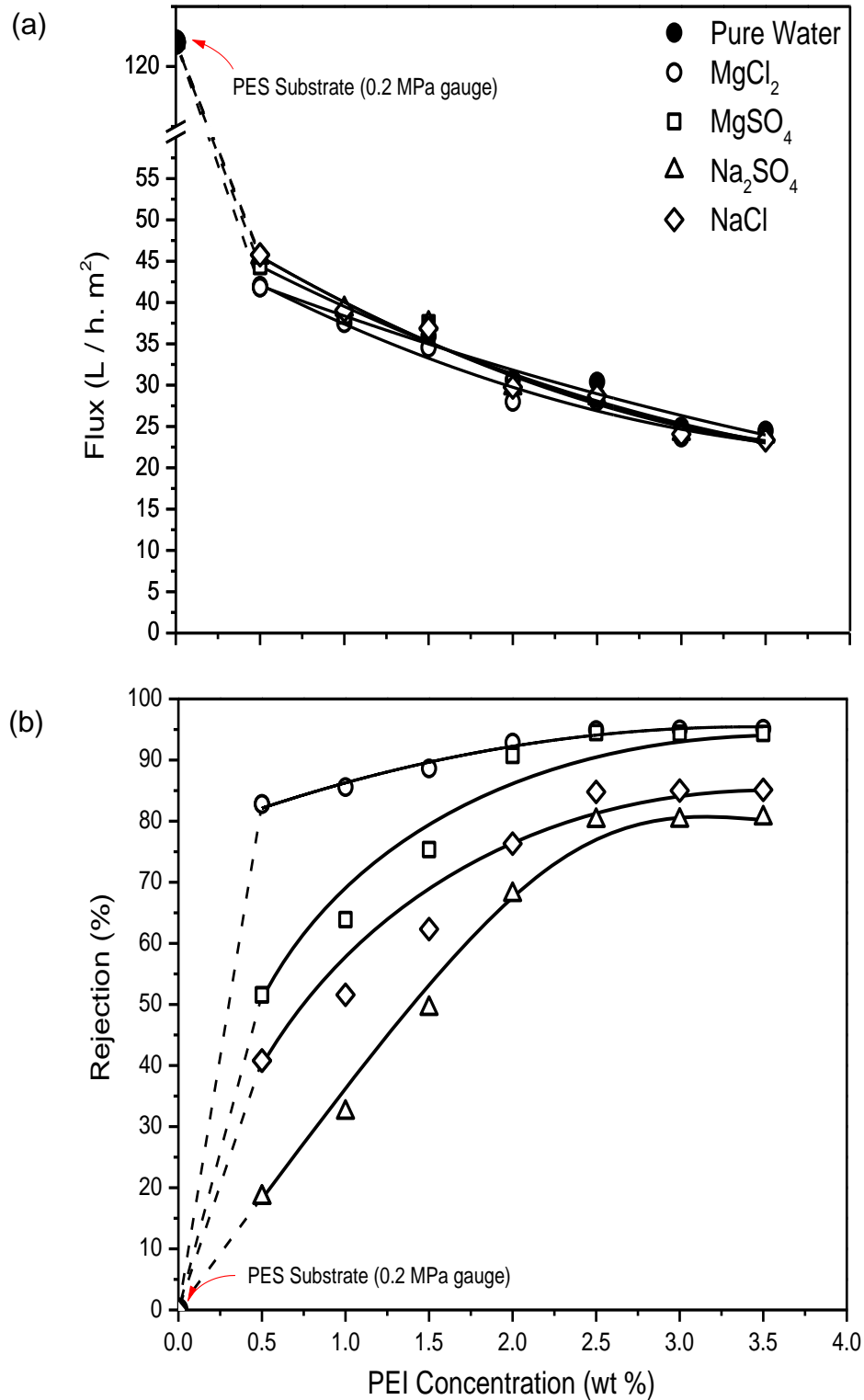
Figure 3.15 Effects of reactant concentrations on (a) permeation flux and (b) salt rejection for (PEI/TMC) membrane (Operating pressure: 0.8 MPa gauge, except for PES substrate which was tested at 0.2 MPa gauge; Salt concentration: 500 ppm; Temperature: 23°C).

When the reactant deposition sequence was reversed, the resulting membrane showed a similar trend in the separation performance when the reactant concentrations varied. This is shown in Figures 3.16(a) and (b) for permeation flux and salt rejection, respectively.
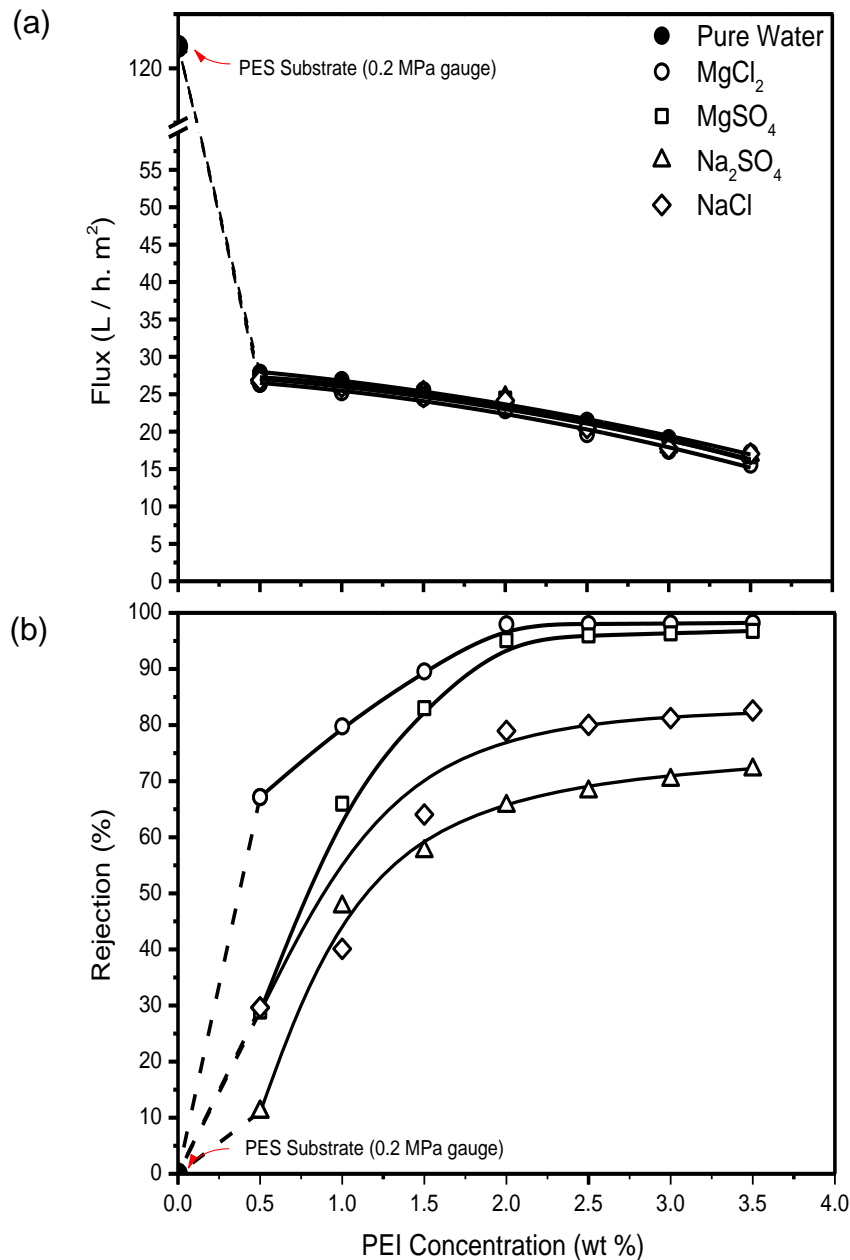
Figure 3.16 Effects of reactant concentrations on (a) permeation flux and (b) salt rejection for (TMC/PEI) membrane (Operating pressure: 0.8 MPa gauge, except for PES substrate which was tested at 0.2 MPa gauge; Salt concentration: 500 ppm; Temperature: 23°C).

Similar results have been reported for other membrane systems [Tang *et al.*, 2008; Liu *et al.*, 2008b; Li *et al.*, 2009b; Kaur *et al.*, 2012]. At a low concentration of the reactants, the polymerization reaction proceeds slowly, which tends to produce a "thin and loose" skin layer, resulting in a high water flux and a low solute rejection. At higher reactant concentrations, a thicker and more compact skin layer will be formed. As a result, the salt rejection increases whereas the water flux decreases.

Comparing the flux data for the two series of membranes, at a given reactant concentration, the (PEI/TMC) membranes are always more permeable than (TMC/PEI) membranes in the experimental range of the reactant concentrations investigated. However, no such a clear trend can be observed for the salt rejections, as shown in Figure 3.17. The (PEI/TMC) membranes have a better rejection to solutes $MgCl_2$ and $MgSO_4$ when the reactant concentration is relatively low in the membrane preparation, and the opposite was observed at higher reactant concentrations. However, for solutes Na_2SO_4 and NaCl, (PEI/TMC) membranes have a better rejection than (TMC/PEI) membranes at either a relatively low or a relatively high reactant concentration, but the (TMC/PEI) membranes formed at a moderate reactant concentration appear to be more selective than the (PEI/TMC) membranes.

Effect of heat treatment temperature

Heat treatment is often used during membrane formation to facilitate the removal of residual organic solvent from nascent skin layer and to promote additional cross-linking by dehydration of unreacted amine and carboxyl groups. Heat treatment has been used to improve the membrane stability and salt rejection of interfacially polymerized membranes [Rao *et al.*, 1997; Zhang *et al.*, 2012], and the thermal treatment conditions (i.e., temperature and time) are found to influence the membrane performance considerably.
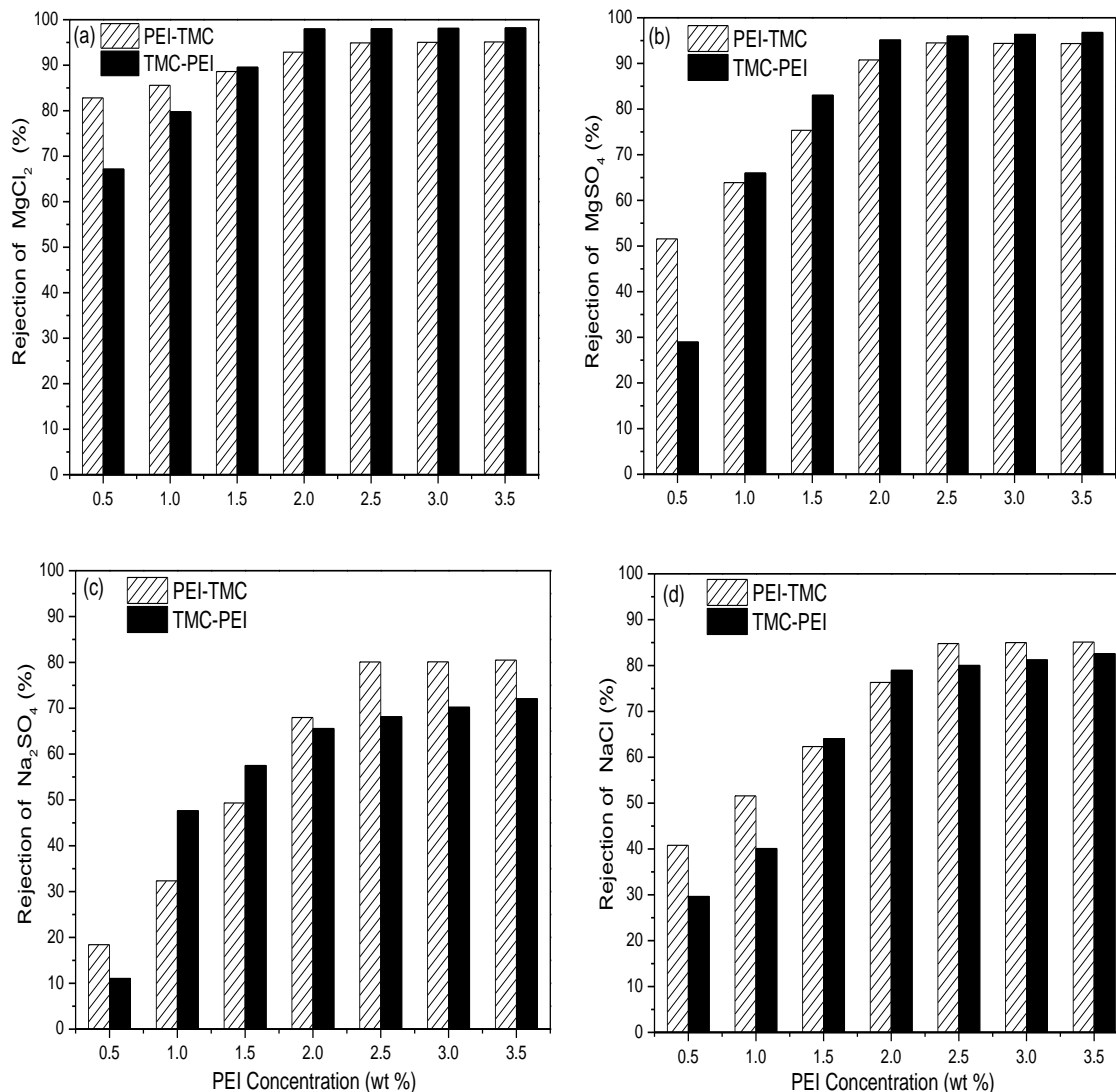
Figure 3.17 Salt rejection of (PEI/TMC) and (TMC/PEI) membranes formed at different reactant concentrations: (a) $MgCl_2$, (b) $MgSO_4$; (c) Na_2SO_4 and (d) NaCl (Operating pressure: 0.8 MPa gauge; Salt concentration: 500 ppm; Temperature: 23°C).

To investigate the effects of heat treatment on the membrane performance, the PES substrate membranes coated with PEI or TMC and the (PEI/TMC) thin film composite membranes were subjected to heat treatment, and the separation performance of the membranes were evaluated.

Figures 3.18(a) and (b) show the permeation flux and salt rejections of PES substrate membrane coated with PEI (i.e., PEI membrane) with and without heat treatment at 95 °C for 20 min. The concentration of PEI in the coating solution was 1.0 wt%. An early study [Cadotte

76

et al., 1974] suggested that PEI could be insolubilized by heat treatment. Upon heating, the PEI coated layer on top of PES substrate will be densified, and the pore size will decrease, resulting in a higher salt rejection and a lower water flux. However, the membrane rejection to Na_2SO_4 was shown to be an exception. After heat treatment, the rejection of Na_2SO_4 was lowered, presumably due to the strong electrostatic interaction between PEI and SO_4^{2-} and weaker repulsive effects to Na^+ than Mg^{2+}.
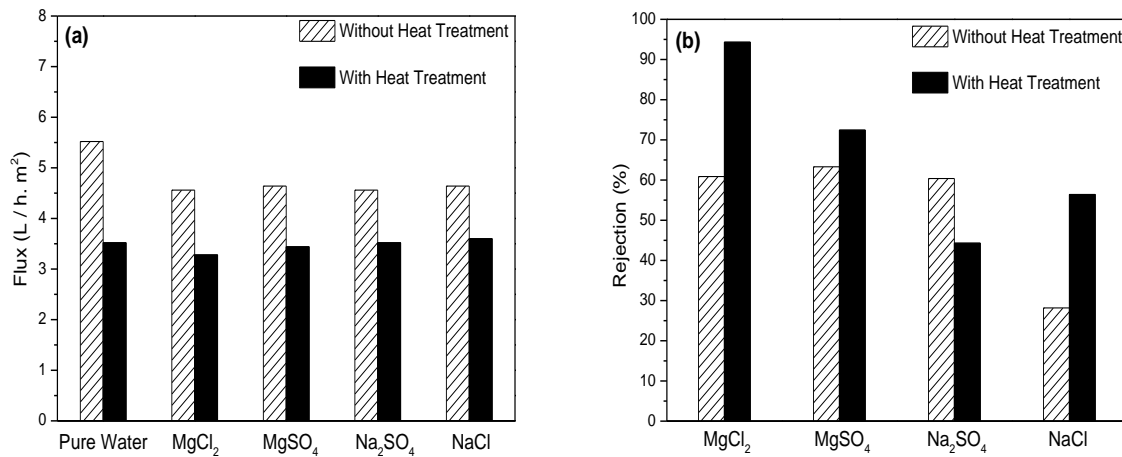
Figure 3.18 Effect of heat treatment on permeation flux (a) and salt rejection (b) for PEI membrane (Operating pressure: 0.8 MPa gauge; Salt concentration: 500 ppm; Temperature: 23°C).

Figures 3.19(a) and (b) show the permeation flux and salt rejection of PES substrate coated with TMC at a concentration of 0.2 wt%. After heat treatment at 95 ℃ for 20 min, the salt rejection increased considerably but at an expense of reduced flux. Nonetheless, the heat treated PEI membrane is shown to be suitable to reject $MgCl_2$ while heat treated TMC membrane is more suitable for $MgSO_4$ and Na_2SO_4 rejections. For solute NaCl, both heat-treated PEI and TMC membranes have a similar rejection, but the former has a higher flux.

77
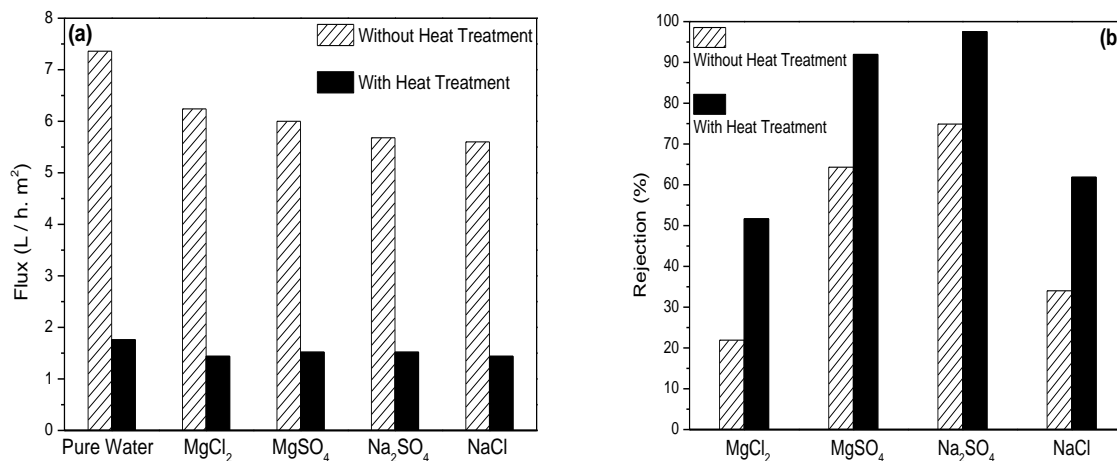
Figure 3.19 Effect of heat treatment on permeation flux (a) and salt rejection (b) for TMC membrane (Operating pressure: 0.8 MPa gauge; Salt concentration: 500 ppm; Temperature: 23°C).

The effects of heat treatment temperature on the separation performance of thin film composite (PEI/TMC) membranes were studied as well. Figures 3.20(a) and (b) show the flux and salt rejection of (PEI/TMC) membranes heat-treated for a period of 20 min at a temperature up to 115 °C. The concentrations of PEI and TMC reactants in their solutions were 2.0 wt% and 0.4 wt%, respectively, during the interfacial polymerization for composite membrane fabrication. This membrane was chosen to investigate the effects of thermal treatment on the separation performance of the membrane because it offered a moderate flux and rejection as shown in Figure 3.15.
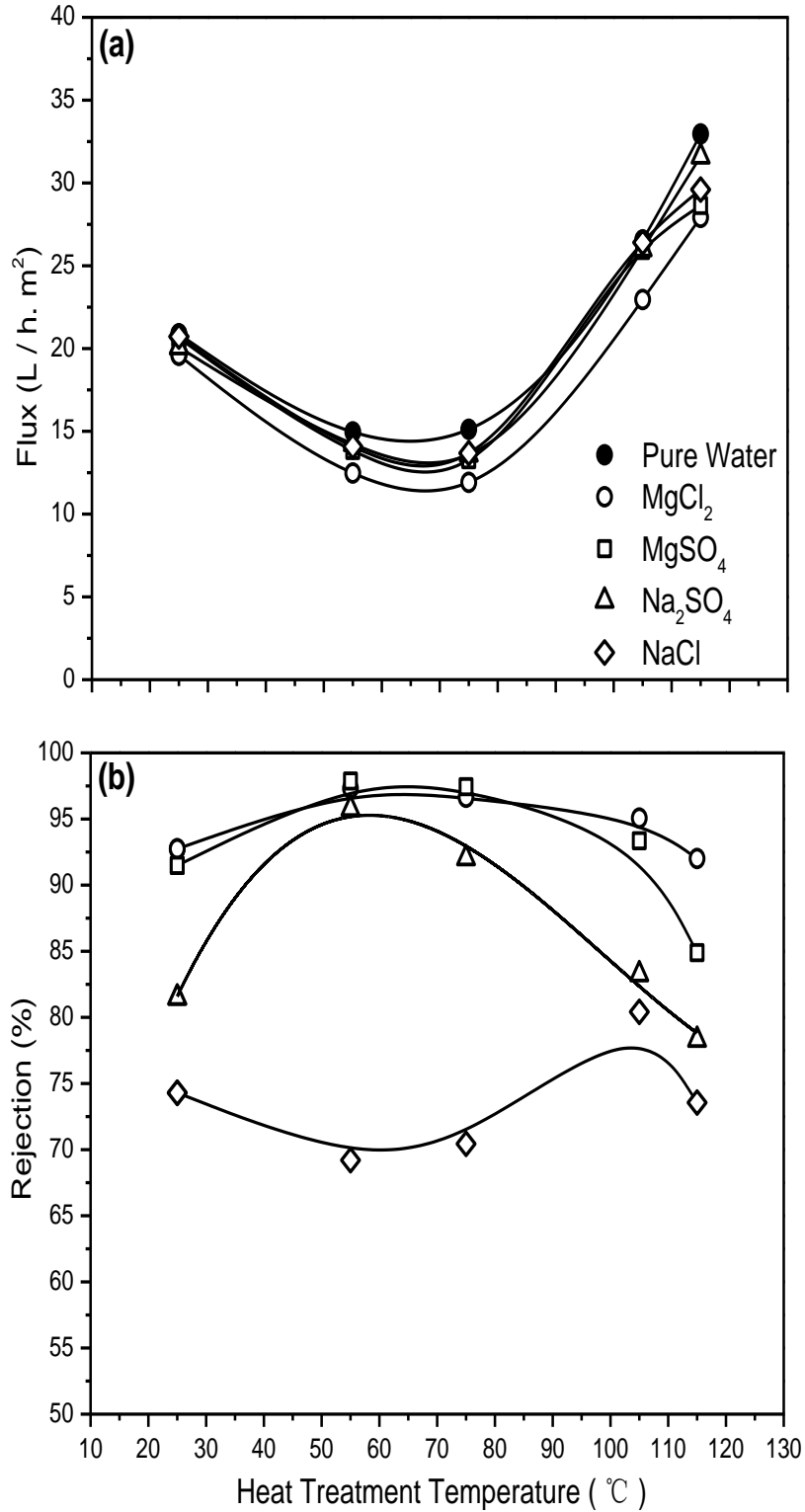
Figure 3.20 Effects of heat treatment temperature on (a) permeation flux and (b) salt rejection for (PEI/TMC) membrane (Operating pressure: 0.8 MPa gauge; Salt concentration: 500 ppm; Temperature: 23°C).

Compared to membranes formed at room temperature, the permeation flux is decreased by heat treatment, and when the heat treatment temperature is high enough, a further increase in the heat treatment temperature will yield an increase in the permeation flux. An opposite trend in the salt rejections is observed for solutes $MgCl_2$, $MgSO_4$ and Na_2SO_4. These results are consistent with the experimental data of Zhang *et al.* [2012] who used piperazine and TMC to form interfacially polymerized membranes. This suggests that the heat treatment of membranes needs to be carried out at appropriate temperatures in order to improve the membrane performance. Proper heat treatment will facilitate interfacial polymerization and lead to a more cross-linked structure, resulting in an increased rejection and a decreased flux. If, however, the heat treatment temperature is too high, the polyamide skin layer will shrink. Because of its ultrathin structure, the thermal shrinkage may cause defects in the skin layer, which compromises salt rejection. An optimization of the heat treatment conditions, which is a subject of further study, will be needed to determine the most suitable parameters for membrane fabrication.

It is interesting to note that unlike solutes $MgCl_2$, $MgSO_4$ and Na_2SO_4 that involve divalent cations or anions, the membrane rejection to NaCl behaved differently as the heat treatment temperature varied. The NaCl rejection did not change drastically over the range of heat treatment temperature (25-105°C) tested. Nonetheless, it is shown that if the heating temperature is high enough, the membrane rejection to NaCl is also affected adversely.

The membranes were shown to be stable. There was no noticeable change in the membrane performance after nanofiltration tests with various solutes. For instance, pristine membrane PES-(PEI/TMC)$_4$ showed a water flux of 19.2 L/(m^2.h) and $MgCl_2$ rejection of 95%, and after extensive tests with various solutes (e.g., NaCl, $MgSO_4$ and Na_2SO_4 at different concentrations)

for over 3 weeks, the membrane maintained essentially the same nanofiltration performance (water flux 19.0 L/(m^2.h) and MgCl$_2$ rejection of 95%).

3.3.3 Membrane performance at different operating conditions

Figures 3.21(a) and (b) show permeation flux and salt rejection of a (PEI/TMC) membrane at different feed concentrations. The concentrations of PEI and TMC reactants in their solutions were 2.0 wt% and 0.4 wt%, respectively, during the interfacial polymerization for composite membrane fabrication. All the membranes used in this section were formed under these reactants concentrations.
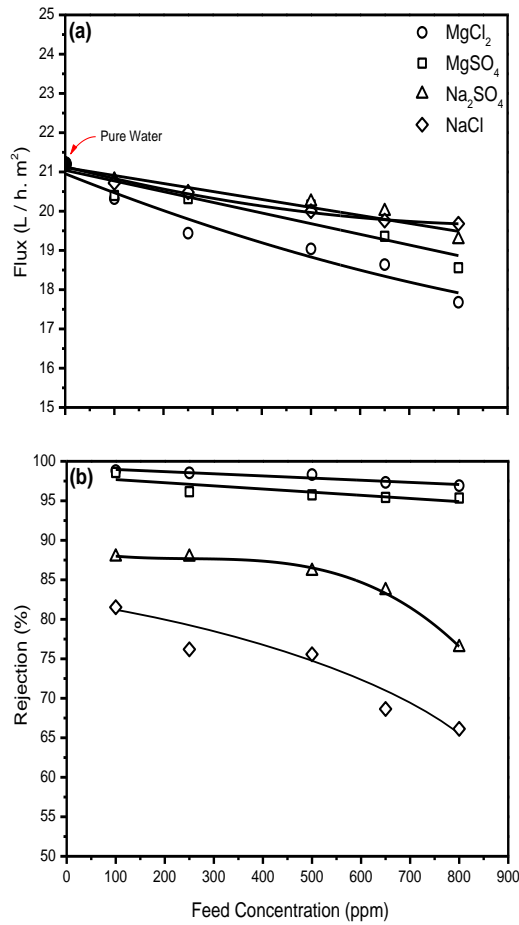
Figure 3.21 Permeation flux (a) and salt rejection (b) of a (PEI/TMC) membrane at different feed concentrations (Operating pressure: 0.8 MPa gauge; Temperature: 23°C).

81

Both permeation flux and salt rejection decreased with an increase in the salt concentration in the feed. It is known that the osmotic pressure will increase with an increase in the salt concentration of the feed solution. For the low concentration salt solution, the osmotic pressure π can be approximated using the Morse equation [Sourirajan and Matsuura, 1985]:

$$\pi = imRT \tag{3.3}$$

where i is the total number of moles of ions given by one mole of the salt, m is the solute molality, R is the gas constant, T is the temperature. At a given temperature, with every 1000 ppm (i.e., 1g/L) increase in the salt concentration in the feed, the increase in the osmotic pressure follows the order of $NaCl > MgCl_2 > Na_2SO_4 > MgSO_4$, as illustrated in Table 3.3. However, the decrease in permeation flux followed the order of $MgCl_2 > MgSO_4 > Na_2SO_4 \approx NaCl$ (see Figure 3.21(a)), and the decrease in salt rejection followed the order of $NaCl > Na_2SO_4 > MgSO_4 \approx MgCl_2$ (see Figure 3.21(b)). Hence, the decreases in permeation flux and salt rejection cannot be attributed merely to the effects of osmotic pressure.

Table 3.3 Increment of osmotic pressure increase with every 1000 ppm increase in the salt concentration in the feed at a given temperature

	$MgCl_2$	$MgSO_4$	Na_2SO_4	NaCl
i	3	2	3	2
Molecular Weight (g/mol)	95	120	142	58.5
$\Delta\pi$/1000 ppm	3/95 = 0.03158	2/120 = 0.01667	3/142 = 0.02113	2/58.5 = 0.03419

To further study the effects of feed concentration on the membrane performance, the mass transfer coefficient k and salt transport parameter B were evaluated based on the transport equations proposed by Sourirajan and Matsuura [1985]:

$$A = (PWP)/(3600M_wS\Delta P) \tag{3.4}$$

$$N_w = A[\Delta P - \pi(x_{sb}) + \pi(x_{sl})] \tag{3.5}$$

$$N_w = B(\frac{1-x_{sl}}{x_{sl}})(\rho_b x_{sb} - \rho_l x_{sl}) \tag{3.6}$$

$$N_w = k\rho_0(1 - x_{sl})\ln\frac{(x_{sb}-x_{sl})}{(x_{s0}-x_{sl})} \tag{3.7}$$

where A is pure water permeability constant (mol/m^2.s.MPa), PWP is pure water permeation rate through given area of membrane surface (kg/h), M_w is molecular weights of water (kg/mol), S is effective membrane area (m^2), ΔP is pressure difference across the membrane (MPa), N_w is mole permeation flux of water through membrane (mol/m^2.s), x_s is mole fraction of salt, x_{s0}, x_{sb} and x_{sl} are mole fraction of feed solution, concentrated boundary solution and the permeated product solution, respectively, $\pi(x_s)$ is osmotic pressure (MPa) corresponding to mole fraction of salt x_s, B is salt transport parameter (m/s), ρ is molar density (mol/m^3), k is mass transfer coefficient for the salt on the high pressure side of the membrane (m/s).

Figures 3.22(a) and (b) show the values of k and B at different feed concentrations for a (PEI/TMC) membrane. The value of k reflects the concentration polarization on the feed side of the membrane. The data in Figure 3.22(a) indicate that the values of k for $MgSO_4$ and $MgCl_2$ are smaller than those for Na_2SO_4 and NaCl, which explains the more significant flux decline for $MgSO_4$ and $MgCl_2$. The quantities of B are characteristics of the membrane to salt transport. It is a function of the chemical nature of the salt, membrane material and the pore size on the membrane surface. A lower value of B indicates less salt transport through the membrane and thus a higher solute rejection. From Figure 3.22(b), we can see that the values of B follow the order of $MgCl_2 < MgSO_4 < Na_2SO_4 < NaCl$, which was in accordance with the reversed order in salt rejection shown in Figure 3.21(b). With an increase in salt concentration in the feed, the value of B increases, which means more salt will pass through the membrane, leading to a

reduced salt rejection. Furthermore, there is a linear relationship between log((B) and log(feed molality) for $MgCl_2$, Na_2SO_4 and NaCl, but not for $MgSO_4$, as shown in Figure 3.22(b). These results are consistent with Yeager *et al.* [1981].
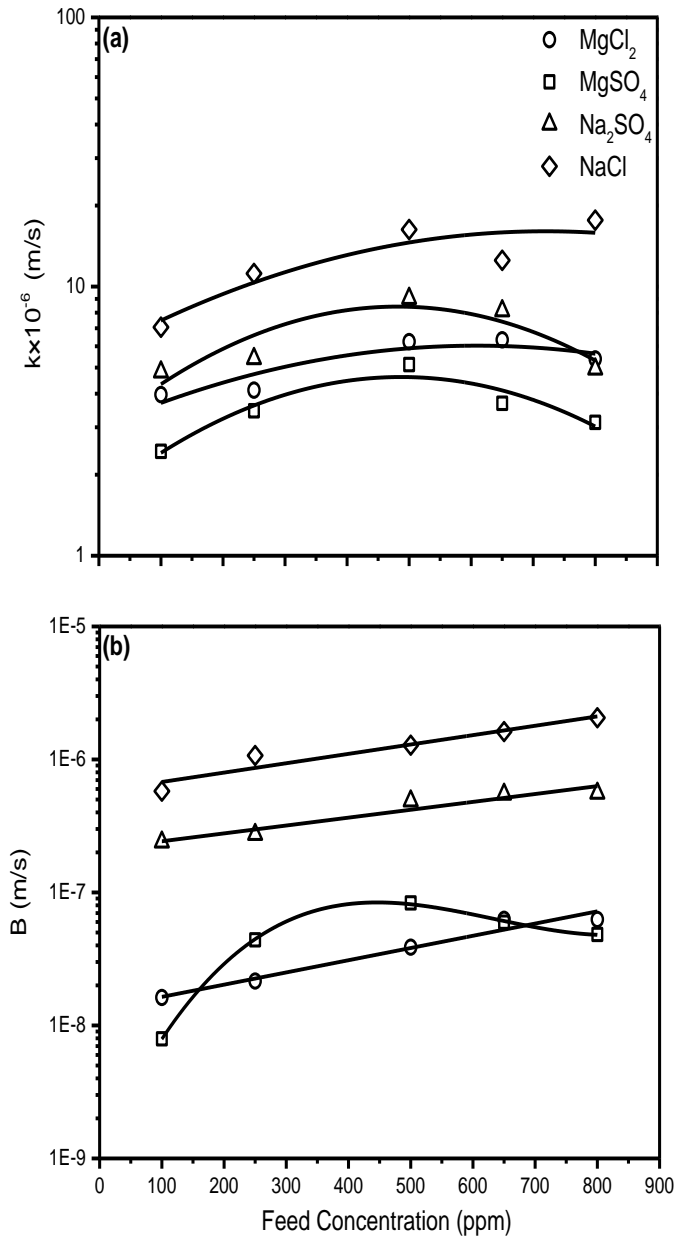
Figure 3.22 Values of mass transfer coefficient k (a) and salt transport parameter B (b) of a (PEI/TMC) membrane at different feed concentrations (Operating pressure: 0.8 MPa gauge; Temperature: 23°C).

Figures 3.23(a) and (b) show permeation flux and salt rejection of a (PEI/TMC) membrane at different operating pressures. As expected, the permeation fluxes increased linearly with an increase in the operating pressure. For the (PEI/TMC) membrane, the value of A, which measures the water permeability, is 0.54 (mol/m^2.s.MPa). This value is very close to the water permeability for the aqueous solute solutions due to the low solute concentrations in the feed. In addition, the linearity also indicates that the thin film composite membranes are mechanically stable under pressure, at least within the experimental range studied.
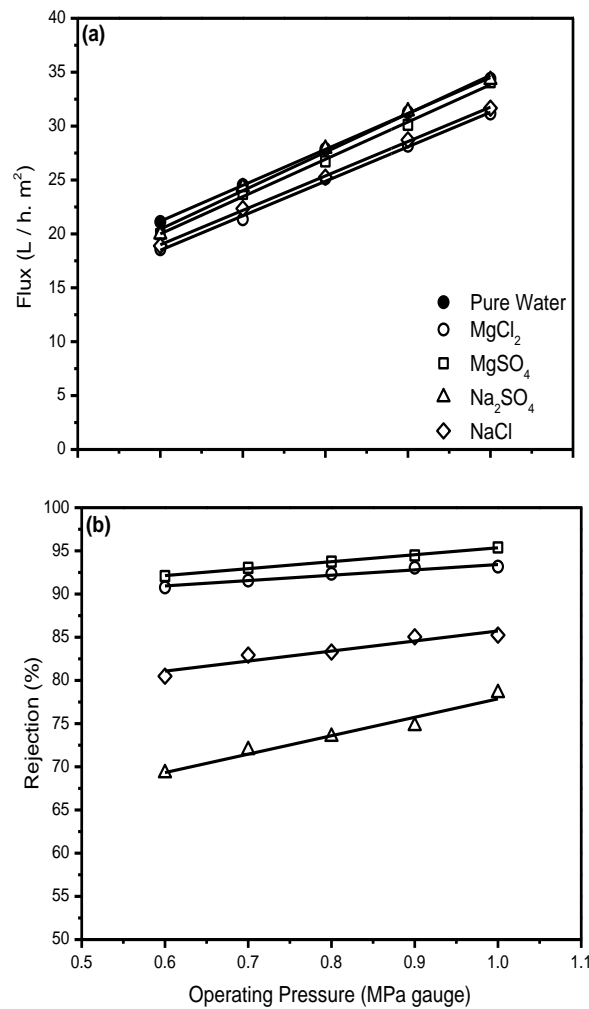
Figure 3.23 Permeation flux (a) and salt rejection (b) of a (PEI/TMC) membrane at different operating pressures (Salt concentration: 500 ppm; Temperature: 23°C).

The salt rejection also increased with an increase in the operating pressure. There are two competing factors dictating the separation behavior of the solutes with an increase in the operating pressure. On the one hand, the water flux increases due to the increased driving force, resulting in lower ion concentrations in the permeate (so-called "dilute effect"). On the other hand, more ions are transported from the bulk solution toward the membrane surface by convection as permeate flux increases, which enhances concentration polarization and subsequently reduces ion rejection [Seidel *et al.*, 2001]. From the calculation, the values of k are always large ($8\text{-}154 \times 10^{-6}$ m/s) within the experimental range. Therefore, there is no significant concentration polarization on the feed side, and the "dilute effect" played a dominant role for the separation, hence resulting in an increase in the salt rejections.

The performance of the (TMC/PEI) membrane at different feed concentrations is shown in Figure 3.24. The permeation flux declines with an increase in feed concentration, and the flux decrease follows the order of $MgCl_2 > NaCl \approx MgSO_4 > Na_2SO_4$. The most significant flux decrease is observed for solute $MgCl_2$, and it can be also attributed to the relatively low value of k. The variations in the value of B with feed concentrations for the (TMC/PEI) membrane are similar to those for (PEI/TMC) membrane.
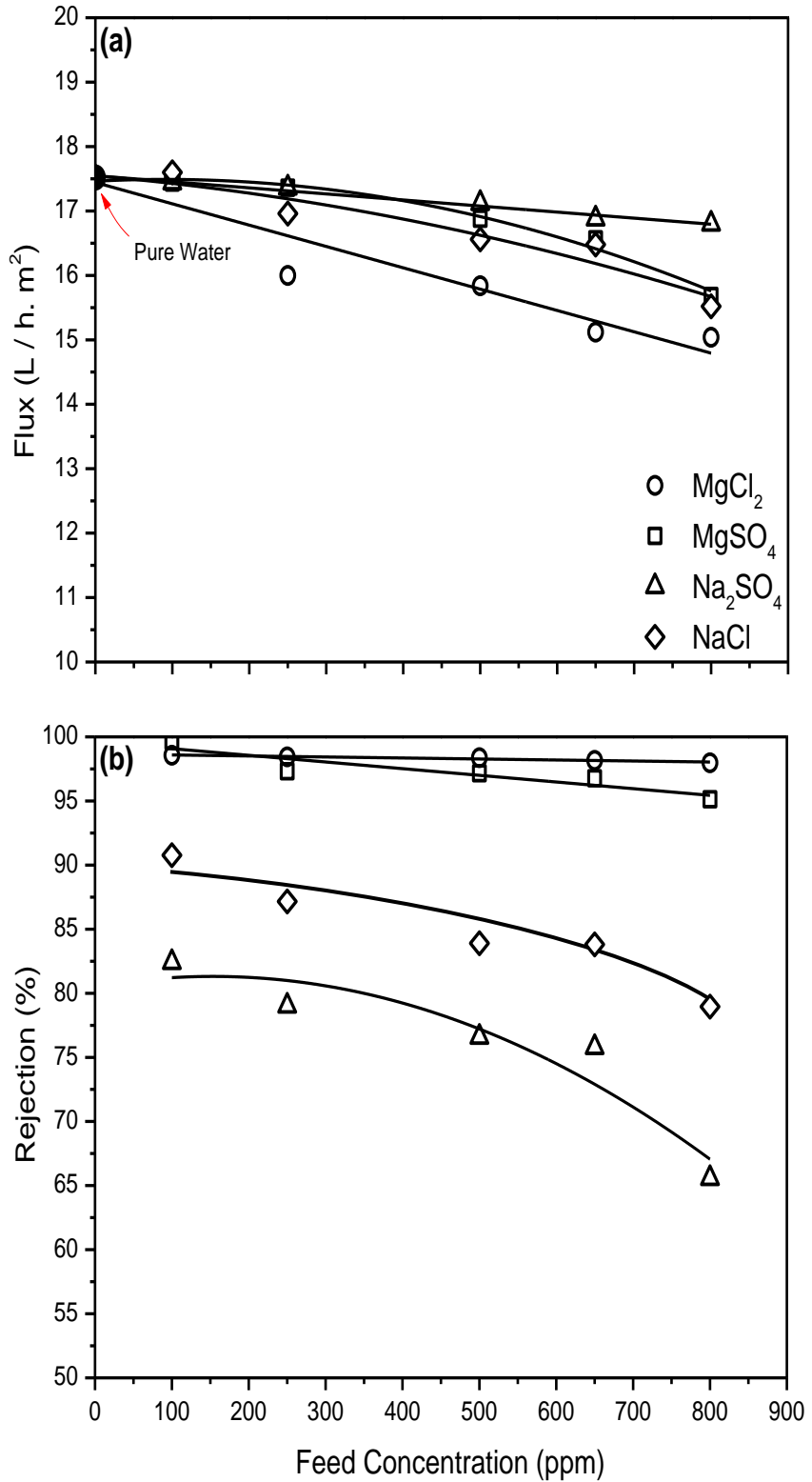
Figure 3.24 Permeation flux (a) and salt rejection (b) of a (TMC/PEI) membrane at different feed concentrations (Operating pressure: 0.8 MPa gauge; Temperature: 23°C).

Figures 3.25(a) and (b) show the permeation flux and salt rejection for the (TMC/PEI) membrane at different operating pressures. The effects of operating pressure on the membrane performance are similar to those for (PEI/TMC) membrane. The A value was determined to be 0.45 (mol/m^2.s.MPa), and this membrane is less permeable than the (PEI/TMC) membrane.
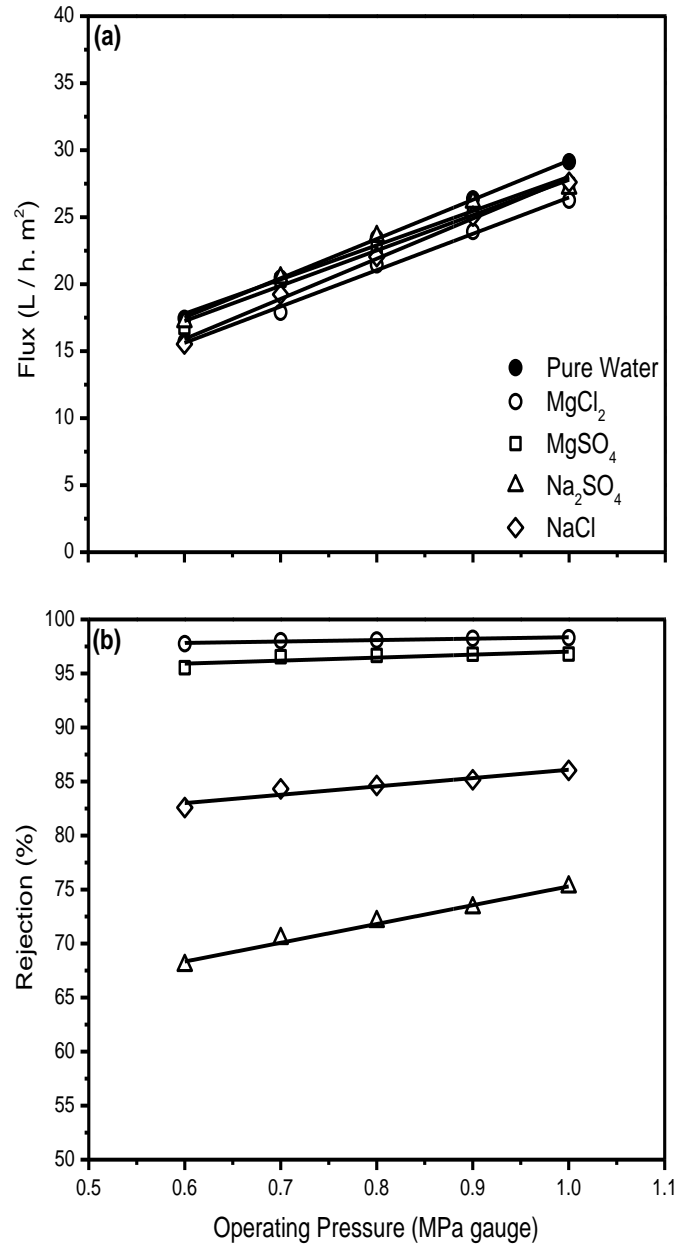
Figure 3.25 Permeation flux (a) and salt rejection (b) of a (TMC/PEI) membrane at different operating pressures (Salt concentration: 500 ppm; Temperature: 23°C).

3.4 Conclusions

Positively charged polyamide thin-film composite nanofiltration membranes were synthesized by interfacial polymerization from polyethylenimine and trimesoyl chloride. The composite membranes were characterized by ATR-FTIR, contact angle measurements, streaming Zeta potential, FE-SEM and AFM. The effects of parameters involved in the membrane fabrication on the separation performance of the membranes were investigated, including the number of cycles of reactant depositions, sequence of reactant depositions, concentration of reactants and the temperature of heat treatment. The influence of operating conditions on the membrane performance, including the feed concentration and operating pressure, was also studied. The following conclusions can be drawn:

(1) The composite membranes fabricated using a PEI-TMC deposition sequence had evenly distributed valley-ridge morphology on the membrane surface, while reversing the reactant deposition sequence (i.e., TMC-PEI) yielded membranes with irregularly distributed nodular structures on the membrane surface.

(2) Increasing the number of cycles of sequential reactant depositions for layer-by-layer buildup, thicker and more compact polyamide top layers could be produced with both reactant deposition sequences. In general, membranes formed by the PEI-TMC deposition sequence were more permeable than membranes formed by the TMC-PEI deposition sequence.

(3) Increasing the reactant concentrations could also form thicker and more compact skin layers, resulting in a decreased permeation flux and an increased salt rejection. At a reactant concentration of 3.5 wt% for PEI and 0.7 wt% for TMC, membrane (PEI/TMC) showed a high salt rejection(95.1% for $MgCl_2$, 94.4% for $MgSO_4$, 80.5% for Na_2SO_4 and 85.1% for

NaCl) with the water permeation flux of 24.5 $L/(m^2.h)$ at 0.8 MPa feed pressure.

(4) The stability and salt rejection of (PEI/TMC) polyamide composite membrane were improved by proper heat treatment. The permeation flux decreased and the salt rejection increased after the membrane was thermally treated at 55°C. However, if the heat treatment temperature was too high, the salt rejection would be affected negatively.

(5) Operating conditions influenced the separation performance. The permeation flux and salt rejection decreased with an increase in the salt concentration in the feed for both (PEI/TMC) and (TMC/PEI) membranes. An opposite trend in the permeation flux and salt rejection was observed when the operating pressure was increased.

Chapter 4.

Thin film composite NF membranes formed from polymeric amine PEI imbedded with monomeric amine PIP and TMC[∗]

4.1 Introduction

The preparation of TFC nanofiltration membranes is mainly based on interfacial polymerization, and many efforts have been made to tailor the structures and properties of polyamide-based TFC membranes to improve the separation performance of the membranes. One approach is to synthesize new monomers for TFC membrane formation based on molecular design. Both new amine monomers (e.g., N-aminoethyl piperazine propane sulfonate [An *et al.*, 2013], 2,5-bis(4-amino-2-trifluoromethyl-phenoxy) benzenesulfonic acid [Liu *et al.*, 2012b], 4,4-bis(4-amino-2-trifluoromethyl-phenoxy) biphenyl-4,4-disulfonic acid [Liu *et al.*, 2012b] , disulfonated bis[4-(3-aminophenoxy)phenyl] sulfone [Xie *et al.*, 2012]) and acyl chloride monomers (e.g., cyclohexane-1,3,5-tricarbonyl chloride [Yu *et al.*, 2009b], 5-chloroformyloxy-isophthaloyl chloride [Liu *et al.*, 2009], isomeric biphenyl tetraacyl chloride [Li *et al.*, 2008]) have been synthesized and used as the reactive monomers for interfacial polymerization. Another approach is to tailor the membrane structures by such post modifications as surface coating [Wu *et al.*, 2010a], radical grafting [Wei *et al.*, 2010], plasma-induced polymerization [Zou *et al.*, 2011] and ion implantation [Mukherjee *et al.*, 2005]. Moreover, incorporation of titanium dioxide [Lee *et al.*, 2008], lithium bromide [Tang *et al.*,

---

[∗] Portions of this work have been published in *React. Funct. Polym.*, 86 (2015) 168-183.

2010] and poly(vinyl alcohol) [An *et al.*, 2011] into the effective skin layer of the membrane during interfacial polymerization has also been carried out to enhance water permeability, salt rejection and antifouling properties.

From the study in Chapter 3, it appeared that polyethylenimine (PEI) is a reactive amine used in interfacial polymerization and the PEI-based TFC membranes showed good nanofiltration performance. In addition to PEI, piperazine (PIP) is another popular amine reactant for fabrication of TFC membranes. Many efforts have been made on controlling and optimizing the formation conditions of piperazine-based membranes and their properties [Cadotte *et al.*, 1979; Cadotte *et al.*, 1981; Kamiyama *et al.*, 1986; Fibiger *et al.*, 1988]. The commercialized PIP/TMC membranes include NS-300, NF, XP, NTR and UTC series membranes, which have been mentioned in Chapter 1. At present, the studies have been expanded to produce novel nanofiltration membranes using this traditional amine [Wang *et al*., 2011a, 2013].

Both PEI and PIP performed well in interfacial polymerization for preparation TFC membranes. However, these two amines have their distinctive characteristics. Due to its macromolecular structure, PEI has a lower reactivity. Therefore, the relatively slow rate of interfacial reaction between PEI and an acyl chloride allows the membrane formation to be controlled more easily. However, the effective layer of the resulting membrane tends to have a loose structure as compared to membranes formed from molecular PIP and an acyl chloride. Therefore, in this chapter, it was decided to use a blend of polymeric amine (PEI) and monomeric amine (PIP) as the aqueous phase reactant and trimesoyl chloride (TMC) as the organic phase reactant for interfacial polymerization. This approach has several potential advantages: (1) the polymer links formed from PIP and TMC, which occurs faster than the PEI-

TMC macromolecular links, will be embedded and anchored in the macromolecular matrixes, thereby enhancing the membrane stability, and (2) the properties of the membrane can be tailored by adjusting the composition of the amine reactants. The sequence of reactant deposition onto the substrate (i.e., amine-acyl chloride or acyl chloride-amine) involved in the interfacial polymerization was also studied to get an insight into the membrane formation.

It should be mentioned that PEI-based TFC membranes are generally positively charged (see Figure 3.5) while PIP-based polyamide layers are negatively charged [Eriksson, 1988]. Due to the Donnan exclusion, the PEI-based TFC membranes tend to have a higher rejection to salts with multivalent cations and monovalent anions (e.g., $MgCl_2$) and a lower rejection to salts having multivalent anions and monovalent cations (e.g., Na_2SO_4). Therefore, an attempt was also made in this study to develop NF membranes with two-plies of polyamide layers comprising of a positively-charged PEI-TMC polyamide layer and a negatively-charged PIP-TMC polyamide layer (Figure 4.1). The multiple-layered polyamide TFC membranes were prepared by two cycles of interfacial polymerization, and two series of membranes (one with a PEI-TMC under-layer and a PIP-TMC top-layer, and the other with a PIP-TMC under-layer and a PEI-TMC top-layer) were prepared to investigate the effect of the membrane structure on NF performance.

The surface properties of the membranes (i.e., chemical composition, surface hydrophilicity, charge, and morphology) of the polyamide selective layer were also characterized and the NF performance of the membranes was evaluated using $MgCl_2$, $MgSO_4$, Na_2SO_4 and NaCl as representative solute salts.
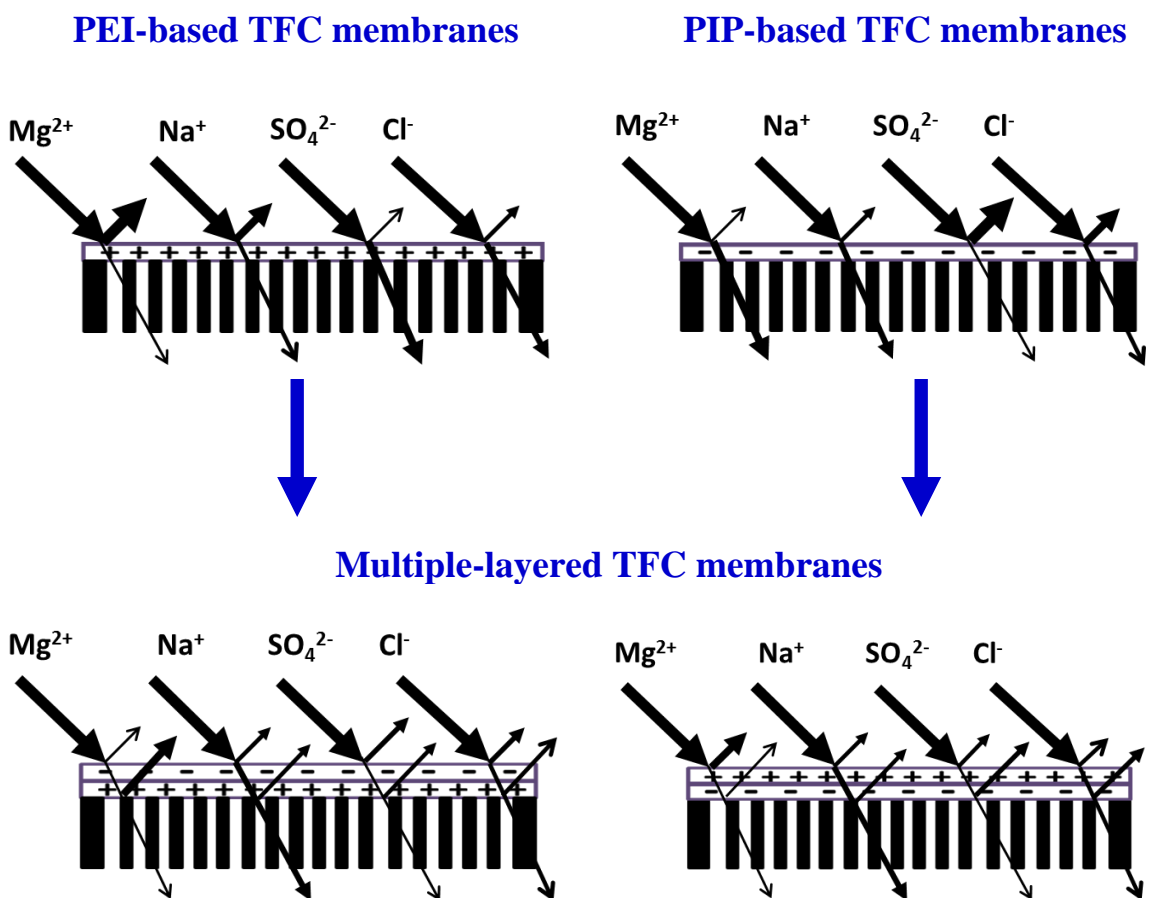
Figure 4.1 Schematic diagram showing the structures of 2-ply polyamide TFC membranes and ion transport through the membranes.

4.2 Experimental

Piperazine (PIP) was purchased from Sigma-Aldrich. Other materials used were the same as described in Chapter 3. Two series of TFC membranes were prepared in this chapter, i.e., membranes with a single polyamide layer and membranes with a two-ply polyamide layer. For the formation of single polyamide layer membranes, the aqueous phase reactant solution was prepared by dissolving predetermined amounts of polyethylenimine (PEI) and piperazine (PIP) in de-ionized water to form a homogeneous solution. The overall concentration of amine (i.e., the total concentration of PEI and PIP) was kept at 3.0 wt%, while the compositions of the

amine mixtures varied from $PEI_{3.0}$-PIP_0, $PEI_{2.7}$-$PIP_{0.3}$, $PEI_{2.4}$-$PIP_{0.6}$, $PEI_{2.1}$-$PIP_{0.9}$, $PEI_{1.8}$-$PIP_{1.2}$, $PEI_{1.5}$-$PIP_{1.5}$, $PEI_{1.2}$-$PIP_{1.8}$, $PEI_{0.9}$-$PIP_{2.1}$, $PEI_{0.6}$-$PIP_{2.4}$, $PEI_{0.3}$-$PIP_{2.7}$ to PEI_0-$PIP_{3.0}$ for different membranes. The subscripts in the membrane designations denote the reactant concentration (in wt%) used in the interfacial polymerization. The pH of the aqueous solutions was about 9.5. The organic phase reactant solution was composed of 0.6 wt% TMC in hexane. The procedures are the same as what was described in section "Preparation of TFC membrane with one polyamide layer" in Chapter 3 except the temperature of heat treatment was changed to 75 °C. The interfacial polymerization was also carried with a reversed sequence of depositions of the reactants onto the substrate, i.e., TMC-(PEI-PIP). The chemical reactions between the amines (i.e., PEI and PIP) and TMC to form polyamides with different chemical structures are illustrated in Figure 4.2.

For the formation of two-ply polyamide layer membranes, two cycles of interfacial polymerization were proceeded. The PES substrate membrane was allowed to contact with an aqueous solution of PEI and then with the TMC solution, thereby forming an interfacially polymerized layer with PEI/TMC crosslinks. Then the membrane was allowed to contact sequentially with an aqueous solution of PIP and TMC to form a second polyamide layer with PIP/TMC crosslinks. The membranes so formed with two plies of polyamide layers were designated as [(PEI/TMC)-(PIP/TMC)]. The membrane formation could also start with interfacial reaction between PIP and TMC, followed by interfacial polymerization of PEI/TMC; such membranes are designated as [(PIP/TMC)-(PEI/TMC)].
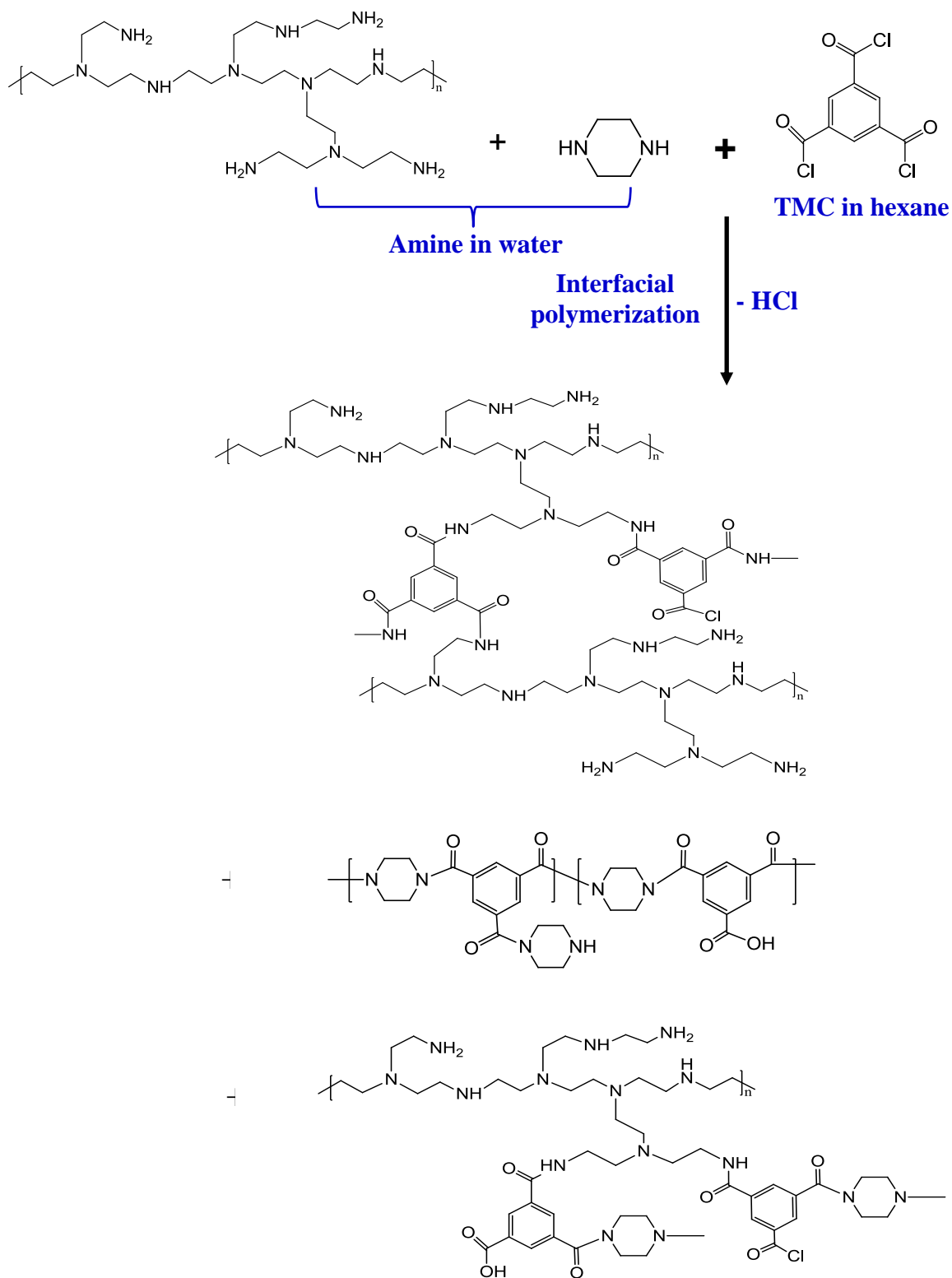
Figure 4.2 Interfacial polymerization between amine mixtures (i.e., PEI+PIP) and TMC for polyamide formation.

The concentration of TMC in the solution was 0.3 wt% for both interfacial reaction cycles. The concentrations of PEI and PIP in their aqueous solutions varied, but the total amine concentration (i.e., the sum of PEI concentration and PIP concentration) was 3.0 wt% for convenience of comparison with the single-ply membranes formed with mixed amines. The procedures are the same as what was described in section "Preparation of TFC membrane with multiple polyamide layer" in Chapter 3 while the temperature of heat treatment was also changed to 75 °C. Based on the sequence of reactant depositions, compositions of the reactants, and the number of interfacially formed polyamide layers in the composite membranes, the designations of the membranes used in this chapter are shown in Table 4.1.

The membrane characterizations (including ATR-FTIR, contact angle test, Zeta potential, FE-SEM and AFM), experimental set up and separation performance measurements are similar as described in Chapter 3.

4.3 Results and discussion

4.3.1 TFC NF membranes with a single layer of polyamide

Chemical composition of polyamide layer

The ATR-FTIR was employed to analyze the chemical composition of the top surface of the composite membrane. Figure 4.3 shows the ATR-FTIR spectra of the pristine PES substrate and thin film composite membranes formed from PEI, mixed amines and PIP. Compared to the PES substrate (Figure 4.3(a)), two new bands at 1640 and 1545 cm^{-1} appeared on the ATR-FTIR spectra for membrane [PEI$_{3.0}$/TMC$_{0.6}$] (Figure 4.3(b)), which are characteristics of the amide-I (C=O stretching) band and the amide-II (N-H) band of the amide groups (-CONH-) formed from PEI and TMC. The band at 1610 cm^{-1} is associated with the hydrogen-bonded C=O of the amide. For membrane [PIP$_{3.0}$/TMC$_{0.6}$] (Figure 4.3 (e)), there is only one band at

around 1629 cm^{-1} for amide-I (C=O stretching) but no band was observed for amide-II (N-H).

This is consistent with the chemical structure of a tertiary amide (-CONR-) without amidic

hydrogen formed from PIP and TMC.

Table 4.1 Designation of membranes based on reactant deposition sequence, concentration of reactant and the number of interfacially formed polyamide layers

Number of polyamide layer	Membrane designation	Description
1-ply[1]	[PEI$_{3.0}$/TMC$_{0.6}$]	One ply of polyamide layer formed from interfacial reaction of surface-deposited PEI (solution concentration 3.0 wt%) with TMC
	[(PEI$_a$–PIP$_b$)/TMC$_{0.6}$]	One ply of polyamide layer formed from interfacial reaction of surface-deposited amine mixture of PEI and PIP with TMC; "a" and "b" are concentrations of PEI and PIP in the amine solution, respectively
	[PIP$_{3.0}$/TMC$_{0.6}$]	One ply of polyamide layer formed from interfacial reaction of surface-deposited PIP (solution concentration 3.0 wt%) with TMC
	[TMC$_{0.6}$/PEI$_{3.0}$]	One ply of polyamide layer formed from interfacial reaction of surface-deposited TMC with PEI (solution concentration 3.0 wt%)
	[TMC$_{0.6}$/(PEI$_a$–PIP$_b$)]	One ply of polyamide layer formed from interfacial reaction of surface-deposited TMC with an amine mixture; "a" and "b" are concentrations of PEI and PIP in the solution, respectively
	[TMC$_{0.6}$/PIP$_{3.0}$]	One ply of polyamide layer formed from interfacial reaction of surface-deposited TMC with PIP (solution concentration 3.0 wt%)
2-ply[2]	[(PEI$_a$/TMC$_{0.3}$)-(PIP$_b$/TMC$_{0.3}$)]	2-ply polyamide layer comprising of a first ply of PEI/TMC crosslinks and a second ply of PIP/TMC crosslinks; "a" and "b" are concentrations of PEI and PIP in their solutions
	[(PIP$_a$/TMC$_{0.3}$)-(PEI$_b$/TMC$_{0.3}$)]	2-ply polyamide layer comprising of a first ply of PIP/TMC crosslinks and a second ply of PEI/TMC crosslinks; "a" and "b" are concentrations of PIP and PEI in their solutions

[1] The TMC concentration was 0.6 wt%
[2] The TMC concentration was 0.3 wt% for every ply
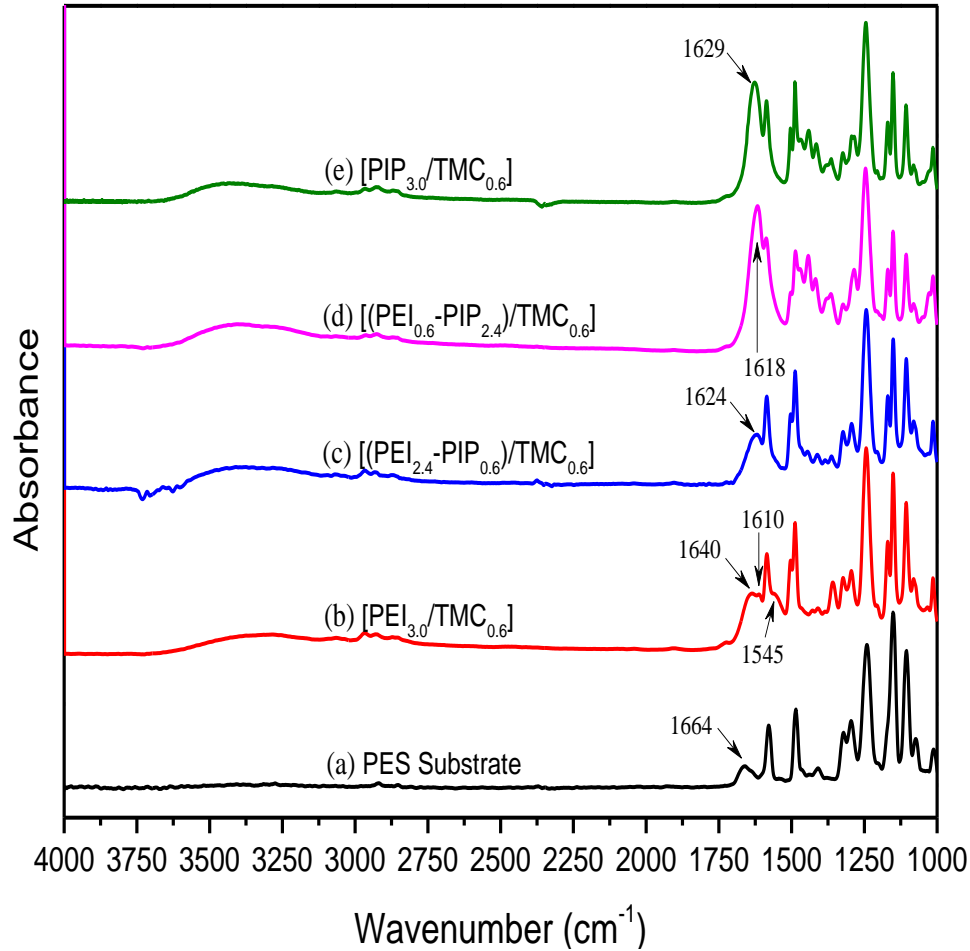
Figure 4.3 ATR-FTIR spectra of (a) PES substrate and single-ply polyamide composite membranes: (b) [$PEI_{3.0}$/$TMC_{0.6}$], (c) [($PEI_{2.4}$-$PIP_{0.6}$)/$TMC_{0.6}$], (d) [($PEI_{0.6}$-$PIP_{2.4}$)/$TMC_{0.6}$] and (e) [$PIP_{3.0}$/$TMC_{0.6}$].

Surface hydrophilicty/hydrophobicity

The surface hydrophilicity of the membranes is evaluated with contact angle measurements.

Figure 4.4 shows the contact angles of the polyamide nanofiltration membranes prepared by

interfacial polymerization from mixed amines of PEI and PIP at different compositions with a

reactant deposition sequence of (PEI+PIP)-TMC. It should be pointed out that the PES

substrate had a contact angle of 86°, and it dropped to 75° after a polyamide layer was formed

on the membrane surface. However, when the PIP concentration in the mixed amine increased

from 0 to 3.0 wt% (that is, the PEI concentration decreased from 3.0 wt% to 0), there was no change in the contact angle. This indicates that the surface hydrophilicity of the polyamide surface layer formed by reacting TMC with the polymeric amine PEI, monomeric amine PIP, or their mixtures at different compositions, is essentially the same.
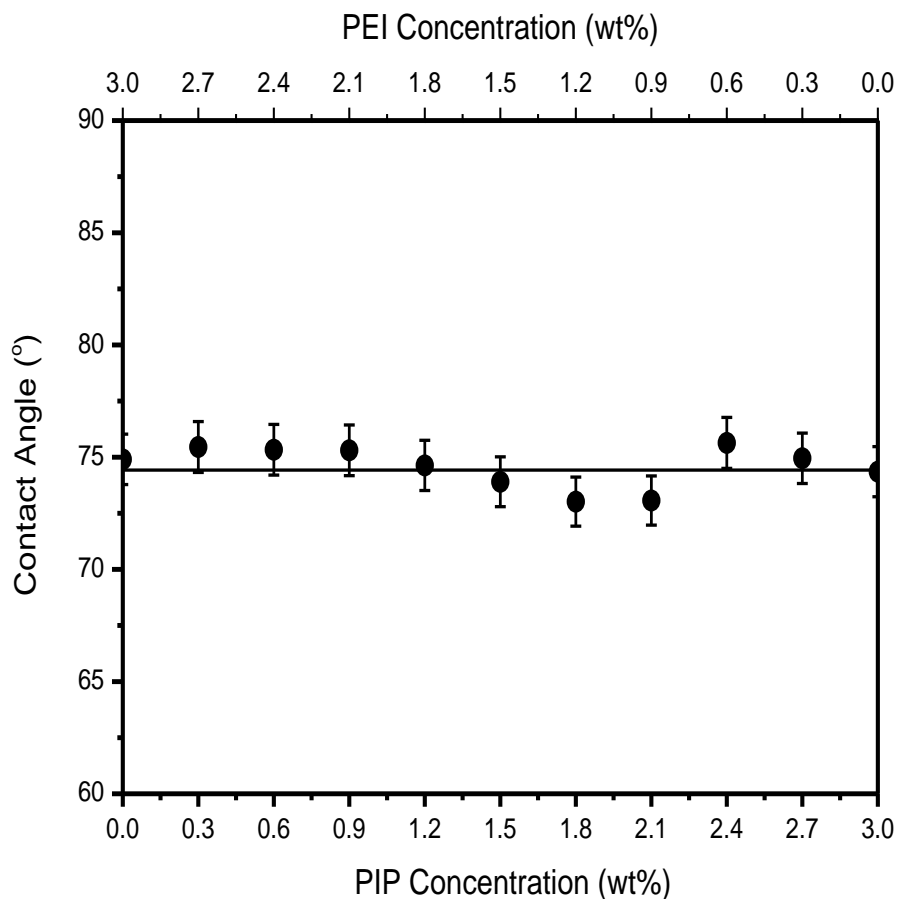
Figure 4.4 Contact angle of water on the surface of single-ply polyamide membranes prepared from reaction of amine mixtures (i.e., PEI+PIP of different compositions) with TMC.

Surface charge

The surface charge characteristics of the membranes were studied in terms of Zeta potential. Figure 4.5(a) shows the Zeta potentials on the membrane surface measured at various pH

values for the polyamide TFC NF membranes formed with PEI, PIP and their mixtures. From Figure 4.5(a), we can find a certain pH value at which the membranes showed no net electrical charge (i.e., Zeta potential of 0 MV). This pH values are the isoelectric points (IEP) of the membranes, which are shown in Figure 4.5(b). The membrane formed from TMC and polymeric amine PEI (i.e., membrane [$PEI_{3.0}$/$TMC_{0.6}$]), which has an isoelectric point of 7.76, is indeed positively charged at the NF performance testing conditions (pH=6.8-7.2). On the other hand, the membrane formed from TMC and monomeric amine PIP (i.e., membrane [$PIP_{3.0}$/$TMC_{0.6}$]) has an isoelectric point of 4.51, and its surface is thus negatively charged under the testing conditions. These results are in agreement with common observations. It is, however, interesting to notice that when a small amount of PIP was present along with PEI for interfacial polymerization with TMC, the membrane surface became more positively charged. Among the membranes tested, membrane [($PEI_{2.7}$-$PIP_{0.3}$)/$TMC_{0.6}$] showed an isoelectric point of 10.0. As the PIP content in the mixed amines continued to increase, the isoelectric point of the resulting membrane decreased.

The above results are not unexpected. It has been illustrated in Figure 3.5 that the PEI-based membrane surface has positive charges due to unreacted primary amines in polyamide membranes, and similar results have also been reported recently by Chung and co-workers [Sun *et al.*, 2012]. When a small amount of PIP was present along with PEI for interfacial reaction with TMC, the reaction between PIP and TMC will occur preferentially over the PEI-TMC reaction because the small PIP molecules have a higher reactivity and mobility than the macromolecular amine PEI. The polymer links formed by PIP-TMC will thus be embedded in the branched PEI macromolecules, and the PIP-TMC polyamide anchored in PEI will restrict the mobility of the polymer chains as well as the diffusivity of TMC molecules across the

interface between the two reacting phases. As such, it becomes more difficult for TMC molecules to access the amines in PEI chains. Therefore, more primary amines in PEI will be left unreacted, resulting in more positive charges on the membrane surface. The ATR-FTIR spectra for membranes [(PEI$_{3.0}$/TMC$_{0.6}$] (Figure 4.3(b)) and [PIP$_{3.0}$/TMC$_{0.6}$] (Figure 4.3(e)) also support the above hypothesis, as shown by the higher band intensity of the amide-I (C=O stretching) in [PIP$_{3.0}$/TMC$_{0.6}$] membrane. However, when the PIP content is sufficiently high, the contribution of negative surface charges from PIP-TMC polyamide will be significant, and the carboxyl groups (-COO$^-$) resulting from the hydrolysis of unreacted acyl chloride (-COCl) also contribute to negative charges on the membrane surface. It can thus be concluded that by controlling the composition of the PIP/PEI mixed amines, the TFC membranes can be tailored to achieve desired surface charge properties (i.e., highly positive, neutral, or highly negative) appropriate for target solutes.

Surface morphology

The surface morphologies of the membranes were examined using FE-SEM, and they are shown in Figure 4.6. Membranes formed from PEI, PIP and mixed amines have different surface morphologies. For instance, membrane [PEI$_{3.0}$/TMC$_{0.6}$] has a quite smooth and uniform surface with occasional small debris (Figure 4.6(a)), and a larger "patch-like" structure is formed on the membrane surface when the amine reactant contained 30 wt% of PIP (i.e., membrane [(PEI$_{2.1}$-PIP$_{0.9}$)/TMC$_{0.6}$]) (Figure 4.6(b)). Two types of structures are observed on the surface of membrane [(PEI$_{0.9}$-PIP$_{2.1}$)/TMC$_{0.6}$] which was formed with 70 wt% PIP in the amine reactant: large ridge-valley structures and small globular structures (Figure 4.6(c)). When the reactant amine is PIP only, the membrane (i.e., [PIP$_{3.0}$/TMC$_{0.6}$]) showed some "planar sheet-like" structures on its surface (Figure 4.6(d)).

AFM was used for topological characterization of the membrane surface to complement with SEM. The three-dimensional scan images (scan size 10 μm × 10 μm) of the membranes are shown in Figure 4.7. The surface roughness in terms of the root mean square roughness is listed in Table 4.2. These results are in agreement with the surface morphologies observed under SEM. There are some small cone-shaped structures dispersed on the surface of membrane [PEI$_{3.0}$/TMC$_{0.6}$] (Figure 4.7(a)), with a root mean square roughness of 22.9 nm. Some small nodules appear on the surface of membrane [(PEI$_{2.1}$-PIP$_{0.9}$)/TMC$_{0.6}$] (Figure 4.7(b)), which has a root mean square roughness of 18.5 nm. There are more nodular structures on the surface of membrane [(PEI$_{0.9}$-PIP$_{2.1}$)/TMC$_{0.6}$] (Figure 4.7(c)), and membrane [PIP$_{3.0}$/TMC$_{0.6}$] shows a nodular aggregated structure on the surface (Figure 4.7(d)). The latter two membranes have much rougher surfaces, with a root mean square roughness of 75.8 and 120.8 nm, respectively.

For membrane [PEI$_{3.0}$/TMC$_{0.6}$], the amine groups are evenly distributed on the polymer chains as determined by its macromolecular structure, which may be attributed to the uniformness of the interfacially polymerized surface layer with relatively low roughness. When the reactant amine is a mixture of PEI and PIP, the local amine-TMC reaction rate varies due to the different reactivity and mobility of the amine sites in small molecules of PIP and macromolecules of PEI, resulting in an uneven structure on the membrane surface. At a low PIP content in the amine mixture, the quantity of crosslinks between PIP and TMC is relatively low, and they are embedded in the PEI macromolecules, resulting in a smooth membrane surface with a few patch-like or nodular structures. When the PIP content in the amine mixture is high enough, the more-rapidly formed PIP/TMC crosslinks will be significant to affect the

more-slowly occurring crosslinking between TMC and amine groups in PEI, resulting in rough surfaces with obvious ridge-valley and even aggregated nodular structures.
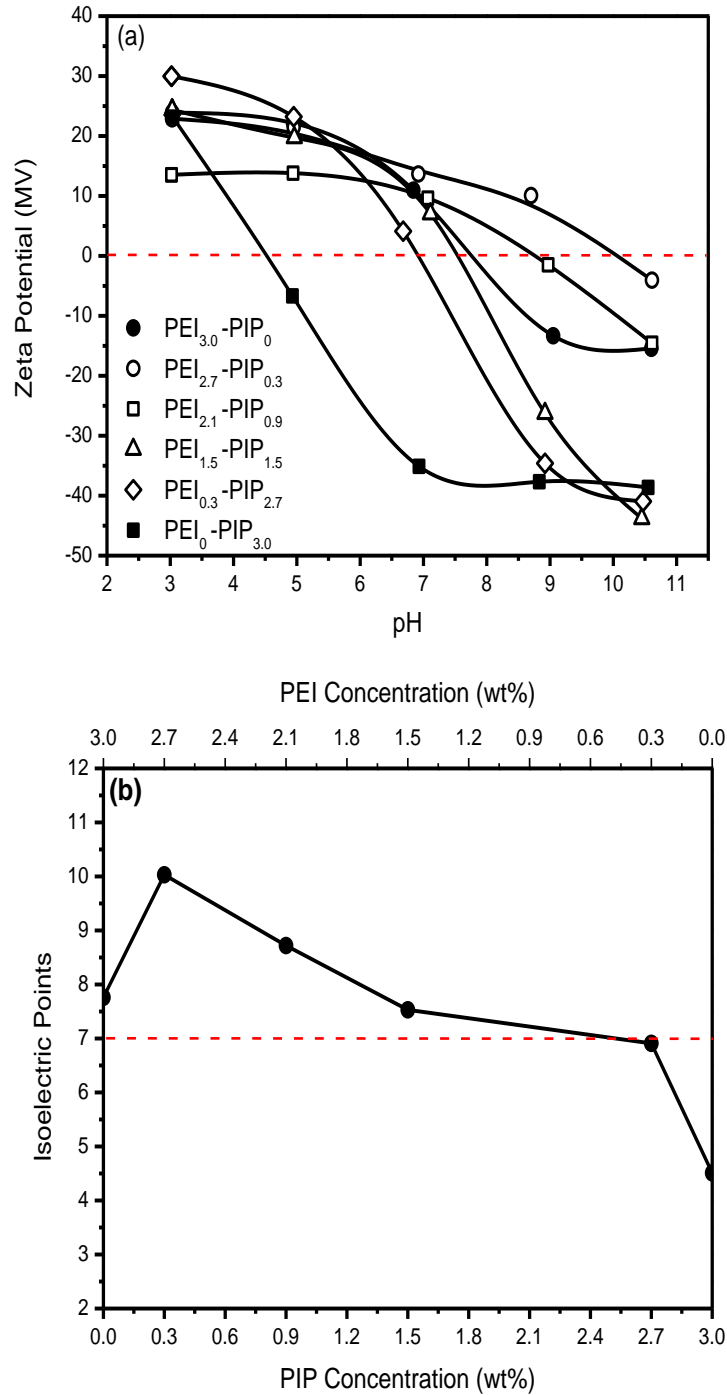
Figure 4.5 Surface charge properties for single-ply polyamide membranes: (a) Zeta potential at various pH values, and (b) isoelectric point. Test conditions: 0.001 M KCl, 25 °C.
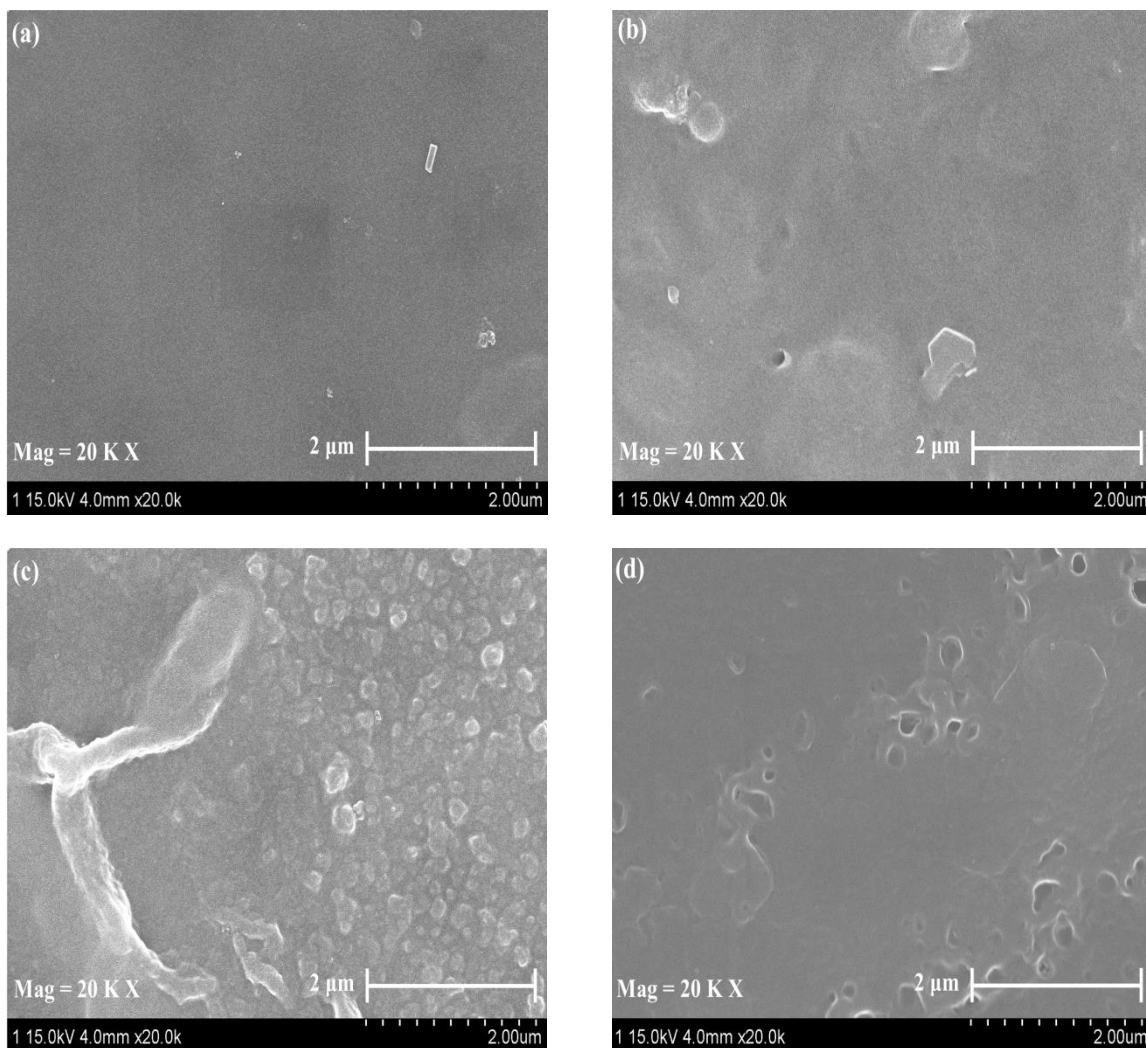
Figure 4.6 Surface images (20,000$\times$) of single-ply polyamide composite membranes: (a) [PEI$_{3.0}$/TMC$_{0.6}$], (b) [(PEI$_{2.1}$-PIP$_{0.9}$)/TMC$_{0.6}$], (c) [(PEI$_{0.9}$-PIP$_{2.1}$)/TMC$_{0.6}$], and (d) [PIP$_{3.0}$/TMC$_{0.6}$].
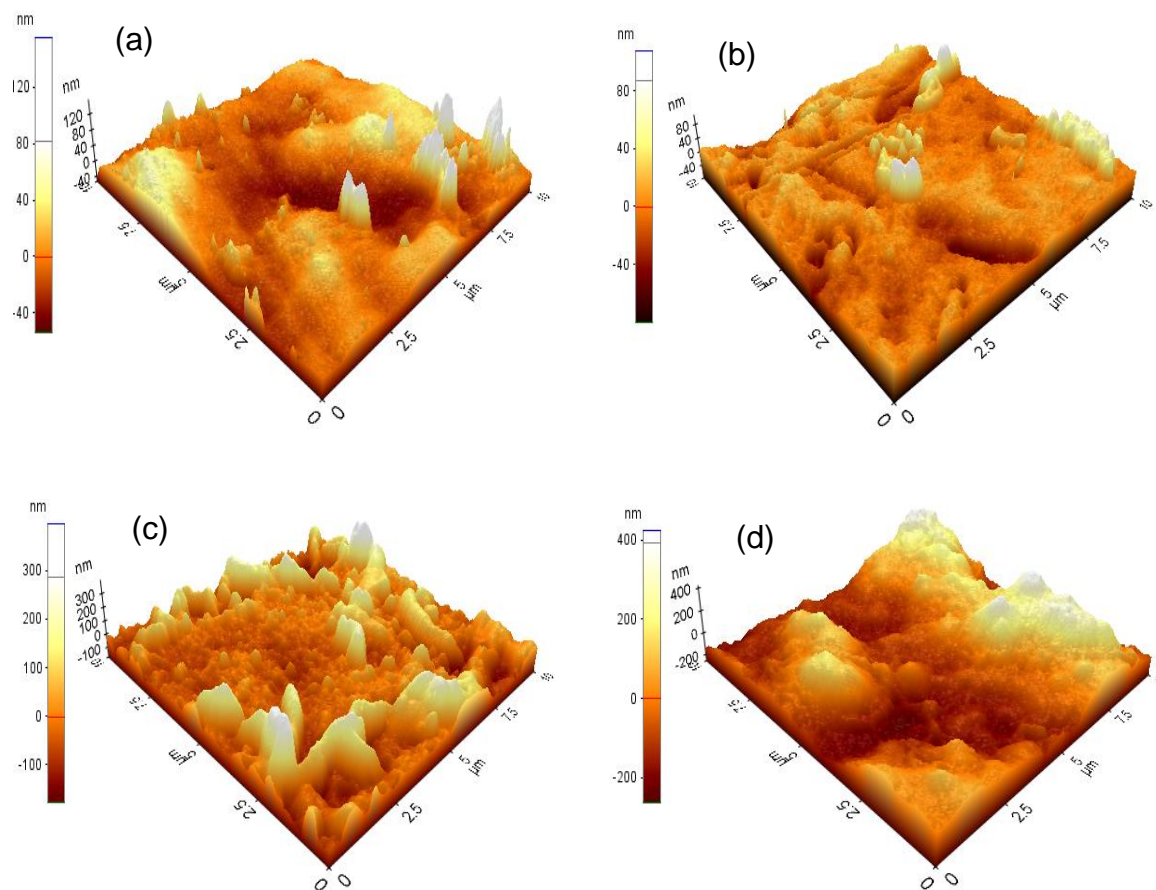
Figure 4.7 AFM images (10 μm × 10 μm) of single-ply polyamide composite membranes: (a) [PEI$_{3.0}$/TMC$_{0.6}$], (b) [(PEI$_{2.1}$-PIP$_{0.9}$)/TMC$_{0.6}$], (c) [(PEI$_{0.9}$-PIP$_{2.1}$)/TMC$_{0.6}$], and (d) [PIP$_{3.0}$/TMC$_{0.6}$].

Table 4.2 Root mean square roughnesses of single-ply polyamide composite membranes based on AFM

Membrane samples	Root mean square roughness (nm)
[PEI$_{3.0}$/TMC$_{0.6}$]	22.9
[(PEI$_{2.1}$-PIP$_{0.9}$)/TMC$_{0.6}$]	18.5
[(PEI$_{0.9}$-PIP$_{2.1}$)/TMC$_{0.6}$]	75.8
[PIP$_{3.0}$/TMC$_{0.6}$]	120.8

Nanofiltration performance

Membranes prepared from a reactant deposition sequence of (PEI+PIP)-TMC

The separation performance of the polyamide thin film composite membranes fabricated by interfacial reaction between TMC and the amine mixtures with different compositions with a reactant deposition sequence of (PEI+PIP)-TMC is shown in Figure 4.8 in terms of permeation flux and salt rejection at a transmembrane pressure of 0.8 MPa gauge.

When the reacting amine is PEI only, the membrane (i.e., [$PEI_{3.0}$/$TMC_{0.6}$]) has a water flux of 9 L/(m^2.h), which is about twice the permeation flux of the membrane formed with PIP and TMC (i.e., [$PIP_{3.0}$/$TMC_{0.6}$]). When a mixed amine of PIP and PEI was used, the permeation flux of the resulting membrane can be enhanced significantly. For instance, using 10 wt% of PIP in the mixed amine for membrane preparation will increase the permeation flux of the membrane (i.e., [($PEI_{2.7}$-$PIP_{0.3}$)/$TMC_{0.6}$)]) to 43-47 L/(m^2.h), depending on the solutes present in the feed solutions. When a mixed amine of PIP and PEI was used, the monomeric amine PIP and polymeric amine PEI behave quite differently in their interfacial reactions with TMC, which makes the overall membrane formation mechanism more complicated. Regardless of the type of the reactant amine, the interface between the aqueous phase and the organic phase is believed to be the first locus of reaction between TMC and the amine. There has been evidence to suggest that after initial interfacial reaction to form a thin layer of crosslinks, further reactions between the two reactants will occur mainly in the organic phase because of highly unfavorable partition coefficient of the acyl chloride in water [Morgan, 1965]. However, for polymeric amine, this will be difficult because of the low mobility of the macromolecules and their unfavorable partition coefficient in the organic phase [Petersen, 1993]. With an amine mixture of PEI and PIP, small molecules of PIP will react with TMC quickly, and the crosslinks so formed will hinder the diffusion of TMC molecules across the interface to react

with the amine groups in PEI. This will make the slow reaction between TMC and PEI even slower. In this case, the selective skin layer will be dominated by PIP/TMC crosslinks embedded in PEI which is more loosely crosslinked by TMC, resulting in a permeability that would be higher than a membrane formed from TMC and PEI alone without PIP. However, as one may expect, too much PIP in the amine mixture will form a dense PIP/TMC crosslink, which will lower the permeation flux of the membrane. As shown in Figure 4.8(a), when the PIP content in the reacting amine solution is sufficiently high, a further increase in the PIP content will reduce permeability of the membrane.

Figure 4.8(b) shows that the rejection of the membranes to $MgCl_2$ is quite high (~95%), and the PIP content in the amine solution during membrane formation has little effect on $MgCl_2$ rejection. This high rejection of $MgCl_2$ may be attributed partially to the positively-charged membrane surfaces. Even membrane [$PIP_{3.0}/TMC_{0.6}$], which has a negatively charged surface, showed a $MgCl_2$ rejection of 90%; this membrane had a high degree of crosslinking of PIP and TMC that makes the membrane dense enough to reject $MgCl_2$ effectively, as shown by its low permeation flux. The membranes showed a higher rejection to $MgSO_4$ than to Na_2SO_4, and there is a similar trend in the effects of PIP content on the rejection of the membranes to these two solutes. With an increase in the PIP content in the amine reactant, the rejections of the membranes to $MgSO_4$ and Na_2SO_4 experienced a decrease initially and then increased when the PIP content in the reactant amine was over 10 wt%. This is easy to understand based on the surface charge and tightness of the skin layer. The Zeta potential on the membrane surface indicates that incorporating a small amount of PIP in the amine mixture makes the membrane surface more positively charged, but the membrane skin layer is relatively loose because of the limited amount of quick-reacting PIP available in the amine solution, as shown by its higher

water flux. This will lower the membrane rejection to Na_2SO_4 more significantly than $MgSO_4$. When the quantity of PIP in the amine reactant increases, the polyamide layer will be increasingly crosslinked but less positively charged, which favors the membrane rejection to $MgSO_4$ and Na_2SO_4. On the other hand, unlike the above solutes with divalent ions, the rejection of the membranes to monovalent salt NaCl showed a continuous decrease with an increase in the PIP content in the amine reactant. This appears to suggest that the electrostatic interaction between the membrane and the monovalent solute is less significant and the membrane structures are in general not tight enough to retain this solute with a smaller molecular size.

Presented in Table 4.3 is a comparison of membrane [(PEI$_{2.4}$-PIP$_{0.6}$)/TMC$_{0.6}$)] with some PEI-based NF membranes developed in laboratories and PIP-based commercial NF membranes in terms of water permeability and salt rejection. Membrane [(PEI$_{2.4}$-PIP$_{0.6}$)/TMC$_{0.6}$)] exhibited a moderate water permeability but a higher NaCl rejection. It is apparent that incorporating a small amount of PIP in PEI for interfacial reaction with TMC would yield membranes with both good permeation flux and solute rejection.
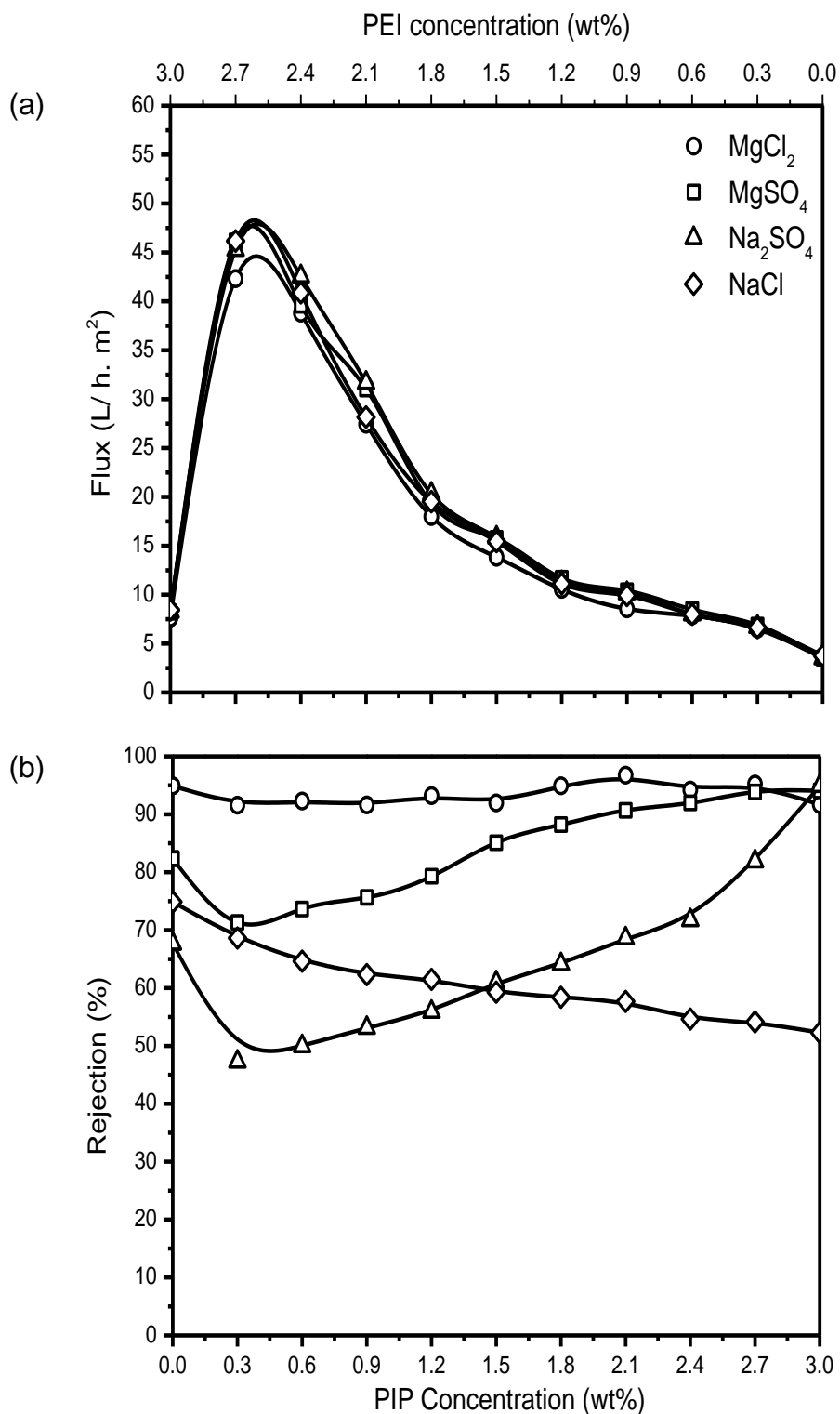
Figure 4.8 Effects of PIP concentration in the amine mixture on (a) permeation flux and (b) salt rejection of the resulting single-ply polyamide membranes prepared by interfacial polymerization with a reactant deposition sequence of (PEI+PIP)-TMC. (Operating pressure, 0.8 MPa gauge; Salt concentration, 500 ppm. Temperature, 23°C).

Table 4.3 Comparison of NF performance of membranes developed in this study* with other NF membranes

Membrane	Pure Water Permeability (L/m^2.h.MPa)	Salt Rejection (%)				Feed Solution Concentration (ppm)	Ref.
		MgCl$_2$	MgSO$_4$	Na$_2$SO$_4$	NaCl		
[(PEI$_{2.4}$-PIP$_{0.6}$)/TMC$_{0.6}$]	50.6	92	74	50	65	500	This work
PEI/TPC (terephthaloyl chloride)	31.0	95	91	75	61	1000	[Chiang *et al.*, 2009]
PEI/TMC	95.0	80	76	51	46		
NS-300	54.6	46	98	98	50	5000	[Kamiyama *et al.*, 1984]
NF40	41.0	/	98	/	35	2000	[Eriksson, 1988]
NF40HF	60.7	20	95	/	40	2000	[Freeman and Stocker, 1987]
XP45	48.6	83	97.5	/	50	2000	[Cadotte *et al.*, 1988]
[(PEI$_{0.6}$/TMC$_{0.3}$)-(PIP$_{2.4}$/TMC$_{0.3}$)]	12.2	98	94	68	78	500	This work
[(PEI$_{0.6}$-PIP$_{2.4}$)/TMC$_{0.6}$]	10.1	94	92	72	55		
[PEI$_{3.0}$/TMC$_{0.6}$]	8.9	95	82	68	75		
[PIP$_{3.0}$/TMC$_{0.6}$]	4.5	92	94	95	52		

* Test temperature was 23 °C

Membranes prepared from a reactant deposition sequence of TMC-(PEI+PIP)

Polyamide composite membranes were also prepared by interfacial polymerization using a reversed sequence of reactant depositions, that is, reactant TMC was deposited on the substrate first, followed by the reactant amine (PEI+PIP). The separation performance of these membranes is shown in Figure 4.9. When the reactant amine was PEI, the resulting membrane [$TMC_{0.6}$/$PEI_{3.0}$] still had a fairly good performance with a water flux of 6.3 L/(m^2.h) at a transmembrane pressure of 0.8 MPa gauge and solute rejections of 95.2% for $MgCl_2$, 90.4% for $MgSO_4$, 58.2% for Na_2SO_4 and 66.2% for NaCl. However, when a mixture of amines was used, the permeation flux of the membrane first increased with an increase in the PIP content in the amine mixture, and then decreased when the PIP content was high enough. A maximum permeability was observed with membrane [$TMC_{0.6}$/($PEI_{0.6}$-$PIP_{2.4}$)] among the membranes prepared. An opposing trend was observed for solute rejections of the membranes except for solutes $MgCl_2$ and NaCl which decreased continuously with an increase in the PIP content in the amine mixture.
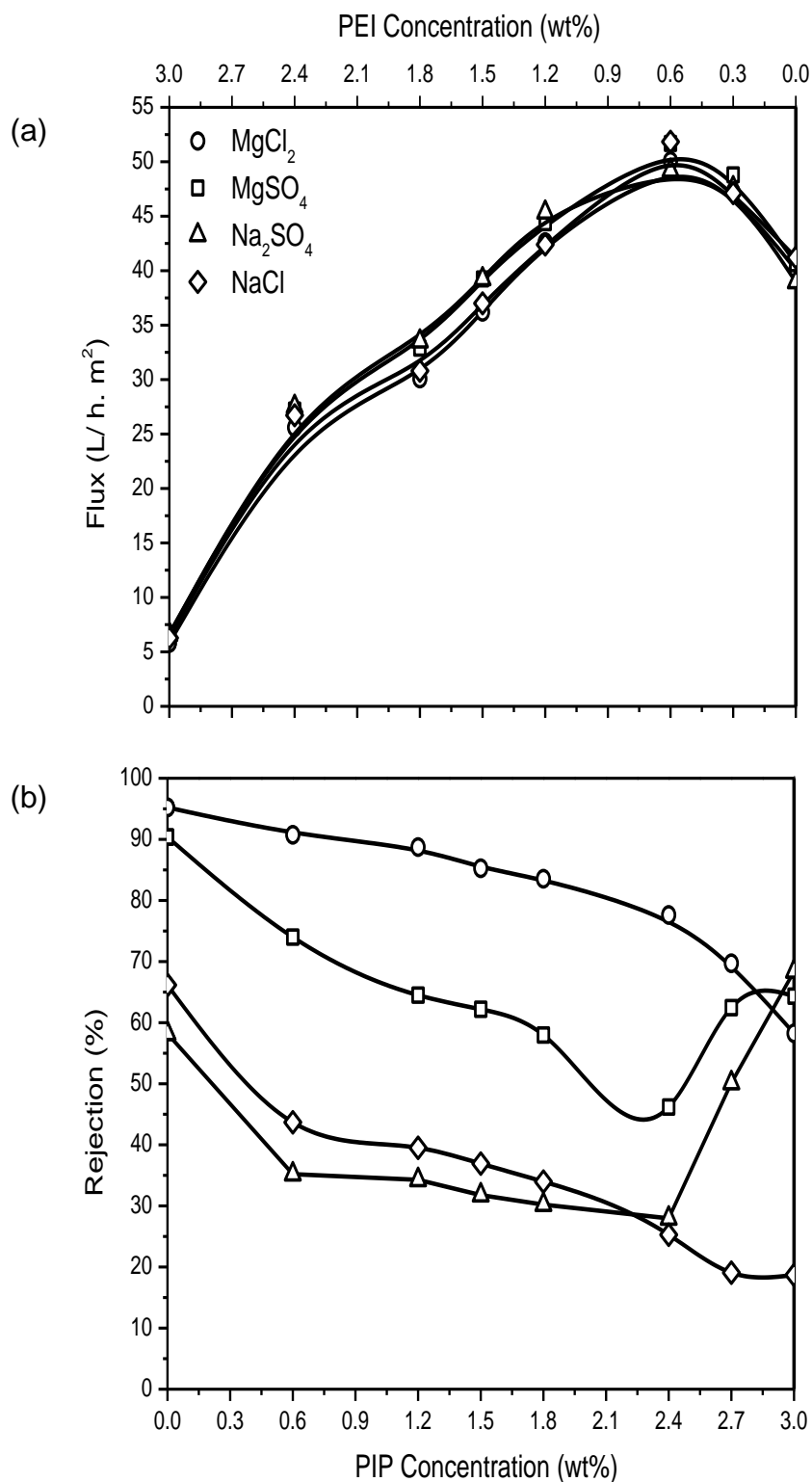
Figure 4.9 Effects of PIP concentration in the amine mixture on (a) permeation flux and (b) salt rejection of the resulting single-ply polyamide membranes prepared by interfacial polymerization with a reactant deposition sequence of TMC-(PEI+PIP). (Operating pressure, 0.8 MPa gauge; Salt concentration, 500 ppm. Temperature, 23°C).

It may be mentioned that when hydrophilic polysulfone or polyethersulfone substrate is used for fabrication of TFC membranes by interfacial polymerization, the aqueous amine solution is often deposited onto the substrate membrane followed by deposition of an organic solution of acyl chloride to induce interfacial polymerization on the substrate surface. The deposition of the aqueous amine as the first reactant onto a hydrophilic substrate favors the reactant loading and adhesion on the substrate surface. However, with polymeric amine PEI, it has been shown that a reversed sequence of reactant depositions (i.e., TMC deposition first, followed by PEI) could also be used to prepare TFC membranes with reasonably good rejections [Wu *et al.*, 2014]. In spite of the weak affinity between PES and TMC, the low mobility and branched structure of the PEI macromolecules were helpful to the formation of the polyamide layer fixed and secured on the substrate. This attribute, however, will gradually diminish with an increase in PIP content when an amine mixture of PIP and PEI is used, resulting in an increased permeation flux and a decreased solute rejection.

To get a better idea about the separation performance of membranes prepared with the two different sequences of reactant depositions, i.e., (PEI+PIP)-TMC vs. TMC-(PEI+PIP), the pure water permeation flux and solute rejection of the membranes are re-plotted in Figures. 4.10 and 11 for direct comparisons. It can be seen that at a PIP content of 0.6 wt% in the amine mixture, the pure water permeation flux of the membranes formed by the (PEI+PIP)-TMC deposition sequence are greater than those of membranes formed by the reverse sequence of reactant depositions (i.e., TMC-(PEI+PIP)). While the membranes formed with both sequences of reactant depositions have similar rejections to $MgCl_2$ and $MgSO_4$, the membranes formed by the deposition sequence of (PEI+PIP)-TMC have a higher rejection to Na_2SO_4 and NaCl than membranes formed by the reversed reactant deposition sequence. In addition, at a higher PIP

114

content in the mixed amine, the membranes formed by the (PEI+PIP)-TMC deposition sequence exhibit lower pure water permeabilities and higher solute rejections for all the four salts tested than membranes formed by the reversed reactant deposition sequence. It appears that the amine-acyl chloride deposition sequence for fabricating membranes using the PEI and PIP mixtures with a small amount of PIP is appropriate, and therefore this sequence was used in studies of multiple-layered TFC membranes.
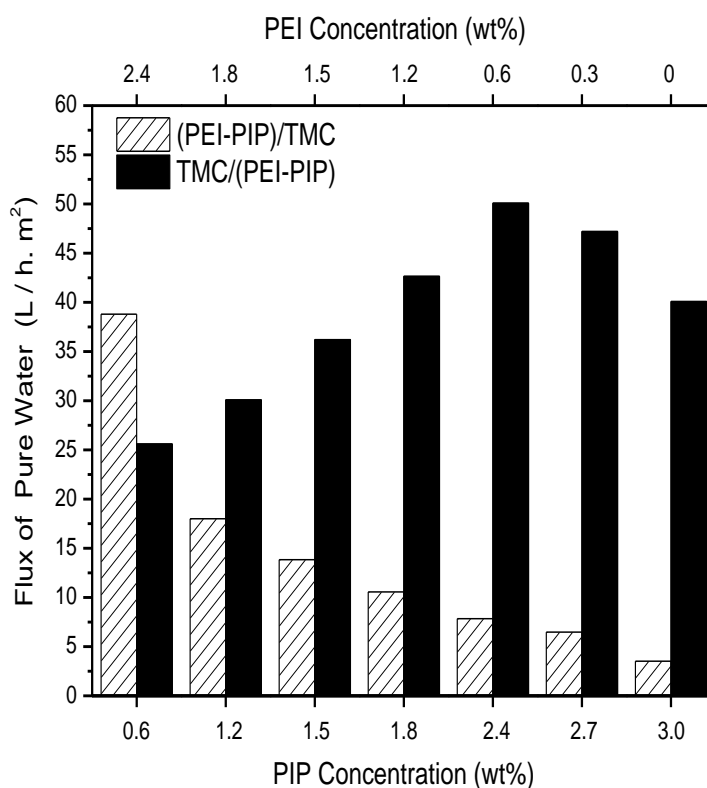
Figure 4.10 Effect of reactant deposition sequence on pure water permeation flux, Temperature, 23°C.
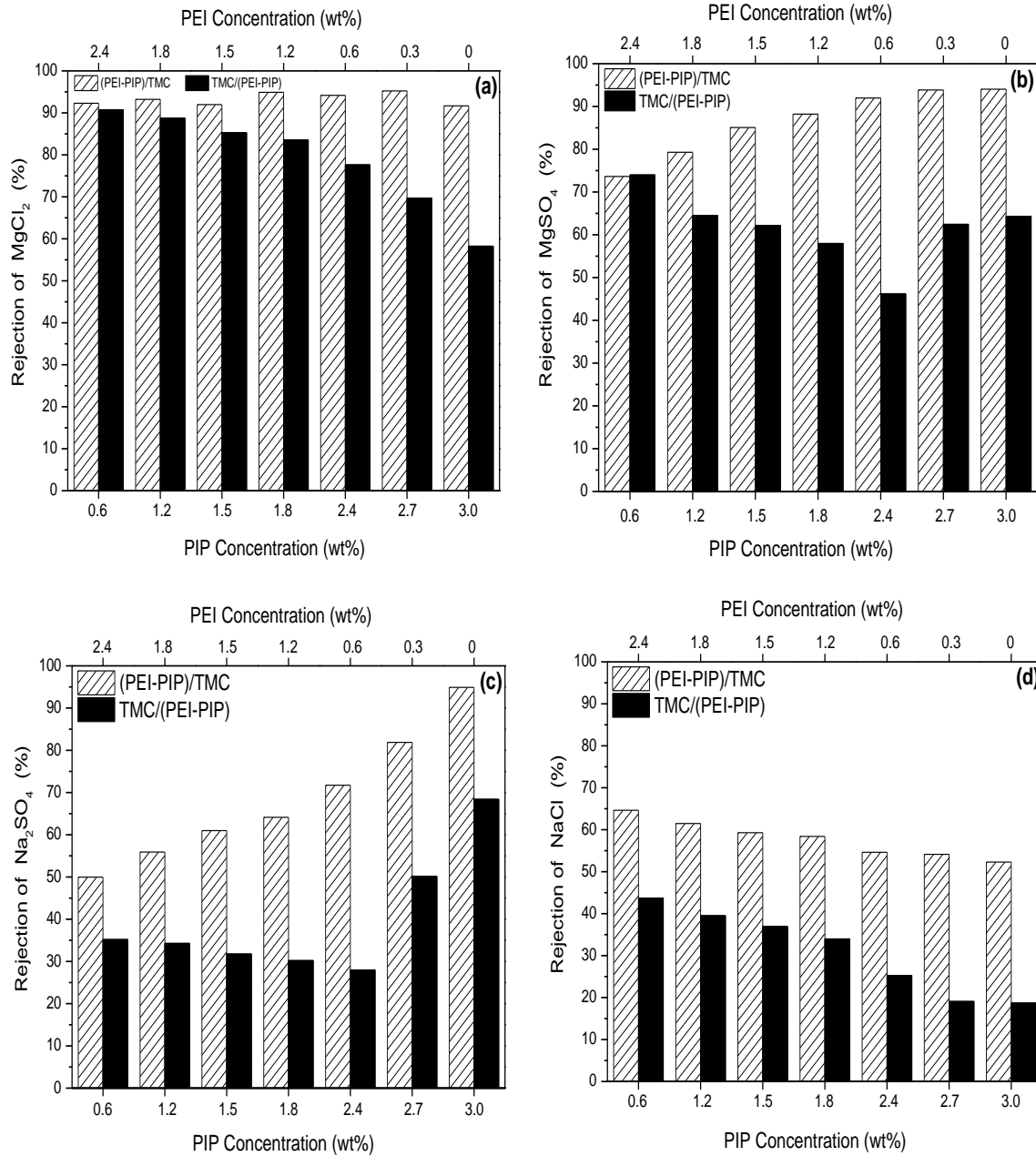
Figure 4.11 Effects of reactant deposition sequence on salt rejection of the single-ply polyamide membranes. Solutes: (a) $MgCl_2$, (b) $MgSO_4$, (c) Na_2SO_4, and (d) NaCl. (Operating pressure, 0.8 MPa gauge; Salt concentration, 500 ppm. Temperature, 23°C).

4.3.2 TFC NF membranes with a two-ply of polyamide layer

Instead of using mixed amines of PIP and PEI, TFC membranes with a two-ply polyamide layer were prepared by two cycles of interfacial polymerizations based on PEI-TMC and PIP-TMC reactions that occurred separately and sequentially. The two-plies of the polyamide layer are not expected to be overlaid perfectly, but instead there will be significant interpenetrations due to their ultrathin thicknesses. Depending on the reactant deposition sequences, two series of membranes may be distinguished: [(PEI/TMC)-(PIP/TMC)] and [(PIP/TMC)-(PEI/TMC)]. The sum of PIP and PEI concentrations was maintained at 3 wt%. In analog to the above study of amine compositions on the membranes formed with mixed amines of PIP and PEI, the effects of PIP to PEI concentration ratio used in preparing the two-ply polyamide layer on the membrane performance were investigated here. For example, membrane [(PEI$_{2.1}$/TMC$_{0.3}$)-(PIP$_{0.9}$/TMC$_{0.3}$)], which was produced using 2.1 wt% of PEI and 0.9 wt% of PIP respectively to form the two polyamide layers sequentially, has a PIP/PEI ratio of 0.9/2.1.

Surface charge

The Zeta potentials on the membrane surface measured at various pH are presented in Figure 4.12(a), and the isoelectric points are shown in Figure 4.12(b). For convenience of comparison, the properties of membranes [PEI$_{3.0}$/TMC$_{0.6}$] and [PIP$_{3.0}$/TMC$_{0.6}$] (representing limiting cases of 0 and infinity in the PIP to PEI concentration ratio) were also shown in the plots. As the PIP/PEI concentration ratio increased, the isoelectric point decreased. Membrane [(PEI$_{0.3}$/TMC$_{0.3}$)-(PIP$_{2.7}$/TMC$_{0.3}$)] showed an isoelectric point of 6.9, indicating that there were still sufficient unreacted amine groups from PEI in producing the first ply of polyamide to render the membrane surface positively charged even at a PIP concentration that was much higher than the PEI concentration.

117
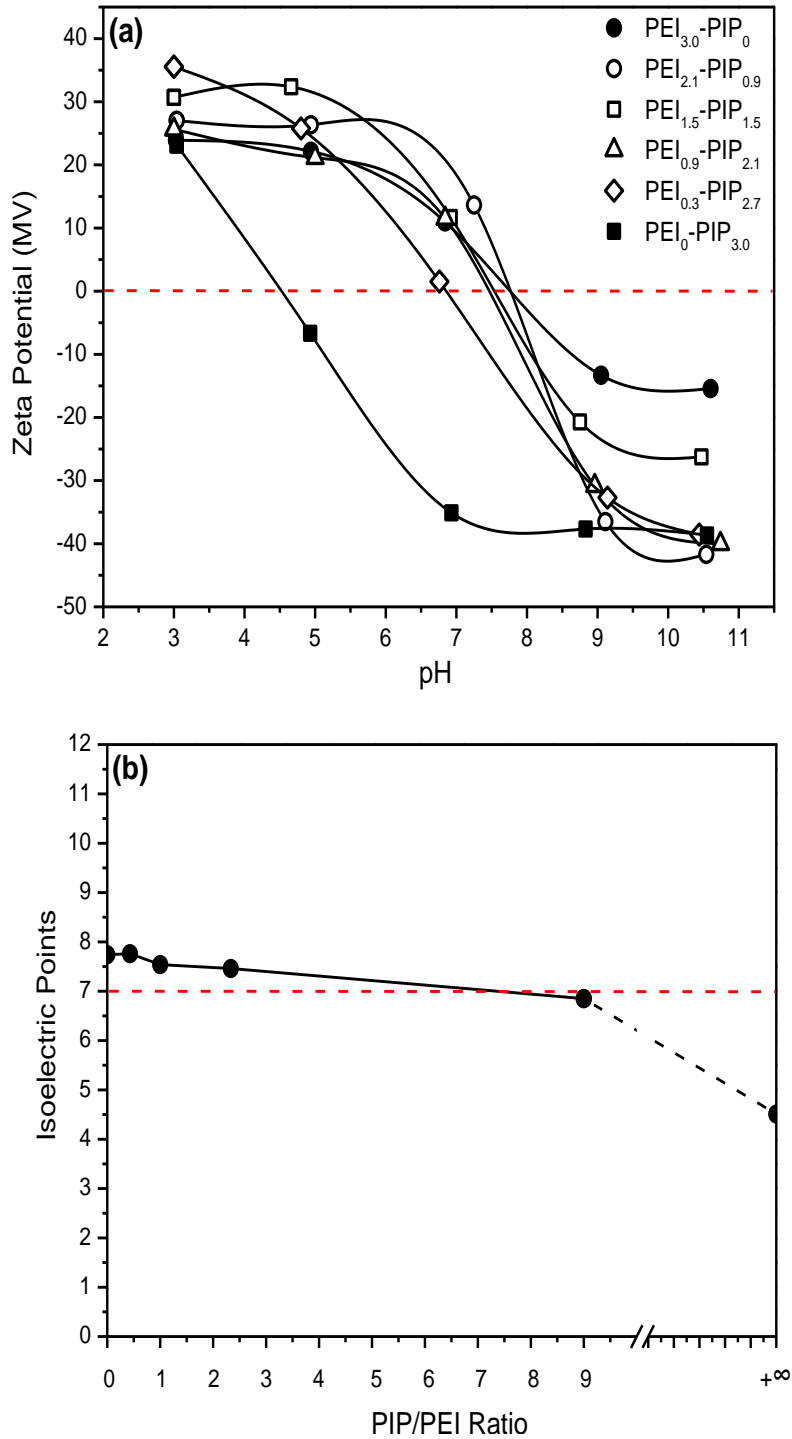
Figure 4.12 Surface charge properties for 2-ply polyamide membranes: (a) Zeta potential at various pH values, (b) isoelectric point. Test conditions: 0.001 M KCl, 25 ℃.

Surface morphology

Figure 4.13 shows the scanning electron microscopic images of the surfaces of three membranes $[(PEI_{2.1}/TMC_{0.3})-(PIP_{0.9}/TMC_{0.3})]$, $[(PEI_{1.5}/TMC_{0.3})-(PIP_{1.5}/TMC_{0.3})]$ and $[(PEI_{0.9}/TMC_{0.3})-(PIP_{2.1}/TMC_{0.3})]$. Their three-dimensional 10 μm × 10 μm AFM scan images are shown in Figure 4.14, and the surface roughnesses of the membranes are presented in Table 4.4.

The SEM images revealed that "patch-like" structures appeared occasionally on the surface of membrane $[(PEI_{2.1}/TMC_{0.3})-(PIP_{0.9}/TMC_{0.3})]$ (Figure 4.13(a)), and many small globular structures were formed on the surface of membrane $[(PEI_{1.5}/TMC_{0.3})-(PIP_{1.5}/TMC_{0.3})]$ (Figure 4.13(b)). Membrane $[(PEI_{0.9}/TMC_{0.3})-(PIP_{2.1}/TMC_{0.3})]$ showed both large and small ridge-valley structures (Figure 4.13(c)). These results are in agreement with the surface morphologies observed under AFM. There are many small cone-shaped structures on the surface of membrane $[(PEI_{2.1}/TMC_{0.3})-(PIP_{0.9}/TMC_{0.3})]$ (Figure 4.14(a)). More small cone-shaped and nodular structures emerged on the surface of membrane $[(PEI_{1.5}/TMC_{0.3})-(PIP_{1.5}/TMC_{0.3})]$, and they were connected with each other to form a large area of aggregated structures (Figure 4.14(b)). The aggregated structure was more obvious for the membrane $[(PEI_{0.9}/TMC_{0.3})-(PIP_{2.1}/TMC_{0.3})]$ (Figure 4.14(c)). Membrane $[(PEI_{2.1}/TMC_{0.3})-(PIP_{0.9}/TMC_{0.3})]$ had a surface roughness of 20.8 nm, which is similar to membrane $[PEI_{3.0}/TMC_{0.3}]$ (22.9 nm). The surface roughness data in Table 4.4 appear to suggest that the uneven structures and roughnesses on the membranes mainly come from the PIP/TMC crosslinks.
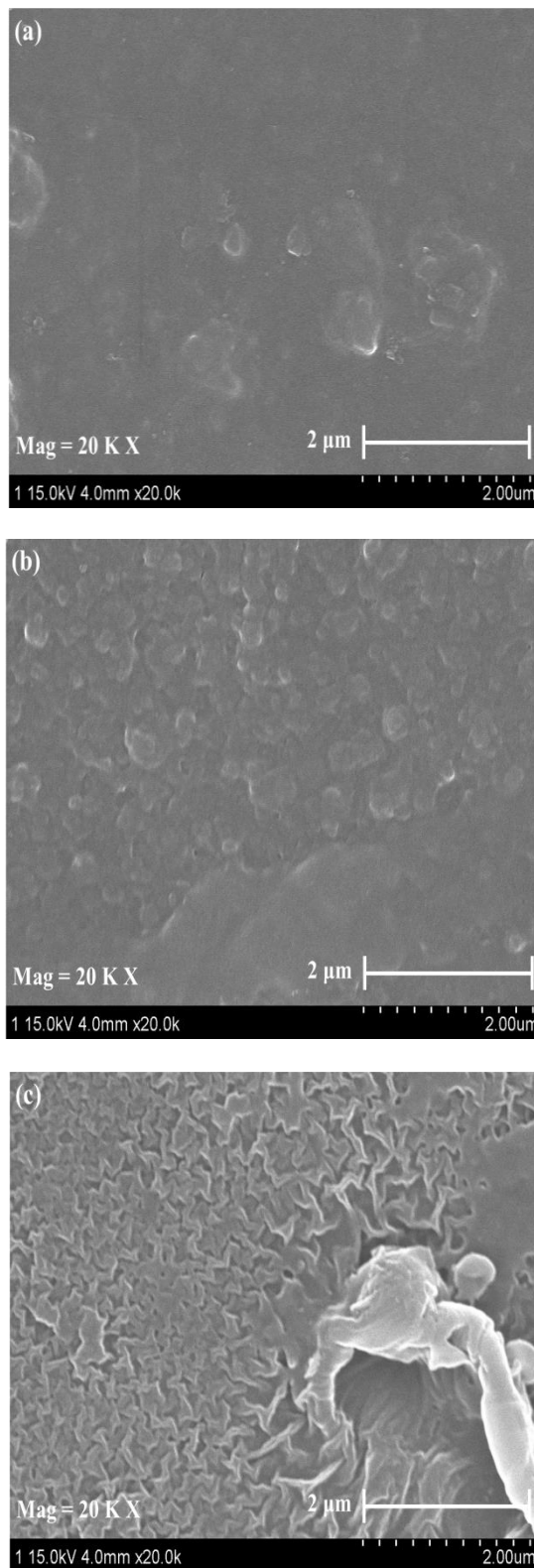
Figure 4.13 Surface images (20,000$\times$) of 2-ply polyamide composite membranes (a) [(PEI$_{2.1}$/TMC$_{0.3}$)-(PIP$_{0.9}$/TMC$_{0.3}$)], (b) [(PEI$_{1.5}$/TMC$_{0.3}$)-(PIP$_{1.5}$/TMC$_{0.3}$)], and (c) [(PEI$_{0.9}$/TMC$_{0.3}$)-(PIP$_{2.1}$/TMC$_{0.3}$)].
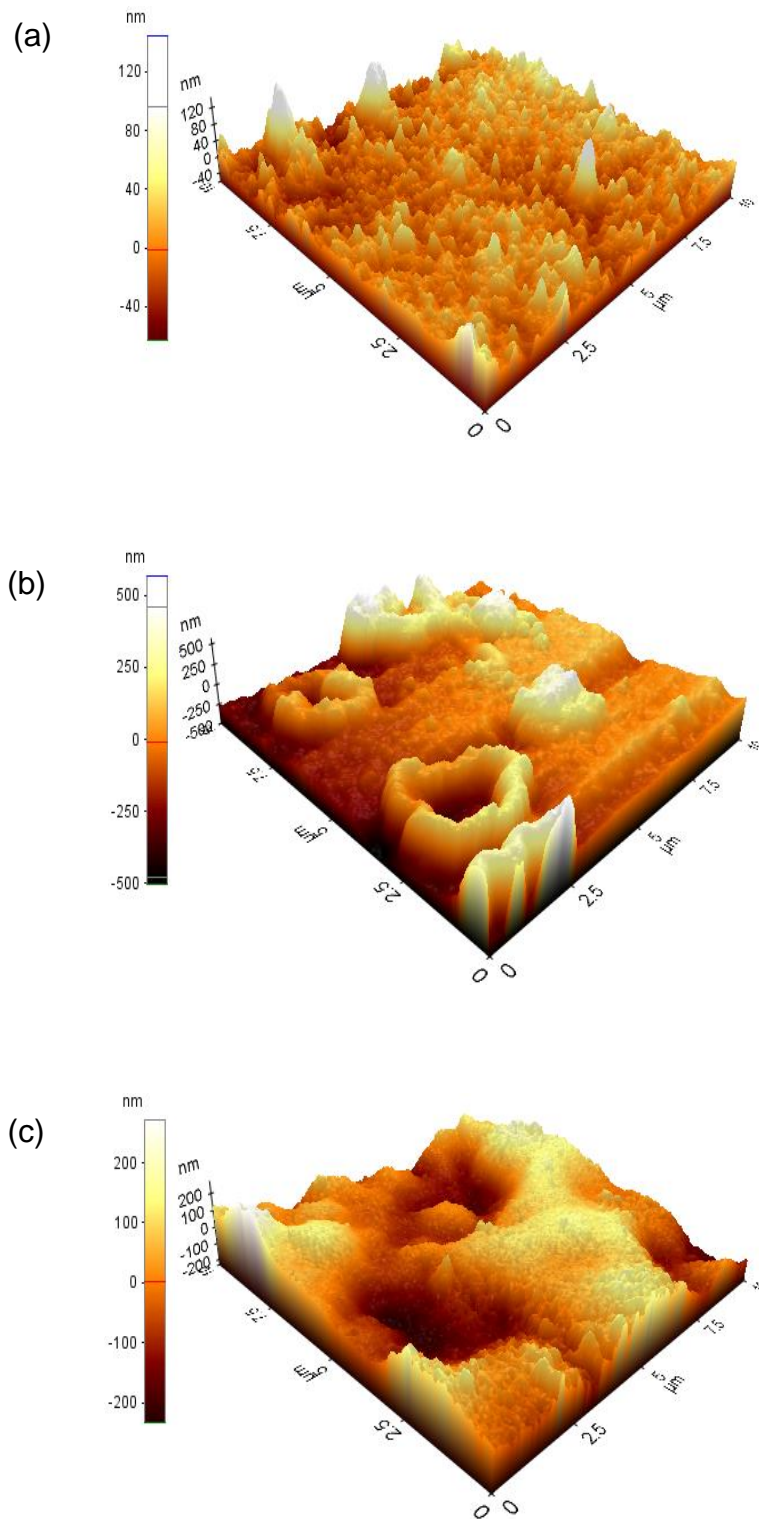
Figure 4.14 AFM images (10 μm × 10 μm) of 2-ply polyamide composite membranes (a) $[(PEI_{2.1}/TMC_{0.3})-(PIP_{0.9}/TMC_{0.3})]$, (b) $[(PEI_{1.5}/TMC_{0.3})-(PIP_{1.5}/TMC_{0.3})]$ and (c) $[(PEI_{0.9}/TMC_{0.3})-(PIP_{2.1}/TMC_{0.3})]$.

Table 4.4 Root mean square roughnesses of 2-ply polyamide composite membranes based on AFM

Membrane samples	Root mean square roughness (nm)
$[(PEI_{2.1}/TMC_{0.3})\text{-}(PIP_{0.9}/TMC_{0.3})]$	20.8
$[(PEI_{1.5}/TMC_{0.3})\text{-}(PIP_{1.5}/TMC_{0.3})]$	53.5
$[(PEI_{0.9}/TMC_{0.3})\text{-}(PIP_{2.1}/TMC_{0.3})]$	93.0

Nanofiltration performance

The two-ply polyamide TFC membranes can be formed by interfacial polymerization through the reactant deposition sequence of (PEI/TMC)-(PIP/TMC), resulting in membranes with a first ply of PEI-based polyamide layer and a second ply of PIP-based polyamide layer. Alternatively, the membrane may have a first ply of PIP-based polyamide layer and a second ply of PEI-based polyamide layer using a reactant deposition sequence of (PIP/TMC)-(PEI/TMC). The separation performance of both types of membranes was studied.

Figure 4.15 showed the permeation flux and salt rejection of the [(PEI/TMC)-(PIP/TMC)] series of membranes. Compared to single-ply PEI-based polyamide membrane $[PEI_{3.0}/TMC_{0.6}]$, the permeation flux of 2-ply polyamide membrane $[(PEI_{2.4}/TMC_{0.3})\text{-}(PIP_{0.6}/TMC_{0.3})]$ was about 50% lower. This means that the presence of the second ply of the PIP/TMC polyamide layer, though formed at a low PIP concentration, contributed significantly to the mass transport resistance. However, the permeation fluxes of the 2-ply polyamide membranes increased with an increase in the PIP/PEI ratio up to a value of 2.33 (i.e., 2.1/0.9), beyond which the membrane permeability began to decrease with a further increase in PIP/PEI ratio. This is understandable because the first ply of PEI-based polyamide layer became thinner and less dense with an increase in the PIP/PEI ratio, while the opposite was true for the second ply of

PIP-based polyamide layer. At a low PIP/PEI ratio, the permeation flux of the membrane would be determined by the first ply polyamide layer, but when PIP/PEI ratio was high enough, the second ply polyamide layer would be more dominating.

There is generally a tradeoff between the membrane permeability and solute rejection. For instance, $[(PEI_{2.4}/TMC_{0.3})-(PIP_{0.6}/TMC_{0.3})]$ membrane showed a lower flux but a higher solute rejection than the single-ply polyamide membrane $[PEI_{3.0}/TMC_{0.6}]$. Nevertheless, the data in Figure 4.15 demonstrate that at a proper PIP/PEI ratio, membranes (e.g., membrane $[(PEI_{0.6}/TMC_{0.3})-(PIP_{2.4}/TMC_{0.3})]$) with both a high permeation flux and salt rejection than conventional single-ply polyamide membranes could be produced using the 2-ply approach. The data of permeation flux and salt rejection for the 2-ply polyamide membrane $[(PEI_{0.6}/TMC_{0.3})-(PIP_{2.4}/TMC_{0.3})]$ and single-ply polyamide membranes $([(PEI_{0.6}-PIP_{2.4})/TMC_{0.3})]$, $[PEI_{3.0}/TMC_{0.6})]$ and $[PIP_{3.0}/TMC_{0.6})])$ were also shown in Table 4.3 for convenience of comparison with other nanofiltration membranes. The 2-ply approach is shown to be advantageous.

The separation performance of 2-ply polyamide membranes comprising of a first ply of PIP-based polyamide layer and a second ply of PEI-based polyamide layer is shown in Figure 4.16. Compared to single-ply PEI-based polyamide membrane, $[(PIP_{0.6}/TMC_{0.3})-(PEI_{2.4}/TMC_{0.3})]$ showed a higher permeation flux and a lower solute rejection. In general, the 2-ply polyamide membranes had a lower permeation flux than those 2-ply polyamide membranes with a first ply of PEI/TMC crosslinks and a second ply of PIP/TMC crosslinks. Nevertheless, the membrane showed a more favorable rejection to Na_2SO_4 and NaCl when the PIP/PEI ratio is relatively high.
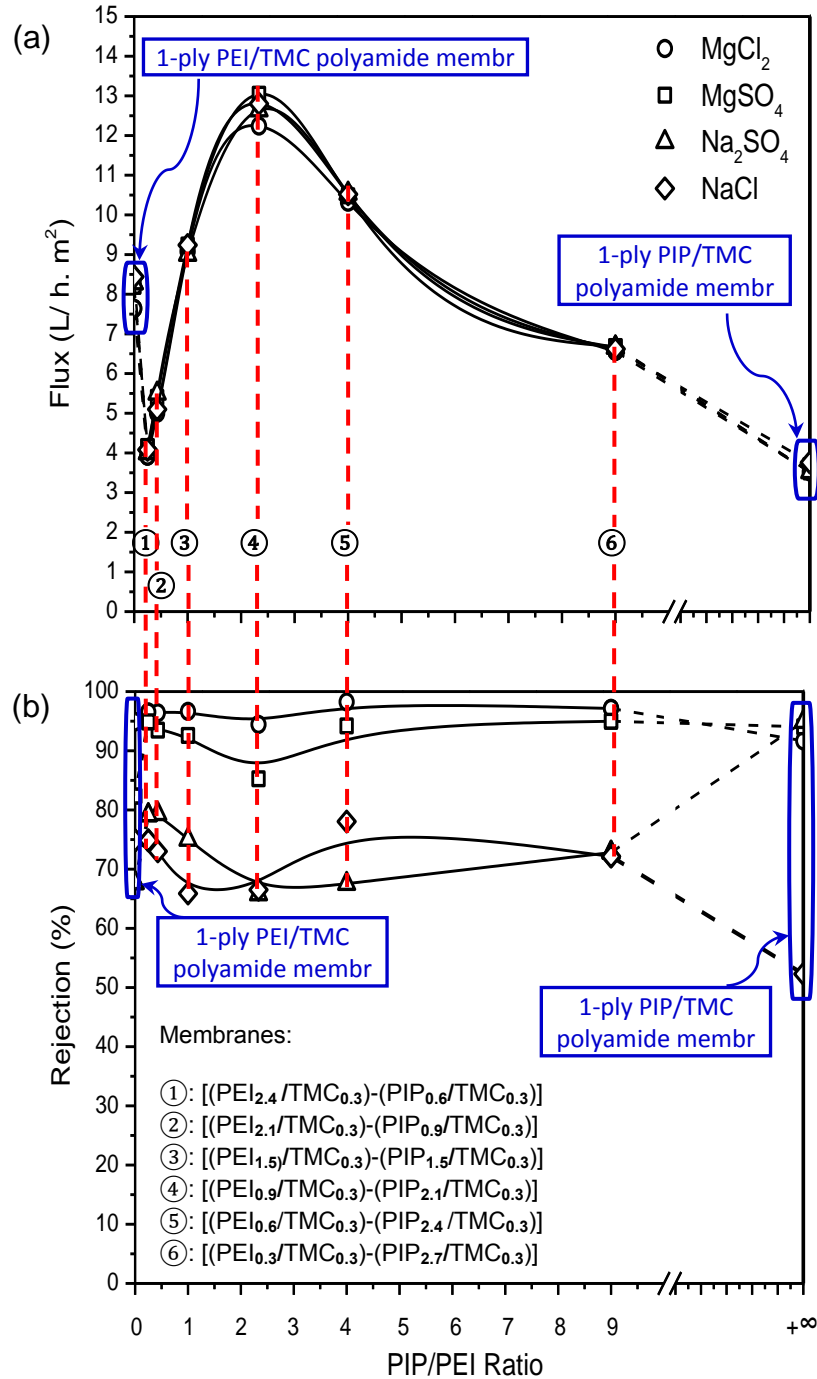
Figure 4.15 Effects of PIP/PEI ratio on (a) permeation flux and (b) salt rejection of the 2-ply polyamide membranes comprising of a first ply of PEI/TMC crosslinks and a second ply of PIP/TMC crosslinks. Identities of the membranes were labeled. Operating pressure, 0.8 MPa gauge; Salt concentration, 500 ppm. Temperature, 23°C.
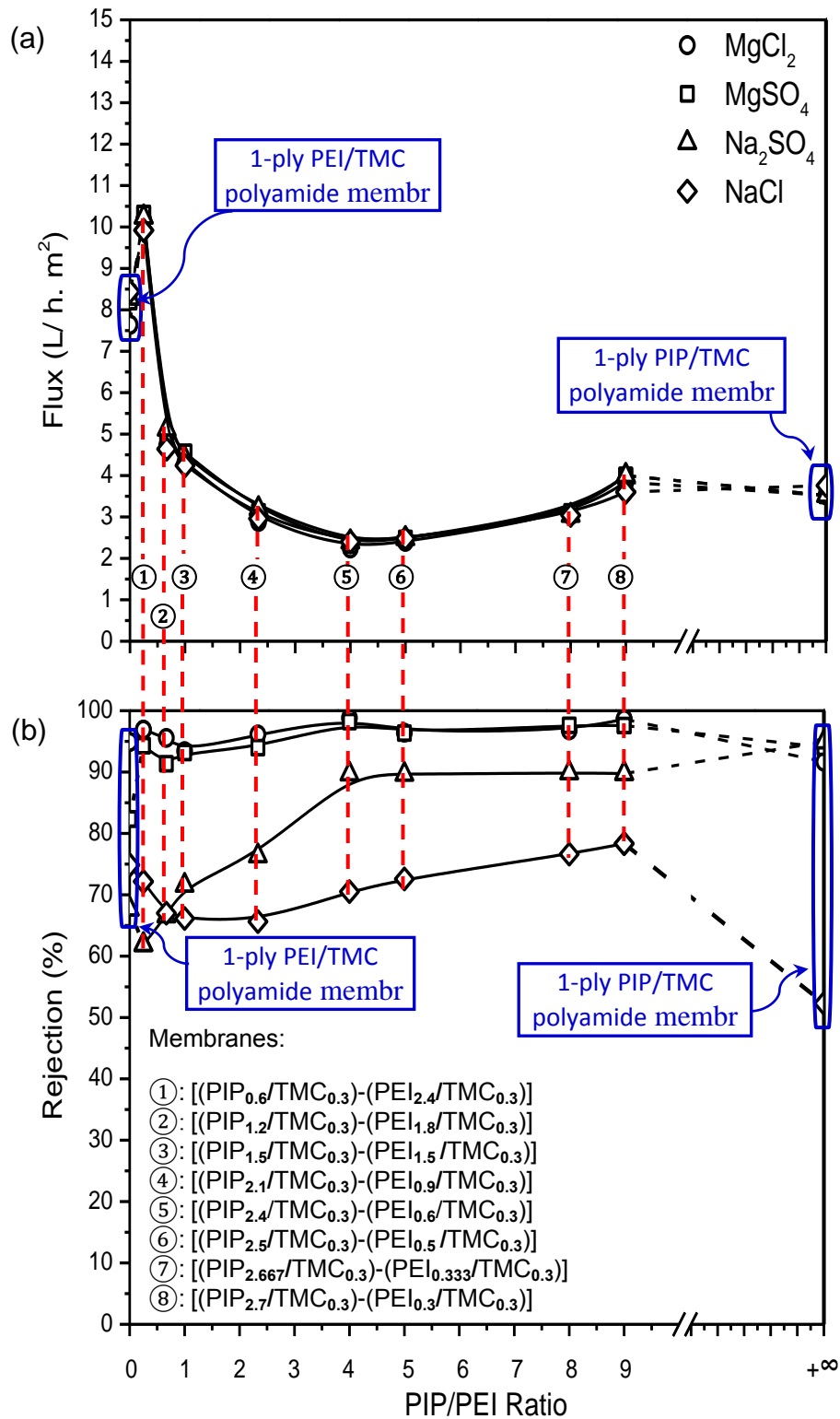
Figure 4.16 Effects of PIP/PEI ratio on (a) permeation flux and (b) salt rejection of the 2-ply polyamide membranes comprising of a first ply of PIP/TMC crosslinks and a second ply of PEI/TMC crosslinks. Identities of the membranes were labeled. Operating pressure, 0.8 MPa gauge; Salt concentration, 500 ppm. Temperature, 23°C.

The separation performance of the 2-ply polyamide membranes (i.e., [(PEI/TMC)-(PIP/TMC)] and [(PIP/TMC)-(PEI/TMC)]) at given PIP and PEI concentrations during the formation of the two plies as well as the single-ply polyamide membranes formed with a mixed amine of PIP and PEI (i.e., [(PEI-PIP)/TMC]) is compared in Figures 4.17 and 18. The following general observations may be made. At a low PIP/PEI concentration ratio, the single-ply polyamide membranes formed with mixed amines of PIP and PEI have a higher pure water permeation flux than the 2-ply polyamide membranes. However, with an increase in the PIP/PEI concentration ratio, the single-ply polyamide membrane became close to [(PEI/TMC)-(PIP/TMC)] in terms of pure water permeation flux, but still higher than the pure water flux of [(PIP/TMC)-(PEI/TMC)]. For the 2-ply polyamide membranes, [(PIP/TMC)-(PEI/TMC)] tended to have a higher pure water flux than [(PEI/TMC)-(PIP/TMC)] at a low PIP/PEI concentration ratio, and the opposite held at a high PIP/PEI concentration ratio. All the membranes showed a $MgCl_2$ rejection of greater than 90%. For the other three solutes, the 2-ply polyamide membranes showed a higher rejection than the membrane having a single-ply of polyamide layer. Especially, [(PIP/TMC)-(PEI/TMC)] exhibited a good rejection to Na_2SO_4 at a relatively high PIP/PEI concentration ratio.

These results suggest that the membranes can be tailored by adjusting the number of deposited polyamide layers, the sequence of reactant depositions, and the compositions (i.e., mixed amines) and concentrations of the reactants during the interfacial polymerization. Factorial design experiments may be used to optimize the membrane fabrication conditions for nanofiltration treatment of target solutes in order for the membrane to work out its full potential.

It should be pointed out that similar to the single-ply membrane, if the deposition sequence was reversed (i.e., deposition of TMC prior to deposition of an amine), whether following a

sequence of TMC/PIP-TMC/PEI or TMC/PEI-TMC/PIP, the resulting membrane had a poor

salt rejection, presumably due to poor spreading and adhesion of TMC from the organic

solution onto a hydrophilic substrate surface.
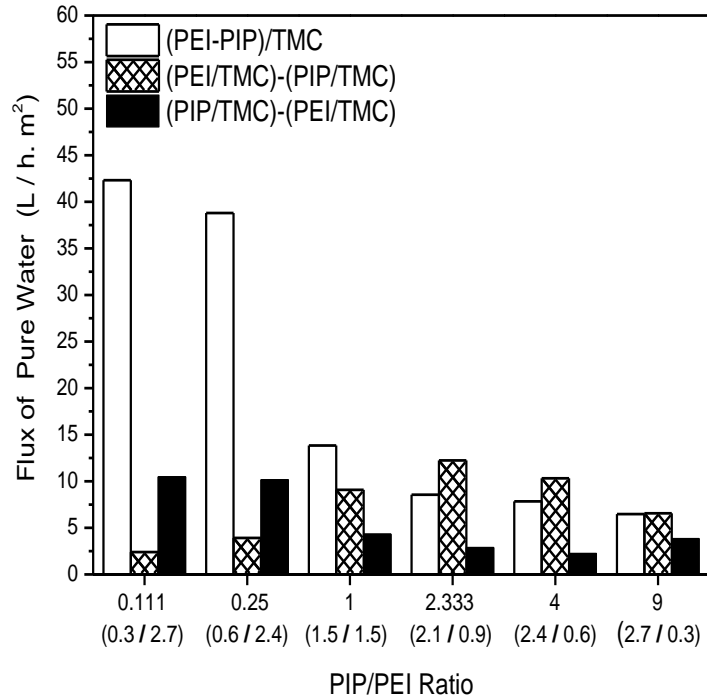
Figure 4.17 A comparison of permeation fluxes of pure water in three types of membranes: Single-ply polyamide membrane [(PEI-PIP)/TMC], and 2-ply polyamide membranes [(PEI/TMC)-(PIP/TMC)] and [(PIP/TMC)-(PEI/TMC)]. Operating pressure, 0.8 MPa gauge; Salt concentration, 500 ppm. Temperature, 23°C.
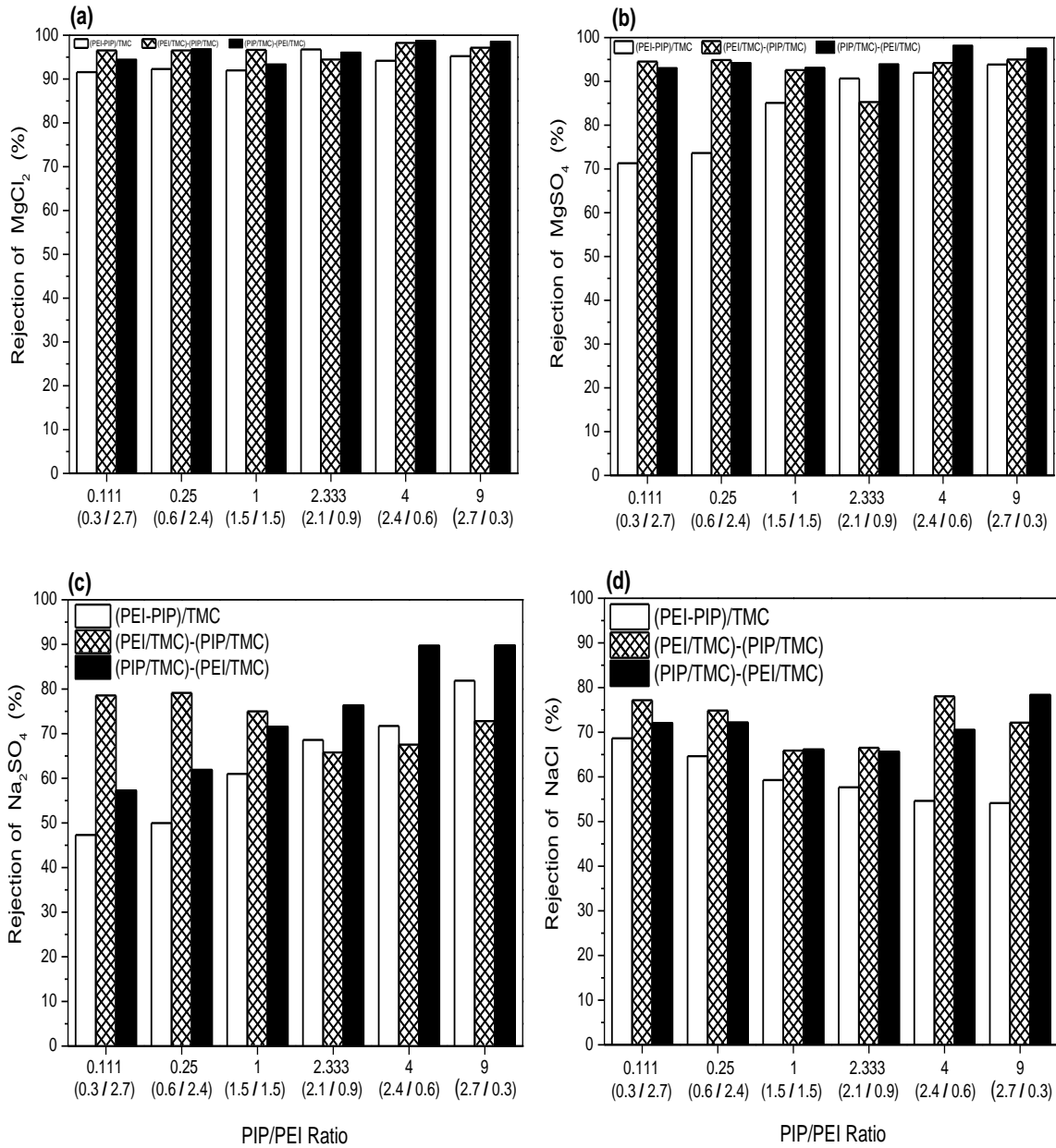
Figure 4.18 A comparison of salt rejections in the three types of membranes: (a) $MgCl_2$, (b) $MgSO_4$, (c) Na_2SO_4, and (d) NaCl. Operating pressure, 0.8 MPa gauge; Salt concentration, 500 ppm. Temperature, 23°C.

4.4 Conclusions

Thin film composite nanofiltration membranes with a single-ply and two-ply polyamide layer were fabricated by interfacial polymerization using polymeric amine polyethylenimine and monomeric amine piperazine. The following conclusions can be drawn from the study:

(1) Incorporation of a small amount of PIP in PEI for interfacial reaction with TMC would increases the permeation flux while still maintaining a good solute rejection.

(2) The 2-ply polyamide membranes showed a higher rejection than the membrane having a single-ply of polyamide layer. At a low PIP/PEI concentration ratio, the single-ply polyamide membranes formed with mixed amines of PIP and PEI tended to have a higher permeation flux than the 2-ply polyamide membranes. However, at a proper PIP/PEI ratio, 2-ply polyamide membranes with both a higher permeation flux and salt rejection than conventional single-ply polyamide membranes could be produced.

(3) For the 2-ply polyamide membranes, [(PIP/TMC)-(PEI/TMC)] showed a higher flux than [(PEI/TMC)-(PIP/TMC)] at a low PIP/PEI concentration ratio, and the opposite was observed at a high PIP/PEI concentration ratio.

(4) Both the single-ply polyamide membranes formed with mixed amines of PEI and PIP and the 2-ply polyamide membranes formed separately with PEI and PIP showed a $MgCl_2$ rejection of greater than 90%. The 2-ply polyamide membranes tended to have a better rejection to NaCl, Na_2SO_4 and $MgSO_4$ than the single-ply polyamide membrane.

Chapter 5.

Effects of chlorine exposure on nanofiltration performance of polyamide membranes[*]

5.1 Introduction

Polyamide-based thin film composite membranes are widely used for reverse osmosis and nanofiltration applications because of their high water fluxes and solute rejections [Lee *et al.*, 2010; Li and Wang, 2010]. However, the amide bonds (-CO-NH-) can be attacked by chlorine, which is commonly used in the form of sodium hypochlorite as a disinfectant to control biofouling or as a membrane cleaning agent [Jadas-Hecart *et al.*, 1992; Wilde and Shealy, 1992; Rajagopal *et al.*, 2003]. Severe chlorine attack will deteriorate the separation performance (e.g., a decline in salt rejection) and degrade the membrane chemically under certain circumstances. The degradation of polyamide membranes normally occurs due to N-chlorination of the amide nitrogen and ring chlorination [Kawaguchi and Tamura, 1984; Glater *et al.*, 1994; Kang *et al.*, 2007], as shown in Figure 5.1. The N-chlorination involves the substitution of hydrogen to chlorine on amide nitrogen to form N-chloroamide (Route A in Figure 5.1). Subjected to further intramolecular Orton rearrangement, the N-bonded chlorine atom can be eliminated to yield molecular chlorine, which will then attack the aromatic ring via electrophilic substitution (Route B in Figure 5.1), resulting in indirect ring chlorination. In addition, when the aromatic ring bonded to the N-H groups of the amide linkages is attacked by active (electrophilic) chlorine,

---

[*] Portions of this work have been accepted by *J. Membr. Sci.*

direct ring chlorination will occur (Route C in Figure 5.1). Besides the vulnerable amide nitrogen, the end amine groups with a high reactivity are also sensitive to oxidation. They are often chlorinated preferentially, breaking the secondary and tertiary amine linkages [Lee *et al.*, 1983; Glater *et al.*, 1994; Wei *et al.*, 2013].
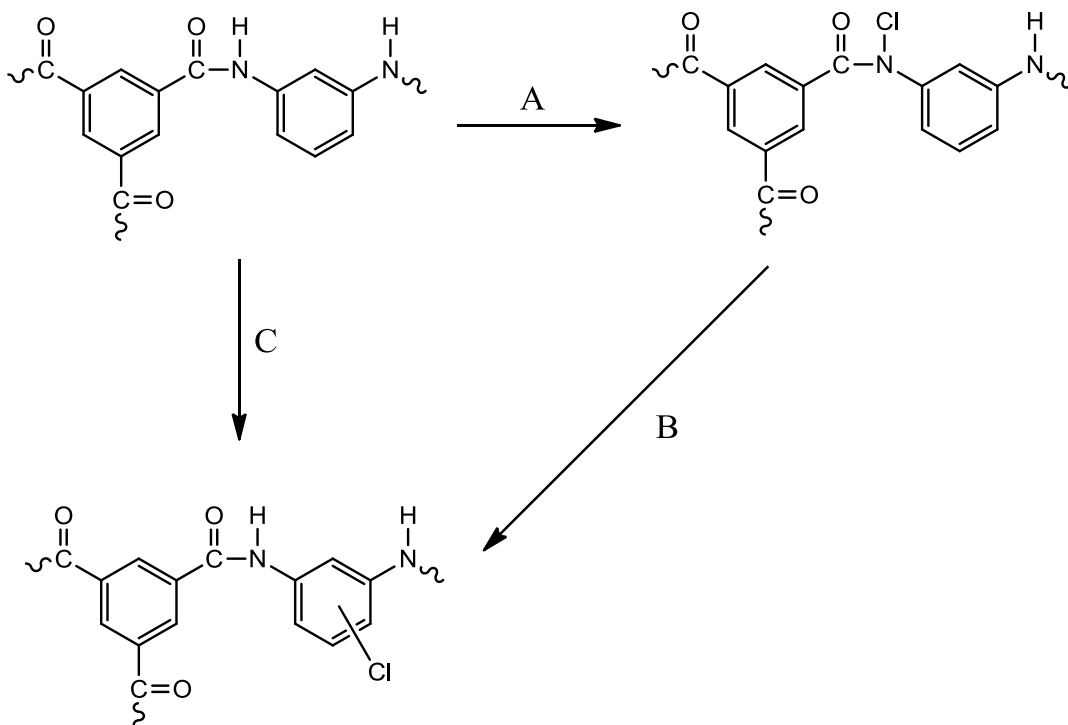
Figure 5.1 Chlorination mechanisms of the fully aromatic polyamide membranes: (A) N-chlorination; (A) and (B) ring chlorination by Orton rearrangement; (C) direct ring chlorination.

In view of the degradation mechanism, it is no surprise that polyethylenimine (PEI) based polyamide thin film composite membranes are sensitive to chlorine. The reactive sites for N-chlorination are readily available in the N-H linkages of the secondary amide bonds. The large number of end amine groups also makes the membrane vulnerable to chlorine attack. Therefore, the objective of the present study was to improve the chlorine resistance of polyamide membranes derived from polymeric amines. We choose to use piperazine (PIP) as an

amine reactant to form an outer layer by interfacial polymerization to protect the interior polyamide sublayer, thereby enhancing the chlorine tolerance of the membrane. As introduced in the previous chapters, piperazine is a traditional secondary amine. Since there is no amidic hydrogen in the tertiary amides formed from piperazine, the chlorine tolerance of a PIP-based polyamide membrane is expected to be enhanced [Credah *et al.*, 1974; Glater *et al.*, 1994]. There have been reports on the low chlorine uptake [Kawaguchi and Tamura, 1984; Konagaya and Watanabe, 2000; Do *et al.*, 2012a] and good chlorine tolerance [Parrini, 1983; Kamiyama *et al.*, 1984; Kurihara *et al.*, 1985; Gaeta *et al.*, 1991; Kurihara and Himeshima, 1991] of PIP-based polyamide membranes. In this chapter, an attempt was made to improve the chlorine resistance of PEI-based nanofiltration membranes by a sequence of interfacial polymerization from PIP and trimesoyl chloride (TMC) on top of PEI-based polyamide layer. The novel multiple-layered polyamide TFC membranes were composed of a PEI-based polyamide inner sublayer and a PIP-based polyamide outer sublayer, which were formed layer-by-layer sequentially by interfacial polymerization. It has been found in Chapter 4 that the [(PEI/TMC)-(PIP/TMC)] series membranes are positively charged even formed at a high PIP/PEI concentration ratio, which is distinct from the negatively charged [PIP/TMC] membranes. These membranes appear higher rejections to $MgCl_2$ and NaCl compared to some commercial PIP-based polyamide nanofiltration membranes (e.g., NS-300, NF40, NF40HF and XP45), and the membrane properties (e.g., surface charge, permeation flux and salt rejection can be tailored by controlling the PIP/PEI ratio [Wu *et al.*, 2015]. In this chapter, the PIP-based polyamide outer sublayer is expected to protect the PEI-based polyamide inner sublayer from chlorine attack. The effects of the distribution of PIP and PEI in the different polyamide sublayers and the number of PIP-based polyamide outer sublayers on the chlorine resistance of the resulting

membranes were studied.

The effects of the chlorination conditions, including pH and concentration of the chlorine solution and exposure time, on the nanofiltration performance of the membranes were studied. It should be noted that the chlorination intensity is customarily measured in the literature by the product of the chlorine concentration (ppm) and the exposure time (h), expressed in the unit of (ppm.h). As such, the chlorine concentration and exposure time may be perceived to be equivalent in terms of their impacts on membrane degradation. However, in view of the different possible chlorination mechanisms involved, the chlorination is unlikely to follow a first order reaction. It is thus reasonable to suspect that the chlorination intensity (ppm.h) alone is inadequate to measure the chlorination conditions. In the literature, the chlorination intensity is often used as a standalone parameter to characterize chlorine resistance of membranes, especially for comparisons of chlorine resistances of different membranes treated at different chlorination conditions. In this chapter, we attempted to elucidate that the joint effects of chlorine concentration and exposure duration on membrane chlorination cannot be represented by the chlorination intensity (ppm.h), a single composite parameter based on a multiplication of the two.

Moreover, although many studies have been done on deterioration of polyamide membranes due to chlorine exposure, the membranes used are primarily negatively-charged reverse osmosis membranes based on aromatic polyamide formed from m-phenylene diamine (MPD) and trimesoyl chloride (TMC). Little work is done on the chlorine resistance properties of positively-charged nanofiltration membranes. This chapter looked into the effects of chlorine exposure on nanofiltration performance of the self-made positively-charged polyamide membranes, which appear higher isoelectric points [Wu *et al.*, 2015] and higher rejections to

divalent cationic salt MgCl$_2$ (shown in Table 5.1) at pH 6.8. The membrane rejections to representative solutes NaCl, MgCl$_2$, MgSO$_4$ and Na$_2$SO$_4$ were evaluated. The changes in chemical composition, surface morphology and surface hydrophilicity of the membranes due to chlorine exposure were also characterized by ATR-FTIR, FE-SEM, AFM and contact angle tests, respectively.

5.2 Experimental

5.2.1 Materials, membrane preparation, characterization and separation performance measurements

The chlorine solution was prepared from a commercially available sodium hypochlorite solution (NaClO, 6% available chlorine, BDH Chemicals). The pH values of the chlorine solution were controlled by using HCl (37%, Sigma-Aldrich) or NaOH (Caledon Laboratories). Other materials used were the same as described in the previous chapters.

The multiple-layered polyamide nanofiltration membranes were prepared by sequential interfacial polymerization from PEI/TMC and PIP/TMC, which has been described in the previous chapters. To investigate the effects of the PIP concentration used in interfacial polymerization on the chlorine resistance of the membranes, 2-ply polyamide membranes with a PEI/TMC inner-layer and a PIP/TMC outer layer were prepared. The concentration of TMC solution used was 0.3 wt%. The concentrations of PEI and PIP were varied, while maintaining a constant total amine concentration of 3.0 wt% in the two cycles of interfacial polymerization (that is, the sum of PEI concentration used in the first cycle of interfacial polymerization and PIP concentration in the second cycle was 3.0 wt%). For comparison purposes, membranes were prepared with the following reactant compositions: [(PEI$_{1.5}$/TMC$_{0.3}$)]$_2$ (i.e., PIP/PEI concentration ratio 0), [(PEI$_{1.0}$/TMC$_{0.3}$)-(PIP$_{2.0}$/TMC$_{0.3}$)] (i.e., PIP/PEI ratio 2) and

[(PEI$_{0.6}$/TMC$_{0.3}$)-(PIP$_{2.4}$/TMC$_{0.3}$)] (i.e., PIP/PEI ratio 4). The subscripts in the membrane designations denote the reactant concentration (in wt%) used in the interfacial polymerization. In addition, membranes comprising of one PEI/TMC inner layer and multiple PIP/TMC polyamide outer layers were prepared to investigate their chlorine resistance. The concentrations of PEI and TMC used for the first cycle of interfacial polymerization were 1.0 wt% and 0.2 wt% respectively. For subsequent cycles of PIP/TMC interfacial polymerizations, different concentrations of PIP and TMC (but at a constant PIP/TMC concentration ratio of 5) were used. Such membranes were designated as [(PEI$_{1.0}$/TMC$_{0.2}$)-(PIP$_x$/TMC$_y$)$_n$], where the subscripts x and y denote the concentrations (in wt%) of PIP and TMC, and n is the number of PIP/TMC layers. The total amine concentration was also maintained as 3.0 wt% for comparison.

Throughout the membrane preparation process, the reactant deposition time and drying time for PEI, PIP and TMC, the heat treatment time and temperature were all the same as Chapter 4. The designations for membranes used in this study are summarized in Table 5.1.

The membrane characterizations (including ATR-FTIR, contact angle test, FE-SEM and AFM), experimental set up and separation performance measurements are similar as described in the previous chapters.

5.2.2 Chlorine treatment

The membranes were immersed in NaClO solutions at different concentrations. The pH values of the solutions were adjusted to 4, 7 and 9 with HCl or NaOH, respectively. The chlorine exposure time was 1 h.

The chlorination intensity is customarily measured with the product of chlorine concentration and exposure time in the unit of (ppm.h). In order to elucidate whether such a composite parameter was adequate to measure chlorine attack to the membrane, two additional

series of experiments were carried out at a chlorine solution at pH of 7. One was at a constant chlorine concentration of 50 ppm for different exposure time (corresponding to chlorination intensities of 50 - 3,000 ppm.h), and the other was at a fixed chlorination intensity of 2000 (ppm.h) with varying chlorine concentrations and exposure time (e.g., 10 ppm for 200 h, 20 ppm for 100 h, and 8000 ppm for 0.25 h). For a given membrane sample, the variations in the permeation flux and salt rejection were found to be less than 2% in duplicate chlorine treatments.

5.3 Result and discussion

5.3.1 Use of PIP/TMC outer layers to improve membrane resistance to chlorine

Surface composition

The chemical compositions of the membrane surface before and after chlorine treatment were analyzed using ATR-FTIR, and the ATR-FTIR spectra are shown in Figure 5.2 for pristine and chlorine treated $[(PEI_{1.5}/TMC_{0.3})]_2$, $[(PEI_{0.6}/TMC_{0.3})-(PIP_{2.4}/TMC_{0.3})]$ and $[(PEI_{1.0}/TMC_{0.2})]$-$[(PIP_{0.67}/TMC_{0.13})]_3$ membranes.

Table 5.1 Designation of membranes (based on reactant deposition sequence, concentration of reactant and the number of interfacially formed polyamide sublayers) as well as water fluxes and solute rejections of pristine membranes[*]

Membrane designation	Description	Pure water flux [L/(m^2.h)]	Solute rejections
[(PEI$_{1.5}$/TMC$_{0.3}$)]$_2$	2-ply polyamide layer formed from interfacial reaction of surface-deposited PEI (solution concentration 1.5 wt%) and TMC (solution concentration 0.3 wt%)	1.76	MgCl$_2$: 96.6% MgSO$_4$: 94.6% Na$_2$SO$_4$: 77.9% NaCl: 86.4%
[(PEI$_{1.0}$/TMC$_{0.3}$)-(PIP$_{2.0}$/TMC$_{0.3}$)]	2-ply polyamide layer comprising of a first ply of PEI/TMC crosslinks and a second ply of PIP/TMC crosslinks; amine concentrations is 1.0 wt% for PEI and 2.0 wt% for PIP, and TMC concentration is 0.3 wt%	13.04	MgCl$_2$: 94.5% MgSO$_4$: 93.3% Na$_2$SO$_4$: 65.8% NaCl: 66.5%
[(PEI$_{0.6}$/TMC$_{0.3}$)-(PIP$_{2.4}$/TMC$_{0.3}$)]	2-ply polyamide layer comprising of a first ply of PEI/TMC crosslinks and a second ply of PIP/TMC crosslinks; amine concentration is 0.6 wt% for PEI and 2.4 wt% for PIP, and TMC concentration is 0.3 wt%	10.32	MgCl$_2$: 98.3% MgSO$_4$: 94.2% Na$_2$SO$_4$: 67.5% NaCl: 78.0%
[(PEI$_{1.0}$/TMC$_{0.2}$)]-[(PIP$_{2.0}$/TMC$_{0.4}$)]	2-ply polyamide layer comprising of a first ply of PEI/TMC crosslinks and a second ply of PIP/TMC crosslinks; amine concentration is 1.0 wt% for PEI and 2.0 wt% for PIP, and TMC concentrations are 0.2 and 0.4 wt% for the two plies, respectively	11.12	MgCl$_2$: 96.6% MgSO$_4$: 93.8% Na$_2$SO$_4$: 63.7% NaCl: 63.7%
[(PEI$_{1.0}$/TMC$_{0.2}$)]-[(PIP$_{1.0}$/TMC$_{0.2}$)]$_2$	3-ply polyamide layer comprising of a first ply of PEI/TMC crosslinks and 2 plies of PIP/TMC crosslinks; amine concentration is 1.0 wt% for PEI and 1.0 wt% for PIP, and TMC concentration is 0.2 wt%	14.64	MgCl$_2$: 89.8% MgSO$_4$: 84.6% Na$_2$SO$_4$: 68.0% NaCl: 53.1%
[(PEI$_{1.0}$/TMC$_{0.2}$)]-[(PIP$_{0.67}$/TMC$_{0.13}$)]$_3$	4-ply polyamide layer comprising of a first ply of PEI/TMC crosslinks and 3 plies of PIP/TMC crosslinks; amine concentration is 1.0 wt% for PEI and 0.67 wt% for PIP, and TMC concentration is 0.13 wt % except for the first ply for which the TMC concentration is 0.2 wt%.	8.24	MgCl$_2$: 83.3% MgSO$_4$: 82.1% Na$_2$SO$_4$: 79.3% NaCl: 35.3%

[*] Test conditions: Temperature 23 °C, transmembrane pressure 0.8 MPa, solute concentration in feed 500 ppm, pH 6.8.

For pristine membrane [(PEI$_{1.5}$/TMC$_{0.3}$)]$_2$, there are two bands at 1640 cm^{-1} and 1550 cm^{-1} that are characteristic of the amide-I (C=O stretching) band and the amide-II (N-H) band of the amide groups (-CONH-) formed form PEI and TMC. The band at 1610 cm^{-1} is related to the hydrogen-bonded C=O of the amide groups [Skrovanek *et al.*, 1986; Belfer *et al.*, 1998]. It is observed that after chlorine treatment the band intensity at 1610 cm^{-1} gradually decreases and eventually disappears when the chlorination intensity is sufficiently strong, and that the band at 1640 cm^{-1} shifts to 1650 cm^{-1} for the chlorine treated [(PEI$_{1.5}$/TMC$_{0.3}$)]$_2$ membrane. These changes are presumably due to the transformation of hydrogen bonding carbonyl (C(=O)-NH, at 1640 cm^{-1}) to non-hydrogen bonding carbonyl (C(=O)-NCl, at 1650 cm^{-1}) [Kwon and Leckio, 2006b; Kang *et al.*, 2007; Buch *et al.*, 2008; Ettori *et al.*, 2011] resulting from the broken hydrogen bonds between C=O and N-H groups. It has been reported that the amine-II band of the membranes will shift to lower wavenumber and the intensity will decrease after chlorine treatment [Belfer *et al.*, 1998; Kwon and Leckie, 2006a, 2006b; Kang *et al.*, 2007; Do *et al.*, 2012a, 2012b; Xu *et al.*, 2013]. However, there's invisible change of amine-II band for chlorinated membranes in present study. This is presumably due to the polymeric structures of amine (PEI in this study), which may influence the sensitivity for detection the change of amide-II characteristic peak [Yu *et al.*, 2011; Liu *et al.*, 2012a; Wu *et al.*, 2014, 2015].

It is interesting that the pristine membrane [(PEI$_{0.6}$/TMC$_{0.3}$)-(PIP$_{2.4}$/TMC$_{0.3}$)] showed only a band at 1629 cm^{-1} for amide-I (C=O stretching) but no band is observed for amide-II (N-H). This is consistent with the chemical structure of a tertiary amide without having amidic hydrogen formed from PIP and TMC. The disappearance of the amide-II (N-H) band also indicates that the PEI-based polyamide inner layer of the membrane is fully covered by the PIP-based polyamide outer layer. In contrast to the spectral changes observed for membrane

$[(PEI_{1.5}/TMC_{0.3})]_2$ due to chlorine treatment, there is no noticeable change in the ATR-FTIR peaks for $[(PEI_{0.6}/TMC_{0.3})-(PIP_{2.4}/TMC_{0.3})]$ membrane. Similar observations were obtained by Do *et al.* [2012a] for the commercial PIP based nanofiltration membrane (i.e., NF270). These results suggest that the outer layer formed at a relatively high PIP concentration is dense enough to help the PEI-based polyamide inner layer against chlorine attack.

Membrane $[(PEI_{1.0}/TMC_{0.2})]-[(PIP_{0.67}/TMC_{0.13})]_3$, which has 3-ply PIP/TMC outer sublayers formed at a relatively low PIP concentration, showed no obvious change in chemical structure on its surface when it was subjected to a chlorine treatment at 500 ppm $\times$ 1 h. However, when the chlorination strength was increased to 3000 ppm $\times$ 1 h, the characteristic band of amide-I (C=O stretching) shifted from 1629 cm^{-1} to 1638 cm^{-1} and the band intensity decreased, which is believed to a result of the bond cleavage of the amide groups. The invisible change of amide-II from PEI/TMC crosslinks may be also ascribed to the influence of polymeric structure of PEI, and the top deposited PIP/TMC crosslinks. In addition, the band intensities at 1441 cm^{-1} and 1414 cm^{-1} corresponding to the C=C stretching of the aromatic ring also decreased. Since no aromatic amine was used for the interfacial polymerization, this spectral change was caused by the degradation of the aromatic ring from the polyethersulfone (PES) substrate.
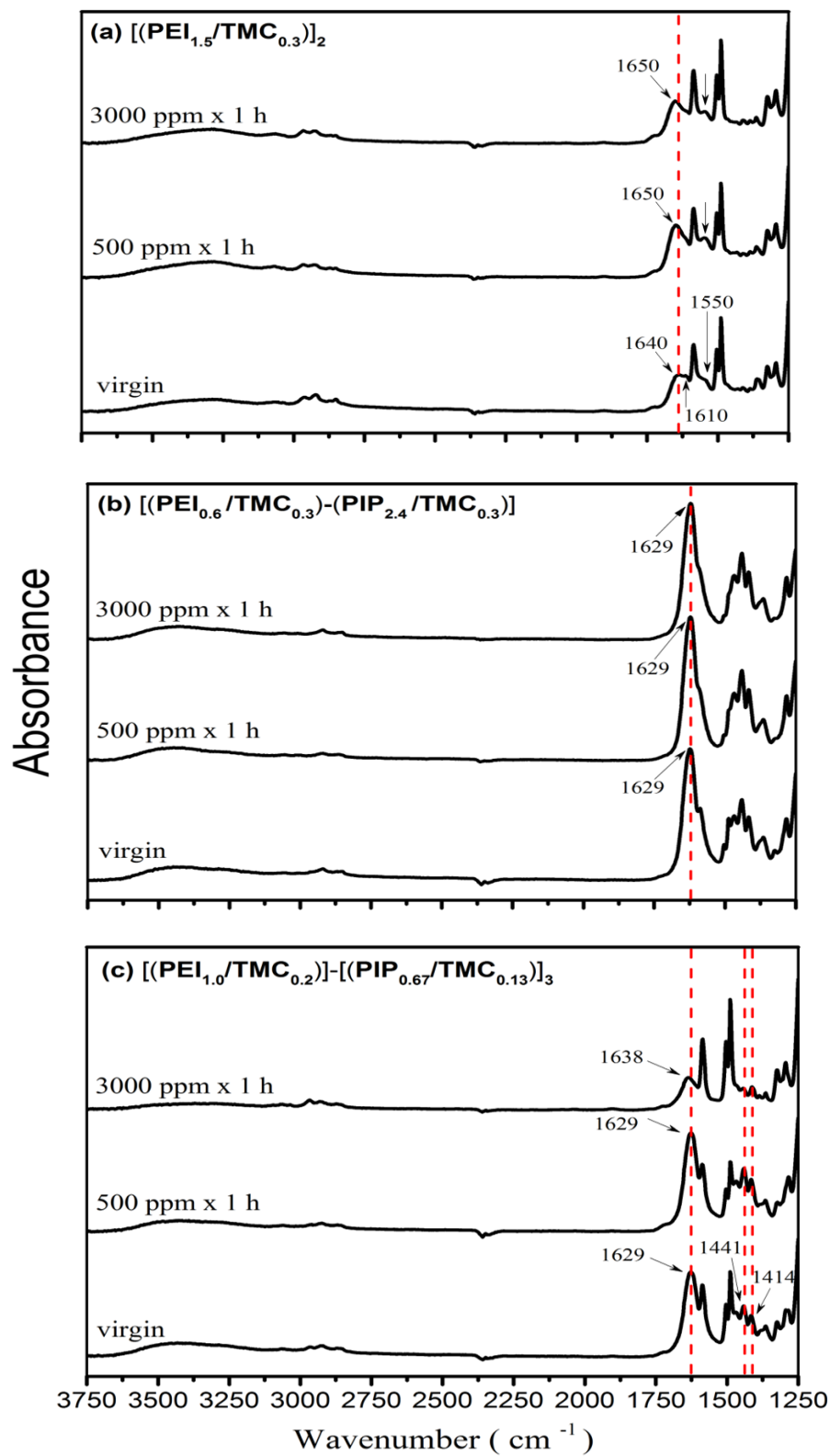
Figure 5.2 ATR-FTIR spectra of membranes (a) $[(PEI_{1.5}/TMC_{0.3})]_2$, (b) $[(PEI_{0.6}/TMC_{0.3})$-$(PIP_{2.4}/TMC_{0.3})]$ and (c) $[(PEI_{1.0}/TMC_{0.2})]$-$[(PIP_{0.67}/TMC_{0.13})]_3$: pristine and chlorinated at pH 7.

Surface morphology

The surface morphology of the membranes was examined using SEM. Figure 5.3 shows the surface images of a few pristine and chlorine treated membranes. It can be seen that various types of structures, including small debris, large "patch-like" structures and small ridge-valley structures, were observed on the surface of pristine $[(PEI_{1.5}/TMC_{0.3})]_2$ membrane (Figure 5.3(a)). After chlorine treatment at 500 ppm × 1 h, some of the surface structures cast off (Figure 5.3(b)). When the chlorination intensity reached 3000 ppm × 1 h, the membrane surface became quite smooth and uniform, and the top polyamide layer appeared to be peeled away (Figure 5.3(c)). *Soice et al.* [2004] and *Xu et al.* [2013] also observed the disappearance of the skin layer from the support layer for MPD-TMC TFC reverse osmosis membranes under harsh chlorination conditions (pH 7, ≥ 10,000 ppm.h). Such membrane degradation can be explained from two aspects. First, the barrier skin layer in a TFC membrane is anchored to the substrate by physical adhesion and mechanical interlocking into the pores of the substrate [Bartels, 1989]. In the multilayered TFC membranes studied here, there may also be interpenetration between the polyamide sublayers in the membrane skin. The strength of physical bonding between the polyamide skin layer and the PES substrate will depend on the degree of membrane swelling and the ductility of the polyamide layer. *Soice et al.* [2004] observed a reduction in the ductility of polyamide film upon chlorine exposure. Thus, the free chlorine can penetrate into the membrane and destroy the membrane structure if the chlorination intensity is strong enough. On the other hand, a strong dose of chlorine can break the polyamide bonds (as confirmed by the ATR-FTIR spectra discussed above) and lead to the collapse of the polymer chains.
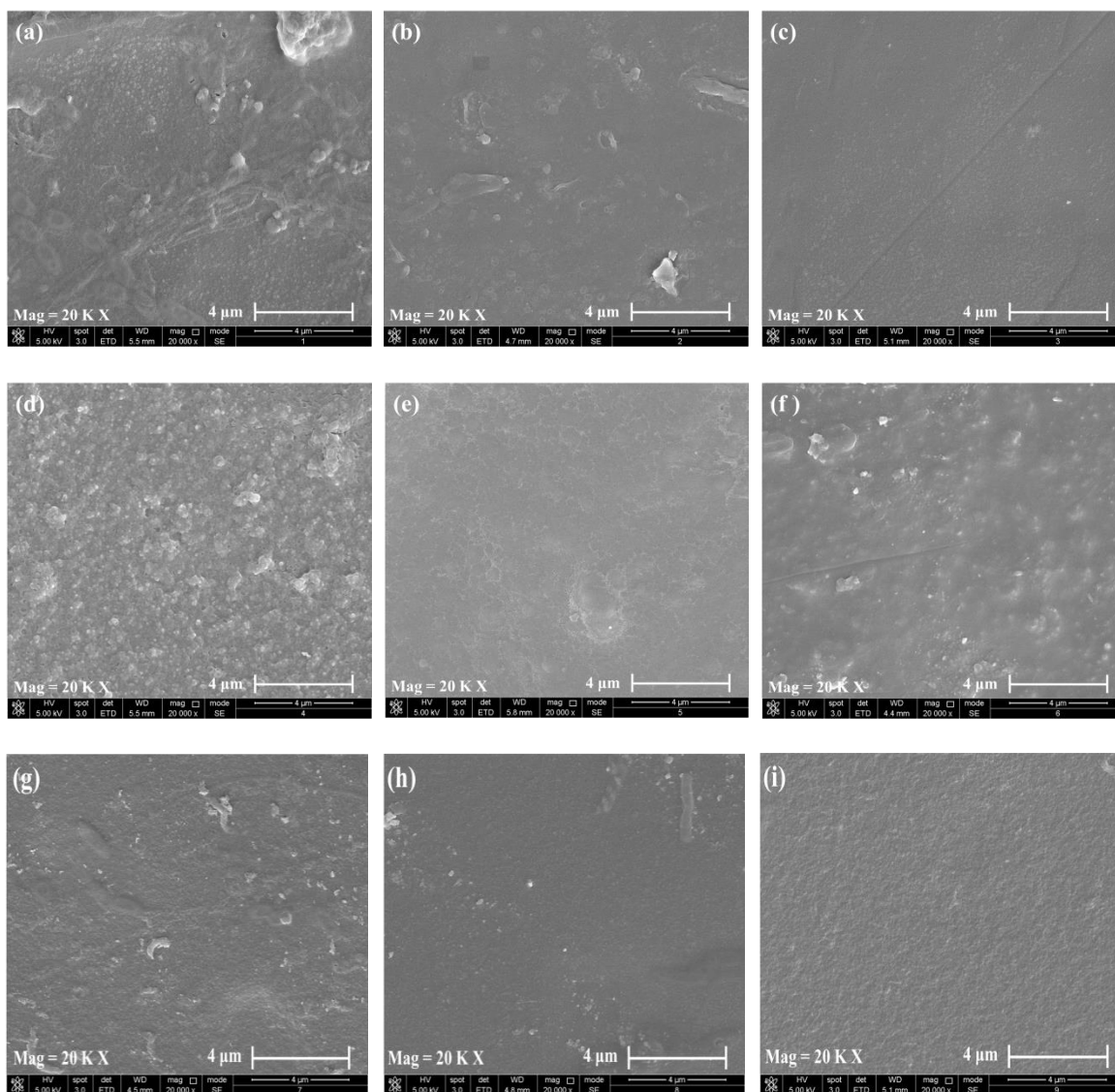
Figure 5.3 Surface images (20,000×) of (a) pristine, (b) chlorinated: 500 ppm ×1 h, (c) chlorinated: 3000 ppm ×1 h for $[(PEI_{1.5}/TMC_{0.3})]_2$ membrane; (d) pristine, (e) chlorinated: 500 ppm ×1 h, (f) chlorinated: 3000 ppm ×1 h for $[(PEI_{0.6}/TMC_{0.3})-(PIP_{2.4}/TMC_{0.3})]$ membrane and (g) pristine, (h) chlorinated: 500 ppm ×1 h, (i) chlorinated: 3000 ppm ×1 h for $[(PEI_{1.0}/TMC_{0.2})]-[(PIP_{0.67}/TMC_{0.13})]_3$ membrane, chlorinated at pH 7.

For membrane $[(PEI_{0.6}/TMC_{0.3})-(PIP_{2.4}/TMC_{0.3})]$, the surface of the pristine membrane looked compact with many globular structures and a few "patch-like" structures (Figure 5.3(d)). After exposure to chlorine at 500 ppm × 1 h, loose cellular structures appeared on the membrane surface (Figure 5.3(e)). When the chlorination intensity was increased to 3000 ppm × 1 h, globular structures, small debris and "patch-like" structures were distributed loosely on

142

the membrane surface (Figure 5.3(f)). Compared the surface morphologies of the pristine membranes [PEI$_{3.0}$/TMC$_{0.6}$] (in Chapter 4), [(PEI$_{1.5}$/TMC$_{0.3}$)]$_2$ (Fig. 3(a)) and [(PEI$_{0.6}$/TMC$_{0.3}$)-(PIP$_{2.4}$/TMC$_{0.3}$)] (Fig. 3(d)), it suggests that the PEI/TMC crosslinks, either formed as a single layer with high PEI concentration (i.e., 3.0 wt%) or a double-layer with low PEI concentration (i.e., 1.5 wt%), are likely to form the "patch-like" structures. Therefore, the small globular structures may come from PIP/TMC crosslinks. The surface morphology of membrane [(PEI$_{0.6}$/TMC$_{0.3}$)-(PIP$_{2.4}$/TMC$_{0.3}$)] indicates that the PEI-based polyamide inner layer can be well covered by the PIP-based polyamide outer layer in membrane [(PEI$_{0.6}$/TMC$_{0.3}$)-(PIP$_{2.4}$/TMC$_{0.3}$)]. The loose cellular structures of chlorine treated membrane at 500 ppm $\times$ 1 h was presumably due to the collapse of the polymer chains caused by moderate degree of chlorine degradation, while the "patch-like" structures observed after exposure to a high dose of chlorine (e.g., 3000 ppm $\times$ 1 h) indicated that when the chlorine treatment intensity was sufficiently high, the PIP-based polyamide outer layer would be degraded and the inner PEI-based polyamide layer would also be affected. However, it may be pointed out that the PIP/TMC crosslinks are shown to be more resistant to chlorine than PEI/TMC crosslinks. Unlike membrane [(PEI$_{1.5}$/TMC$_{0.3}$)]$_2$, there was no peeling off of the polyamide skin layer from membrane [(PEI$_{0.6}$/TMC$_{0.3}$)-(PIP$_{2.4}$/TMC$_{0.3}$)]. This is another indication that applying an outer polyamide sublayer based on PIP/TMC crosslinks on top of an inner polyamide sublayer based on PEI/TMC improves the chlorine resistance of the membranes.

In view that at given membrane formation conditions, the use of an additional PIP/TMC sublayer would decrease the membrane permeability, it was thus decided to use lower amine concentrations when fabricating membranes with multiple PIP/TMC sublayers in order to minimize the reduction in membrane permeability. It was found that the membrane

$[(PEI_{1.0}/TMC_{0.2})]\text{-}[(PIP_{0.67}/TMC_{0.13})]_3$, which consists of 3 PIP/TMC sublayers, has similar

changes on the surface morphology due to chlorine treatment (Figures 5.3(g), (h) and (i)) as the

membrane $[(PEI_{0.6}/TMC_{0.3})\text{-}(PIP_{2.4}/TMC_{0.3})]$.

The AFM analyses of the membrane surface are in agreement with the SEM observations.

The surface roughness data are shown in Table 5.2. For purpose of illustration, Figure 5.4

shows the surface images of pristine and chlorine-treated $[(PEI_{0.6}/TMC_{0.3})\text{-}(PIP_{2.4}/TMC_{0.3})]$

membranes. There were some polymer aggregates on the surface of the pristine membrane

(Figure 5.4(a)), with a root mean square roughness of 190.4 nm. After exposure to chlorine at

500 ppm for 1 h, some nodular structures showed up on the membrane surface (Figure 5.4(b))

and the membrane surface became smoother (roughness 68.4 nm). With a further increase in

the chlorine exposure intensity to 3,000 ppm $\times$ 1 h, the nodular structures became smaller and

more scattered (Figure 5.4(c)), while the membrane surface roughness remained essentially the

same.

Table 5.2 Root mean square roughness of the pristine and chlorinated (at pH 7) $[(PEI_{0.6}/TMC_{0.3})\text{-}(PIP_{2.4}/TMC_{0.3})]$ membrane analyzed by AFM

Chlorination condition	Root mean square roughness (nm)
0	190.4
500 ppm $\times$ 1 h	68.4
3000 ppm $\times$ 1 h	67.4
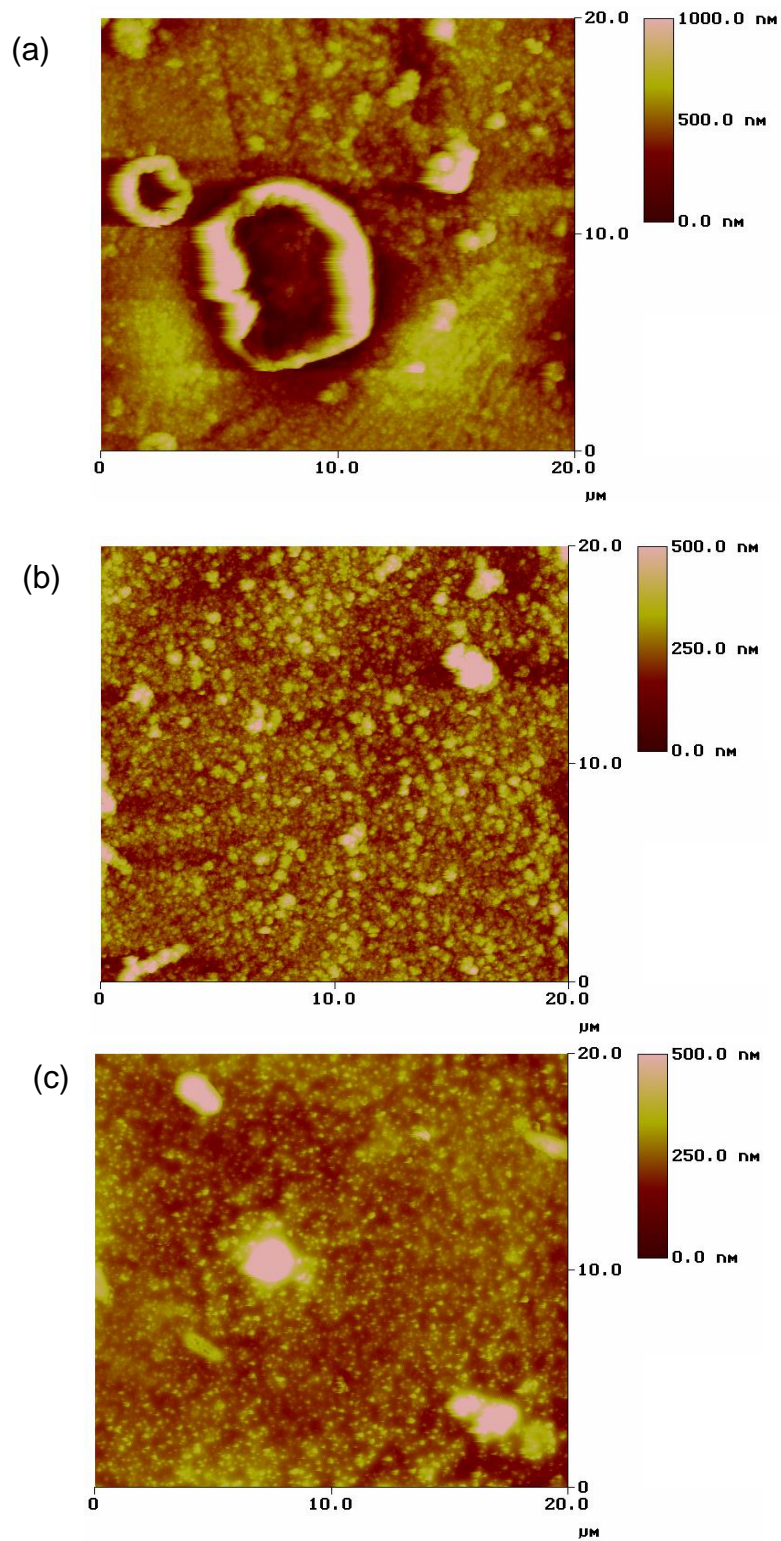
Figure 5.4 AFM images (20 μm × 20 μm) of (a) pristine, (b) chlorinated: 500 ppm × 1 h, (c) chlorinated: 3000 ppm × 1 h for [(PEI$_{0.6}$/TMC$_{0.3}$)-(PIP$_{2.4}$/TMC$_{0.3}$)] membrane, chlorinated at pH 7.

145

NF performance

To evaluate the nanofiltration performance of the membranes after exposure to chlorine, normalized permeation flux and solute rejection were used. They were defined as the flux and salt rejection of the chlorine-treated membrane relative to those of the pristine membrane. Figure 5.5 shows the normalized pure water flux of three membranes after exposure to chlorine at different intensities: $[(PEI_{1.5}/TMC_{0.3})]_2$, $[(PEI_{1.0}/TMC_{0.3})-(PIP_{2.0}/TMC_{0.3})]$ and $[(PEI_{0.6}/TMC_{0.3})-(PIP_{2.4}/TMC_{0.3})]$. The normalized rejections of the membranes to solutes $MgCl_2$, $MgSO_4$, Na_2SO_4 and NaCl are shown in Figure 5.6. The water flux and solute rejection of the pristine membranes are shown in Table 5.1.
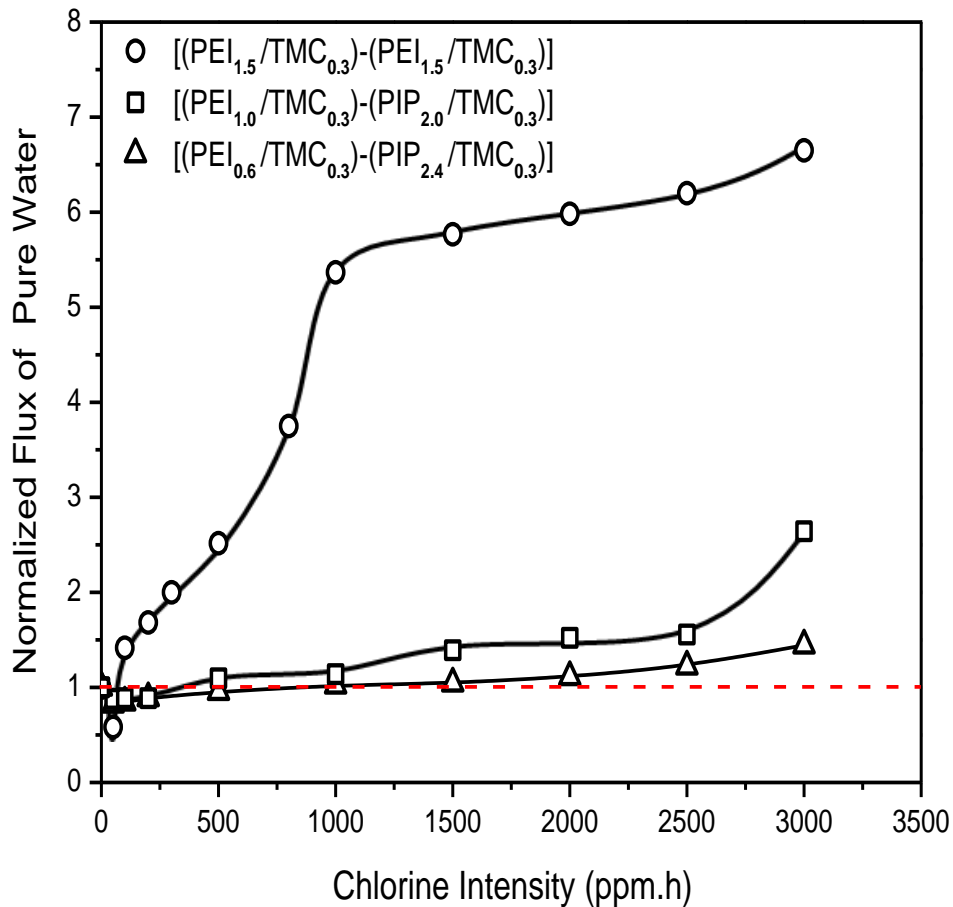
Figure 5.5 Normalized flux of pure water for membranes $[(PEI_{1.5}/TMC_{0.3})]_2$, $[(PEI_{1.0}/TMC_{0.3})-(PIP_{2.0}/TMC_{0.3})]$ and $[(PEI_{0.6}/TMC_{0.3})-(PIP_{2.4}/TMC_{0.3})]$, chlorinated at pH 7.

Figure 5.6 Normalized rejections of (a) $MgCl_2$, (b) $MgSO_4$, (c) Na_2SO_4 and (d) NaCl for membranes $[(PEI_{1.5}/TMC_{0.3})]_2$, $[(PEI_{1.0}/TMC_{0.3})-(PIP_{2.0}/TMC_{0.3})]$ and $[(PEI_{0.6}/TMC_{0.3})-(PIP_{2.4}/TMC_{0.3})]$, chlorinated at pH 7.

For membrane $[(PEI_{1.5}/TMC_{0.3})]_2$, the water flux experienced a 50% decrease initially when the membrane was subjected to chlorine treatment at 50 ppm $\times$ 1 h, and then increased substantially (more than 5 times) when the chlorination intensity increased to 1000 ppm $\times$ 1 h. After that, a further increase in the chlorination intensity resulted in a more moderate increase in the water flux. Membrane $[(PEI_{1.0}/TMC_{0.3})-(PIP_{2.0}/TMC_{0.3})]$ showed a slight decrease in

water flux when exposed to chlorine at 50 ppm $\times$ 1 h, and then increased to 1.5 times that of the pristine when the chlorination intensity was increased to 2500 ppm $\times$ 1 h. Membrane [(PEI$_{0.6}$/TMC$_{0.3}$)-(PIP$_{2.4}$/TMC$_{0.3}$)] showed a similar trend, and the membrane flux was affected by the chlorine exposure less significantly.

As for the solute rejection, all the three membranes showed a decreasing trend in the membrane rejections to MgCl$_2$ and NaCl with an increase in the chlorination intensity. Among the three membranes, membrane [(PEI$_{0.6}$/TMC$_{0.3}$)-(PIP$_{2.4}$/TMC$_{0.3}$)] was affected by chlorine least significantly; chlorine treatment at a high intensity of 3000 ppm $\times$ 1 h resulted in only a 20% reduction in NaCl rejection and a 3% reduction in MgCl$_2$ rejection. Interestingly, this membrane showed an improved rejection to solutes MgSO$_4$ and Na$_2$SO$_4$ after exposure to chlorine as compared to the pristine membrane. However, both the membranes [(PEI$_{1.5}$/TMC$_{0.3}$)]$_2$ and [(PEI$_{1.0}$/TMC$_{0.3}$)-(PIP$_{2.0}$/TMC$_{0.3}$)] showed a fluctuated trend of rejections to solutes MgSO$_4$ and Na$_2$SO$_4$ after exposure to chlorine.

The declines in both the membrane flux and rejection to MgCl$_2$ and NaCl at a low intensity of chlorine exposure are believed to result from conformational deformations of the polyamide chains. It has been shown that the intermolecular hydrogen bonds will be disrupted and the symmetry of the polyamide network will be destroyed by N-chlorination [Avlonitis *et al*., 1992; Kwon and Leckie, 2006a, 2006b]. The conformational changes of the polymer chains due to partial destruction of the polyamide rigid structure will enhance the free volume and flexibility of the polymer, making it easier for the solutes to pass the membrane. On the other hand, the polymer chains are more vulnerable to collapse under pressure [Kwon and Leckio, 2006b], and compaction of the membrane barrier layer under operating pressure (which was 0.8 MPa in the present study) will lead to a decrease in membrane permeability. In addition, membrane

exposure to a low concentration chlorine at pH 7 can make the membrane surface more hydrophobic (which will be shown later), and this will also tend to decrease the water flux [Koo *et al.*, 1986]. However, at a high intensity of chlorine exposure, polyamide will be hydrolyzed, resulting in an increase in the water flux. The hydrolysis is expected to influence solute rejections differently, depending on the nature of the solutes. The degradation of the crosslinked structure will in general decrease the salt rejection. However, from the observations of the decreased isoelectrical points in previous studies [Kwon and Leckie, 2006a; Do *et al*., 2012a, 2012b; Xu *et al.*, 2013], it has been confirmed that the surface of the chlorinated membrane will become more negatively charged, presumably due to the inhibition of NH_2^+/NH_3^+ groups and increase of COO^- groups. This relatively negatively charged surface favors the rejection of multivalent anionic solutes (i.e., $MgSO_4$ and Na_2SO_4), which may explain the different behavior of the membranes to reject different solutes, as shown in Figure 5.6.

Based on the flux and rejection data shown in Figures 5.5 and 5.6, it is evident that the chlorine tolerance of membrane was improved by using the PIP/TMC outer layer. To further investigate the protective effect of PIP-based polyamide outer layers against chlorine, membranes with different numbers of PIP/TMC sublayers were prepared and tested for nanofiltration performance. Figures 5.7 and 5.8 show the normalized pure water flux and solute rejections, respectively, for membranes $[(PEI_{1.0}/TMC_{0.2})]$-$[(PIP_{2.0}/TMC_{0.4})]$, $[(PEI_{1.0}/TMC_{0.2})]$-$[(PIP_{1.0}/TMC_{0.2})]_2$ and $[(PEI_{1.0}/TMC_{0.2})]$-$[(PIP_{0.67}/TMC_{0.13})]_3$. Their water flux and solute rejection before chlorine exposure are shown in Table 5.1. The permeation flux increased with an increase in the intensity of chlorine exposure, and the impact of chlorine on the membrane permeability is in the order of $[(PEI_{1.0}/TMC_{0.2})]$-$[(PIP_{2.0}/TMC_{0.4})]$ < $[(PEI_{1.0}/TMC_{0.2})]$-

$[(PIP_{1.0}/TMC_{0.2})]_2 < [(PEI_{1.0}/TMC_{0.2})]\text{-}[(PIP_{0.67}/TMC_{0.13})]_3$. Their rejections to $MgCl_2$ and NaCl decreased with increased chlorine exposure intensity, while the opposite was observed for Na_2SO_4 rejection. Apparently, exposure of the membrane to chlorine is not always detrimental to the membrane performance, and one may take advantage of the chlorine treatment to improve both permeation flux and solute retention for certain feed systems (e.g., Na_2SO_4 solutions). For $MgSO_4$ rejection, there was only 8% decline for the membranes $[(PEI_{1.0}/TMC_{0.2})]\text{-}[(PIP_{2.0}/TMC_{0.4})]$ and $[(PEI_{1.0}/TMC_{0.2})]\text{-}[(PIP_{1.0}/TMC_{0.2})]_2$, and 5% decline for the membrane $[(PEI_{1.0}/TMC_{0.2})]\text{-}[(PIP_{0.67}/TMC_{0.13})]_3$ when the chlorine exposure intensity was 3000 ppm $\times$1 h.
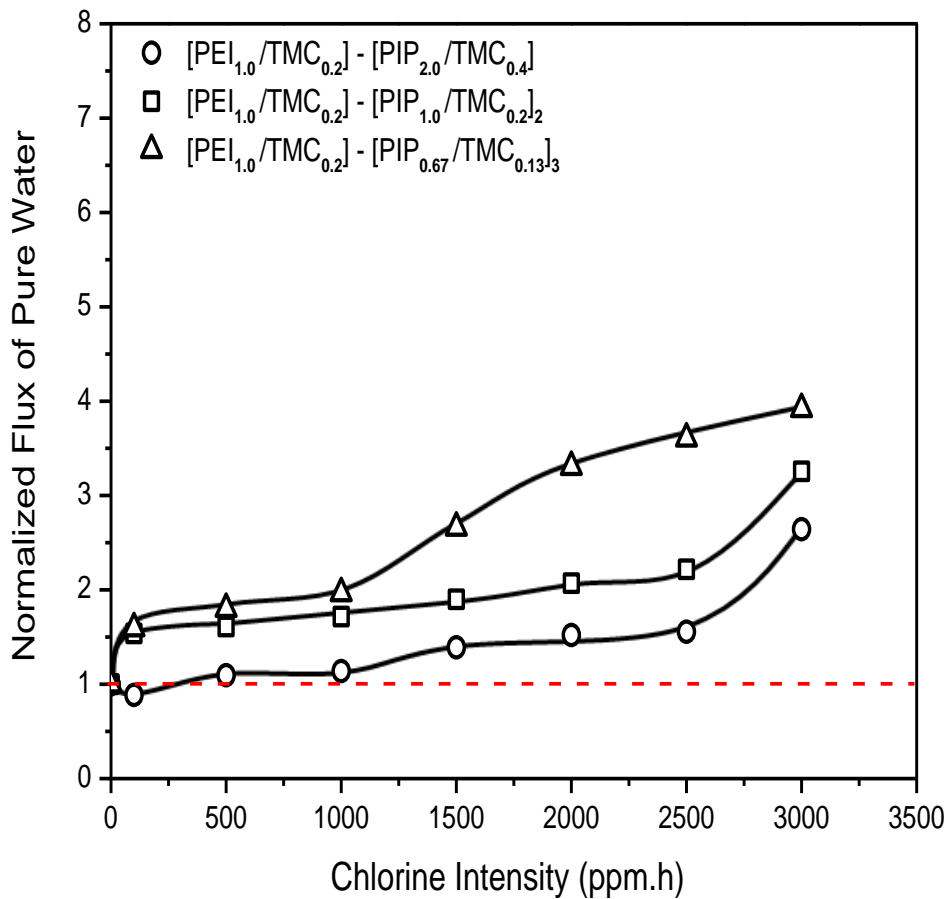
Figure 5.7 Normalized flux of pure water for membranes $[(PEI_{1.0}/TMC_{0.2})]\text{-}[(PIP_{2.0}/TMC_{0.4})]$, $[(PEI_{1.0}/TMC_{0.2})]\text{-}[(PIP_{1.0}/TMC_{0.2})]_2$ and $[(PEI_{1.0}/TMC_{0.2})]\text{-}[(PIP_{0.67}/TMC_{0.13})]_3$, chlorinated at pH 7.
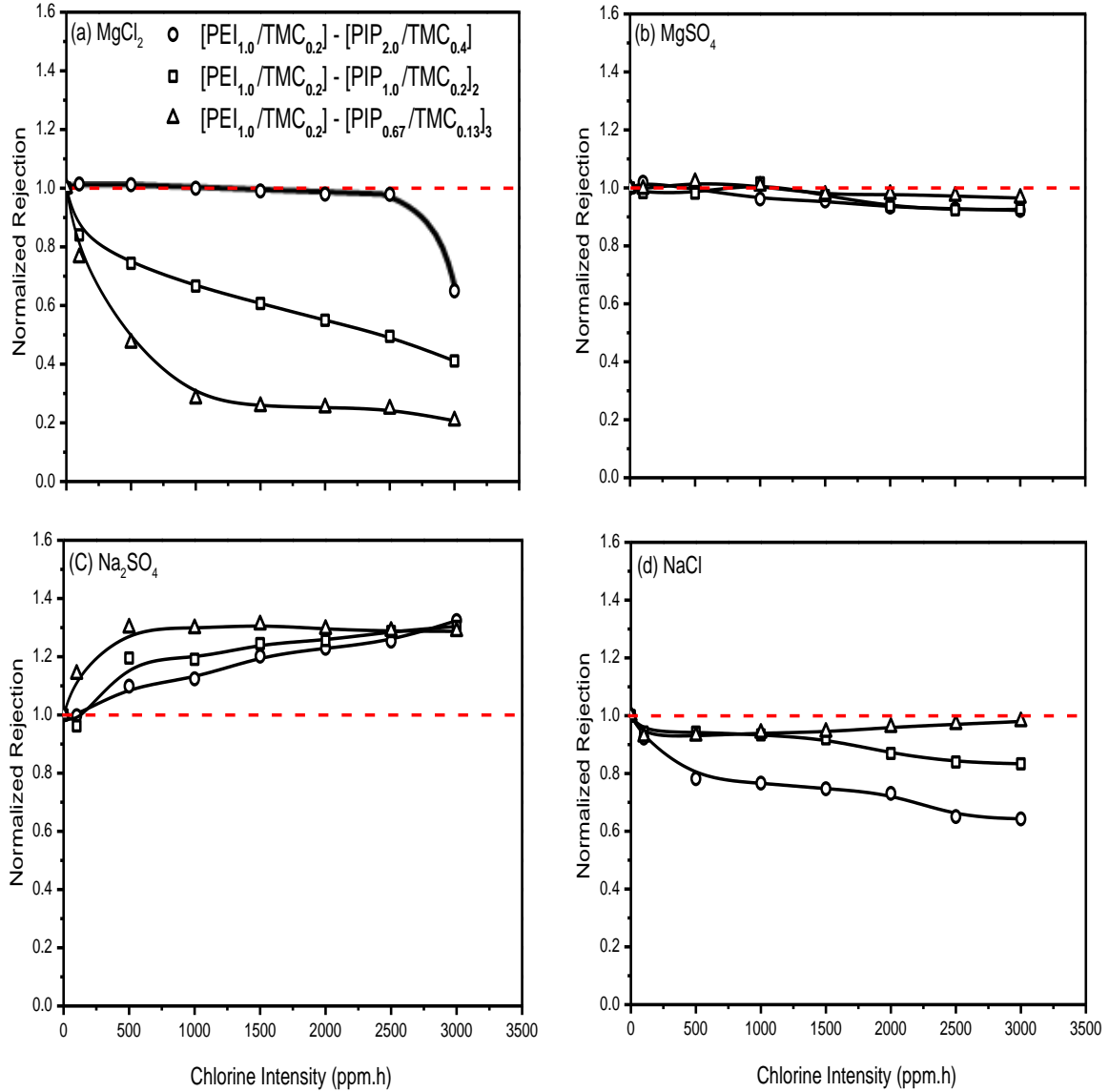
Figure 5.8 Normalized rejections of (a) MgCl$_2$, (b) MgSO$_4$, (c) Na$_2$SO$_4$ and (d) NaCl for membranes [(PEI$_{1.0}$/TMC$_{0.2}$)]-[(PIP$_{2.0}$/TMC$_{0.4}$)], [(PEI$_{1.0}$/TMC$_{0.2}$)]-[(PIP$_{1.0}$/TMC$_{0.2}$)]$_2$ and [(PEI$_{1.0}$/TMC$_{0.2}$)]-[(PIP$_{0.67}$/TMC$_{0.13}$)]$_3$, chlorinated at pH 7.

Comparing the performance of membranes with a single PIP/TMC sublayer (i.e., membrane [(PEI$_{1.0}$/TMC$_{0.2}$)]-[(PIP$_{2.0}$/TMC$_{0.4}$)]) and membranes with multiple PIP/TMC sublayers formed at lower reactant concentrations (with a fixed PIP to TMC concentration ratio), it is shown that membranes with a PIP/TMC outer layer formed at high concentrations are more resistant to chlorine attack than membranes with multiple PIP/TMC outer layers formed at low

concentrations. This is understandable based on the following considerations. A higher reactant concentration tends to produce a denser and thicker PIP/TMC polyamide networks. Each of the PIP/TMC sublayer (i.e., $[(PIP_{0.67}/TMC_{0.13})]$) in the multiple-layers membranes is expected to be thinner with a looser structure than a single sublayer of $[(PIP_{2.0}/TMC_{0.4})]$. In spite of the plural PIP/TMC sublayers, they may not be sufficient to fully cover and protect the interior PEI/TMC crosslinks that are susceptible to chlorine degradation and hydrolysis. From a solute retention point of view, membrane $[(PEI_{1.0}/TMC_{0.2})]-[(PIP_{2.0}/TMC_{0.4})]$ has the best chlorine resistance among the three membranes investigated here, whereas membrane $[(PEI_{1.0}/TMC_{0.2})]-$ $[(PIP_{0.67}/TMC_{0.13})]_3$ will be preferred for nanofiltration of Na_2SO_4 solutions since a controlled chlorine exposure will improve the membrane permeability and selectivity.

5.3.2 Effects of pH of chlorine solution on the degradation process

Membrane $[(PEI_{1.0}/TMC_{0.2})]-[(PIP_{2.0}/TMC_{0.4})]$ was used to further study the effects of pH of the chlorine solution on the separation performance of the chlorine-exposed membranes, and the results are presented in Figures 5.9 and 5.10 for water flux and solute rejections, respectively. It is shown that at either an alkaline or acidic pH, the impact of chlorine exposure on the water flux is greater than at a neutral solution pH. As expected, the exposure of the membrane to chlorine solutions at an alkaline or acidic pH also resulted in a more significant reduction in the solute rejections, except for Na_2SO_4 which showed an increased rejection.
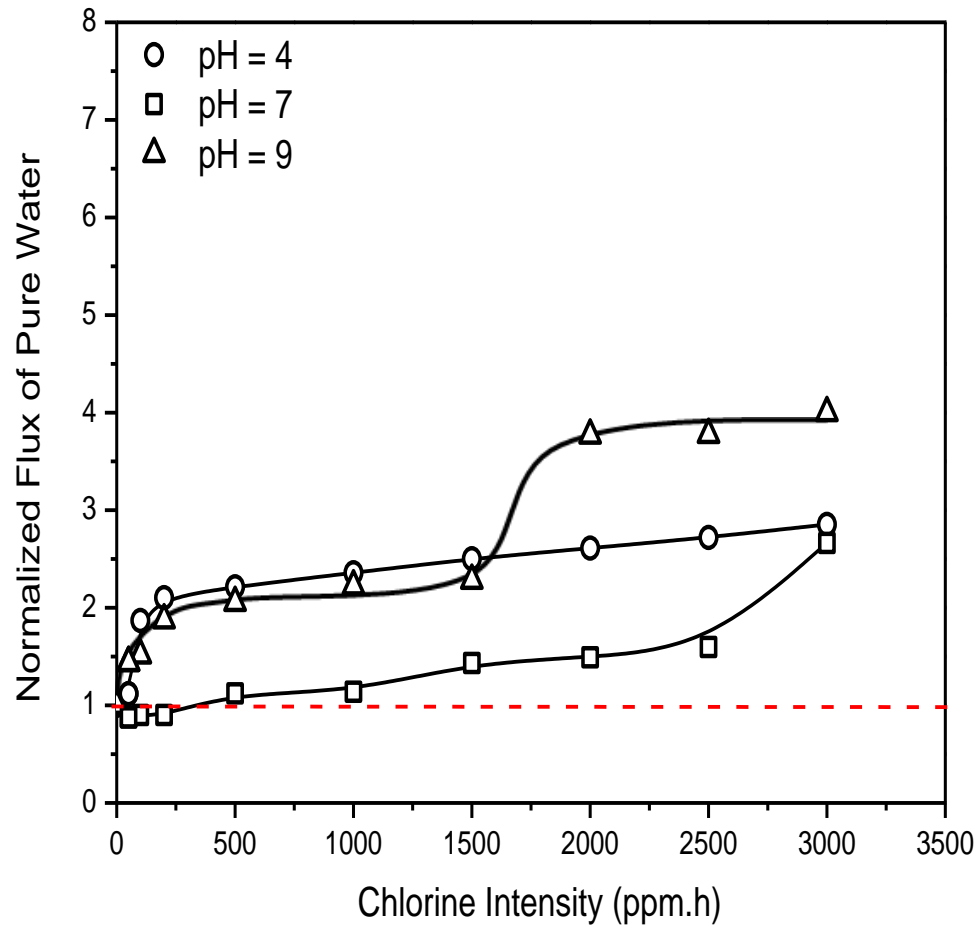
Figure 5.9 Normalized flux of pure water for membrane $[(PEI_{1.0}/TMC_{0.2})]-[(PIP_{2.0}/TMC_{0.4})]$, chlorinated at pH 4, 7 and 9.
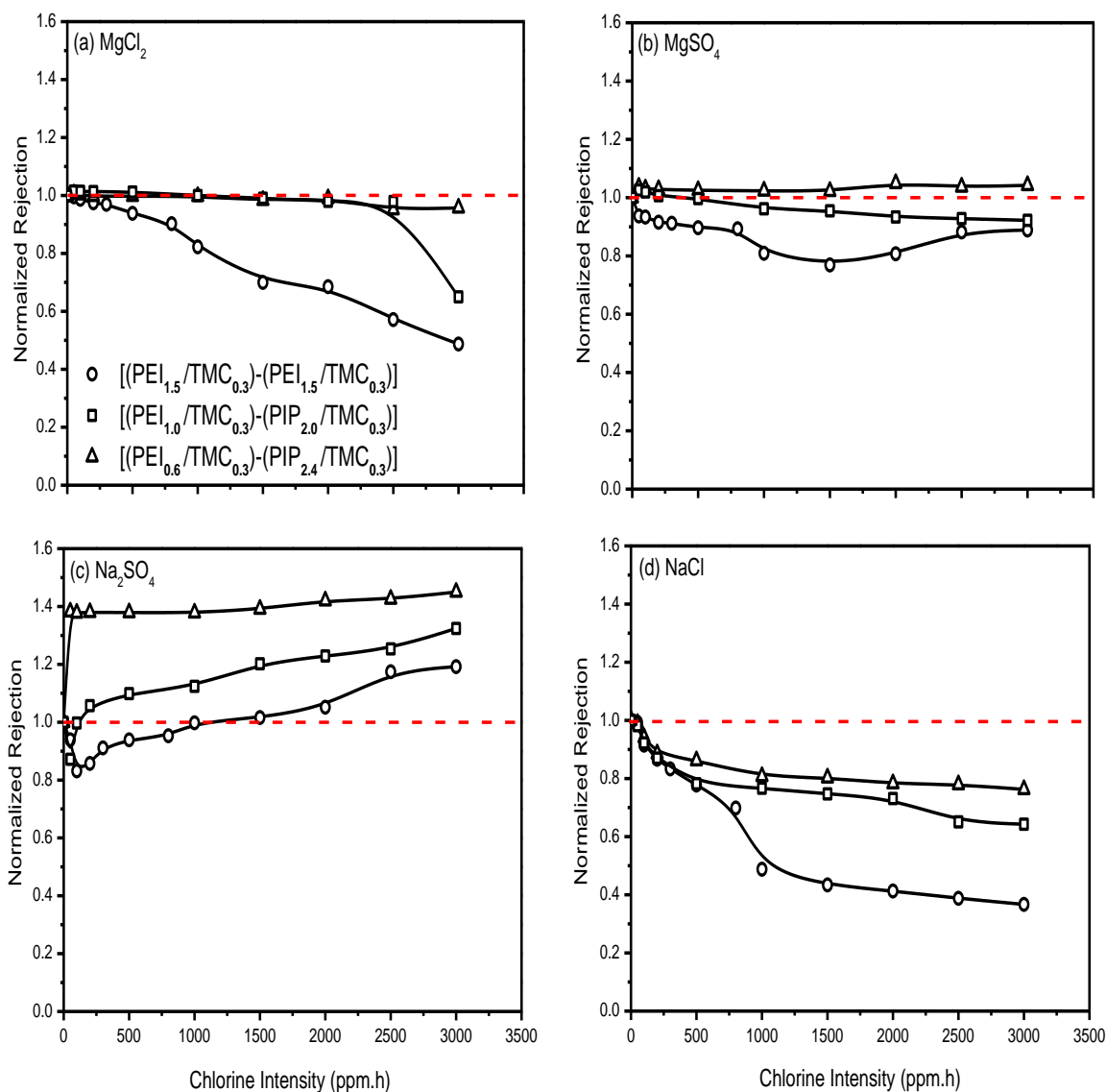
Figure 5.10 Normalized rejections of (a) $MgCl_2$, (b) $MgSO_4$, (c) Na_2SO_4 and (d) NaCl for membrane $[(PEI_{1.0}/TMC_{0.2})]$-$[(PIP_{2.0}/TMC_{0.4})]$, chlorinated at pH 4, 7 and 9.

These results can be explained in the following. The reactivity of chlorine in the solution depends on the pH, and so does the degradation of polyamide membranes. At pH <7.5, which is equal to the pKa of the hypochlorous acid (HClO), the protonated species (HClO) is predominant, and at a pH higher than the pKa, the deprotonated species (ClO⁻) will be predominant, as shown in Figure 5.11 [Ettori *et al.*, 2011; Xu *et al.*, 2013]. Hypochlorous acid (HClO) is known to be more reactive than hypochlorite ions (ClO⁻). Thus, at a lower acidic pH

condition, the membrane will be degraded more significantly. Severe degradation of polyamide membranes by chlorine at pH 4 has also been observed by others [Kang *et al.*, 2007; Gu *et al.*, 2012; Xu *et al.*, 2013]. At an alkaline pH, ClO$^-$ will be the major chlorine species which are not strongly reactive to degrade polyamide [Soice *et al.*, 2003]. However, an alkaline environment (pH > 7) favors the chlorine-induced hydrolysis because of the abundant OH$^-$ groups available, and a high alkaline pH will facilitate the hydrolysis [Do *et al.*, 2012b]. This is because the active chlorine (HClO in this case) attacks the electron-rich N atoms of C−N bonds, which are weakened as the shared pair of electrons are drawn to the N atoms [Do *et al.*, 2012a], resulting in positively charged C atoms. These electrophiles will be stabilized by the nucleophilic OH$^-$ in the solution. As such, the chlorine-induced hydrolysis of polyamide will be enhanced by OH$^-$. However, it should be mentioned that in the absence of chlorine, the membrane may still be hydrolyzed at proper acidic or alkaline conditions. This is supported by the solute rejection data of the membrane after exposure for 1 h to chlorine-free acidic or alkaline solutions with different pH values, as shown in Figure 5.12, where the normalized rejection is the solute rejection of the membrane after alkaline or acid treatment in the absence of chlorine relative to the solute rejection of the pristine membrane. The membrane rejection to Na$_2$SO$_4$ increased when subjected to either acidic or alkaline treatments because of COO$^-$ produced on the membrane surface from hydrolysis.
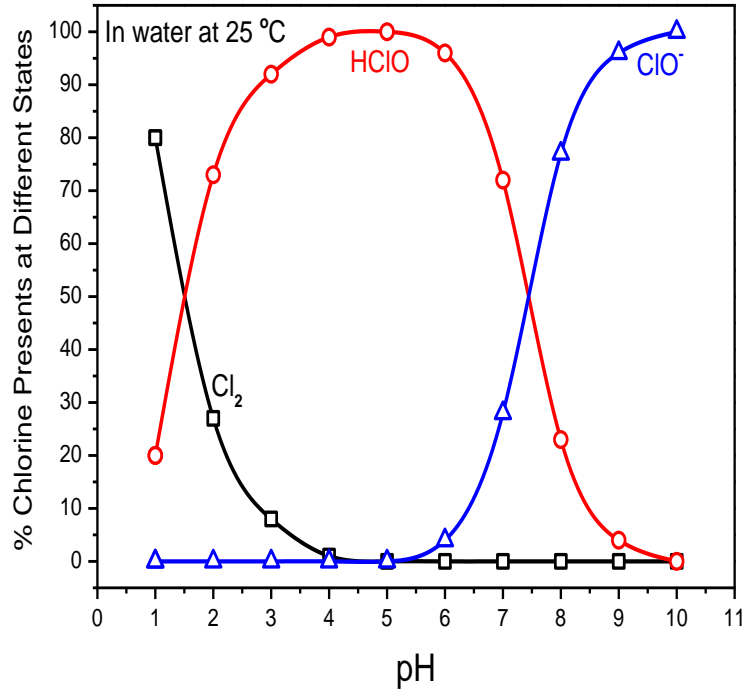
Figure 5.11 Percentage chlorine in water (25 ℃) presents at different states as a function of pH [Ettori *et al.*, 2011; Xu *et al.*, 2013].
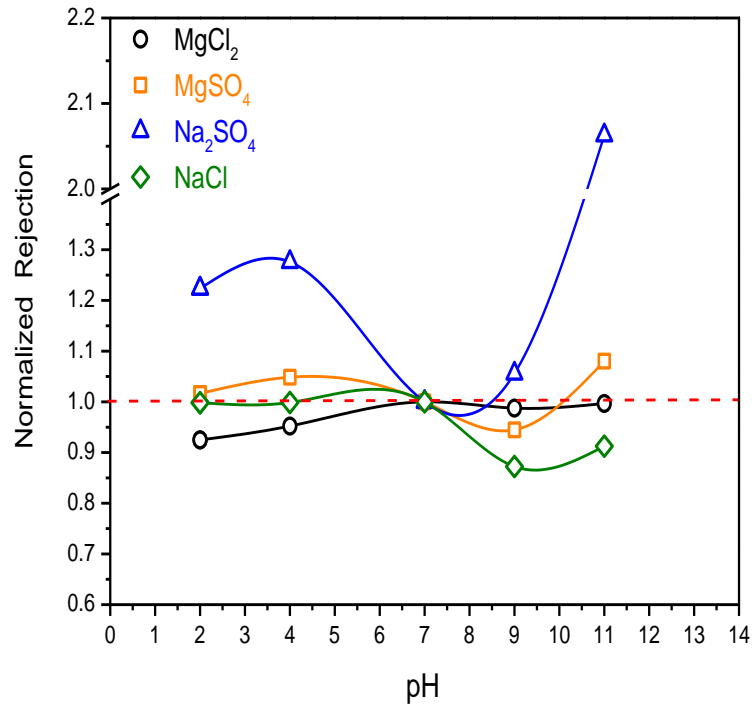
Figure 5.12 Normalized rejections of $MgCl_2$, $MgSO_4$, Na_2SO_4 and NaCl for membrane [$(PEI_{1.0}/TMC_{0.2})$]-[$(PIP_{2.0}/TMC_{0.4})$] treated with chlorine-free solutions at different pHs.

The change in contact angle on the membrane after chlorine exposure at pH 4, 7 and 9 is shown in Figure 5.13. At a given pH, the contact angle decreased with an increase in the chlorination intensity, except in a small range of low chlorination intensities (0-250 ppm.h). There are two opposing effects on the membrane hydrophilicity caused by the chlorination process. While the hydrophobic chlorine atoms bound to the membrane surface will decrease the surface hydrophilicity, the carboxylic groups produced by hydrolysis will tend to increase the surface hydrophilicity. The latter will be dominant when the chlorination intensity is high enough. The membrane chlorinated at pH 4 appeared to be more hydrophilic than the membrane chlorinated at pH 9, presumably due to chloramines and other derivatives from the end amine groups reacting with chlorine at a high pH [Soice et al., 2003].
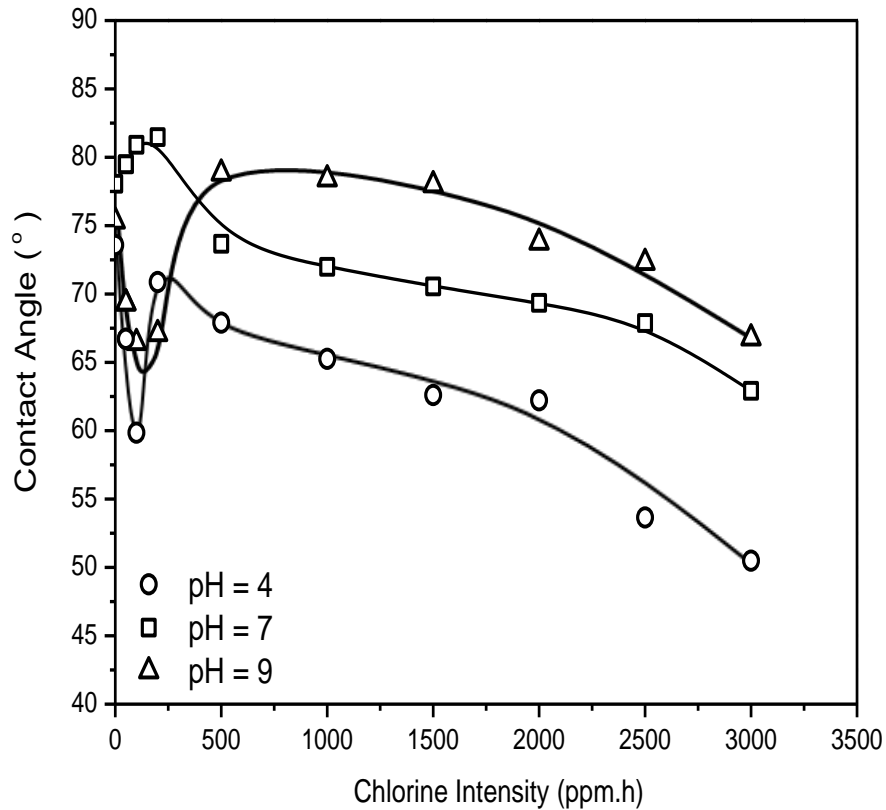
Figure 5.13 Contact angle of membrane [(PEI$_{1.0}$/TMC$_{0.2}$)]-[(PIP$_{2.0}$/TMC$_{0.4}$)], chlorinated at pH 4, 7 and 9.

5.3.3 Effects of chlorine concentration and exposure time on membrane degradation

In evaluating chlorine-resistance of membranes, the chlorine intensity is often reported as a product of the total chlorine concentration (ppm) and exposure time (h). This will lead one to perceive that the chlorine solution concentration and exposure time are equivalent with regard to their impacts on membrane degradation are concerned. In order to clarify this, two chlorination protocols were used for comparisons. The first protocol (designated as P-1) involved membrane exposures to chlorine solutions at different concentrations for a constant exposure time of 1 h, and the second protocol (designated as P-2) involved membrane exposure to chlorine at a fixed concentration of 50 ppm for different duration. In both cases, the chlorine solutions were at a pH of 7. Figures 5.14 and 5.15 show respectively the normalized flux and solute rejections of chlorine-treated membrane $[(PEI_{1.0}/TMC_{0.2})]$-$[(PIP_{2.0}/TMC_{0.4})]$ as a function of chlorine intensity expressed in (ppm.h).

Generally, the membrane under the P-2 chlorination protocol showed a larger magnitude in the flux increase and better normalized rejections to all four tested solutes. Thus, it is apparent that the chlorine intensity (ppm.h) is not a unique parameter to measure the impact of chlorination on the membrane. The impact of chlorination is mainly determined by the rate and duration of the chlorination process. The chlorine concentration affects the rate of the degradation reaction, and theoretically there is no guarantee of a first order reaction in view of the different chlorination mechanisms involved. As such, the chlorine concentration and chlorination time will have different effects on the membrane degradation, though the impact will be increasingly significant at an increased chlorine concentration (i.e., faster reaction rate) or for a prolonged duration of exposure. This analysis is consistent with the observed convex trend of the permeation flux with respect to chlorine concentration for a constant exposure time (Figure 5.14, protocol P-1). On the other hand, it is generally believed that the hydrogen bonds

between C=O and N-H groups can break at a low to moderate chlorine intensity, and chemical cleavage of amide linkages will begin to occur when chlorine oxidation is powerful enough [Glater *et al.*, 1994; Kwon and Leckio, 2006b]. It is thus understandable that for experimental protocol P-2, in spite of the constant chlorine concentration (50 ppm) used, there was a nonlinear change in the permeation flux with chlorination time (Figure 5.14, protocol P-2). This is also in agreement with the contact angle of the membrane presented in Figure 5.16, where the chlorine concentration for a fixed exposure time is shown to affect the membrane surface more significantly than the chlorination time at a given chlorine concentration.
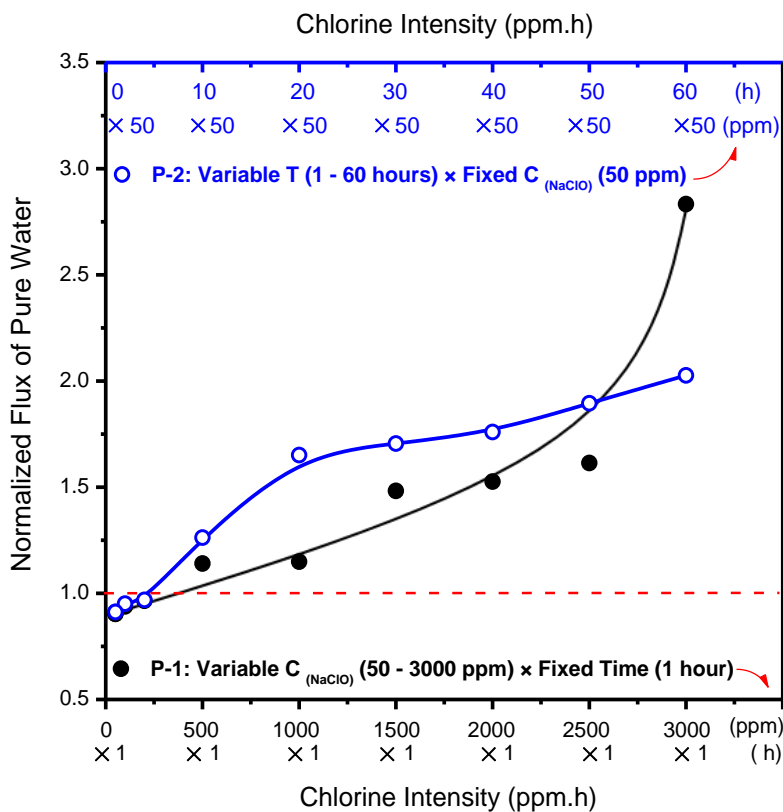
Figure 5.14 Normalized flux of pure water for membrane [(PEI$_{1.0}$/TMC$_{0.2}$)]-[(PIP$_{2.0}$/TMC$_{0.4}$)], chlorinated by P-1 and P-2, at pH 7.
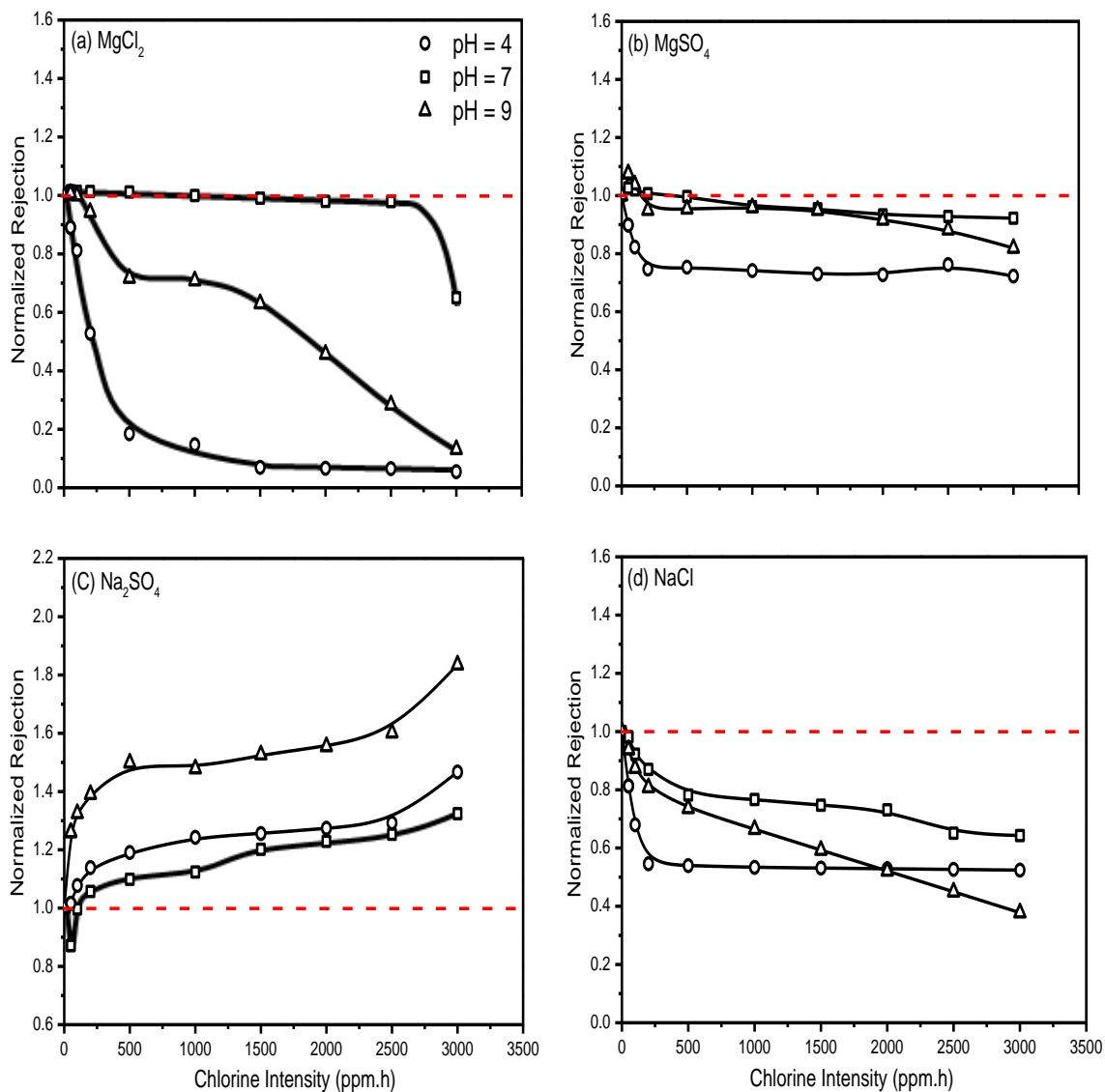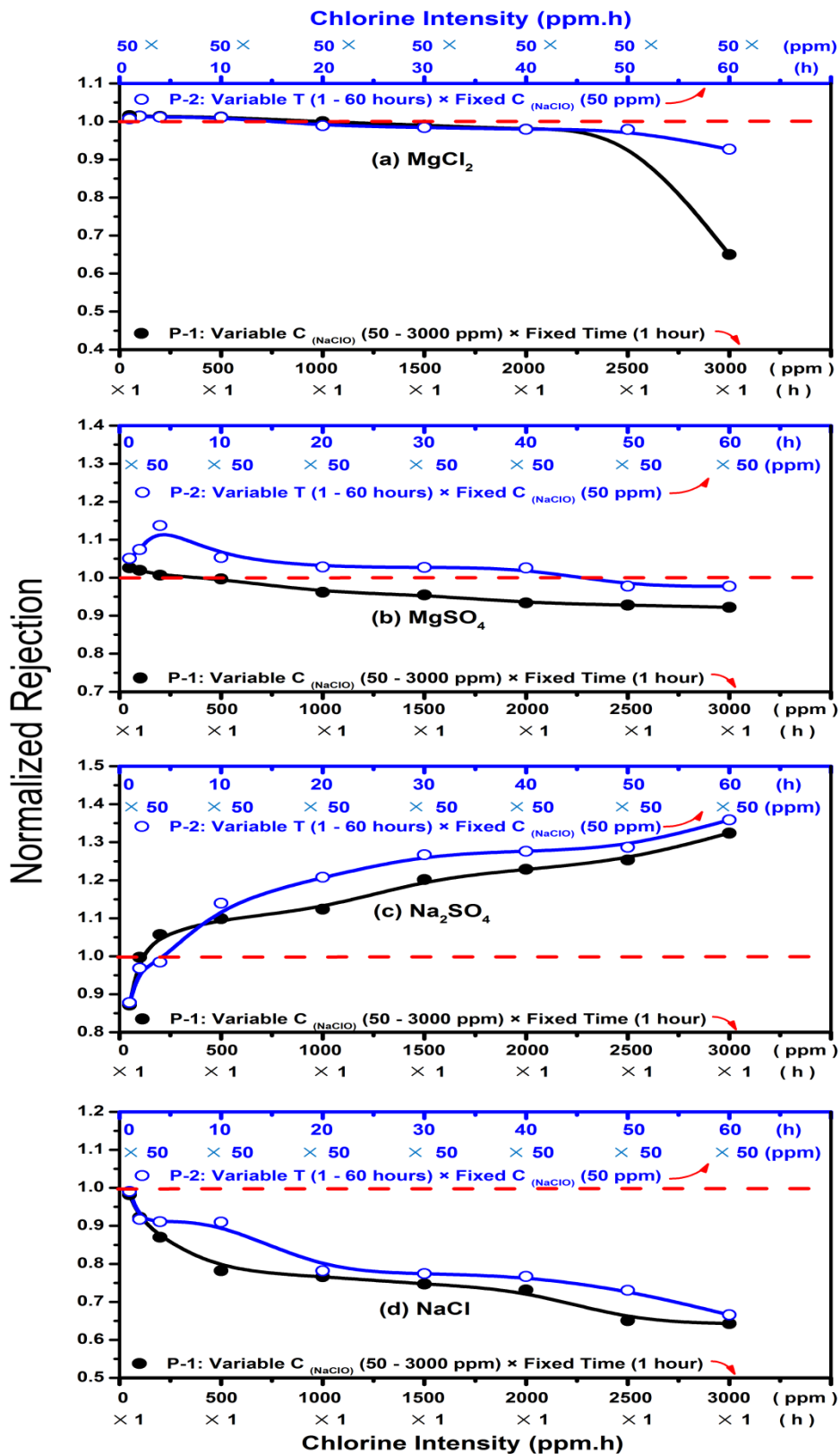
Figure 5.15 Normalized rejections of (a) $MgCl_2$, (b) $MgSO_4$, (c) Na_2SO_4 and (d) NaCl for membrane $[(PEI_{1.0}/TMC_{0.2})]-[(PIP_{2.0}/TMC_{0.4})]$, chlorinated by P-1 and P-2, at pH 7.

160
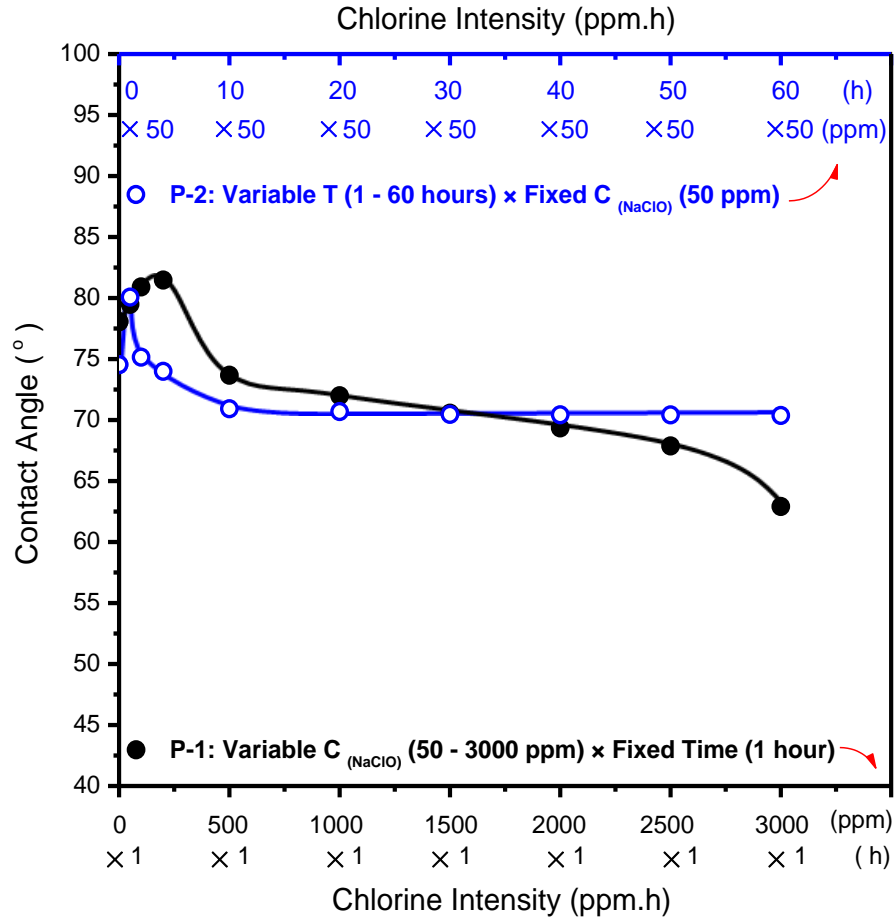
Figure 5.16 Contact angle of membrane [(PEI$_{1.0}$/TMC$_{0.2}$)]-[(PIP$_{2.0}$/TMC$_{0.4}$)], chlorinated by P-1 and P-2, at pH 7.

To further illustrate that the effects of chlorine concentration and exposure time are not equivalent with respect to membrane chlorination, the membranes was treated at different chlorine concentrations and exposure time while maintaining a fixed chlorination intensity of 2000 (ppm.h) at pH 7. Figure 5.17 shows the nanofiltration performance of the membrane after chlorine treatment. It is clearly shown that the chlorination intensity in (ppm.h), which is a composite parameter based on the product of chlorine concentration and chlorination time, is inadequate to characterize the chlorination conditions over a broad range. In other words, both chlorine concentration and exposure duration are significant factors influencing membrane chlorination, but their joint effects cannot be quantified by a simple multiplication of the two.

The data in the figure also clearly showed that chlorine exposure of the membrane increased the permeation flux, whereas the solute rejections would increase or decrease, depending on the charge properties of the solutes. The variations in the membrane performance are also reflected in the hydrophilicity of the membrane surface, as shown in Figure 5.18. It may be hypothesized that the membrane surface is quite sensitive to chlorine, even at low concentrations. When the chlorine concentration is sufficiently high (e.g., 8000 ppm), severe cleavage of the amide bonds may occur even for a short period of chlorine exposure, resulting in a significant reduction in the solute rejection. Nonetheless, it is important to notice that exposure of the membrane to chlorine at low concentrations can enhance the permeation flux effectively without a significant loss in solute rejections for $MgCl_2$ and $MgSO_4$ (and, to a lesser extent, NaCl), whereas the membrane retention to Na_2SO_4 will also be enhanced. This suggests that chlorine treatment of membranes under proper conditions can be exploited to improve the nanofiltration performance of the membranes.
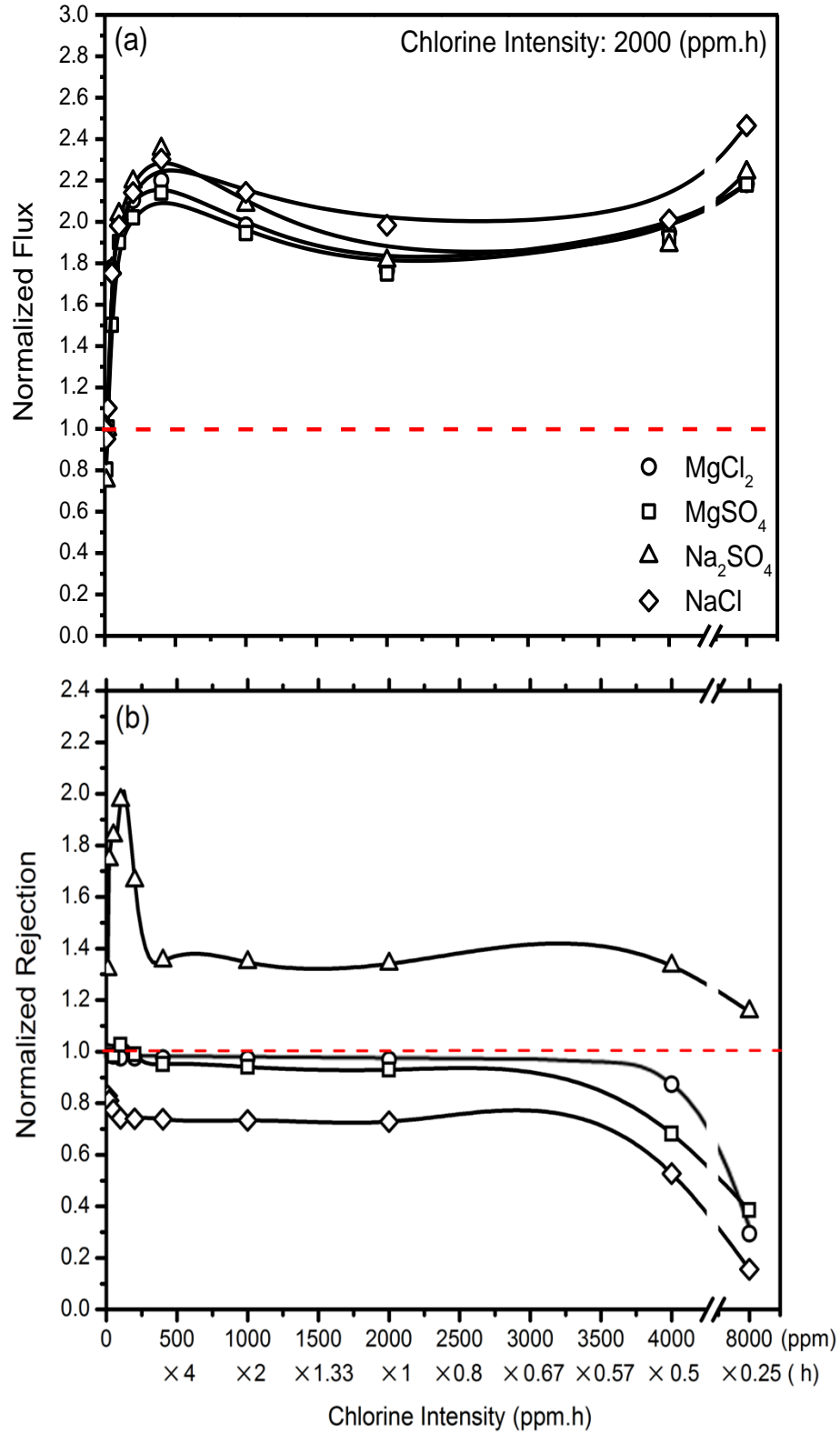
Figure 5.17 Normalized flux (a) and rejection (b) for membrane $[(PEI_{1.0}/TMC_{0.2})]-[(PIP_{2.0}/TMC_{0.4})]$ chlorinated under 2000 (ppm.h) with different chlorine concentration and exposure time, at pH 7.
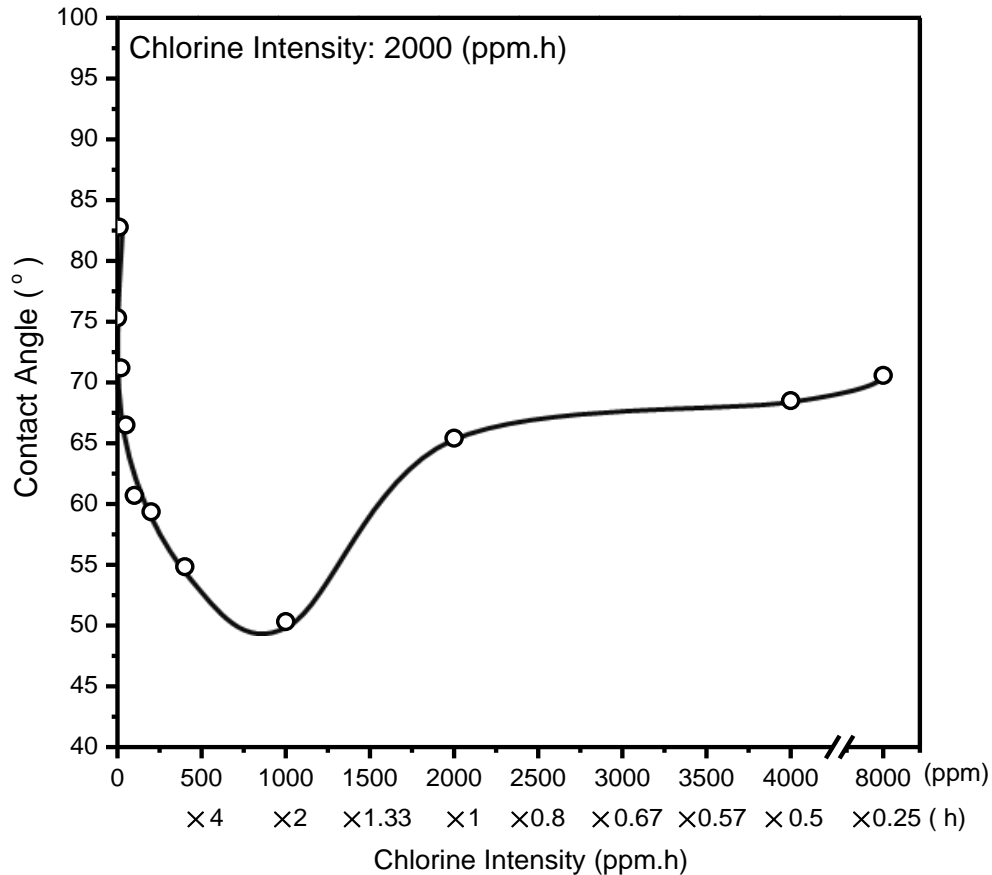
Figure 5.18 Contact angle of membrane [(PEI$_{1.0}$/TMC$_{0.2}$)]-[(PIP$_{2.0}$/TMC$_{0.4}$)] chlorinated under 2000 (ppm.h) with different chlorine concentration and exposure time, at pH 7.

5.4 Conclusions

The effects of chlorine exposure on the nanofiltration performance of positively-charged polyamide membrane were investigated. The pristine and chlorinated membranes were characterized by ATR-FTIR, FE-SEM, AFM and contact angle measurements, and the effects of the chlorination conditions (pH, chlorine concentration, exposure duration) on the membrane performance were studied. The following conclusions can be drawn from this study:

(1) Composite membranes comprising of a PEI-based polyamide inner sublayer and a PIP-based polyamide outer sublayer were fabricated via layer-by-layer sequential interfacial

164

polymerization, and the chlorine resistance of the membranes was improved by the outer sublayer based on PIP/TMC crosslinks.

(2) In general, membrane chlorination resulted in an increase in membrane permeability, whereas the solute rejection could increase or decrease, depending on the charge properties of the solutes.

(3) The water flux of the membrane was enhanced effectively after chlorine treatment at low concentrations without compromising solute rejections for $MgCl_2$ and $MgSO_4$ (and, to a lesser extent, NaCl); the membrane retention of Na_2SO_4 was actually enhanced by the chlorine treatment. This suggests that chlorination under proper conditions may be exploited to improve the nanofiltration performance of the membranes.

(4) At a given chlorine concentration, the effect of membrane chlorination was intensified at either alkaline or acidic pHs as compared to membrane chlorination at pH 7.

(5) The customarily used chlorination intensity (ppm.h), a composite parameter based on the product of chlorine concentration and chlorination time, was inadequate as a standalone parameter to characterize the chlorination conditions. Caution should be exercised in using this parameter as the extent of membrane chlorination is not a linear function of the chlorine concentration.

Chapter 6.

Modification of polyamide TFC membrane with self-polymerized polydopamine for pervaporative dehydration of ethylene glycol

6.1 Introduction

Thin film composite (TFC) membranes prepared by interfacial polymerization are generally used for reverse osmosis (RO) [Baroña *et al.*, 2012; Zhao and Ho, 2014] or nanofiltration (NF) [Wu *et al.*, 2014, 2015]. The aforementioned work in Chapter 2 reveals that polyamide TFC membranes hold promise for pervaporation as well. However, the monomers need to be selected and the membrane formation procedures need to be tailored to produce membranes with desired properties. Rather than developing new reactive monomers or tailoring interfacial polymerization conditions, modification of the polyamide TFC membrane based on its inherent properties appears to be easier to accomplish. Albo *et al*. [2014] treated commercial RO (SWC5, ESPA2 and CPA5) membranes by different solvent immersion and drying processes, and the membranes were evaluated for isopropanol dehydration by pervaporation. Xu *et al*. [2010] assembled polyelectrolytes onto an interfacially polymerized polyamide membrane for dehydration of ethylene glycol, and Zhang *et al*. [2013] further improved the stability of the polyelectrolyte membranes. Therefore, an attempt was made to modify our polyamide nanofiltration membranes for pervaporation uses. Surface coating is a facial and versatile method for surface modification because of a simple contact between the membrane surface and the solution. Inspired by the adhesive proteins secreted by mussels for attachment to wet surfaces [Waite and Tanzer, 1981], polydopamine has been extensively used in surface coatings

by taking advantage of its good adhesion to a wide range of surfaces as well as its good stability and durability in various environments (except in strong alkaline solutions (pH >13)) [Lee *et al.*, 2007; Bernsmann *et al.*, 2009; Xi *et al.*, 2009]. The good adhesive property derives from its spontaneous self-polymerization ability at an oxidative and slightly basic pH condition. In the application of membranes, polydopamine can be used for the formation of the selective skin layer or merely for the surface modification. Composite membranes formed by simply coating polydopamine on a substrate have been used for the dehumidification of propylene gas [Pan *et al.*, 2009], pervaporative desulfurization [Li *et al.*, 2009a] and salt separation [Li *et al.*, 2012]. The anti-fouling properties of the commercial RO membranes [Kasemset *et al.*, 2013; Karkhanechi *et al.*, 2014] and the permeation flux of the commercial ultrafiltration (UF) membranes [Xi *et al.*, 2009] were reported to have been improved by surface coating of polydopamine.

Based on prior work about TFC pervaporation membranes and the properties of polydopamine, in this work, we modified the polyamide nanofiltration membranes to make them suitable for pervaporation applications by depositing the self-polymerized polydopamine. The polydopamine can be the outer layer if it is deposited onto a polyamide layer pre-formed by interfacial polymerization. It can also act as a transition layer between the substrate and the polyamide if deposited before the polyamide layer formation by interfacial polymerization. This approach has several potential advantages: (1) the process of interfacial polymerization for the polyamide layer formation has been studied in details in our previous chapters, so that the properties of the polyamide layer can be easily controlled and tailored, (2) the membrane properties can be tailored by interfacial polymerization and polydopamine deposition independently, (3) the polydopamine deposition is a simple process which does not need any

catalyst, organic solvent or rigorous conditions, (4) the catechol groups of dopamine can react with amines under oxidizing conditions via Michael addition or Schiff base reactions [Burzio and Waite, 2000; LaVoie *et al.*, 2005], which will enhance the anchoring of the polydopamine layer onto the polyamide layer and further improve the membrane stability. In the present work, the effects of the number and sequence of the polydopamine depositions on the pervaporation performance of the resulting membranes will be studied.

The separation performance of the formed membranes was evaluated for the dehydration of ethylene glycol. Ethylene glycol is commercially produced from hydrolysis of ethylene oxide in the presence of large amount of excess water. It is used as an antifreeze in automobiles, deicing agent for aircrafts and absorbent to scrub water vapor in natural gas industry. All these applications involve separation of water from the spent ethylene glycol. Although ethylene glycol and water do not form azeotrope over the entire composition range, its high boiling point (197.3 ℃) makes the separation of water from ethylene glycol energy-intensive if multi-stage evaporation or distillation is used. From an energy consumption standpoint, pervaporation will be more competitive than distillation, especially at relatively low water concentrations in the feed. In this study, the effects of feed water concentration and operating temperature on the pervaporation performance were investigated. Since many chemical processes and gas processing generate waste streams containing mixed organic/inorganic solutes, so the pervaporation performance of the membrane for the ternary system ethylene glycol/water/inorganic salts will also be examined. The effects of the salt contents (NaCl in this study) in the feed and the operating temperature on the dehydration performance of the ternary system ethylene glycol/water/NaCl will be investigated.

6.2 Experimental

6.2.1 Materials

Dopamine hydrochloride and tris(hydroxymethyl)aminomethane (Tris) were purchased from Sigma-Aldrich. Ethylene glycol was purchased from VWR International. The aqueous solutions of ethylene glycol used as feeds in pervaporation experiments were prepared by blending ethylene glycol with de-ionized water at pre-determined concentrations. Other materials were the same as used before.

6.2.2 Membrane preparation

The composite membranes consist of a polyamide layer and one or more polydopamine layer. The polyamide layer was formed by interfacial polymerization from polyethylenimine (PEI) and trimesoyl chloride (TMC) using a PEI concentration of 4.0 wt% and TMC concentration of 0.8 wt%. The procedures of interfacial polymerization to form a single polyamide layer have been described in Chapter 3 and the chemical reaction between PEI and TMC to form the polyamide has been illustrated in Figure 3.4. The polydopamine layer was formed by self-polymerization of dopamine, and a possible mechanism for oxidative self-polymerization of dopamine is presented in Figure 6.1 [Xi *et al.*, 2009; Li *et al.*, 2012]. Dopamine was dissolved in a 15 mM Tris buffer (pH=8.8) at a concentration of 0.4 wt%. The self-polymerized polydopamine layers can be formed either after or before the formation of the polyamide layer. The deposition time was 24 h and 5 h respectively for the polydopamine layer formed after and before the polyamide layer. After the formation of a polydopamine or polyamide layer, the membrane was washed and rinsed thoroughly with de-ionized water and then thermally treated at 75 ℃ for 20 min. Figure 6.2 shows the process of synthesizing the thin film composite

membranes by the sequential steps of polydopamine and polyamide formation by self-polymerization and interfacial polymerization, respectively.

It should be mentioned that to ensure the skin layer formation occurred only on the surface of the PES side, the substrate was so mounted so as to keep the PES surface exposed. This way, the deposition solutions only contacted with the PES surface and the microporous substructure of the nonwoven fabric would not be blocked by the macromolecules.

The polyamide layer and polydopamine layer are designated as "PA" and "PD", respectively. Based on the sequence and the number of the depositions in the composite membranes, the designations of the membranes used in this study are shown in Table 6.1.
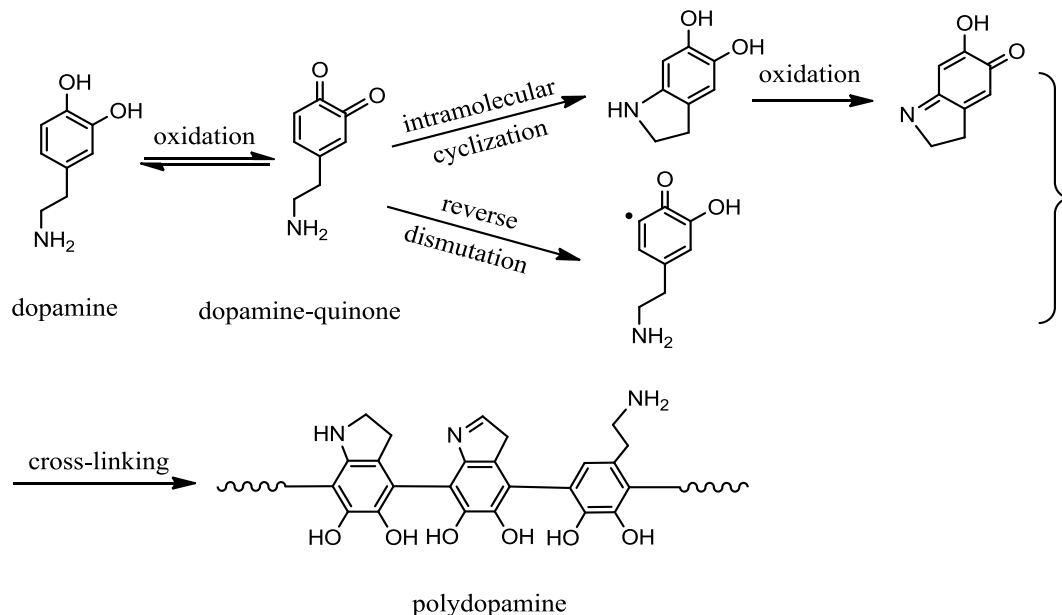
Figure 6.1 The possible mechanism of dopamine self-polymerization [Xi *et al.*, 2009; Li *et al.*, 2012].

170
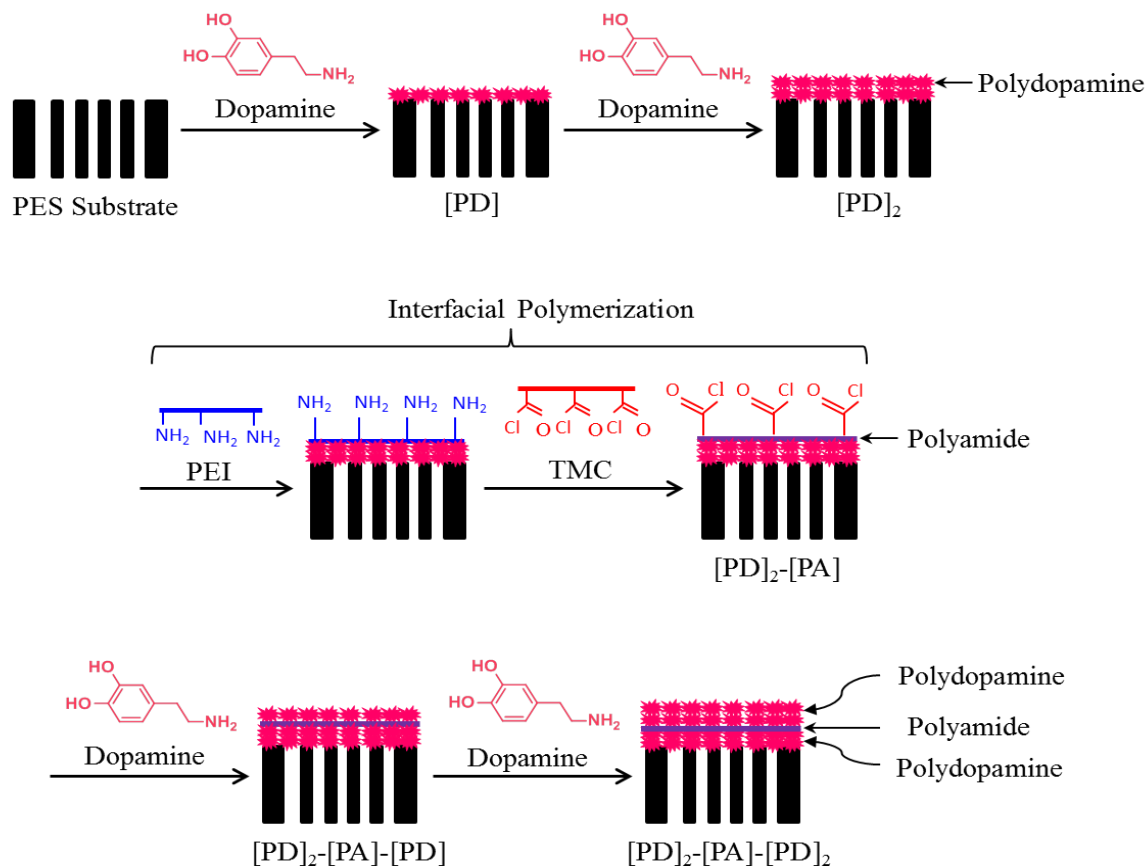
Figure 6.2 Schematic diagram showing the procedure to prepare thin film composite membrane [PD]$_2$-[PA]-[PD]$_2$ by polydopamine deposition and interfacial polymerization.

Table 6.1 Designation of membranes based on the sequence and the number of the depositions

Number of depositions	Membrane designation	Description
0	PES	PES substrate
1	[PA]	One ply of polyamide formed on the substrate
2	[PA]-[PD]	One ply of polyamide and one ply of polydopamine formed on the substrate sequentially
3	[PA]-[PD]$_2$	One ply of polyamide and two plies of polydopamine formed on the substrate sequentially
4	[PD]-[PA]-[PD]$_2$	One ply of polydopamine, one ply of polyamide and two plies of polydopamine formed on the substrate sequentially
5	[PD]$_2$-[PA]-[PD]$_2$	Two plies of polydopamine, one ply of polyamide and two plies of polydopamine formed on the substrate sequentially

171

6.2.3 Membrane characterization

ATR-FTIR, FE-SEM and contact angle test for analyzing the chemical composition, morphology and hydropilicity of the membrane surface are the same as described before. The sorption uptakes of pure water and pure ethylene glycol in the active layer of the composite membrane were measured to study the effect of preferential sorption on the pervaporation performance. After drying in a vacuum oven at 80 °C for 1 day, the PES substrate (weight W_1) and the composite membrane (weight W_2) samples of the same area were immersed in the same liquid at room temperature to reach sorption equilibrium. Then the weights of the membrane samples (W_3 for the substrate and W_4 for the composite membrane) were determined quickly after gently blotting away the excess liquid on the surface. Since the weight of the dry skin layer (W_2-W_1) was very small and could not be accurately determined, the swelling degree of skin layer by the liquid sorbent, which was equal to $[(W_4-W_3)-(W_2-W_1)]/(W_2-W_1)$, was difficult to evaluate. It was thus decided to use the water to ethylene glycol sorption uptake ratio (mol/mol) [which is equal to $(62/18)(W_4-W_3)_{water}/(W_4-W_3)_{glycol}$] to measure the selective sorption of the two liquid in the membrane. This way, the liquid uptake in the porous substrate of the composite membrane was rightfully separated because it was the permeant sorption in the active skin layer of the membrane that was relevant to pervaporation. Note the molar sorption uptake ratio was used as it characterizes the solubility selectivity pertaining to the membrane permeability.

6.2.4 Pervaporation

Figure 6.3 is a schematic diagram of the experimental set up for pervaporation tests. The membrane was mounted in a permeation cell with an effective area of 21.23 cm^2. The feed solution was pumped from the feed tank to the membrane surface, and the retentate was

circulated back to the feed tank. The permeate side was evacuated, and the permeate pressure was maintained below 1.7 kPa absolute. The permeate vapor was all condensed and collected in a cold trap immersed in liquid nitrogen. The permeability and selectivity of the membrane were evaluated in terms of permeation flux (J) and separation factor (α),

$$J = \frac{Q}{S\Delta t} \tag{6.1}$$

$$\alpha = \frac{X_{wl}/(1-X_{wl})}{X_{w0}/(1-X_{w0})} \tag{6.2}$$

where Q is the quantity of permeate (g) collected over a time interval Δt (h), S is the effective area of the membrane (m^2), and X_{w0} and X_{wl} are the mass fractions of water in the feed and permeate, respectively. The permeate composition was analyzed with a refractometer (ATAGO, Japan), equipped with a digital thermal meter and a circulating water bath (HAAKE FE 2, Germany). The calibrations of ethylene/water mixtures were attached in Appendix C. The partial permeation flux of water and ethylene glycol can be calculated from the total permeation flux and the permeate composition, that is, $J_{water} = JX_{wl}$ and $J_{EG} = J(1-X_{wl})$. The permeation was considered to have reached steady state when the permeation flux and permeate composition became constant. Generally, the steady state of permeation was attained within 3 h after a pervaporation run was initiated. The removed water by membranes was compensated by adding the same amount water into feed to maintain the constant feed composition.
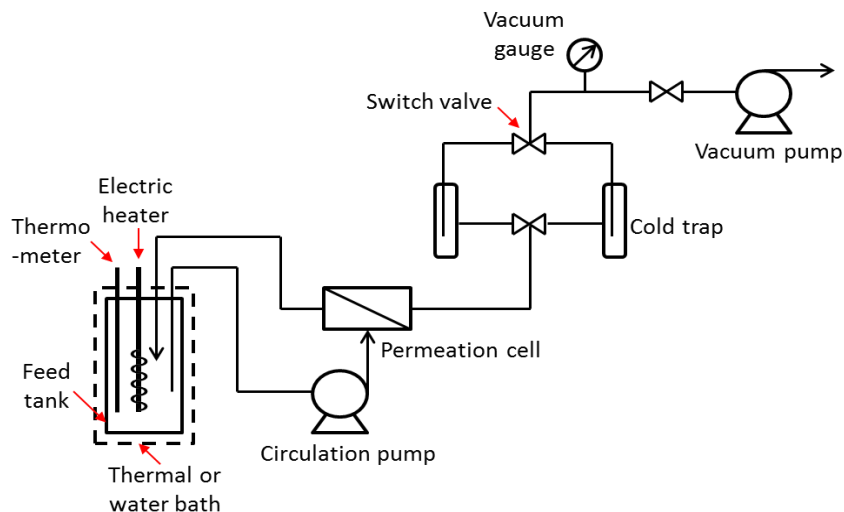
Figure 6.3 Schematic diagram of experimental setup for pervaporation.

The effects of feed water concentration (0.5-20 wt%) and operating temperature (25-55 ℃) on the membrane performance were studied. The operating temperature was controlled using a thermal/water bath. The influences of inorganic salt on the performance of the membranes [PD]$_2$-[PA]-[PD]$_2$ were studied by adding various amounts of NaCl into the ethylene glycol/water mixtures. Dehydrations of ethylene glycol/water/NaCl mixtures were performed at different contents of NaCl and water concentrations. After a pervaporation run for dehydrations of ethylene glycol/water/NaCl mixtures, the membrane was thoroughly washed by circulating pure water on the feed side for 2 h, followed by pervaporation of pure water at room temperature for 3 h to wash away any salt from the membrane. The pervaporation data reported were an average value of at least two measurements and the experimental error in the measurements was ~5%.

174

6.3 Result and discussion

6.3.1 Modification of TFC polyamide membranes with polydopamine

Effects of polydopamine depositions on pervaporation performance

The water concentration in the permeate and total permeation flux of the dopamine-free polyamide membrane and polydopamine modified membranes are shown in Figure 6.4 for the separation of water from ethylene glycol at 38 ℃ at a feed water concentration of 9.5 wt%.

Figure 6.4 Effects of the number of layers deposited in the membrane (as shown in Table 6.1) on (a) water concentration in permeate and (b) total permeation flux. Feed composition: 9.5 wt% water + 90.5 wt% ethylene glycol, Temperature: 38 ℃.

175

The data in Figure 6.4 show that the membrane [PA] exhibited a total permeation flux of $100 \text{ g/(m}^2\text{.h)}$ and a water concentration of 51 wt% in the permeate. This membrane is intended for nanofiltration and its skin layer is not dense enough to yield a relatively high selectivity in pervaporation. However, the polydopamine deposition improves the membrane selectivity substantially. With only one layer of polydopamine deposited on the outer surface of the polyamide membrane, the water content in the permeate increases to 85 wt%. When 2 layers of polydopamine were deposited on the surface of the polyamide membrane, the water content in the permeate continues to increase to 89 wt%. From the above pervaporation data, it appears clear that the deposition of polydopamime on the outer surface will improve the membrane selectivity. On the other hand, since the substrate used for preparing the polyamide nanofiltration membranes is a microporous PES ultrafiltration membrane, it may be hypothesized that if the pore size of the substrate can be decreased by depositing a layer of polydopamine as a gutter layer between the substrate and the interfacially formed polyamide, a further improvement in the pervaporation performance of the resulting composite membrane may be achieved. To demonstrate this concept, membranes [PD]-[PA]-[PD]$_2$ and [PD]$_2$-[PA]-[PD]$_2$ were prepared by depositing polydopamine onto the PES substrate before the polyamide layer was formed by interfacial polymerization and this is followed by additional polydopamine deposition on the outer surface of the membrane. As shown in Figure 6.4(a), the water content in the permeate continues to increase to 92 wt% and 96 wt% with membranes [PD]-[PA]-[PD]$_2$ and [PD]$_2$-[PA]-[PD]$_2$, respectively, which confirms that the pervaporation performance can be further improved by adding a polydopamine gutter layer in the membrane. It may be pointed out that due to its rigid supramolecular structure, while polydopamine can be hydrated in aqueous solutions (which is desirable for pervaporative dehydration of solvents), polydopamine

176

films may crack upon drying under high internal stresses [Yang and Zhao, 2011]. Therefore, instead of forming a thicker [PD] layer on top of a [PA] sublayer, the [PA] sublayer was sandwiched by the [PD] sublayers in the above membranes in anticipation that this would improve the membrane stability.

It is interesting to notice from Figure 6.4(b) that the total permeation flux also increases when the polydopamine layer is incorporated into the membrane either as a gutter layer for polyamide formation or as an outer surface layer. Based on the solution-diffusion model, the permeability of a component (i.e., water or ethylene glycol) is affected by both the selective sorption onto the membrane surface and the molecular diffusion through the membrane. Each polydopamine layer deposited (either as the outer layer or the gutter layer) onto the membrane will increase the resistance to mass transfer due to the increased diffusion path that both water and ethylene glycol need to pass through. However, as shown in Figure 6.5(a), the lower contact angles of the modified membranes indicate that the deposited polydopamine layers, especially on the outer surface, will improve the affinities of both water and ethylene glycol to the membranes. The sorption uptakes of water also increase when the membranes are modified, as shown in Figure 6.5(b). These results mean that the increased diffusion resistance may be compensated by the enhanced solubility, resulting in an increase in the permeation flux.

The partial fluxes of water and ethylene glycol in the polyamide membrane and the polydopamine modified membranes are shown in Figure 6.6. It is interesting to note that the added polydopamine layers have a negative effect on the permeation of ethylene glycol but a positive effect on the permeation of water. This may be explained by the solution-diffusion model. From a sorption point of view, the lower contact angles of ethylene glycol than that of water shown in Figure 6.5(a) reveal that both the polyamide surface and the polydopamine

surface have a better affinity to ethylene glycol than to water. This is not surprising since ethylene glycol has more –OH groups than water and thus there is a strong affinity between ethylene glycol and the polymer. Similar results have been observed in previous studies for poly(N,N-dimethylaminoethyl methacrylate)/polysulfone composite membranes [Du *et al.*, 2008]. However, the preferential sorption of water or ethylene glycol in the membranes is affected by the affinity between the membrane and the permeating, and the difference in their molecular sizes [Huang, 1991]. Considering the latter effect, the smaller water molecules will diffuse in the membrane faster. It appears that the effect of molecular size on the preferential sorption is more dominating than that of affinity, resulting in an increased water/ethylene glycol sorption uptake ratio, as shown in Figure 6.5(b). This dominating effect is becoming more significant when the film becomes denser [Huang, 1991]. Thus, the increased polydopmine depositions tend to result in a denser skin layer of the membrane, leading to the increased sorption selectivity of water over ethylene glycol. In addition, from a diffusion point of view, the permeation of the smaller water molecules is favored over the larger ethylene glycol molecules. Figure 6.6 shows that the partial fluxes of water and ethylene glycol in the polyamide membrane are very close. The polydopamine modified membranes showed a substantially higher water flux than ethylene glycol, and with the increased number of polydopamine deposition, the total permeation flux is mainly determined by the water flux. Figure 6.7 shows the separation factors of the polyamide membrane and the polydopamine modified membranes. Clearly, an increase in the membrane selectivity was achieved by the deposition of the polydopamine either as an outer layer or as a gutter layer. The separation factor of membrane $[PD]_2$-$[PA]$-$[PD]_2$ is 219 when the feed water concentration is 9.5 wt%.
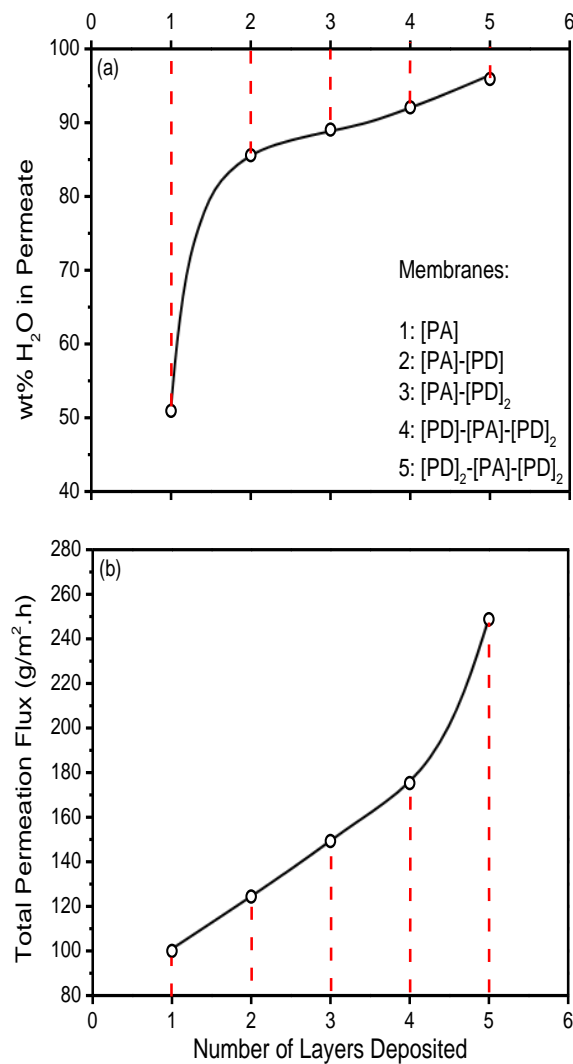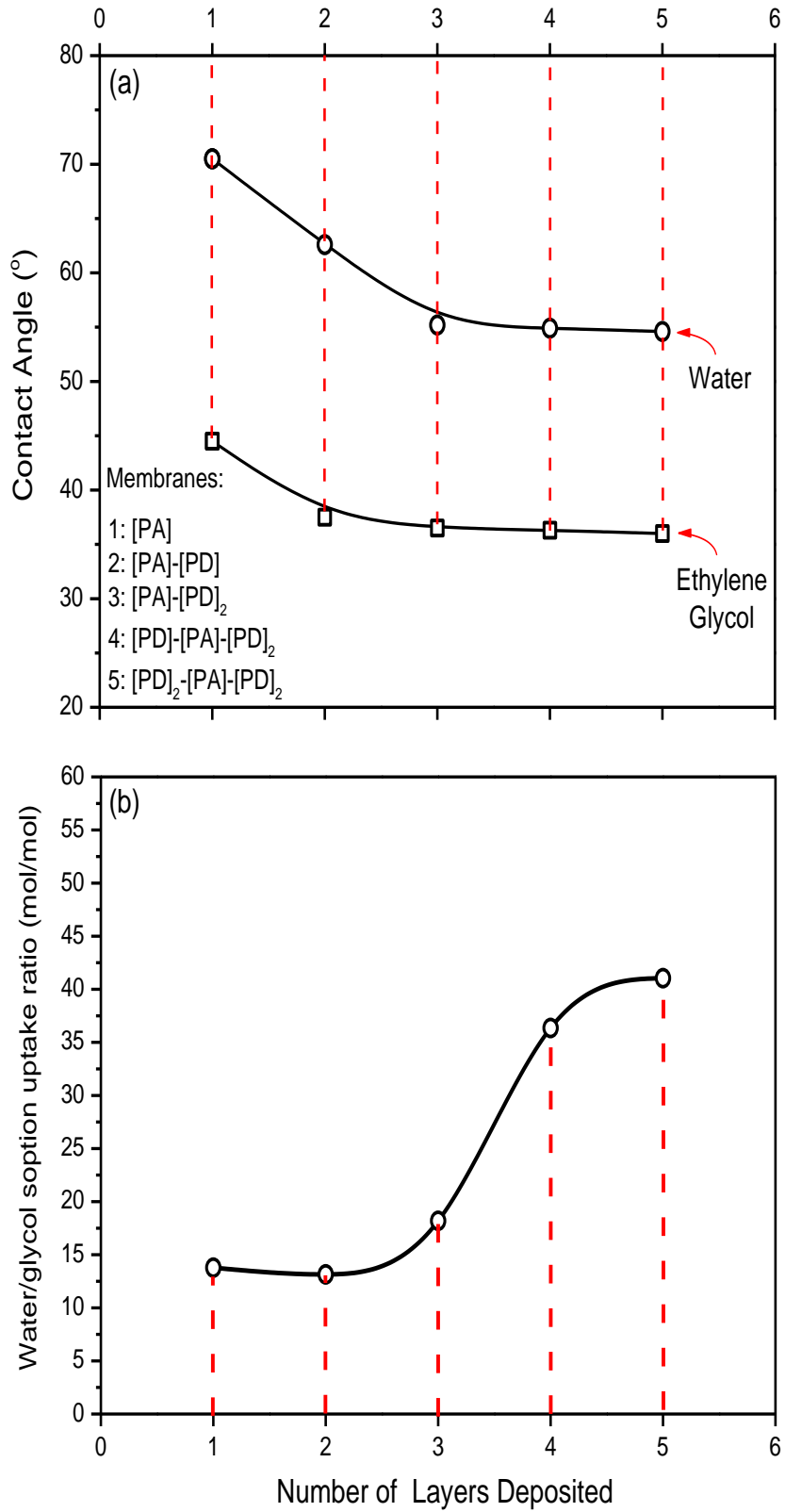
Figure 6.5 Effects of the number of layers deposited in the membrane (as shown in Table 6.1) on (a) contact angle and (b) water/ethylene glycol sorption uptake ratio.
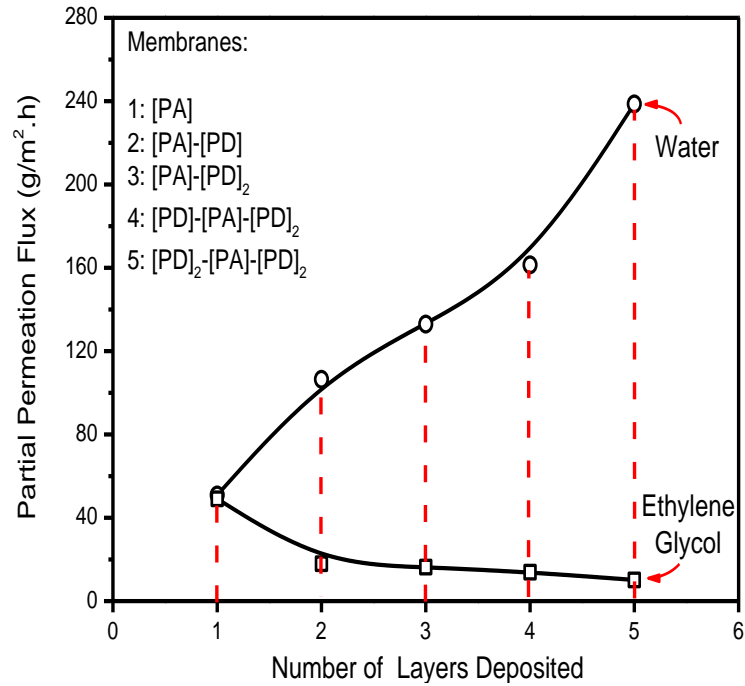
Figure 6.6 Effects of the number of layers deposited in the membrane (as shown in Table 6.1) on the partial fluxes of water and ethylene glycol. Feed composition: 9.5 wt% water + 90.5 wt% ethylene glycol, Temperature: 38 ℃.
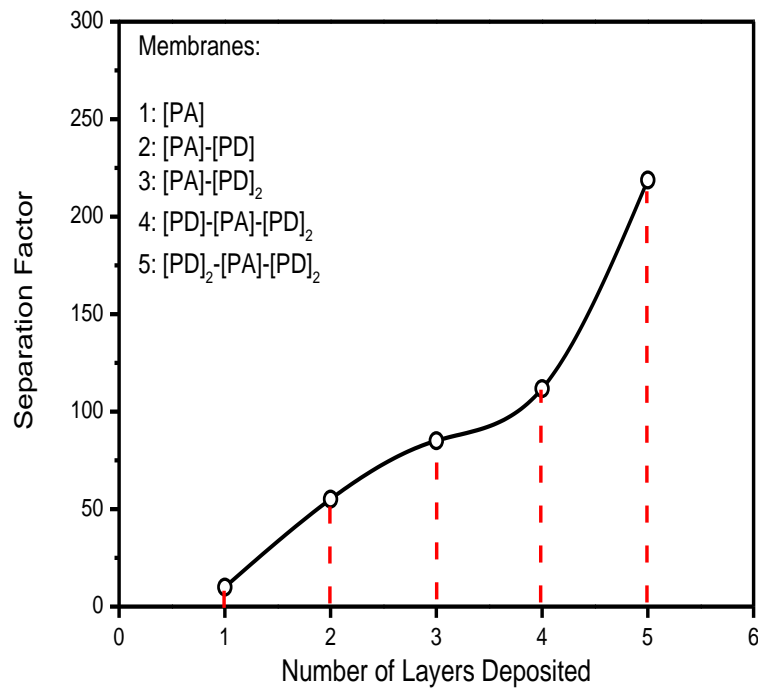
Figure 6.7 Separation factors for the polyamide membrane and polydopamine modified membranes. Feed composition: 9.5 wt% water + 90.5 wt% ethylene glycol, Temperature: 38 ℃.

Generally, hydrophilic membranes are suitable for solvent dehydration since water preferentially permeates through the membrane. However, due to the strong hydrophilicity of the diol compound, ethylene glycol also has a high affinity to hydrophilic materials. The results from a previous study [Du *et al.*, 2008] and the present study show that if the skin layer is dense enough, a good performance in the dehydration of ethylene glycol can still be obtained using a highly hydrophilic membrane where the selectivity is derived from the difference in the permeant diffusivity. As a result, the deposition of polydopamine either as an outer layer or as a gutter layer will improve the membrane selectivity for the separation of water from ethylene glycol by pervaporation. In the following, membrane [PD]$_2$-[PA]-[PD]$_2$ was selected for further studies to evaluate the effects of feed water concentration, operating temperature and NaCl contents in the feed on the separation performance. It should be pointed out that this proof-of-concept study was aimed to demonstrate the feasibility of modifying polyamide nanofiltration membranes for pervaporation applications by simply depositing polydopamine onto the polyamide nanofiltration membrane. The membrane modification conditions (e.g., the concentration of dopamine, the deposition time and the number of polydopamine/polyamide layers) were not optimized and the separation data presented here do not represent the best membrane performance that could be obtained.

Chemical composition

The chemical composition of the top surface for the composite membranes was analyzed by ATR-FTIR. Figure 6.8 shows the ATR-FTIR spectra of the pristine PES substrate and thin film composite membranes with polydopamine/polyamide depositions. Compared to the PES substrate, several new peaks appeared on the ATR-FTIR spectra for [PD] membrane: 3310 cm^{-1} (N-H/O-H stretching), 1640 cm^{-1} (overlap of C=C resonance vibration in aromatic ring and N-

H bending vibration), 1505 cm^{-1} (N-H scissoring), 1365 cm^{-1} (phenolic O-H bending) and 1170 cm^{-1} (phenolic C-O stretching). These new adsorption peaks prove the existence of polydopamine layer on the PES substrate membrane. For membrane [PD]$_2$-[PA], the peaks at 1651 cm^{-1} and 1545 cm^{-1} are characteristics of amide-I (C=O stretching) band and amide-II (N–H) band of the amide groups (–CONH–). The peak around 1650 cm^{-1} becomes broader for membrane [PD]$_2$-[PA]-[PD] since it overlaps with characteristic peaks of C=C resonance vibration, N-H bending vibration and C=O stretching vibration. The band intensities at 3310 cm^{-1} and 1650 cm^{-1} increase with an increase in the polydopamine deposition layers. In addition, we can see that the PES substrate is white, and the membrane became brown when deposited with 1 layer of polydopamine, and the color turned to be darker with additional polydopamine depositions. All the above results confirm that polydopamine and polyamide have been deposited on the substrate surface.

Surface morphology

The surface morphologies of the membranes were examined using FE-SEM. Figure 6.9 shows the surface images of PES substrate and thin film composite membranes with polydopamine/polyamide depositions. As described in Chapter 3, the PES substrate shows a relatively flat and smooth surface (Figure 6.9(a)). It is obvious to see the small patch-like and large fractal-like aggregated structures on the surface of [PD] membrane (Figure 6.9(b)), which proves the deposition of polydopamine on the substrate. However, the polydopamine deposition is not evenly distributed on the surface, and one layer polydopamine deposition is not dense enough to fully cover the surface of substrate. After one more layer of polydopamine deposition and one layer of polyamide formed on the surface, membrane [PD]$_2$-[PA] appears a dense morphology (Figure 6.9(c)), and the surface of substrate is almost fully covered by the

top depositions. With further deposition of polydopamine, membrane [PD]₂-[PA]-[PD] shows a much denser and more compact surface than membrane [PD]₂-[PA] (Figure 6.9(d)). For comparison, the surface image of membrane [PA] (formed from 4.0 wt% PEI and 0.8 wt%) were also shown in Figure 6.9(e). Clearly, both two polydopamine modified composite membranes show denser and more compact surface than this dopamine-free polyamide membrane.
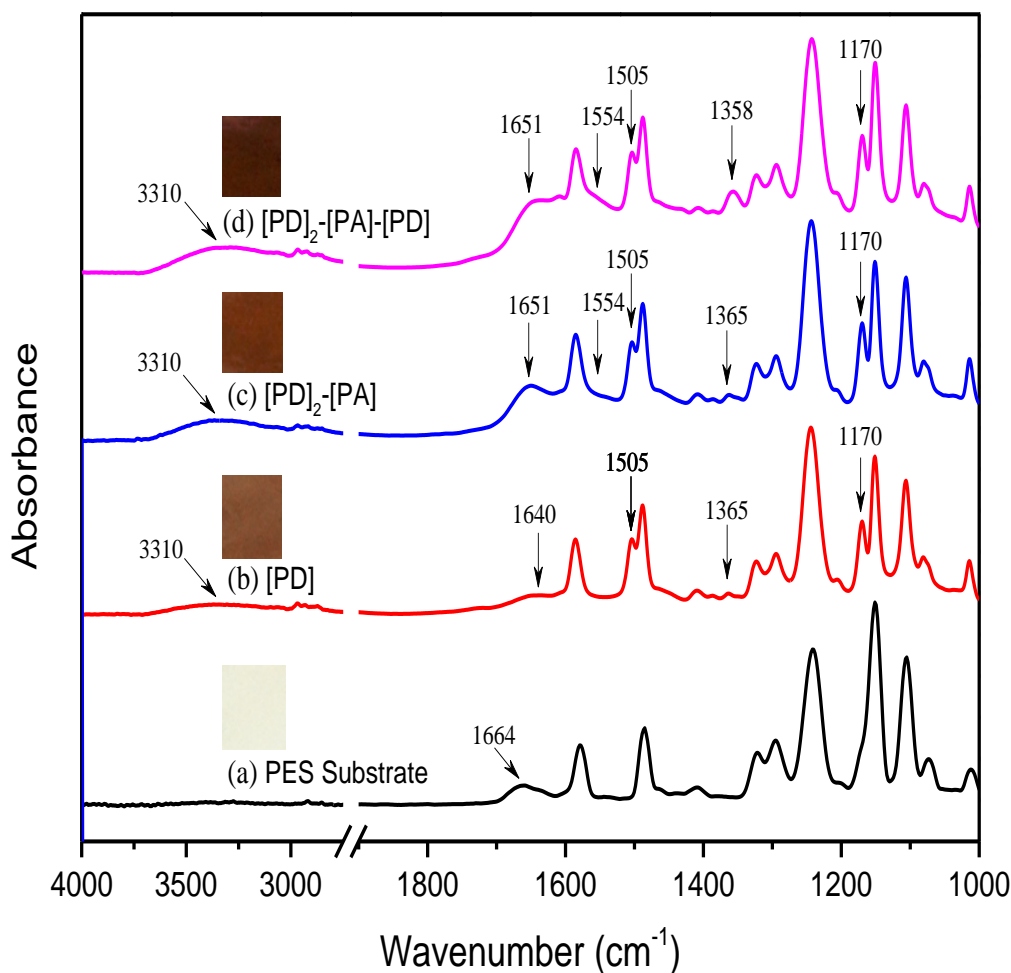
Figure 6.8 ATR-FTIR spectra of (a) PES substrate and thin film composite membranes: (b) [PD], (c) [PD]₂-[PA] and (d) [PD]₂-[PA]-[PD].
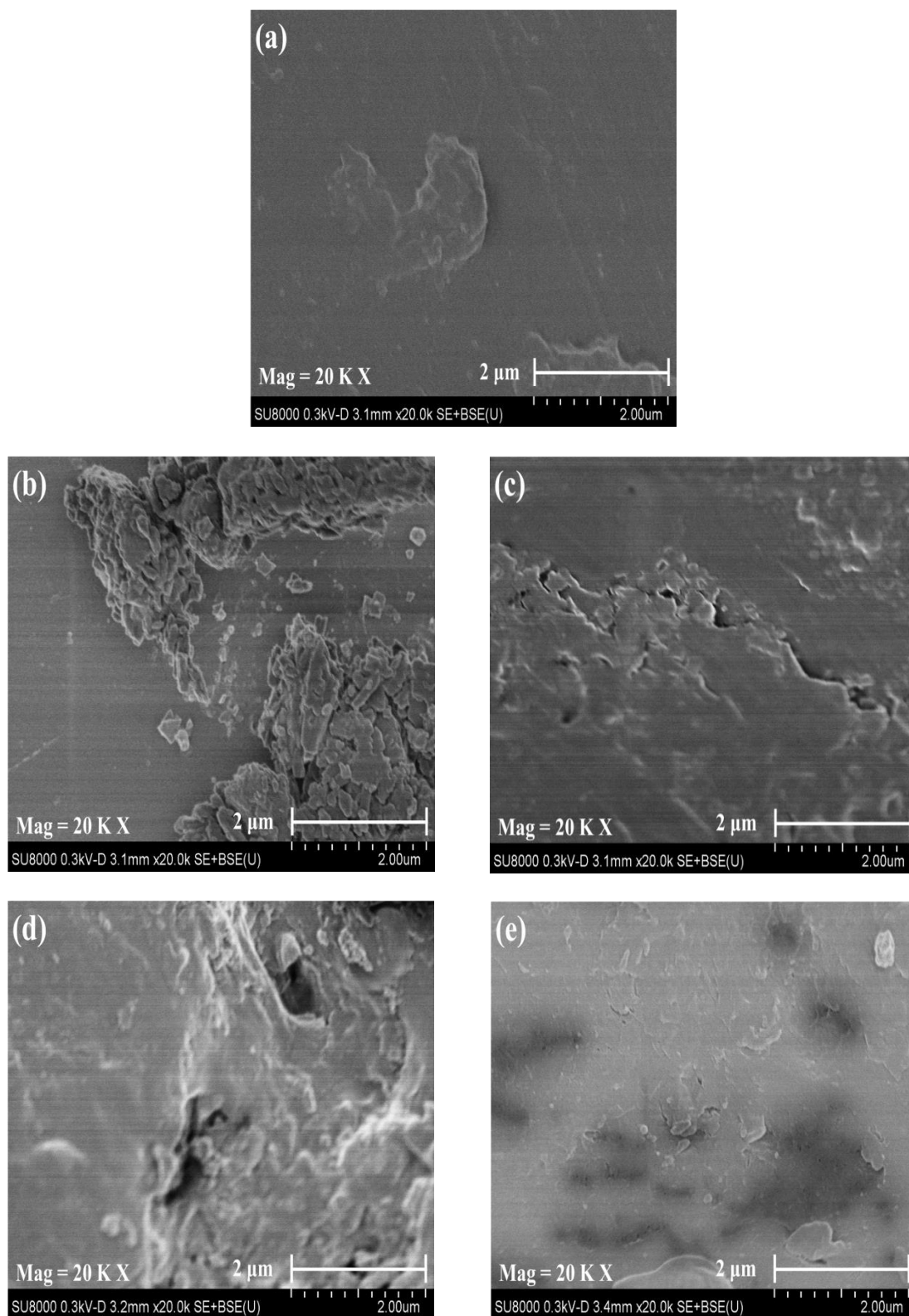
Figure 6.9 Surface images (20,000×) of (a) PES substrate and thin film composite membranes: (b) [PD], (c) [PD]$_2$-[PA], (d) [PD]$_2$-[PA]-[PD] and (e) [PA]

6.3.2 Pervaporation performance of membrane [PD]$_2$-[PA]-[PD]$_2$

Effect of feed concentration

To investigate the influence of feed water concentration on the performance of membrane [PD]$_2$-[PA]-[PD]$_2$ for the dehydration of ethylene glycol, pervaporation experiments were carried out at 38 °C at feed water concentrations ranging from 0.5 to 20 wt%. This concentration range is of industrial interest, particularly for ethylene glycol regeneration related to natural gas dehydration by ethylene glycol. Figures 6.10(a) and (b) show water concentrations in the permeate and the total permeation flux as a function of feed water concentration.

At a feed water concentration of 0.5 wt%, the water concentration in the permeate is 81 wt%. The total permeation flux increases almost linearly with an increase in the feed water concentration. This trend was also observed in other studies on hydrophilic composite membranes for dehydration of ethylene glycol [Xu *et al.*, 2010; Hu *et al.*, 2012]. An increase in feed water concentration increases the driving force for water permeation. Due to the high hydrophilictity of the membrane polymer, the free volume in the polymer increases and the polymer chains become more flexible, thus making the permeant molecules to penetrate through the membrane more easily. For comparison with conventional distillation, the vapor-liquid equilibrium (VLE) data for ethylene glycol/water mixtures [Perry and Green, 1999] were also plotted in Figure 6.10(a). It is clear that pervaporative separation with membrane [PD]$_2$-[PA]-[PD]$_2$ is more selective than distillation for dehydration of ethylene glycol, especially at relatively low feed water concentrations.

185
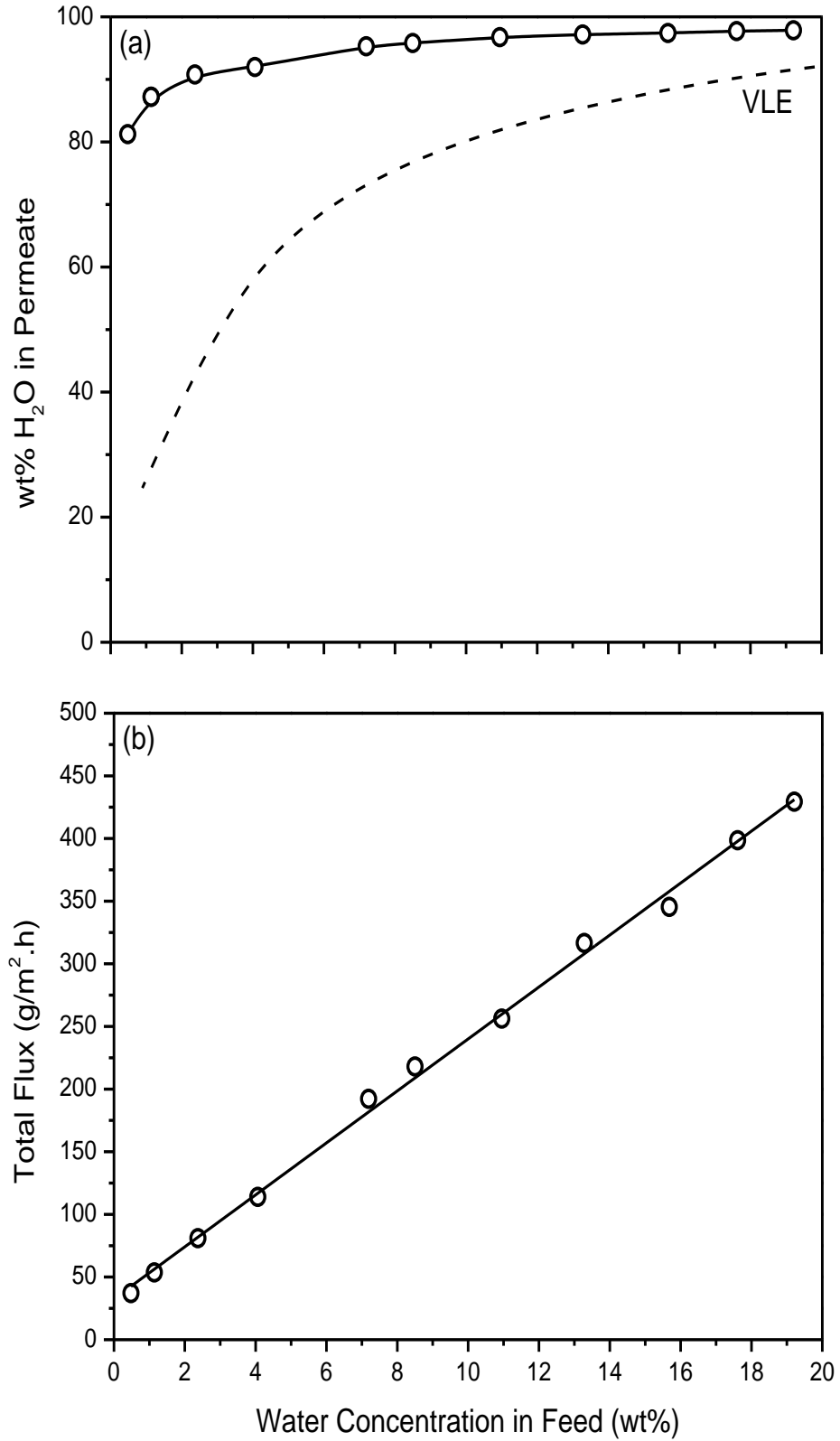
Figure 6.10 Effects of feed water concentration on (a) water concentration in permeate and (b) total permeation flux through membrane [PD]$_2$-[PA]-[PD]$_2$, Temperature: 38 °C.

Figures 6.11(a) and (b) show the partial fluxes of water and ethylene glycol at different feed water concentrations. The partial flux of water is approximately proportional to feed water concentration, while the partial flux of ethylene glycol increases slightly when the feed water concentration increases from 0.5 wt% to 4.0 wt% and then remains almost constant when further increasing the feed water content. In the binary mixture of water and ethylene glycol, an increase in water content means a decrease in the content of ethylene glycol, and thus the driving force for ethylene glycol permeation decreases. However, an increased feed water concentration will make the membrane more swollen which facilitates the permeability of ethylene glycol in spite of its reduced driving force. Nevertheless, this trend will not continue indefinitely if the feed water concentration is high enough. The separation factor of this membrane varies with feed water concentration, as shown in Figure 6.12. A trade-off relationship between the permeation flux and separation factor is observed for this membrane. At 0.5 wt% water in feed, the separation factor is relatively high (i.e, 992). It drops to 388 when feed water concentration is reduced to 2.4 wt%. Above 4.0 wt% feed water, a further increase in the feed water content will not decrease the separation factor significantly.
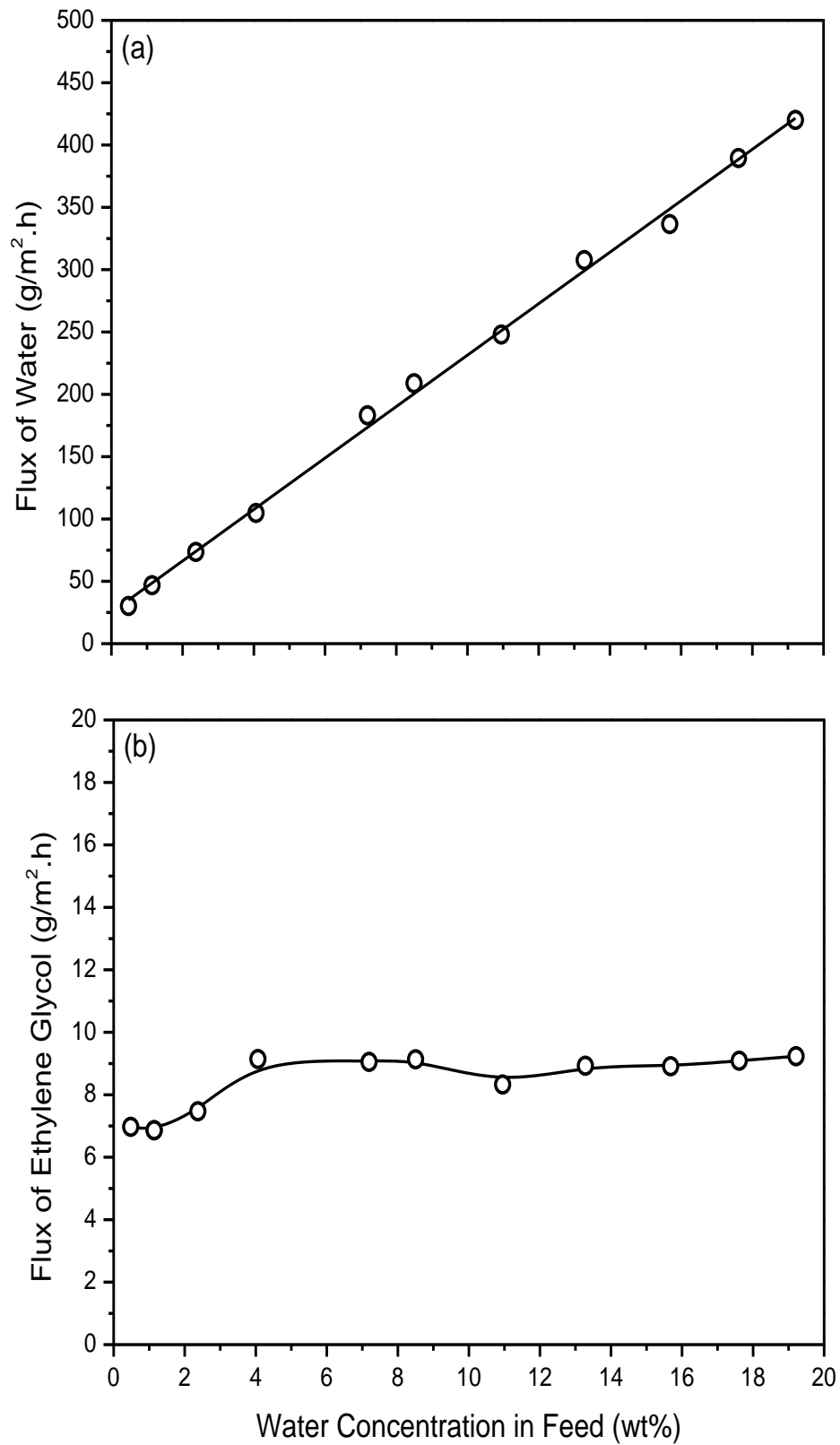
Figure 6.11 Effects of feed water concentration on partial permeation fluxes of (a) water and (b) ethylene glycol through membrane [PD]$_2$-[PA]-[PD]$_2$, Temperature: 38 ℃.
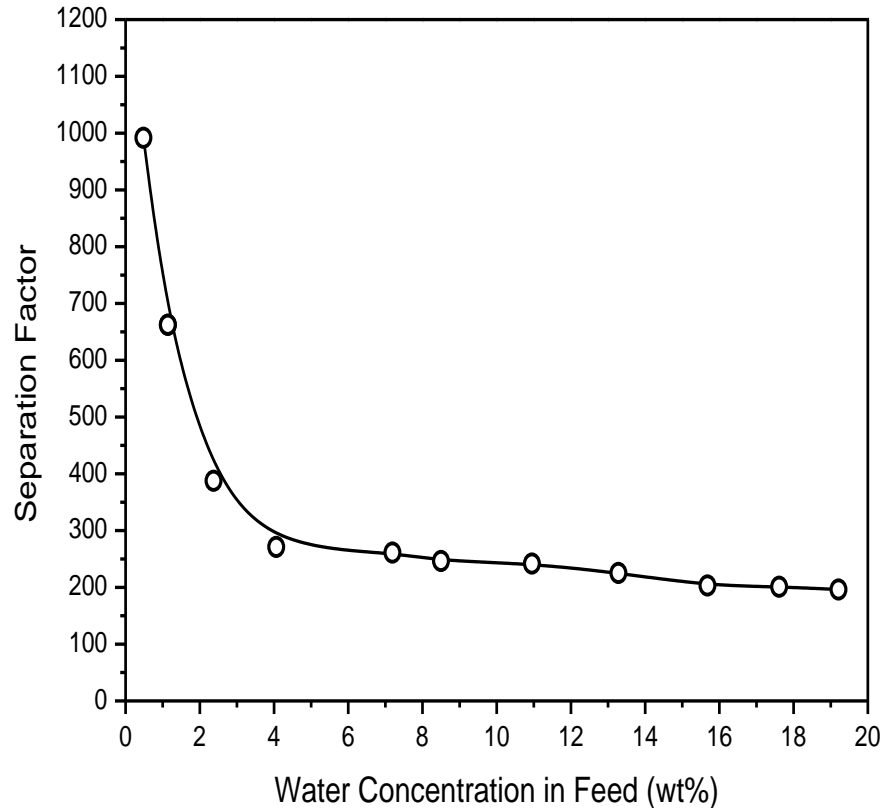
Figure 6.12 Effects of feed water concentration on separation factor for separation of water from ethylene glycol using membrane $[PD]_2$-$[PA]$-$[PD]_2$, Temperature: 38 °C.

Effect of operating temperature

Temperature is an important parameter in pervaporation since it influences the solubility and diffusivity of the permeating species in the membrane as well as driving force for permeation. Figure 6.13 shows the partial fluxes of water and ethylene glycol through membrane $[PD]_2$-$[PA]$-$[PD]_2$ at various temperatures ranging from 25-55 °C. It is shown that both the permeation fluxes of water and ethylene glycol increase with an increase in temperature. Generally, elevating the temperature will increase the thermal motion of the polymer chains and thus increasing the free volume inside the membrane, thereby increasing the diffusivity of the permeant in the membrane. In addition, the vapor pressures of water and ethylene glycol will both increase with an increase in temperature, thus increasing the driving force for the mass

189

transport through the membrane. All these factors will enhance the permeation flux. The temperature dependence of the permeation flux appears to flow an Arrhenius type of relationship,

$$J_i = J_{i0} \exp(-\frac{E_{Ji}}{RT}) \tag{6.3}$$

where E_{Ji} is the apparent activation energy for permeation, which represents the overall temperature dependence of permeation flux. The apparent activation energies for water and ethylene glycol at different feed water concentrations are shown in Table 6.2. The data in Table 6.2 show that at a given feed water concentration, the apparent activation energy for ethylene glycol permeation is larger than that for water permeation (i.e., $E_{J(Ethylene\ glycol)} > E_{J(Water)}$). Compared to water permeation, ethylene glycol has a larger molecular size and lower driving force (i.e., lower partial vapor pressure), which makes it more difficult to transport through the membrane, thus having a higher activation energy. The apparent activation energy was calculated from the slope of the Arrhenius plots. The temperature affects the permeation flux of ethylene glycol more significantly than it does for water. This explains the general decreasing tendency of the separation factor with an increase in temperature, as shown in Figure 6.14. In addition, over the temperature range tested, the feed water concentration has little effect on the permeation flux of ethylene glycol, but enhances the permeation flux of water, which results in a slight decrease in the separation factor at a relatively high feed water content, as shown in Figure 6.14.
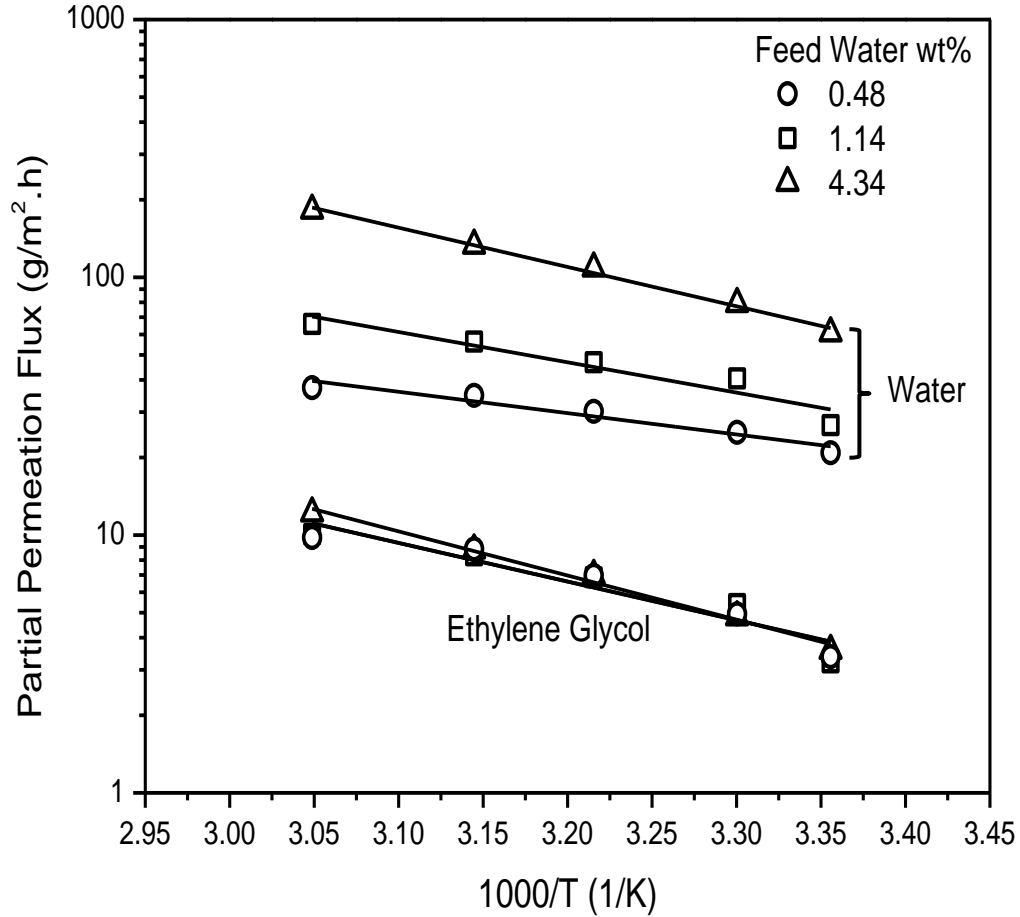
Figure 6.13 Effects of temperature on partial permeation fluxes of water and ethylene glycol through membrane $[PD]_2$-$[PA]$-$[PD]_2$ at different feed water concentrations.

Table 6.2 The activation energy based on permeation flux (E_J) and membrane permeance (E_P) for water and ethylene glycol at different feed water concentrations

Feed water concentration (wt%)	Water		Ethylene glycol	
	E_J (kJ/mol)	E_P (kJ/mol)	E_J (kJ/mol)	E_P (kJ/mol)
0.48	15.85	-28.57	28.64	-39.71
1.14	22.51	-25.93	28.73	-40.32
4.34	29.17	-15.51	32.77	-30.95
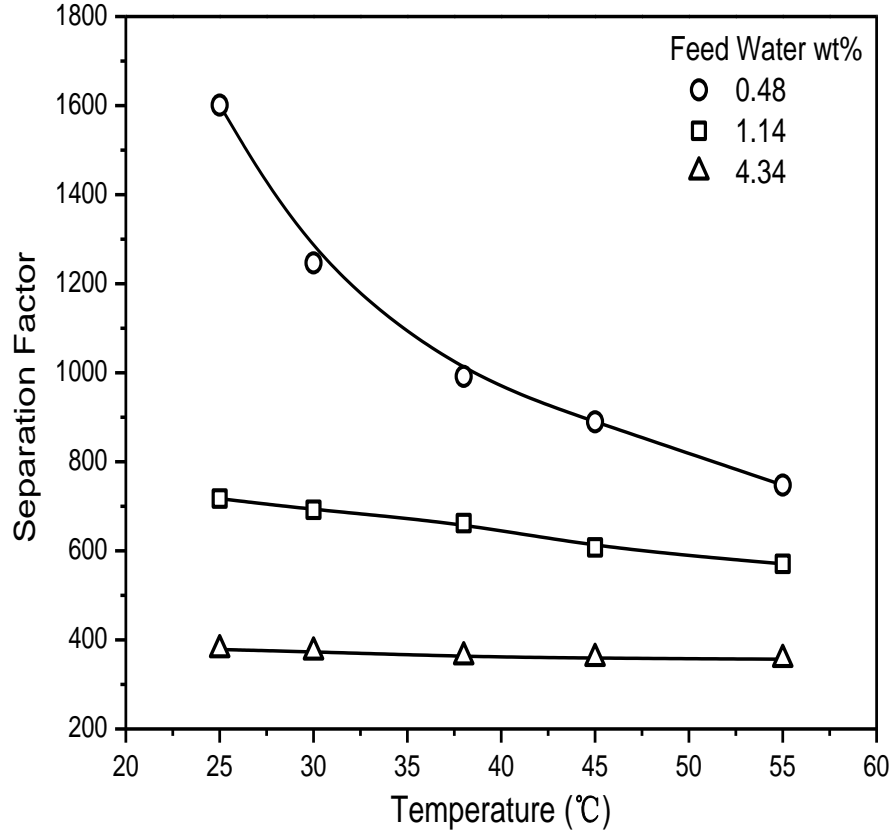
Figure 6.14 Effects of temperature on separation factor for separation of water from ethylene glycol using membrane $[PD]_2$-$[PA]$-$[PD]_2$.

It should be pointed out that the apparent activation energy based on permeation flux characterizes the overall temperature dependence of permeation flux, which has accounted for the effects of temperature on the driving force for mass transport. In order to evaluate the influence of the temperature on the membrane permeability, the membrane permeance was estimated in analog to gas permeation using permeation flux normalized by driving force for permeation, and the temperature dependence of the membrane permeance was also found to follow an Arrhenius relationship,

$$(P_i/l) = \frac{J_i}{p_i^S x_{io}\, \gamma_i - p_i^P x_{il}} = (P_{i0}/l)\exp(-\frac{E_{Pi}}{RT}) \tag{6.4}$$

where (P_i/l) is the permeance of the membrane, p^s is the saturated vapor pressure that can be calculated from the Antoine equation [Yaws *et al.*, 2009], γ is the activity coefficient in the liquid phase which can be calculated by the Wilson equation [Gmehling and Onken, 1977], p^p is the permeate vapor pressure, x_{i0} and x_{il} are the mole fractions in the feed and permeate respectively, E_P is the activation energy based on membrane permeability, and subscript i represents component i. Figure 6.15 shows the membrane permeance as a function of the reciprocal of temperature. The E_p values determined from the Arrhenius plots for water and ethylene glycol at different feed water concentrations are shown in Table 6.2. It appears that the temperature has a negative impact on the membrane permeability for both water and ethylene glycol. Based on the solution-diffusion model, the membrane permeability is determined by the solubility and diffusivity. As a first approximation [Feng and Huang, 1996],

$$E_P = E_D + \Delta H_S \tag{6.5}$$

where E_D is the activation energy for diffusion and ΔH_S is the heat of sorption. The diffusion process needs energy thus the value of E_D is positive. However, the sorption process is often exothermic and the value of ΔH_S is negative. The negative values of E_P suggest that the exothermic sorption process (i.e, negative value of ΔH_S) overweighs the diffusion process (i.e, positive value of E_D). That is to say, the reduction in solubility overweighs the increase in diffusivity, resulting in a decrease in the membrane permeability. Therefore, the observed increase in permeation flux is mainly caused by the increase in driving force. Moreover, the negative temperature dependence of the permeance of ethylene glycol appears to be more significant than that of water. However, as discussed before, the increase in permeation flux for ethylene glycol is more obvious than that for water when raising the temperature. These two

opposite trends suggest that the increased driving force caused by the increased temperature has

a more significant effect for ethylene glycol permeation than permeation of water.
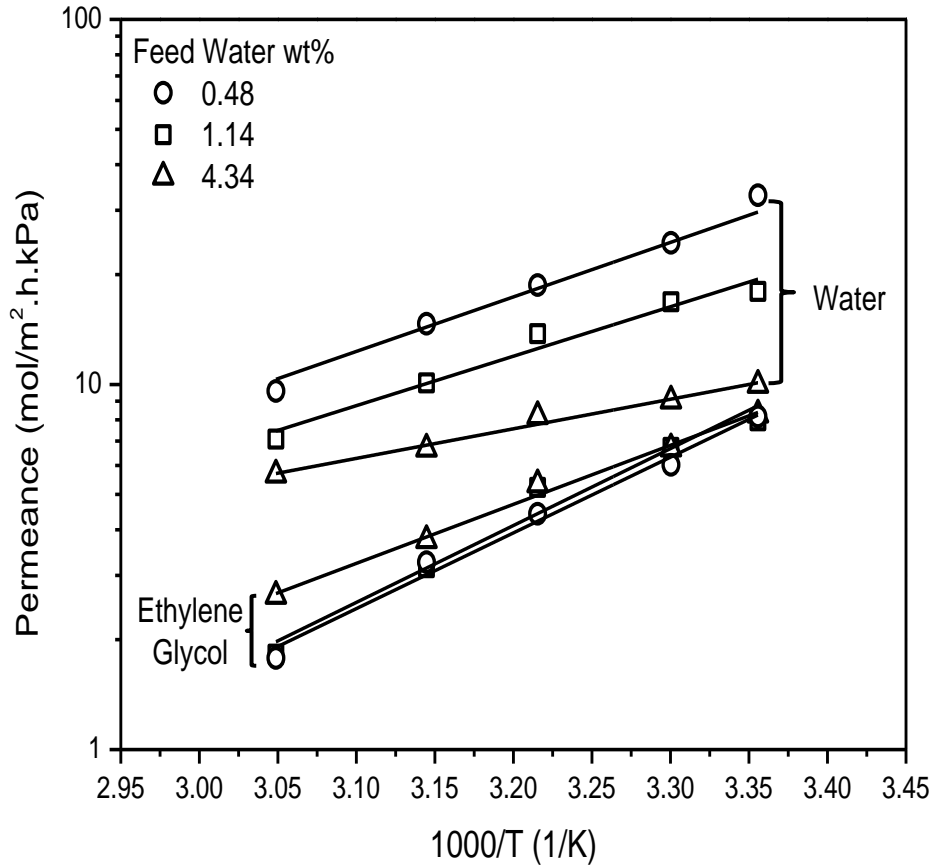
Figure 6.15 Effects of temperature on permeance of water and ethylene glycol through membrane [PD]$_2$-[PA]-[PD]$_2$ at different feed water concentrations.

At a given temperature, the permeance of water through the membrane is higher than that of

ethylene glycol, as shown in Figure 6.15. This can be ascribed to the smaller size of water,

which diffuses through the membrane more easily. Similar observations were also obtained by

Wang *et al*. [2011b] who used polybenzimidazole (PBI)/polyetherimide (PEI) membranes for

the dehydration of ethylene glycol. Furthermore, an increase in the feed water concentration

tends to increase the permeance of ethylene glycol, while the opposite is true for water. As

discussed in Section 6.3.2 ("Effect of feed concentration"), a higher feed water concentration would make the membrane more swollen that facilitates the permeability of ethylene glycol. However, the water molecules tend to form clusters at higher contents, making them more difficult to diffuse [Hirai and Nakajima, 1989]. Similar results were also observed with other hydrophilic membranes for dehydration of ethylene glycol [Hu *et al.*, 2012].

The overall separation in pervaporation may be approximated with selective evaporation of the liquid and selective permeation through the membrane [Wijmans and Baker, 1993]. The selectivity of the membrane for permeation water to ethylene glycol, i.e., the permeance ratio of water to ethylene glycol, is shown to be in the range of 1.21-5.39 within the studied temperature and feed water concentration ranges. Comparing the permeance ratio with the relatively high overall separation factor (i.e., 357-1601), it is clear that the contribution of the selective evaporation is more significant than that of the selective permeation. This is not surprising in view of the large difference in the volatilities of the two permeants. However, the selective permeation through the membrane is also important since a good separation is achieved by the mutual contribution of selective evaporation and selective permeation.

Effect of NaCl contents in feed

Many chemical processes and gas processing generate waste streams containing mixed organic/inorganic solutes, which will interact with the membrane surface and influence the separation performance. Up to now, only a few studies addressed the effects of salts in the feed mixtures on the membrane performance for the dehydration of organic solvents [Heisler *et al.*, 1956; Misra *et al.*, 1973; Shah *et al.*, 1999; Yang *et al.*, 2014]. In the present study, the effects of NaCl in the feed and temperature on the performance of membrane [PD]$_2$-[PA]-[PD]$_2$ for dehydration of ethylene glycol in the presence of NaCl were studied.

Figures 6.16(a) and (b) show the water concentration in the permeate and the total permeation flux as a function of NaCl content in the feed. For convenience of discussion, the salt concentration in the feed was expressed in terms of molality (i.e., the number of moles of NaCl per kg of the water/ethylene glycol solvent), while the water and ethylene glycol concentrations in the feed mixtures are on a salt-free basis. With an increase in the NaCl concentration in the feed mixture, there's more water content in the permeate and the increasing trend is more significant at lower water concentrations in the feed. However, the total permeation flux decreases with an increase in NaCl content in the feed mixture. Figure 6.17 shows the partial permeation fluxes of water and ethylene glycol at different feed NaCl concentrations. It is not surprising to see that both permeation fluxes of water and ethylene glycol decrease with an increase in NaCl content in the feed, and the reduction is more significant for ethylene glycol than for water, especially at lower feed water concentrations. Similar results were also observed by Heisler *et.al.* [1956] and Misra *et.al.* [1973] who used cellulose films for the dehydration of ethanol and methanol, respectively.
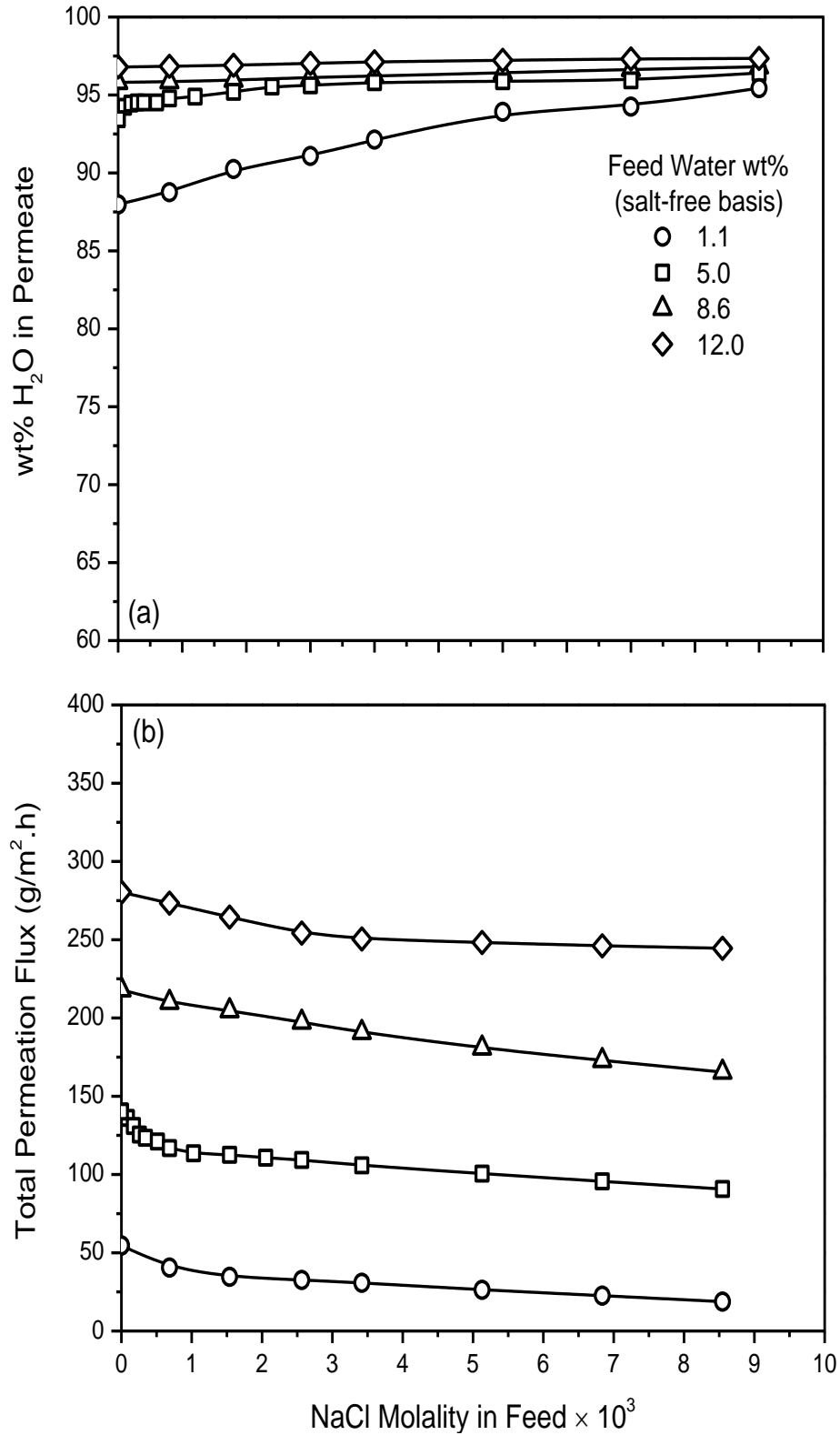
Figure 6.16 Effects of NaCl molality in the feed mixtures on (a) water concentration in permeate and (b) total permeation flux through membrane $[PD]_2$-$[PA]$-$[PD]_2$, Temperature: 38 °C.
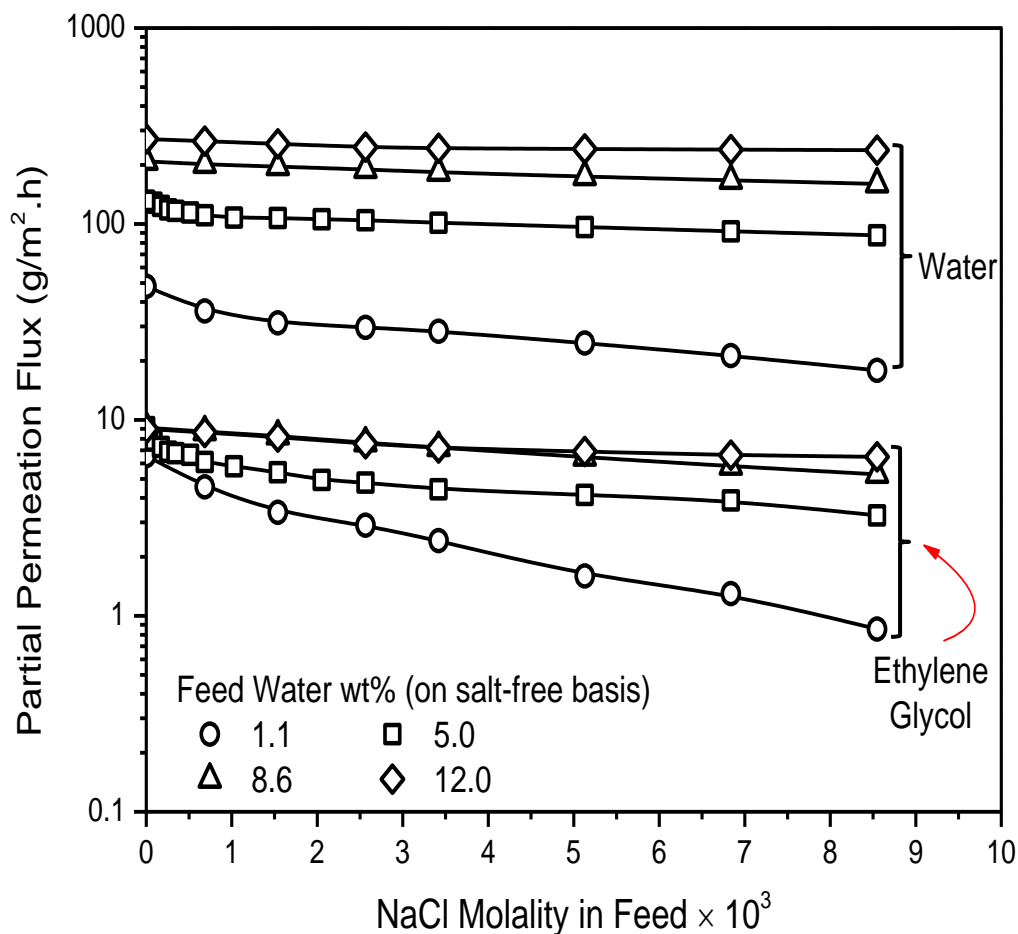
Figure 6.17 Effects of NaCl molality in the feed mixtures on partial permeation fluxes of water and ethylene glycol through membrane [PD]$_2$-[PA]-[PD]$_2$, Temperature: 38 °C.

The coupling effects between permeating components in the feed mixture often exist in pervaporation. For binary mixtures of ethylene glycol/water, the presence of water will increase the permeation of ethylene glycol due to the increased swelling of the membrane and the interaction between ethylene glycol and water. However, the presence of NaCl in the feed solution will make the situation much different. Firstly, the strong polar-polar interactions between NaCl and water will decrease the activity of water and make it less evaporative, and thus decrease the permeation flux of water. On the other hand, the stronger interactions can also result in a shielding effect of water which weakens the interactions between ethylene glycol and

water, and reduces the swelling of the membrane. Therefore, the facilitating effect of water on the permeation of ethylene glycol will be depressed, resulting in a decreased permeation of ethylene glycol. Moreover, it is believed that there are interactions between a charged membrane surface and the inorganic ions [Ball, 2010], which makes the membrane surface more hydrophilic. During the pervaporation process, the NaCl molecules either adhere to or become trapped in the membrane alone with the permeation of water and ethylene glycol. The good interactions between water and NaCl make the water molecules easily pass through the membrane, whereas the poor interactions between ethylene glycol and NaCl help restrict the passage for ethylene glycol molecules. This explains the relatively significant permeation reduction of ethylene glycol and the increased water content in the permeate. Based on the analysis above, it is understandable that there is a gradual increase in separation factor due to presence of NaCl in the feed mixtures, as shown in Figure 6.18. Similarly, the increase in the separation factor is more significant for the feed mixtures at a lower water content. Clearly, the presence of NaCl alters the permeability of water and ethylene glycol in the membrane due to the different NaCl-water and NaCl-ethylene glycol interactions. The separation factor is influenced by both the salt concentration and the ratio of water/ethylene glycol in the feed, and the effects of these two variables are interrelated.
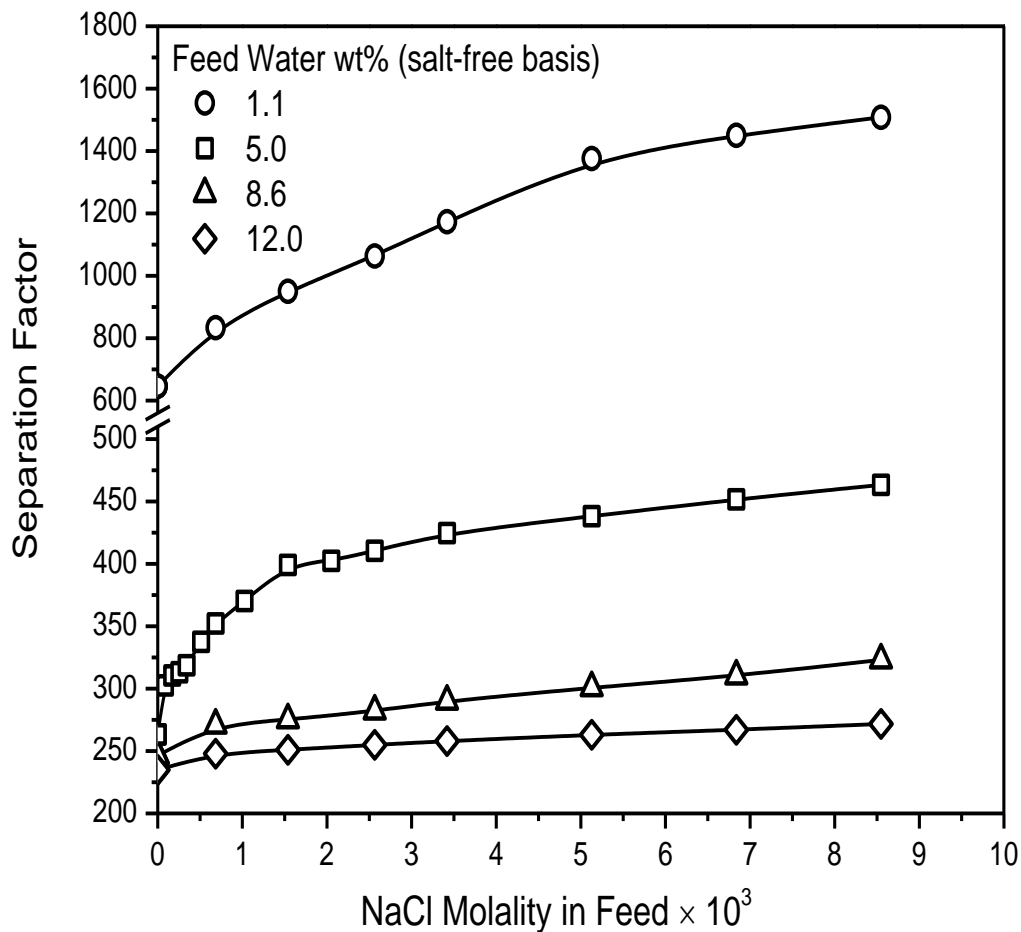
Figure 6.18 Effects of NaCl molality in the feed mixtures on separation factor for separation of water from ethylene glycol using membrane $[PD]_2$-$[PA]$-$[PD]_2$, Temperature: 38 °C.

The effects of temperature on the membrane performance for the ternary feed mixtures (i.e., ethylene glycol/water/NaCl) were also investigated. Figure 6.19 shows the logarithmic fluxes of water and ethylene glycol for the feeds with different NaCl concentrations through membrane $[PD]_2$-$[PA]$-$[PD]_2$ as a function of the reciprocal of temperature ranging from 25-55 °C. Here the feed water concentration was fixed at 1.14 wt% (salt-free basis). Generally, both the permeation fluxes of water and ethylene glycol increase with an increase in temperature, but decrease with an increase in the NaCl content in the feed. Similarly, the apparent activation energies E_J for permeation can be calculated from the slopes of the plots,

and they are presented in Table 6.3. An increase in the salt concentration in the feed increases $E_{J(water)}$ while $E_{J(Ethylene\ glycol)}$ decreases. It is well known that inorganic salts can decrease the activity of water and increase the activity of organic compounds in the mixture [Kujawski and Krajewski, 2007; Martíñez *et al.*, 2012]. The activity coefficients predicted using Aspen Plus, shown in Table 6.4, demonstrate this trend. The changes in the activities of the permeating components in the feed due to addition of NaCl help us to understand the change of the apparent activation energy for the permeation of water and ethylene glycol. In addition, it can be observed that the effect of temperature on the permeation flux of water becomes more significant at a higher NaCl content in the feed. The activity and mobility of NaCl is enhanced by increasing the temperature, resulting in a more significant facilitating effect for the permeation of water. Therefore, the water content in the permeate increases with temperature, resulting in an increased separation factor, as shown in Figures 6.20(a) and (b).

This [PD]$_2$-[PA]-[PD]$_2$ membrane was shown to be stable. There was no noticeable change in the membrane performance after pervaporation test with various feed mixtures at different temperatures for a prolonged period of experiments. For example, this membrane showed a total permention flux of 53.7 g/(m^2.h) and a water/ethylene glycol separation factor of 662 for a feed containing 1.14 wt% water (salt-free basis), and after extensive tests with various feed mixtures (e.g., binary ethylene glycol/water solutions and ternary ethylene glycol/water/NaCl solutions with different compositions) at different temperatures for over 3 months, the membrane maintained essentially the same pervaporation performance, with a total permention flux of 57.8 g/(m^2.h) and a separation factor of 640 for a feed containing 1.25 wt% water (salt-free basis).
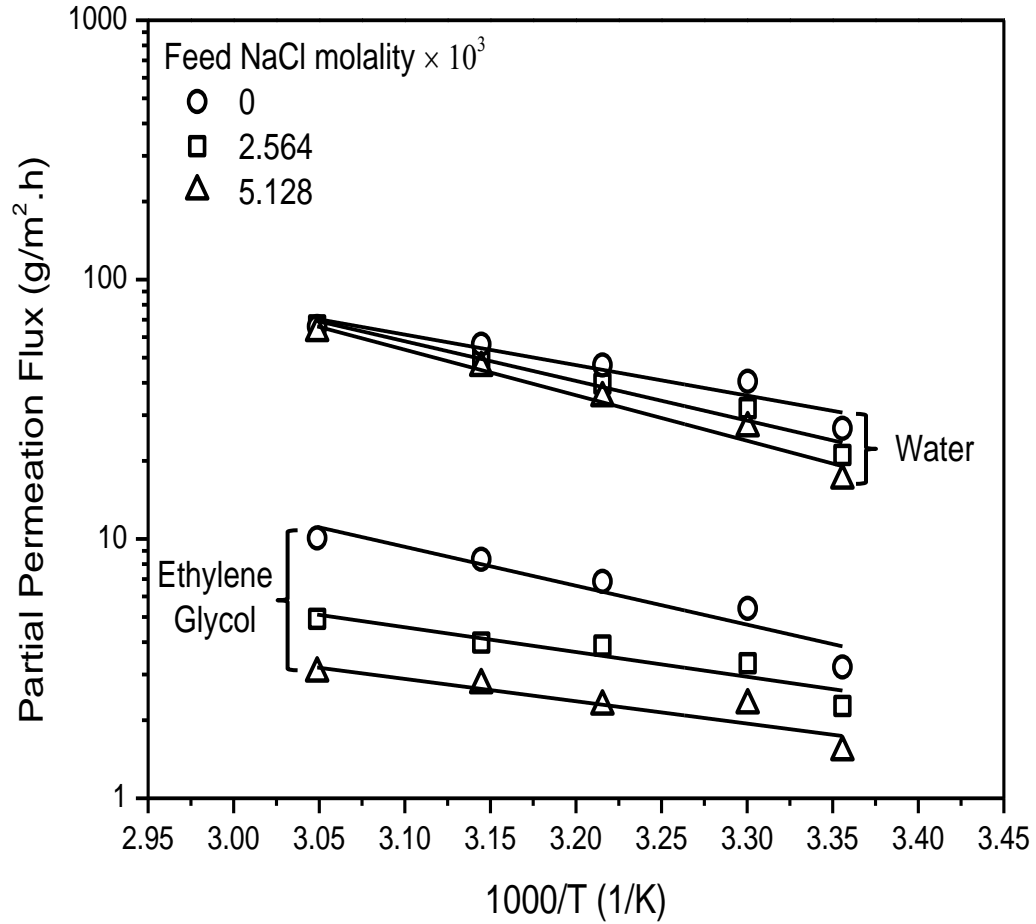
Figure 6.19 Effects of temperature on partial permeation fluxes of water and ethylene glycol through membrane [PD]$_2$-[PA]-[PD]$_2$ at different feed NaCl concentrations, Feed water concentration: 1.14 wt% (salt-free basis).

Table 6.3 Apparent activation energy based on permeation flux (E$_J$) for water and ethylene at different feed NaCl concentrations. Feed water concentration: 1.14 wt% (salt-free basis)

Feed NaCl molality $\times 10^3$	E$_J$ (kJ/mol)	
	Water	Ethylene glycol
0	22.51	28.73
2.564	29.28	18.27
5.128	33.61	16.48
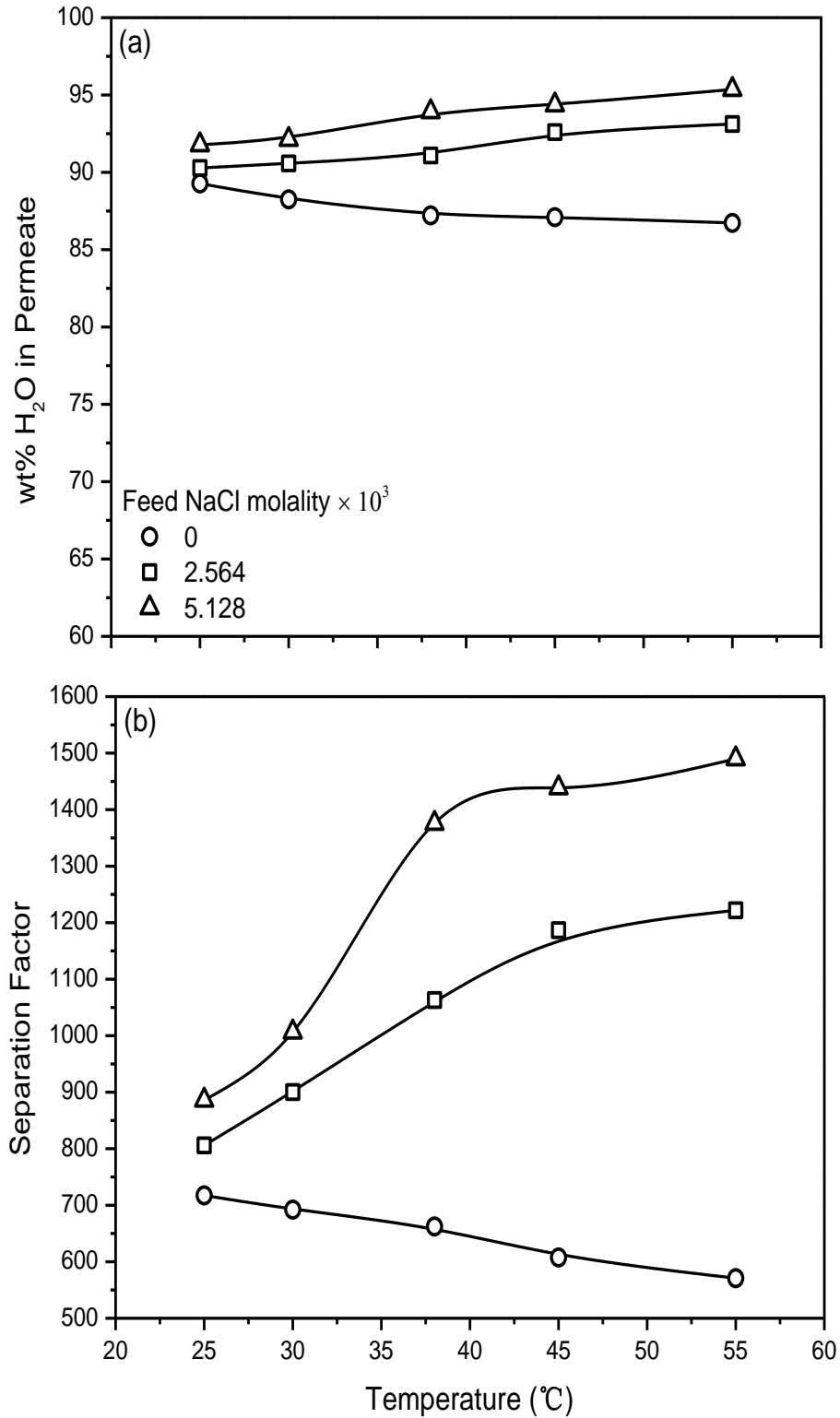
Figure 6.20 Effects of temperature on (a) water concentration in permeate and (b) separation factor for separation of water from ethylene glycol using membrane $[PD]_2$-$[PA]$-$[PD]_2$ at different feed NaCl concentrations, Feed water concentration: 1.14 wt% (salt-free basis).

Table 6.4 Activity coefficient γ for water and ethylene at different feed NaCl concentrations predicted by Aspen Plus. Feed water concentration: 1.14 wt% (salt-free basis)

Feed NaCl molality $\times 10^3$	Temperatures (℃)	Activity coefficient (γ)	
		Water	Ethylene glycol
0	25	0.814268	0.999825
	30	0.821999	0.999830
	35	0.829546	0.999834
	45	0.844115	0.999842
	55	0.858021	0.999849
2.564	25	0.673440	1.123749
	30	0.674925	1.125865
	35	0.677530	1.129738
	45	0.681709	1.136185
	55	0.690442	1.150070
5.128	25	0.597746	1.288267
	30	0.600443	1.292300
	35	0.604972	1.299733
	45	0.611900	1.312158
	55	0.625725	1.338904

6.4 Conclusions

Thin film composite polyamide membrane was modified with self-polymerized polydopamine for the dehydration of ethylene glycol. The effect of the number and sequence of the polydopamine depositions on the pervaporation performance were studied. The effects of feed water concentration, operating temperature and inorganic salt in the feed on the pervaporation performance were also investigated, and the following conclusions can be drawn:

(1) Deposition of one or two layers of polydopamine either as an outer layer (i.e., on top of the polyamide) or as a gutter layer (i.e., between the polyamide and the substrate) would

increase both the total permeation flux and permselectivity for the separation of water from ethylene glycol by pervaporation.

(2) The permeation flux increased and the separation factor tended to decrease with an increase in feed water concentration. To address concerns about the rigidity of the supramolecular structures of PD, a PA sublayer was sandwiched in between two PD sublayers, and the $[PD]_2$-$[PA]$-$[PD]_2$ membrane showed a total permeation flux of 81.0 $g/(m^2.h)$ and a separation factor of 388 for a feed containing 2.4 wt% water at 38 ℃.

(3) The permeation flux increased and the separation factor decreased with an increase in operating temperature. The positive temperature dependence of permeation flux was mainly ascribed to the increased driving force for permeation.

(4) The presence of inorganic salt NaCl in the feed solution decreased both the permeation flux of water and ethylene glycol, but the decrease in ethylene glycol flux was more significant, resulting in an improved separation factor. Unlike the pervaporation of binary ethylene glycol/water, when NaCl was present in the ethylene glycol/water solutions, the separation factor for pervaporative dehydration of ethylene glycol increased with an increase in temperature.

Chapter 7.

General conclusions, contributions and recommendations

7.1 General conclusions and contributions to original research

Thin film composite membranes based on interfacial polymerization for salt separation and ethylene glycol dehydration were prepared and studied. The general conclusions drawn from this study and related contributions to original research are as follows:

7.1.1 Fabrication of TFC NF membranes with good separation performance

(1) Positively charged polyamide TFC nanofiltration membranes with single-layered and multi-layered structures were prepared by interfacial polymerization from polyethylenimine (PEI) and trimesoyl chloride (TMC). Multi-layered membranes were prepared by a sequence of reactant depositions and reactions. The membrane properties could be tailored by adjusting the reactant concentrations or the number of cycles of the sequential reactant depositions. The resulting membrane formed by a single cycle of interfacial polymerization with 3.5 wt% PEI and 0.7 wt% TMC showed a good nanofiltration performance; salt rejections of 95.1% for $MgCl_2$, 94.4% for $MgSO_4$, 80.5% for Na_2SO_4 and 85.1% for NaCl with a pure water permeation flux of 24.5 $L/(m^2.h)$ were obtained at a feed solute concentration of 500 ppm and transmembrane pressure of 0.8 MPa gauge.

(2) Monomeric amine piperazine (PIP) was embedded with polymeric amine PEI for fabricating TFC nanofiltration membranes. Membranes with a single-ply polyamide layer were produced by reacting TMC with mixed amines of PEI and PIP, and the incorporation

of 10 wt% PIP in PEI resulted in a 6-fold increase in water permeation flux while still maintaining a 91.6% $MgCl_2$ rejection. 2-ply polyamide membranes were prepared by two cycles of PEI-TMC and PIP-TMC interfacial reactions separately, and they showed a higher rejection than the single-ply polyamide membrane.

7.1.2 Investigation of membrane formation process

Both the amine-acyl chloride and acyl chloride-amine reactant deposition sequences involved in interfacial polymerization were studied to provide an insight into the membrane formation. With polymeric amine PEI, these two sequences could produce TFC membranes with reasonably good rejections. The composite membranes fabricated using a PEI-TMC deposition sequence had evenly distributed valley-ridge morphology on the membrane surface, while reversing the reactant deposition sequence (i.e., TMC-PEI) yielded membranes with irregularly distributed nodular structures on the membrane surface. In addition, membranes formed by the PEI-TMC deposition sequence were more permeable than membranes formed by the TMC-PEI deposition sequence. However, with monomeric amine PIP embedded into PEI for membrane formation, only the amine-acyl chloride sequence was suitable to produce membranes with good selectivity.

7.1.3 Study of chlorine treatment

(1) Composite membranes comprising of a PEI-based polyamide inner sublayer and PIP-based polyamide outer sublayers were fabricated via layer-by-layer sequential interfacial polymerization, and the chlorine resistance of the membranes was improved by the outer sublayers based on PIP/TMC crosslinks.

(2) The effects of chlorine exposure on the nanofiltration performance of the resulting membranes were investigated at different chlorination conditions (pH and chlorine

concentration). In general, membrane chlorination resulted in an increase in membrane permeability and a decrease in solute rejections (except for solute Na_2SO_4). In addition, at a given chlorine concentration, the effect of membrane chlorination was intensified at either an alkaline or an acidic pH as compared to membrane chlorination at pH 7. Properly controlling the chlorination conditions could improve the nanofiltration performance by effectively enhancing water flux without compromising solute rejections.

(3) The effects of chlorine concentration and exposure time are not equivalent with respect to membrane chlorination. The customarily used chlorination intensity (ppm.h), a composite parameter based on the product of chlorine concentration and chlorination time, was found to be inadequate as a standalone parameter to characterize the chlorination conditions. Caution should be exercised in using this parameter as the extent of membrane chlorination is not a linear function of the chlorine concentration.

7.1.4 Modification of TFC NF membranes for use in pervaporation

(1) Thin film composite nanofiltration membranes based on PEI/TMC were modified for use in pervaporation by deposition of one or two layers of polydopamine either as an outer layer (i.e., on top of the polyamide) or as a gutter layer (i.e., between the polyamide and the microporous substrate). Such modifications would increase the total permeation flux and effectively improve the membrane selectivity for pervaporative separation of water from ethylene glycol. The resulting membrane showed a total permeation flux of 81.0 $g/(m^2.h)$ and a separation factor of 388 for a feed containing 2.4 wt% water at 38 °C.

(2) The effects of feed water concentration, operating temperature and salt contents (NaCl) in the feed on the pervaporation performance were investigated. The membrane was preferentially permeable to water. The positive temperature dependence of permeation flux

was mainly ascribed to the increased driving force for permeation. If inorganic salt NaCl was present in the feed mixture, both permeation fluxes of water and ethylene glycol decreased, but the water content in the permeate increased.

7.2 Recommendations for future work

7.2.1 Interfacially polymerized TFC nanofiltration membranes

Development of new applications

TFC membranes formed by interfacial polymerization from PEI or PEI embedded with PIP in this study showed good selectivity for separation of inorganic salts from water. In addition to the inorganic salts, the emergence of organic contaminants is another concern with regard to the water treatment. The efficiency of organic contaminants removal by commercial NF membranes has been investigated [Yangali-Quintanilla *et al.*, 2010; Bellona *et al.*, 2012; Azaïs *et al.*, 2014]. It is expected that our laboratory made membranes are also suitable for separating organic contaminants from water. The organic matters in wastewater mainly include pharmaceutically active compounds (PhACs), endocrine disrupter compounds (EDCs), disinfection by-products, personal care products and other organic compounds from various industries. It is recommended to investigate the selectivity of the membranes for removal of these organic contaminants from water.

Improvement of chlorine resistance by introducing polyester segments

As mentioned in Chapter 2, TFC membranes based on polyesters, especially aromatic polyesters, are perceived to have better chlorine resistance than polyamide membranes since polyesters have no amidic hydrogen vulnerable to chlorine attack. Therefore, another attempt for improving the chlorine resistance of PEI-based nanofiltration membranes may be made by incorporating an interfacially polymerized polyester outer sublayer on top of the PEI-based

inner sublayer. Due to their rigid structures, aromatic polyesters should be more resistant to chlorine than aliphatic polyesters. However, the reactivity of alcohol/phenol is lower than amine. For fabricating a dense skin top layer, preliminary work should be focused on the membrane preparation conditions (e.g., adding acid acceptor or additives to facilitate the interfacial reaction) to identify suitable strategies for the membrane improvement.

From Chapter 5, we found that the chlorine exposure improved the membrane retention of Na_2SO_4, and increased the water flux without compromising solute rejections for $MgCl_2$ and $MgSO_4$ at low chlorine concentrations. These results suggested that the chlorine treatment could also be used as a membrane modification method. However, the conditions of chlorine exposure (e.g., chlorine concentration and exposure time) for improving the separation performance still need to be further investigated.

Investigation of fouling resistance

Membrane fouling is another obstacle that limits the development of TFC nanofiltration membranes. Based on different foulants, membrane fouling includes colloidal fouling, organic fouling, inorganic fouling and biofouling. Positively charged PEI-based nanofiltration membranes are expected to have a good fouling resistance to positively charged foulants [Zhou *et al.*, 2009]. However, the fouling behavior of commonly encountered protein foulants (e.g., bovine serum albumin (BSA)) on the newly developed membranes is still yet to be studied. The fouling issues also related to membrane cleaning for flux recovery. The physical methods for membrane cleaning include backwashing, introducing a gas to the washing solution and pulsation. Chemical cleaning reagents can also be introduced into membrane cleaning processes. For instance, protein and polysaccharide could be oxidized into small molecules by NaClO and then removed from membrane surface. NaOH would increase the solubility of

organic foulants, HCl would help the removal of mineral deposits and surfactants would break the "organic-metal" complex. Therefore, the membrane cleaning conditions, involving in the type of cleaning reagent, pH of the cleaning solution and the cleaning time, are another interesting aspect to be examined.

7.2.2 TFC pervaporation membranes

Optimization of membrane preparation/modification conditions

In this study, the deposition of the self-polymerized polydopamine layers was proved to be feasible to modify PEI-based nanofiltration membrane for use in pervaporative separations of solvents. However, the membrane modification conditions studied were not optimized. In order to improve the separation properties of the polydopamine modified polyamide TFC membranes, parameters involved in the procedure of membrane fabrication/modification, such as the number of polydopamine and polyamide depositions, the concentration of polydopamine and polyamide depositions, the time for polydopamine and polyamide depositions, need to be further investigated.

Development of new applications

The polydopamine modified polyamide TFC membranes showed a good selectivity for separation of water from ethylene glycol. These membranes are expected to be suitable for the dehydration of other organic solvents (e.g., triethylene glycol, propylene glycol, ethanol, and isopropanol) by pervaporation, and the membrane performance for such separations need to be determined experimentally. The effects of feed composition, operating temperature and the presence of inorganic component in feed on the membrane performance can also be investigated.

This thesis work is expected to lead to 4 refereed publications. Two manuscripts have already been published: one in Journal of Membrane Science, and the other in Reactive & Functional Polymers (an invited contribution). The third one has been accepted by Journal of Membrane Science, and another one will be submitted to Journal of Membrane Science soon.

References

Akbari, A., S. Desclaux, J. C. Rouch, P. Aptel and J. C. Remigy, New UV-photografted nanofiltration membranes for the treatment of colored textile dye effluents, *J. Membr. Sci.*, 286 (2006) 342-350.

Albo, J., J.Wang and T. Tsuru, Application of interfacially polymerized polyamide composite membranes to isopropanol dehydration: Effect of membrane pre-treatment and temperature, *J. Membr. Sci.*, 453 (2014) 384-393.

An, Q., F. Li, Y. Ji and H. Chen, Influence of polyvinyl alcohol on the surface morphology, separation and anti-fouling performance of the composite polyamide nanofiltration membranes, *J. Membr. Sci.*, 367 (2011) 158-165.

An, Q., W. S. Hung, S. C. Lo, Y. H. Li, M. D. Guzman, C. C. Hu, K. R. Lee, Y. C. Jean and J. Y. Lai, Comparison between free volume characteristics of composite membranes fabricated through static and dynamic interfacial polymerization processes, *Macromolecules*, 45 (2012) 3428-3435.

An, Q. F., W. D. Sun, Q. Zhao, Y. L. Ji and C. J. Gao, Study on a novel nanofiltration membrane prepared by interfacial polymerization with zwitterionic amine monomers, *J. Membr. Sci.*, 431 (2013) 171-179.

Arthur, S. D. and D. Wilmington, Reverse osmosis membranes of polyamideurethane, US Pat. 5,085,777, (1992).

Avlonitis, S., W. T. Hanbury and T. Hodgkiess, Chlorine degradation of aromatic polyamides, *Desalination*, 85 (1992) 321-334.

Azaïs, A., J. Mendret, S. Gassara, E. Petit, A. Deratani and S. Brosillon, Nanofiltration for wastewater reuse: Counteractive effects of fouling and matrice on the rejection of pharmaceutical active compounds, *Sep. Purif. Technol.*, 133 (2014) 313-327.

Baker, R. W., *Membrane Technology and Applications, 3rd Edition*, John Wiley, (2012).

Ball, V., Impedance spectroscopy and zeta potential titration of dopa-melanin films produced by oxidation of dopamine, *Colloids and Surf. A: Physicochem. Eng. Aspects*, 363 (2010) 92-97.

Baroña, G. N. B., J. Lim and B. Jung, High performance thin film composite polyamide reverse osmosis membrane prepared via m-phenylenediamine and 2,2' benzidinedisulfonic acid, *Desalination*, 291 (2012) 66-77.

Bartels, C. R., K. L. Kreuz and A. Wachtel, Structure-performance relationships of composite membranes: porous support densification, *J. Membr. Sci.*, 32 (1987) 291-312.

Bartels, C. R., A surface science investigation of composite membranes, *J. Membr. Sci.*, 45 (1989) 225-245.

Belfer, S., Y. Purinson and O. Kedem, Surface modification of commercial polyamide reverse osmosis membranes by radical grafting: An ATR-FTIR study, *Acta Polym.*, 49 (1998) 574-582.

Bellona, C., D. Heil, C. Yu, P. Fu and J. E. Drewes, The pros and cons of using nanofiltration in lieu of reverse osmosis for indirect potable reuse applications, *Sep. Purif. Technol.*, 85 (2012) 69-76.

Berezkin, A. V. and A. R. Khokhlov, Mathematical modeling of interfacial polycondensation, *J. Polym. Sci., Ser B: Polym. Phys.*, 44 (2006) 2698-2742.

Bernsmann, F., A. Ponche, C. Ringwald, J. Hemmerlé, J. Raya, B. Bechinger, J. C. Voegel, P. Schaaf and V. Ball, Characterization of dopamine-melanin growth on silicon oxide, *J. Phys. Chem. C*, 113 (2009) 8234-8242.

Boricha, A. G. and Z. V. P. Murthy, Preparation, characterization and performance of nanofiltration membranes for the treatment of electroplating industry effluent, *Sep. Purif. Technol.*, 65 (2009) 282-289.

Buch, P. R., D. J. Mohan and A. V. R. Reddy, Preparation, characterization and chlorine stability of aromatic-cycloaliphatic polyamide thin film composite membranes, *J. Membr. Sci.*, 309 (2008) 36-44.

Burzio, L. A. and J. H. Waite, Cross-linking in adhesive quinoproteins: studies with model decapeptides, *Biochemistry*, 39 (2000) 11147-11153.

Cadotte, J. E. and L. T. Roxelle, In-situ-formed condensation polymers for reverse osmosis membranes, NTIS Report No. PB-229337, (1972).

Cadotte, J. E., C. V. K. Jr, K. E. Cobian and L. T. Rozelle, In-situ-formedcondensation polymers for reverse osmosis: second phase, NTIS Report No. PB-234198, (1974).

Cadotte, J. E., K. E. Cobian, R. H. Forester and R. J. Petersen, Continued evaluation of in-situ-formed condensation polymers for reverse osmosis membranes, NTIS Report No. PB-253193, (1976).

Cadotte, J. E., Reverse osmosis membrane, US Pat. 4,039,440, (1977).

Cadotte, J. E., M. J. Steuck and R. J. Petersen, Research on in-situ-formed condensation polymers for reverse osmosis membranes, NTIS Report No. PB- 288387, (1978).

Cadotte, J. E., R. S. King and N. A. Newkumet, Advanced poly (piperazineamide) reverse osmosis membranes, NTIS Report No. PB80-127574, (1979).

Cadotte, J. E., R. S. King, R. J. Majerle and R. J. Petersen, Interfacial synthesis in the preparation of reverse osmosis membranes, *J. Macromol. Sci., Part A: Pure Appl. Chem.*, A15 (1981) 727-755.

Cadotte, J. E., Interfacially synthesized reverse osmosis membrane, US Pat. 4,277,344, (1981a).

Cadotte, J. E., Reverse osmosis membrane, US Pat. 4,259,183, (1981b).

Cadotte, J. E., R. Forester, M. Kim, R. Petersen and T. Stocker, Nanofiltration membranes broaden the use of membrane separation technology *Desalination*, 70 (1988) 77-88.

Chai, G. Y. and W. B. Krantz, Formation and characterization of polyamide membranes via interfacial polymerization, *J. Membr. Sci.*, 93 (1994) 175-192.

Chen, G., S. Li, X. Zhang and S. Zhang, Novel thin-film composite membranes with improved water flux from sulfonated cardo poly(arylene ether sulfone) bearing pendant amino groups, *J. Membr. Sci.*, 310 (2008) 102-109.

Chen, J., J. Li, Z. P. Zhao, D. Wang and C. X. Chen, Nanofiltration membrane prepared from polyacrylonitrile ultrafiltration membrane by low-temperature plasma: 5. Grafting of styrene in vapor phase and its application, *Surf. Coat. Technol.*, 201 (2007) 6789-6792.

Chen, J., X. Chen, X. Yin, J. Ma and Z. Jiang, Bioinspired fabrication of composite pervaporation membranes with high permeation flux and structural stability, *J. Membr. Sci.*, 344 (2009) 136-143.

Chiang, Y., Low fouling ultrafiltration and nanofiltration membranes fabricated by zwitterionic surface modification, Ph.D Thesis, National Central University, Taiwan, (2009).

Chiang, Y., Y. Hsub, R. Ruaan, C. Chuang and K. Tung, Nanofiltration membranes synthesized from hyperbranched polyethyleneimine, *J. Membr. Sci.*, 326 (2009) 19-26.

Choi, H. S., T. Hinob, M. Shibata, Y. Negishi and H. Ohya, The characteristics of a PAA-PSf composite membrane for separation of water-ethanol mixtures through pervaporation, *J. Membr. Sci.*, 72 (1992) 259-266.

Credah, L., A. Chiolle and P. Parrini, New polymer materials for reverse osmosis membranes, *Desalination*, 14 (1974) 137-150.

Dalwani, M., G. Bargeman, S. S. Hosseiny, M. Boerrigter, M. Wessling and N. E. Benesa, Sulfonated poly(ether ether ketone) based composite membranes for nanofiltration of acidic and alkaline media, *J. Membr. Sci.*, 381 (2011) 81-89.

Do, V. T., C. Y. Tang, M. Reinhard and J. O. Leckie, Degradation of polyamide nanofiltration and reverse osmosis membranes by hypochlorite, *Environ. Sci. Technol.*, 46 (2012a) 852-859.

Do, V. T., C. Y. Tang, M. Reinhard and J. O. Leckie, Effects of Chlorine Exposure Conditions on Physiochemical Properties and Performance of a Polyamide Membrane-Mechanisms and Implications, *Environ. Sci. Technol.*, 46 (2012b) 13184-13192.

Du, J. R., A. Chakma and X. Feng, Dehydration of ethylene glycol by pervaporation using poly(N,N-dimethylaminoethyl methacrylate)/polysulfone composite membranes, *Sep. Purif. Technol.*, 64 (2008) 63-70.

215

Eriksson, P., Water and salt transport through two types of polyamide composite membranes, *J. Membr. Sci.*, 36 (1988) 297-313.

Ettori, A., E. G. Maurinc, J. C. Schrotter, P. Aimar and C. Causserand, Permeability and chemical analysis of aromatic polyamide based membranes exposed to sodium hypochlorite, *J. Membr. Sci.*, 375 (2011) 220-230.

Fathizadeh, M., A. Aroujalian, A. Raisi and M. Fotouhi, Preparation and characterization of thin film nanocomposite membrane for pervaporative dehydration of aqueous alcohol solutions, *Desalination*, 314 (2013) 20-27.

Feng, X. and R. Y. M. Huang, Estimation of activation energy for permeation in pervaporation processes, *J. Membr. Sci.*, 118 (1996) 127-131.

Fibiger, R. F., J. Y. Koo, D. J. Forgach, R. J. Petersen, D. S. Schmidt, R. A. Wessling and T. F. Stocker, Novel polyamide reverse osmosis membranes, US Pat. 4,769,148, (1988).

Freeman, S. D. N. and T. F. Stocker, Comparison of two thin-film composite membranes: low pressure FT-30 to very low pressure NF40HF, *Desalination*, 62 (1987) 183-191.

Freger, V., Nanoscale heterogeneity of polyamide membranes formed by interfacial polymerization, *Langmuir*, 19 (2003) 4791-4797.

Freger, V., Kinetics of film formation by interfacial polycondensation, *Langmuir*, 21 (2005) 1884-1894.

Gaeta, S. N., E. Petrocchi, E. Negri and E. Drioli, Chlorine resistance of polypiperazineanide membranes and modules, *Desalination*, 83 (1991) 383.

Glater, J., S.-k. Hong and M. Elimelech, The search for a chlorine-resistant reverse osmosis membrane, *Desalination*, 95 (1994) 325-345.

Gmehling, J. and U. Onken, *Vapor-Liquid Equilibrium Data Collection, Chemistry Data Series, Vol. 1, Pt. 1, Aqueous-Organic Systems*, DECHEMA, Frankfurt, (1977).

Gu, J. E., B. M. Jun and Y. N. Kwon, Effect of chlorination condition and permeability of chlorine species on the chlorination of a polyamide membrane, *Water Res.*, 46 (2012) 5389-5400.

Guo, R., X. Fang, HongWu and Z. Jiang, Preparation and pervaporation performance of surface crosslinked PVA/PES composite membrane, *J. Membr. Sci.*, 322 (2008) 32-38.

Heisler, E. G., A. S. Hunter, J. Scillano and R. H. Treadway, Solute and temperature effects in the pervaporation of aqueous alcoholic solutions, *Science*, 124 (1956) 77-79.

Hirai, Y. and T. Nakajima, Sorption behavior of water vapor into polyelectrolyte complex of poly(acrylic acid)/poly(4-vinylpyridine), *J. Appl. Polym. Sci.*, 37 (1989) 2275-2281.

Hu, S. Y., Y. Zhang, D. Lawless and X. Feng, Composite membranes comprising of polyvinylamine-poly(vinylalcohol) incorporated with carbon nanotubes for dehydration of ethylene glycol by pervaporation, *J. Membr. Sci.*, 34-44 (2012) 417-418.

Huang, R. Y. M. (Eds.), *Pervaporation membrane separation process*, Elsevier, 1991,

Huang, S. H., C. J. Hsu, D. J. Liaw, C. C. Hu, K. R. Lee and J. Y. Lai, Effect of chemical structures of amines on physicochemical properties of active layers and dehydration of isopropanol through interfacially polymerized thin-film composite membranes, *J. Membr. Sci.*, 307 (2008) 73-81.

Huang, S. H., G. J. Jiang, D. J. Liaw, C. L. Li, C. C. Hu, K. R. Lee and J. Y. Lai, Effects of the polymerization and pervaporation operating conditions on the dehydration performance of interfacially polymerized thin-film composite membranes, *J. Appl. Polym. Sci.*, 114 (2009) 1511-1522.

Huang, S. H., W. S. Hung, D. J. Liaw, H. A. Tsai, G. J. Jiang, K. R. Lee and J. Y. Lai, Positron annihilation study on thin-film composite pervaporation membranes: Correlation between polyamide fine structure and different interfacial polymerization conditions, *Polymer*, 51 (2010a) 1370-1376.

Huang, S. H., W. S. Hung, D. J. Liaw, C. H. Lo, W. C. Chao, C. C. Hu, C. L. Li, K. R. Lee and J. Y. Lai, Interfacially polymerized thin-film composite polyamide membranes: Effects of annealing processes on pervaporative dehydration of aqueous alcohol solutions, *Sep. Purif. Technol.*, 72 (2010b) 40-47.

Huang, S. H., Y. Y. Liu, Y. H. Huang, K. S. Liao, C. C. Hu, K. R. Lee and J. Y. Lai, Study on characterization and pervaporation performance of interfacially polymerized polyamide thin-film composite membranes for dehydrating tetrahydrofuran, *J. Membr. Sci.*, 470 (2014) 411-420.

Jadas-Hecart, A., A. E. Morer, M. Stitou, P. Bouillot and B. Legube, The chlorine demand of a treated water, *Water Res.*, 26 (1992) 1073-1084.

Jahanshahi, M., A. Rahimpour and M. Peyravi, Developing thin film composite poly(piperazine-amide) and poly(vinyl-alcohol) nanofiltration membranes, *Desalination*, 257 (2010) 129-136.

Jayarani, M. M., R. R. Rajamohanan, S. S. Kulkarniand and U. K. Kharul, Synthesis of model diamide, diester and esteramide adducts and studies on their chlorine tolerance, *Desalination*, 130 (2000) 1-16.

Jayarani, M. M. and S. S. Kulkarni, Thin-film composite poly(esteramide)-based membranes, *Desalination*, 130 (2000) 17-30.

Jenkins, M. and M. B. Tanner, Operational experience with a new fouling resistant reverse osmosis membrane, *Desalination*, 119 (1998) 243-249.

Kamiyama, Y., N. Yoshioka, K. Matsui and K. Nakagome, New thin-film composite reverse osmosis membranes and spiral wound modules, *Desalination*, 51 (1984) 79-92.

Kamiyama, Y., N. Yoshioka and K. Nakagome, Composite semipermeable membrane, US Pat. 4,619,767, (1986).

Kang, G. D., C. J. Gao, W. D. Chen, X. M. Jie, Y. M. Cao and Q. Yuan, Study on hypochlorite degradation of aromatic polyamide reverse osmosis membrane, *J. Membr. Sci.*, 300 (2007) 165-171.

Kang, G. D. and Y. M. Cao, Development of antifouling reverse osmosis membranes for water treatment: A review, *Water Res.*, 46 (2012) 584-600.

Karkhanechi, H., R. Takagi and H. Matsuyama, Biofouling resistance of reverse osmosis membrane modified with polydopamine, *Desalination*, 336 (2014) 87-96.

Kasemset, S., A. Lee, D. J. Miller, B. D. Freeman and M. M. Sharma, Effect of polydopamine deposition conditions on fouling resistance, physical properties, and permeation properties of reverse osmosis membranes in oil/water separation, *J. Membr. Sci.*, 425-426 (2013) 208-216.

Kaur, S., S. Sundarrajan, R. Gopal and S. Ramakrishna, Formation and characterization of polyamide composite electrospun nanofibrous membranes for salt separation, *J. Appl. Polym. Sci.*, 124 (2012) E205-E215.

Kawada, I., K. Inoue, Y. Kazuse, H. Ito, T. Shintani and Y.Kamiyama, New thin-film composite low pressure reverse osmosis membranes and spiral wound modules *Desalination*, 64 (1987) 387-401.

Kawaguchi, T. and H. Tamura, Chlorine-resistant membrane for reverse osmosis. I. correlation between chemical structures and chlorine resistance of polyamides, *J. Appl. Polym. Sci.*, 29 (1984) 3359-3367.

Kemperman, A. J. B., H. H. M. Rolevink, T. v. d. Boomgaard and H. Strathmann, Hollow-fiber-supported liquid membranes with improved stability for nitrate removal, *Sep. Purif. Technol.*, 12 (1997) 119-134.

Kemperman, A. J. B., H. H. M. Rolevink, D. Bargeman, T. v. d. Boomgaard and H. Strathmann, Stabilization of supported liquid membranes by interfacial polymerization top layers, *J. Membr. Sci.*, 138 (1998) 43-55.

Kim, H. J., S. S. Nah and B. R. Min, A new technique for preparation of PDMS pervaporation membrane for VOC removal, *Adv. Environ. Res.*, 6 (2002) 255-264.

Kim, J. J., K. Chang and S. Y. Kwak, Composite reverse osmosis membrane having active layer of aromatic polyester or copolymer of aromatic polyester and aromatic polyamide, US Pat. 5,593,588, (1997).

Kim, S. H., S. Y. Kwak, B. H. Sohn and T. H. Park, Design of TiO_2 nanoparticle selfassembled aromatic polyamide thin-film-composite (TFC) membrane as an approach to solve biofouling problem, *J. Membr. Sci.*, 211 (2003) 157-165.

Konagaya, S. and O. Watanabe, Influence of chemical structure of isophthaloyl dichloride and aliphatic, cycloaliphatic, and aromatic diamine compound polyamides on their chlorine resistance, *J. Appl. Polym. Sci.*, 76 (2000) 201-207.

Koo, J. Y., R. J. Petersen and J. E. Cadotte, ESCA characterization of chlorine damaged polyamide reverse osmosis membrane, *Polym. Prepr. (Am. Chem. Scc., Div. Polym Chem.)*, 27 (1986) 391-392.

Korikov, A. P., P. B. Kosaraju and K. K. Sirkar, Interfacially polymerized hydrophilic microporous thin film composite membranes on porous polypropylene hollow fibers and flat films, *J. Membr. Sci.*, 279 (2006) 588-600.

Kosaraju, P. B. and K. K. Sirkar, Interfacially polymerized thin film composite membranes on microporous polypropylene supports for solvent-resistant nanofiltration, *J. Membr. Sci.*, 321 (2008) 155-161.

Kujawski, W. and S. R. Krajewski, Influence of inorganic salt on the effectiveness of liquid mixtures separation by pervaporation, *Sep. Purif. Technol.*, 57 (2007) 495-501.

Kurihara, M., T. Uemura, Y. Nakagawa and T. Tonomura, The thin-film composite low pressure reverse osmosis membranes, *Desalination*, 54 (1985) 75-88.

Kurihara, M. and Y. Himeshima, The major development of the evolving reverse osmosis membranes and ultrafiltration membranes, *Polym. J.*, 23 (1991) 513-520.

Kwak, S. Y., M. O. Yeom, I. J. Roh, D. Y. Kim and J. J. Kim, Correlations of chemical structure, atomic force microscopy (AFM) morphology, and reverse osmosis (RO) characteristics in aromatic polyester high-flux RO membranes, *J. Membr. Sci.*, 132 (1997) 183-191.

Kwon, Y. N. and J. O. Leckie, Hypochlorite degradation of crosslinked polyamide membranes: I. Changes in chemical/morphological properties, *J. Membr. Sci.*, 283 (2006a) 21-26.

Kwon, Y. N. and J. O. Leckio, Hypochlorite degradation of crosslinked polyamide membranes II. Changes in hydrogen bonding behavior and performance, *J. Membr. Sci.*, 282 (2006b) 456-464.

La, Y. H., R. Sooriyakumaran, D. C. Miller, M. Fujiwara, Y. Terui, K. Yamanaka, B. D. McCloskey, B. D. Freeman and R. D. Allen, Novel thin film composite membrane containing ionizable hydrophobes: pH-dependent reverse osmosis behavior and improved chlorine resistance, *J. Mater. Chem.*, 20 (2010) 4615-4620.

Lau, W. J., A. F. Ismail, N. Misdan and M. A. Kassim, A recent progress in thin film composite membrane: A review, *Desalination*, 287 (2012) 190-199.

LaVoie, M. J., B. L. Ostaszewski, A. Weihofen, M. G. Scholssmacher and D. J. Selkoe, Dopamine covalently modifies and functionally inactivates parkin, *Nat. Med.*, 11 (2005) 1214-1221.

Lee, E. K., W. C. Babcock, R. P. Brass, P. A. Bresnahan and M. B. Chidlaw, Novel composite membranes, NTIS Report No. PB 83-243170, (1983).

Lee, H., S. M. Dellatore, W. M. Miller and P. B. Messersmith, Mussel-inspired surface chemistry for multifunctional coatings, *Science*, 318 (2007) 426-430.

Lee, H. S., S. J. Im, J. H. Kim, H. J. Kim, J. P. Kim and B. R. Min, Polyamide thin-film nanofiltration membranes containing TiO_2 nanoparticles, *Desalination*, 219 (2008) 48-56.

Lee, K. P., T. C. Arnot and D. Mattia, A review of reverse osmosis membrane materials for desalination-Development to date and future potential, *J. Membr. Sci.*, 370 (2010) 1-22.

Letterman, R. D., *Water Quality and Treatment, 5th Edition*, McGraw-Hill, (1999).

Li, B., W. Liu, Z. Jiang, X. Dong, B. Wang and Y. Zhong, Ultrathin and stable active layer of dense composite membrane enabled by poly(dopamine), *Langmuir*, 25 (2009a) 7368-7374.

Li, D. and H. Wang, Recent developments in reverse osmosis desalination membranes, *J. Mater. Chem.*, 20 (2010) 4551-4566.

Li, L., B. Wang, H. Tan, T. Chen and J. Xu, A novel nanofiltration membrane prepared with PAMAM and TMC by in situ interfacial polymerization on PEK-C ultrafiltration membrane, *J. Membr. Sci.*, 269 (2006) 84-93.

Li, L., S. Zhang, X. Zhang and G. Zheng, Polyamide thin film composite membranes prepared from 3,4',5-biphenyl triacyl chloride, 3,3',5,5'-biphenyl tetraacyl chloride and m-phenylenediamine, *J. Membr. Sci.*, 289 (2007) 258-267.

Li, L., S. Zhang, X. Zhang and G. Zheng, Polyamide thin film composite membranes prepared from isomeric biphenyl tetraacyl chloride and m-phenylenediamine, *J. Membr. Sci.*, 315 (2008) 20-27.

Li, L., S. Zhang and X. Zhang, Preparation and characterization of poly(piperazineamide) composite nanofiltration membrane by interfacial polymerization of 3,3',5,5'-biphenyl tetraacyl chloride and piperazine, *J. Membr. Sci.*, 335 (2009b) 133-139.

Li, X., L. Zhu, J. Jiang, Z. Yi, B. Zhu and Y. Xu, Hydrophilic nanofiltration membranes with self-polymerized and strong-adhered polydopamine as separating layer, *Chin. J. Polym. Sci.*, 30 (2012) 152-163.

Lin, W., T. Zhu, Q. Li, S. Yi and Y. Li, Study of pervaporation for dehydration of caprolactam through PVA/nano silica composite membranes, *Desalination* 285 (2012) 39-45.

Linggawati, A., A. W. Mohammad and Z. Ghazali, Effect of electron beam irradiation on morphology and sieving characteristics of nylon-66 membranes, *Eur. Polym. J.*, 45 (2009) 2797-2804.

Linggawati, A., A. W. Mohammad and C. P. Leo, Effects of APTEOS content and electron beam irradiation on physical and separation properties of hybrid nylon-66 membranes, *Materials Chemistry and Physics*, 133 (2012) 110-117.

Liu, J. Q., Z. L. Xu, X. H. Li, Y. Zhang, Y. Zhou, Z. X. Wang and X. J. Wang, An improved process to prepare high separation performance PA/PVDF hollow fiber composite nanofiltration membranes, *Sep. Purif. Technol.*, 58 (2007a) 53-60.

Liu, L., S. Yu, Y. Zhou and C. Gao, Study on a novel polyamide-urea reverse osmosis composite membrane (ICIC-MPD) I. Preparation and characterization of ICIC-MPD membrane, *J. Membr. Sci.*, 281 (2006a) 88-94.

Liu, L., S. Yu, L. Wu and C. Gao, Study on a novel polyamide-urea reverse osmosis composite membrane (ICIC-MPD) II. Analysis of membrane antifouling performance, *J. Membr. Sci.*, 283 (2006b) 133-146.

Liu, L., S. Yu, L. Wu and C. Gao, Study on a novel antifouling polyamide-urea reverse osmosis composite membrane (ICIC-MPD) III. Analysis of membrane electrical properties, *J. Membr. Sci.*, 310 (2008a) 119-128.

Liu, M., S. Yu, J. Tao and C. Gao, Preparation, structure characteristics and separation properties of thin-film composite polyamide-urethane seawater reverse osmosis membrane, *J. Membr. Sci.*, 325 (2008b) 947-956.

Liu, M., D. Wu, S. Yu and C. Gao, Influence of the polyacyl chloride structure on the reverse osmosis performance, surface properties and chlorine stability of the thin-film composite polyamide membranes, *J. Membr. Sci.*, 326 (2009) 205-214.

Liu, M., Y. Zheng, S. Shuai, Q. Zhou, S. Yu and C. Gao, Thin-film composite membrane formed by interfacial polymerization of polyvinylamine (PVAm) and trimesoyl chloride (TMC) for nanofiltration, *Desalination*, 288 (2012a) 98-107.

Liu, Y., S. Zhang, Z. Zhou, J. Ren, Z. Geng, J. Luan and G. Wang, Novel sulfonated thin-film composite nanofiltration membranes with improved water flux for treatment of dye solutions, *J. Membr. Sci.*, 394-395 (2012b) 218-229.

Liu, Y. L., C. H. Yu, K. R. Lee and J. Y. Lai, Chitosan/poly(tetrafluoroethylene) composite membranes using in pervaporation dehydration processes, *J. Membr. Sci.*, 287 (2007b) 230-236.

Martínez, R., M. T. Sanz, S. Beltrán and E. Corcuera, Activity coefficients at infinite dilution of volatile compounds in water: effect of temperature and salt concentration, *J. Chem. Eng. Data*, 57 (2012) 1480-1485.

Matsuura, T., *Synthetic Membranes and Membrane Separation Processes,* CRC Press, (1993).

Misra, A., F. W. Kroesser and R. A. Sheldon, The effect of solutes on the pervaporation of water-methanol mixtures through cellophane, *J. Polym. Sci: Polym Symposia*, 41 (1973) 145-153.

Mohammad, A. W., N. Hilal and M. N. A. Seman, A study on producing composite nanofiltration membranes with optimized properties, *Desalination*, 158 (2003) 73-78.

Morgan, P. W., *Condensation Polymers: By Interfacial and Solution Methods,* Interscience Publishers, (1965).

Mudahar, J. M., Thin film composite membranes based on polyester amides, Ph.D Thesis, Pune University, Pune, (1998).

Mukherjee, P., K. L. Jones and J. O. Abitoye, Surface modification of nanofiltration membranes by ion implantation, *J. Membr. Sci.*, 254 (2005) 303-310.

Mulder, M., *Basic Principles of Membrane Technology, 2nd Edition*, Kluwer Academic Publishers, (1997).

Naylor, T. d., *Polymer Membranes - Materials, Structures and Separation Performance, Rapra Review Reports,* Rapra Technology Ltd, (1996).

Ohyaal, H., M. Shibata, Y. Negishi, Q. H. Guo and H. S. Choi, The effect of molecular weight cut-off of PAN ultrafiltration support layer on separation of water-ethanol mixtures through pervaporation with PAA-PAN composite membrane, *J. Membr. Sci.*, 90 (1994) 91-100.

Pan, F., H. Jia, S. Qiao, Z. Jiang, J. Wang, B. Wang and Y. Zhong, Bioinspired fabrication of high performance composite membranes with ultrathin defect-free skin layer, *J. Membr. Sci.*, 341 (2009) 279-285.

Parrini, P., Polypiperazinamides: new polymers useful for membrane processes, *Desalination*, 48 (1983) 67-78.

Perry, R. H. and D. W. Green (Eds.), *Perry's Chemical Engineers' Handbook*, McGraw-Hill, 1999,

Petersen, R. J., Composite reverse osmosis and nanofiltration membranes, *J. Membr. Sci.*, 83 (1993) 81-150.

Pourjafar, S., A. Rahimpour and M. Jahanshahi, Synthesis and characterization of PVA/PES thin film composite nanofiltration membrane modified with TiO_2 nanoparticles for better performance and surface properties, *J. Ind. Eng. Chem.*, 18 (2012) 1398-1405.

Qiu, C., F. Xu, Q. T. Nguyen and Z. Ping, Nanofiltration membrane prepared from cardo polyetherketon ultrafiltration membrane by UV-induced grafting method, *J. Membr. Sci.*, 255 (2005) 107-115.

Qiu, C., Q. T. Nguyen and Z. Ping, Surface modification of cardo polyetherketone ultrafiltration membrane by photo-grafted copolymers to obtain nanofiltration membranes, *J. Membr. Sci.*, 295 (2007) 88-94.

Rajagopal, S., G. V. d. Velde, M. V. d. Gaag and H. A. Jenner, How effective is intermittent chlorination to control adult mussel fouling in cooling water systems ?, *Water Res.*, 37 (2003) 329-338.

Rao, A. P., N. V. Desai and R. Rangarajan, Interfacially synthesized thin film composite RO membranes for seawater desalination, *J. Membr. Sci.*, 124 (1997) 263-272.

Rautenbach, R. and A. Gröschl, Separation potential of nanofiltration membranes, *Desalination*, 77 (1990) 73-84.

Razdan, U. and S. S. Kulkarni, Nanofiltration thin-film-composite polyesteramide membranes based on bulky diols, *Desalination*, 161 (2004) 25-32.

RiIey, R. L., C. E. MiIstead, A. L. LIoyd, M. W. Seroy and M. Tagami, Spiral-wound thin-film composite membrane systems for brackish and seawater desalination by reverse osmosis, *Desalination*, 23 (1977) 331-355.

Riley, R. L., H. K. Lonsdale, C. R. Lyons and U. Merten, Preparation of ultrathin reverse osmosis membranes and the attainment of theoretical salt rejection, *J. Appl. Polym. Sci.*, 11 (1967) 2143-2158.

Rozelle, L. T., J. E. Cadotte, K. E. Cobian and C. V. Kopp, Nonpolysaccharide membranes for reverse osmosis: NS-100 membranes, in: S. Sourirajan (Ed.), *Reverse Osmosis and Synthetic Membranes*, National Research Council Canada, Ottawa, 1977, pp. 249-262.

Seidel, A., J. J. Waypa and M. Elimelech, Role of charge (Donna) exclusion in removal of arsenic from water by a negatively charged porous nanofiltration membrane, *Environ. Eng. Sci.*, 18 (2001) 105-113.

Seman, M. N. A., M. Khayet and N. Hilal, Nanofiltration thin-film composite polyester polyethersulfone-based membranes prepared by interfacial polymerization, *J. Membr. Sci.*, 348 (2010) 109-116.

Seman, M. N. A., M. Khayet and N. Hilal, Development of antifouling properties and performance of nanofiltration membranes modified by interfacial polymerisation, *Desalination*, 273 (2011) 36-47.

Shah, D., D. Bhattacharyya, A. Ghorpade and W. Mangum, Pervaporation of pharmaceutical waste streams and synthetic mixtures using water selective membranes, *Environ. Prog.*, 18 (1999) 21-29.

Skrovanek, D. J., P. C. Painter and M. M. Coleman, Hydrogen bonding in polymers. 2. Infrared temperature studies of Nylon 11, *Macromolecules* 19 (1986) 699-705.

Soice, N. P., A. C. Maladono, D. Y. Takigawa, A. D. Norman, W. B. Krantz and A. R. Greenberg, Oxidative degradation of polyamide reverse osmosis membranes: Studies of molecular model compounds and selected membranes, *J. Appl. Polym. Sci.*, 90 (2003) 1173-1184.

Soice, N. P., A. R. G. W. B. Krantz and A. D. Norman, Studies of oxidative degradation in polyamide RO membrane barrier layers using pendant drop mechanical analysis, *J. Membr. Sci.*, 243 (2004) 345-355.

Song, Y., F. Liu and B. Sun, Preparation, characterization, and application of thin film composite nanofiltration membranes, *J. Appl. Polym. Sci.*, 95 (2005) 1251-1261.

Sourirajan, S. and T. Matsuura, *Reverse Osmosis / Ultrafiltration Process Principles,* National Research Council Canada, (1985).

Sun, S. P., T. A. Hatton, S. Y. Chan and T. S. Chung, Novel thin-film composite nanofiltration hollow fiber membranes with double repulsion for effective removal of emerging organic matters from water, *J. Membr. Sci.*, 401-402 (2012) 152-162.

Tang, B., Z. Huo and PeiyiWu, Study on a novel polyester composite nanofiltration membrane by interfacial polymerization of triethanolamine (TEOA) and trimesoyl chloride (TMC) I. Preparation, characterization and nanofiltration properties test of membrane, *J. Membr. Sci.*, 320 (2008) 198-205.

Tang, B., C. Zou and P. Wu, Study on a novel polyester composite nanofiltration membrane by interfacial polymerization. II. The role of lithium bromide in the performance and formation of composite membrane, *J. Membr. Sci.*, 365 (2010) 276-285.

Waite, J. H. and M. L. Tanzer, Polyphenolic substance of mytilus edulis: novel adhesive containing L-dopa and hydroxyproline, *Science*, 212 (1981) 1038-1040.

Wang, H., L. Li, X. Zhang and S. Zhang, Polyamide thin-film composite membranes prepared from a novel triamine 3,5-diamino-N-(4-aminophenyl)-benzamide monomer and m-phenylenediamine, *J. Membr. Sci.*, 353 (2010) 78-84.

Wang, H., Q. Zhang and S. Zhang, Positively charged nanofiltration membrane formed by interfacial polymerization of 3,3',5,5'-biphenyl tetraacyl chloride and piperazine on a poly(acrylonitrile) (PAN) support, *J. Membr. Sci.*, 378 (2011a) 243-249.

Wang, T., Y. Yang, J. Zheng, Q. Zhang and S. Zhang, A novel highly permeable positively charged nanofiltration membrane based on a nanoporous hyper-crosslinked polyamide barrier layer, *J. Membr. Sci.*, 448 (2013) 180-189.

Wang, Y., T. S. Chung, B. W. Neoa and M. Gruender, Processing and engineering of pervaporation dehydration of ethylene glycol via dual-layer polybenzimidazole (PBI)/polyetherimide (PEI) membranes, *J. Membr. Sci.*, 378 (2011b) 339-350.

Wei, X., Z. Wang, Z. Zhang, J. Wang and S. Wang, Surface modification of commercial aromatic polyamide reverse osmosis membranes by graft polymerization of 3-allyl-5,5-dimethylhydantoin, *J. Membr. Sci.*, 351 (2010) 222-233.

Wei, X., Z. Wang, J. Xu, J. Wang and S. Wang, Surface modification of commercial aromatic polyamide reverse osmosis membranes by crosslinking treatments, *Chin. J. Chem. Eng.*, 21 (2013) 473-484.

Wijmans, J. G. and R. W. Baker, A simple predictive treatment of the permeation process in pervaporation, *J. Membr. Sci.*, 79 (1993) 101-113.

Wilde, E. W. and R. L. Shealy, Chlorination and dechlorination of nuclear-reactor cooling water, *Water Res.*, 26 (1992) 539-545.

Willem, D. R. J., R. C. J. Nicolaa and Z. Arie, Semipermeable composite membrane, method for the preparation of such a membrane, and its use, EP. 0,780,152, (1997).

Wu, D., X. Liu, S. Yu, M. Liu and C. Gao, Modification of aromatic polyamide thin-film composite reverse osmosis membranes by surface coating of thermo-responsive copolymers P(NIPAM-co-Am). I: Preparation and characterization, *J. Membr. Sci.*, 352 (2010a) 76-85.

Wu, D., Y. Huang, S. Yu, D. Lawless and X. Feng, Thin film composite nanofiltration membranes assembled layer-by-layer via interfacial polymerization from polyethylenimine and trimesoyl chloride, *J. Membr. Sci.*, 472 (2014) 141-153.

Wu, D., S. Yu, D. Lawless and X. Feng, Thin film composite nanofiltration membranes fabricated from polymeric amine polyethylenimine imbedded with monomeric amine piperazine for enhanced salt separations, *React. Funct. Polym.*, 86 (2015) 168-183.

Wu, H., B. Tang and P. Wu, MWNTs / polyester thin film nanocomposite membrane: an approach to overcome the trade-off effect between permeability and selectivity, *J. Phys. Chem. C*, 114 (2010b) 16395-16400.

Xi, Z. Y., Y. Y. Xu, L. P. Zhu, Y. Wang and B. K. Zhu, A facile method of surface modification for hydrophobic polymer membranes based on the adhesive behavior of poly(DOPA) and poly(dopamine), *Jounal of Membrane Science*, 327 (2009) 244-253.

Xie, W., G. M. Geise, B. D. Freeman, H.-S. Lee, G. Byun and J. E. McGrath, Polyamide interfacial composite membranes prepared from m-phenylene diamine, trimesoyl chloride and a new disulfonated diamine, *J. Membr. Sci.*, 403-404 (2012) 152-161.

Xu, J., C. Gao and X. Feng, Thin-film-composite membranes comprising of self-assembled polyelectrolytes for separation of water from ethylene glycol by pervaporation, *J. Membr. Sci.*, 352 (2010) 197-284.

Xu, J., Z. Wang, X. Wei, S. Yang, J. Wang and S. Wang, The chlorination process of crosslinked aromatic polyamide reverse osmosis membrane: New insights from the study of self-made membrane, *Desalination*, 313 (2013) 145-155.

Yang, F. and B. Zhao, Adhesion properties of self-polymerized dopamine thin film, *Open Surf. Sci. J.*, 3 (2011) 115-122.

Yang, J., H. Li, J. Xu, J. Wang, X. Meng, K. Bai, J. Lu, Y. Zhang and D. Yin, Influences of inorganic salts on the pervaporation properties of zeolite NaA membranes on macroporous supports, *Microporous Mesoporous Mater.*, 192 (2014) 60-68.

Yang, Z., Cyanuric chloride based chlorine-resistant nanofiltration membrane, Master's Thesis, National Central University, Taiwan, (2008).

Yangali-Quintanilla, V., S. K. Maeng, T. Fujioka, M. Kennedy and G. Amy, Proposing nanofiltration as acceptable barrier for organic contaminants in water reuse, *J. Membr. Sci.*, 362 (2010) 334-345.

Yaroshchuk, A. E., Rejection mechanisms of NF membranes, *Membr. Technol.*, 100 (1998) 9-12.

Yaws, C. L., P. K. Narasimhan and C. Gabbula, *Yaws' Handbook of Antoine Coefficients for Vapor Pressure*, 2nd Electronic ed., Knovel, (2009).

Yeager, H. L., T. Matsuura and S. Sourlrajan, Some characteristics of rromatic polyamide-hydrazide (1:1) copolymer membranes for reverse osmosis transport, *Ind. Eng. Chem. Process. Des. Dev.*, 20 (1981) 451-456.

Yu, S., M. Liu, X. Liu and C. Gao, Performance enhancement in interfacially synthesized thin-film composite polyamide-urethane reverse osmosis membrane for seawater desalination, *J. Membr. Sci.*, 342 (2009a) 313-320.

Yu, S., M. Liu, Z. Lü, Y. Zhou and C. Gao, Aromatic-cycloaliphatic polyamide thin-film composite membrane with improved chlorine resistance prepared from m-phenylenediamine-4-methyl and cyclohexane-1,3,5-tricarbonyl chloride, *J. Membr. Sci.*, 344 (2009b) 155-164.

Yu, S., M. Ma, J. Liu, J. Tao, M. Liu and C. Gao, Study on polyamide thin-film composite nanofiltration membrane by interfacial polymerization of polyvinylamine (PVAm) and isophthaloyl chloride (IPC), *J. Membr. Sci.*, 379 (2011) 164-173.

Zhang, L., P. Yu and Y. Luo, Dehydration of caprolactam-water mixtures through cross-linked PVA composite pervaporation membranes, *J. Membr. Sci.*, 306 (2007) 93-102.

Zhang, R. X., J. Vanneste, L. Poelmans, A. Sott, X. L. Wang and B. V. d. Bruggen, Effect of the manufacturing conditions on the structure and performance of thin-film composite membranes, *J. Appl. Polym. Sci.*, 125 (2012) 3755-3769.

Zhang, Y., J. W. Rhim and X. Feng, Improving the stability of layer-by-layer self-assembled membranes for dehydration of alcohol and diol, *J. Membr. Sci.*, 444 (2013) 22-31.

Zhao, L. and W. S. W. Ho, Novel reverse osmosis membranes incorporated with a hydrophilic additive for seawater desalination, *J. Membr. Sci.*, 455 (2014) 44-54.

Zhao, Z. P., J. Li, D. X. Zhang and C. X. Chen, Nanofiltration membrane prepared from polyacrylonitrile ultrafiltration membrane by low-temperature plasma: 1. Graft of acrylic acid in gas, *J. Membr. Sci.*, 232 (2004) 1-8.

Zhao, Z. P., J. Li, J. Chen and C. X. Chen, Nanofiltration membrane prepared from polyacrylonitrile ultrafiltration membrane by low-temperature plasma: 2. Grafting of styrene in vapor phase, *J. Membr. Sci.*, 251 (2005a) 239-245.

Zhao, Z. P., J. Li, D. Wang and C. X. Chen, Nanofiltration membrane prepared from polyacrylonitrile ultrafiltration membrane by low-temperature plasma: 4. grafting of N-vinylpyrrolidone in aqueous solution, *Desalination*, 184 (2005b) 37-44.

Zhen, H., S. M. J. Jang, W. K. Teo and K. Li, Modified silicone–PVDF composite hollow-fiber membrane preparation and its application in VOC separation, *J. Appl. Polym. Sci.*, 99 (2006) 2497-2503.

Zhou, Y., S. Yu, M. Liu and C. Gao, Preparation and characterization of polyamide-urethane thin-film composite membranes, *Desalination*, 180 (2005) 189-196.

Zhou, Y., S. Yu, C. Gao and X. Feng, Surface modification of thin film composite polyamide membranes by electrostatic self deposition of polycations for improved fouling resistance, *Sep. Purif. Technol.*, 66 (2009) 287-294.

Zhu, Y., S. Xia, G. Liu and W. Jin, Preparation of ceramic-supported poly(vinyl alcohol)–chitosan composite membranes and their applications in pervaporation dehydration of organic/water mixtures, *J. Membr. Sci.*, 349 (2010) 341-348.

Zou, H., Y. Jin, J. Yang, H. Dai, X. Yu and J. Xu, Synthesis and characterization of thin film composite reverse osmosis membranes via novel interfacial polymerization approach, *Sep. Purif. Technol.*, 72 (2010) 256-262.

Zou, L., I. Vidalis, D. Steele, A. Michelmore, S. P. Low and J. Q. J. C. Verberk, Surface hydrophilic modification of RO membranes by plasma polymerization for low organic fouling, *J. Membr. Sci.*, 369 (2011) 420-428.

Zuo, J., Y. Wang, S. P. Sun and T. S. Chung, Molecular design of thin film composite (TFC) hollow fiber membranes for isopropanol dehydration via pervaporation, *J. Membr. Sci.*, 405-406 (2012) 123-133.

Zuo, J. and T. S. Chung, Design and synthesis of a fluoro-silane amine monomer for novel thin film composite membranes to dehydrate ethanol via pervaporation, *J. Mater. Chem. A*, 1 (2013) 9814-9826.

Zuo, J., Y. Wang and T. S. Chung, Novel organic - inorganic thin film composite membranes with separation performance surpassing ceramic membranes for isopropanol dehydration, *J. Membr. Sci.*, 433 (2013) 60-71.

Zuo, J., J. Y. Lai and T. S. Chung, In-situ synthesis and cross-linking of polyamide thin film composite (TFC) membranes for bioethanol applications, *J. Membr. Sci.*, 458 (2014) 47-57.

Appendix A

Sample calculations

A.1 Nanofiltration performance

Water permeation flux

The water permeation flux was calculated from the following data:

Feed: $MgCl_2$-H_2O

Effective membrane area (S): 12.56 cm^2

Operating pressure: 0.8 MPa

Operating temperature: 23 ℃

Quantity of permeate collected (Q): 22.21 mL

Time interval (Δt): 1 h

$MgCl_2$ concentration in feed (c_{s0}): 525.07 mg/L

$MgCl_2$ concentration in permeate(c_{sl}): 7.67 mg/L

Water permeation flux: $J = \dfrac{Q}{S\Delta t} = \dfrac{22.21\times10^{-3}}{12.56\times10^{-4}\times1} = 17.68$ L/(m^2.h)

Salt rejection

$r = \left(1 - \dfrac{c_{sl}}{c_{s0}}\right) \times 100\% = \left(1 - \dfrac{7.67}{525.07}\right) \times 100\% = 98.54\%$

A.2 Pervaporation performance

Total permeation flux

The total permeation flux was calculated from the following data:

Feed mixture: Ethylene glycol-H_2O

Feed water concentration (X_{w0}): 2.37 wt%

Effective membrane area (S): 21.23 cm^2

Operating temperature: 311 K

Quantity of permeate collected (Q): 0.172 g

Time interval (Δt):1 h

Water content in permeate (X_{wl}): 90.40 wt%

$$J = \frac{Q}{S\Delta t} = \frac{0.172}{21.23\times10^{-4}\times1} = 81.03 \text{ g/(m}^2\text{.h)}$$

Partial permeation flux

$J_{water} = JX_{wl} = 81.03\times0.9040 = 73.25$ g/(m^2.h)

$J_{EG} = J(1-X_{wl}) = 81.03\times(1-0.9040) = 7.78$ g/(m^2.h)

Separation factor

$$\alpha = \frac{X_{wl}/(1-X_{wl})}{X_{w0}/(1-X_{w0})} = \frac{0.9040/(1-0.9040)}{0.0237/(1-0.0237)} = 387.9$$

Membrane permeance

The permeance of water was calculated from the following data:

Operating temperature: 311 K

Partial permeation flux of water (J_w): 46.86 g/(m^2.h)

Saturated vapor pressure of water at 311 K (p_w^s): 5.95 kPa

Mole fraction of water in feed (x_{w0}): 0.038212

Activity coefficient of water (γ_w): 0.82955 (Predicted by Aspen Plus)

Permeate vapor pressure of water (p_w^p): $\approx$0 kPa

Mole fraction of water in permeate (x_{wl}): 0.96179

The permeance of water:

$$\left(P_w/l\right) = \frac{J_w}{p_w^s x_{w0}\, \gamma_w - p_w^p x_{wl}} = \frac{46.86/18.02}{5.95 \times 0.038212 \times 0.82955} = 13.79 \text{ mol/(m}^2.\text{h.kPa)}$$

Apparent activation energy

The temperature dependence of permeation flux and membrane permeance can be expressed by Arrhenius equation and the apparent activation energy based on permeation flux (E_J) and membrane permeability (E_P) can be obtained from the plots of ($\ln J$) vs ($1/T$) and [$\ln (P_i/l)$] vs ($1/T$) based on the following equations:

$$\ln J = \ln J_0 - \frac{E_J}{R}\frac{1}{T} \tag{A2.1}$$

$$\text{Slope}_1 = -E_J/R \tag{A2.2}$$

$$\ln(P_i/l) = \ln\left(\frac{P_{io}}{l}\right) - \frac{E_P}{R}\frac{1}{T} \tag{A2.3}$$

$$\text{Slope}_2 = -E_P/R \tag{A2.4}$$

The apparent activation energies of water based on permeation flux (E_J) and membrane permeability (E_P) were calculated from the following data[*]:

Temperature (°C)	1000/T (K)	Permeation flux (mol/(m^2.h)	Permeance [mol/(m^2.h.kPa)]
25	3.35570	1.02	17.98
30	3.30033	1.56	16.85
38	3.21543	1.80	13.79
45	3.14465	2.16	10.10
55	3.04878	2.53	7.08

* Feed water concentration: 1.14 wt%

$\text{Slope}_1 = -2.7152$, $E_J = -(-2.7152 \times 8.314) = 22.57$ kJ/mol

$\text{Slope}_2 = 3.1209$, $E_P = -(3.1209 \times 8.314) = -25.95$ kJ/mol

Appendix B

Calculations of "salt transport parameter-B" and "mass transfer coefficient for the salt- k"

The "salt transport parameter – B" and "mass transfer coefficient for the salt-k" mentioned in

Chapter 3 was calculated from the following data:

Feed: $MgCl_2$-H_2O

Effective membrane area: 12.56 cm^2

Operating pressure: 0.8 MPa

Operating temperature: 23 °C

Pure water permeation flux: 21.2 L/(m^2.h)

$MgCl_2$ concentration in feed: 525.07 mg/L

$MgCl_2$ molecular weight: 95 g/mol

$MgCl_2$ molality in feed: 525.07/1000/95 = 0.00552705 mol/L

Water permeation flux in the presence of $MgCl_2$: 17.68 L/(m^2.h)

Salt rejection: 98.54%

$\rho_0 = \rho_b = \rho_l = \rho = 1000 / 18.02 = 55.3$ mol/L

The detailed calculations are illustrated as follows:

Mole permeation flux of pure water: $N_w = (21.2 \times 1000)/(18.02 \times 3600) = 0.32646$ mol/(m^2.s)

Pure water permeability constant: A $= 0.32646/0.8 = 0.41$ mol/(m^2.s.MPa)

$MgCl_2$ molality in the permeate solution: $0.00552705 \times (1-0.9854) = 8.0695 \times 10^{-5}$ mol/L

Mole permeation flux of water in the presence of $MgCl_2$:

$$N_w = \frac{(17.68 \times 1000)}{(18.02)(3600)[1 + \frac{8.0695 \times 10^{-5} \times 95}{1000}]} = 0.2725 \text{ mol/(m}^2.\text{s)}$$

Osmotic pressure for 0.1 mol/L $MgCl_2$ solution at 25 ℃ is 641 KPa [Matsuura, 1993]

Osmotic pressure for the permeate solution: π (x_{sl})=$8.0695 \times 10^{-5} \times 641/0.1 = 0.51725$ KPa

Osmotic pressure for the concentrated boundary solution:

π (x_{sb}) = ΔP+ π (x_{sl}) $-$ N_w/A = 800+0.51725-[0.2725/(0.41$\times 10^{-3}$)] = 135.883 KPa

$MgCl_2$ molality in the concentrated boundary solution:

135.883 $\times$0.1/641 = 0.021198612 mol/L

Mole fractions:

x_{s0} = (0.005527025)/(0.005527025+1000/18.02) = 0.000099587

x_{sb} = (0.021198612)/(0.021198612+1000/18.02) = 0.000381853

x_{sl} = (8.0695×10^{-5})/(8.0695×10^{-5} +1000/18.02) = 0.000001454

Salt transport parameter:

$$B = \frac{N_w}{\rho(x_{sb} - x_{sl})(\frac{1 - x_{sl}}{x_{sl}})} = \frac{(0.2725 \times 10^{-3})}{(55.3)(0.000381853 - 0.000001454)(\frac{1 - 0.000001454}{0.000001454})}$$

$$= 1.8835 \times 10^{-8} \text{ (m/s)}$$
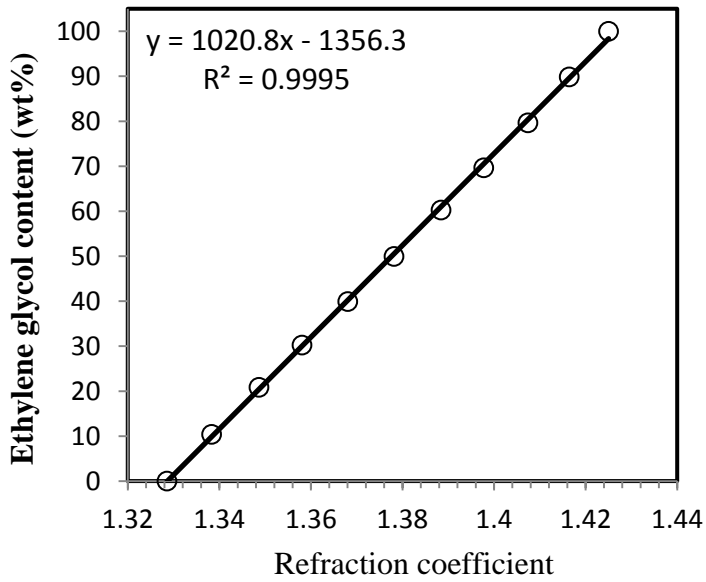
Mass transfer coefficient for the salt:

$$k = \frac{N_w}{\rho(1 - x_{sl})\ln\left[\frac{(x_{sb} - x_{sl})}{(x_{s0} - x_{sl})}\right]} = \frac{(0.2725 \times 10^{-3})}{(55.3)(1 - 0.000001454)ln\left[\frac{(0.000381853 - 0.000001454)}{(0.000099587 - 0.000001454)}\right]}$$

$$= 3.666 \times 10^{-6} \text{ (m/s)}$$

Appendix C

Calibrations of ethylene glycol/water mixtures by refractometer

Ethylene glycol content: 0-100 wt%

$y = 1020.8x - 1356.3$
$R^2 = 0.9995$

Ethylene glycol content: 0-20 wt%

$y = 1037.9x - 1378.4$
$R^2 = 0.9991$